Quantum revivals and generation of non-classical states in an N spin system

Shane Dooley

Department of Physics and Astronomy

University of Leeds

A thesis submitted for the degree of

Doctor of Philosophy

30th September 2014

Intellectual Property and Publication Statements

The candidate confirms that the work submitted is his own, except where work which has formed part of jointly authored publications has been included. The contribution of the candidate and the other authors to this work has been explicitly indicated below. The candidate confirms that appropriate credit has been given within the thesis where reference has been made to the work of others.

Chapter 5 is based on the publication:

> Shane Dooley, Francis McCrossan, Derek Harland, Mark J. Everitt and Timothy P. Spiller. Collapse and revival and cat states with an N-spin system. *Phys. Rev. A* **87** 052323 (2013).

Francis McCrossan contributed to the preminary investigations that led to this paper. Derek Harland and Mark Everitt contributed spin Wigner function plots. Timothy P. Spiller supervised the project. All other work is directly attributable to Shane Dooley.

Section 4.4 and chapter 6 and are based on the publication:

> Shane Dooley and Timothy P. Spiller. Fractional revivals, multiple-Schrödinger-cat states, and quantum carpets in the interaction of a qubit with N qubits. *Phys. Rev. A* **90** 012320 (2014).

Timothy P. Spiller supervised the project. All other work is directly attibutable to Shane Dooley.

Acknowledgements

First, I would like to thank my supervisor, Tim Spiller, for his support and patience throughout my PhD, and for always having time for me when I knocked on his door.

I have been fortunate to have learned from many people over the last four years, including collaborators Mark Everitt, Derek Harland and Jaewoo Joo; fellow PhD students Terrence Farrelly, Suva De, Andreas Kurcz, Jonathan Busch, Abbas Al-Shimary, Veiko Palge, Luis Rico Gutierrez, Tom Barlow, Oleg Kim, James DeLisle and Monovie Asita; and summer students Francis McCrossan and Anthony Hayes. I would especially like to thank Tim Proctor, Adam Stokes and Paul Knott at Leeds for all the "board sessions".

The last four months of my PhD were spent at NTT Basic Research Laboratories in Japan, and I am very grateful to Bill Munro for giving me that opportunity. Also at NTT, I would like to thank Yuichiro Matsuzaki and George Knee for many interesting discussions, and at NII Tokyo, Kae Nemoto, Emi Yukawa and Burkhard Scharfenberger.

Finally, I would like to thank my parents, Carmel and Brendan, my brother Mark and my sister Niamh for their love and support.

Abstract

The generation of non-classical states of large quantum systems is an important topic of study. It is of fundamental interest because the generation of larger and larger non-classical states extends quantum theory further and further into the classical domain, and it is also of practical interest because such states are an important resource for quantum technologies.

The focus of this thesis is the "spin star model" for the interaction of a single spin-1/2 particle with N other spin-1/2 particles. Although this is a simple model, we show that its dynamics include many interesting quantum phenomena, including fractional revival, and Jaynes-Cummings-like collapse and revival. Starting with a spin coherent state of the N spin system – an easily prepared state, in principle – we show that these dynamics can be used to generate a wide variety of non-classical states of the N spin system, including Schrödinger cat states, GHZ states, multiple-Schrödinger cat states and spin squeezed states.

Contents

Chapter 1

Introduction

Since the 1920's, there has been much interest in the generation of quantum states that call attention to the differences between the familiar classical world of our experience and the underlying quantum world. A famous early example is the Schrödinger's cat thought experiment [Schrödinger (1935)], where a cat is neither "alive" nor "dead" but is entangled with a decaying atom in such a way that it is in a quantum superposition of "alive" and "dead". The phrase "Schrödinger's cat" has since spread beyond the physics community into popular culture where – along with the Heisenberg uncertainty principle – it represents the strangeness of quantum physics. Even within physics, its technical meaning has expanded to include a quantum superposition of *any* two "classical" states. Steady progress in the control of quantum systems has led to generation of such states in experiments on small quantum systems. For example, a Schrödinger's cat state of 100 photons has been generated recently in a superconducting cavity resonator [Vlastakis *et al.* (2013)]. A significant challenge is to generate such "non-classical states" for larger and larger quantum systems, which would be convincing evidence that quantum physics describes the world at macroscopic scales (but that the quantum effects are usually suppressed by interaction with the environment [Schlosshauer (2007); Zurek (2003)]).

Another dimension to this progress is the so-called "second quantum revolution": the emerging field of quantum technology [Dowling & Milburn (2003)]. The aim of quantum technology is to engineer systems based on the laws of quantum physics, giving an improvement in some task over what is possible within a

classical framework. In every quantum technology, non-classical states (like the Schrödinger cat state) are an important resource.

The most well-known example of a proposed quantum technology is a *quantum computer*: a computer that operates on the principles of quantum physics. In principle, such a computer would be much more powerful than any classical computer. However, this requires precise control of a large quantum system and careful shielding of the system from unwanted interactions with its environment. Although there has been much progress in this direction, quantum computers are still far from reaching their full potential.

A more mature quantum technology is *quantum communication*. In particular, quantum key distribution uses the principles of quantum physics to guarantee secure communication. There are already several companies selling commercial quantum key distribution systems.

Another example of quantum technology is in the field of metrology (the science of measurement). In *quantum metrology*, a quantum system is used as a probe to measure some other system. By preparing the probe in a "non-classical" state it turns out that it is possible to significantly improve the precision of the measurement compared to the precision that is achieved by preparing the probe in a "classical" state.

In this thesis our primary motivation is the generation of non-classical states of spin systems for quantum metrology. After giving some necessary background material in chapter 2, we review (in chapter 3) quantum metrology, and in particular, the problem of estimating an unknown magnetic field with a system of N spin-1/2 particles. Then, in chapter 4 we turn to the main focus of this thesis: the *spin star model*. This model describes the interaction of a single central spin with N outer spins that do not interact among themselves. We suggest that there are several promising candidates systems for implementation of the spin star model and we derive two effective Hamiltonians for the model in two different parameter regimes.

In chapter 5 we show that there is a parameter regime where the spin star model behaves like the well-known Jaynes-Cummings model for the interaction of an harmonic oscillator and a two-level system. We find interesting dynamics, such as "collapse and revival", analogous to that in the Jaynes-Cummings model

and we propose that these dynamics can be used to generate Schrödinger cat states of the N spin system. The results presented in this section correspond to the publication [Dooley *et al.* (2013)]:

> Shane Dooley, Francis McCrossan, Derek Harland, Mark J. Everitt and Timothy P. Spiller. Collapse and revival and cat states with an N-spin system. *Phys. Rev. A* **87** 052323 (2013).

In the following two chapters we investigate dynamics of the spin star model beyond the Jaynes-Cummings approximation. In chapter 6 we identify a parameter regime where the dynamics of the spin star model leads to "multiple Schrödinger cat states", superpositions of more than two distinct classical states. This generation of "multiple Schrödinger cat states" is closely connected to the interesting phenomenon of "fractional revival". This chapter is based on the publication [Dooley & Spiller (2014)]:

> Shane Dooley and Timothy P. Spiller. Fractional revivals, multiple-Schrödinger-cat states, and quantum carpets in the interaction of a qubit with N qubits. *Phys. Rev. A* **90** 012320 (2014).

In chapter 7 we discuss the generation of another type of non-classical state, *spin squeezed states*, in the spin star model. We focus on a particular implementation of the spin star model by an ensemble of nitrogen vacancy centres in diamond interacting with a flux qubit. We take into account various realistic modifications to the spin star model and we claim that generation of spin squeezed states is experimentally feasible. The results in this chapter will be presented in a forthcoming paper. In the concluding chapter we summarise our results and we mention some areas of future research.

In this thesis we aim to convince the reader that the spin star model is a promising model for the generation of non-classical states for quantum metrology, and that the generation of these states is closely related to various interesting revival phenomena.

Chapter 2

Background

In this chapter we review some of the basic properties of a system of N spin-1/2 particles and we introduce some of the ideas that will be used in later chapters. Since there are many similarities with the quantum harmonic oscillator we begin with a discussion of that system. In section 2.1.2 we review the phase space pictures that give a convenient visualisation of states of the quantum harmonic oscillator. In section 2.1.3 we discuss various non-classical oscillator states including quadrature squeezed states, number squeezed states and superpositions of coherent states. Then, in sections 2.2.2 and 2.2.3, we describe the analogous phase space pictures and non-classical states for the spin system. Finally, in section 2.3 we discuss a limit in which the spin system and the harmonic oscillator are mathematically identical.

2.1 The quantum harmonic oscillator

The quantum harmonic oscillator is one of the most important systems in quantum physics because the harmonic potential is often a good first approximation for an oscillating particle since this is the first non-vanishing term in the expansion about any potential well minimum. It is also important because the dynamics of many continuous physical systems with periodic, or vanishing, boundary conditions can be described as a superposition of an infinite number of modes, each one like an harmonic oscillator [Merzbacher (1977)]. An important example is the electromagnetic field in a one-dimensional cavity [Gerry & Knight (2005)].

The position and momentum observables $\hat{x}$ and $\hat{p}$ for a quantum harmonic oscillator obey the canonical commutation relation

$$[\hat{x}, \hat{p}] = i, \tag{2.1}$$

where here, and throughout this thesis, we set $\hbar = 1$. The Hamiltonian for the quantum harmonic oscillator is

$$\hat{H}_{QHO} = \frac{1}{2m}\hat{p}^2 + \frac{m\omega^2}{2}\hat{x}^2, \tag{2.2}$$

where m is the mass of the particle and ω is the angular frequency of the harmonic oscillator. It is convenient to write this in terms of the dimensionless observables $\hat{X} = \sqrt{m\omega}\,\hat{x}$ and[1] $\hat{P} = \frac{1}{\sqrt{m\omega}}\,\hat{p}$ so that

$$\hat{H}_{QHO} = \frac{\omega}{2}\left(\hat{P}^2 + \hat{X}^2\right). \tag{2.3}$$

Defining the (non-Hermitian) operator

$$\hat{a} = \frac{1}{\sqrt{2}}\left(\hat{X} + i\hat{P}\right), \tag{2.4}$$

allows us to write the Hamiltonian for the quantum harmonic oscillator as

$$\hat{H}_{QHO} = \omega\left(\hat{a}^\dagger\hat{a} + \frac{1}{2}\right). \tag{2.5}$$

We can also write $\hat{X}$ and $\hat{P}$ in terms of $\hat{a}$ and $\hat{a}^\dagger$:

$$\hat{X} = \frac{1}{\sqrt{2}}(\hat{a} + \hat{a}^\dagger) \qquad ; \qquad \hat{P} = \frac{i}{\sqrt{2}}(\hat{a}^\dagger - \hat{a}). \tag{2.6}$$

From (2.1), the commutator of $\hat{a}$ and $\hat{a}^\dagger$ is

$$\left[\hat{a}, \hat{a}^\dagger\right] = 1. \tag{2.7}$$

The eigenstates of the Hamiltonian $\hat{H}_{QHO}$ are the eigenstates of the operator $\hat{a}^\dagger\hat{a}$. These are called *Fock states* and are labelled by non-negative integers, $n = 0, 1, 2...$:

[1] If we reintroduce Planck's constant these scaling factors are $\sqrt{\frac{m\omega}{\hbar}}$ and $\sqrt{\frac{1}{\hbar m\omega}}$ which do indeed have units of distance^{-1} and momentum^{-1} respectively.

$$\hat{a}^\dagger \hat{a} \left|n\right\rangle = n \left|n\right\rangle . \tag{2.8}$$

The eigenvalue associated with the eigenstate $|n\rangle$ of $\hat{H}_{QHO}$ is thus $\omega\left(n + \frac{1}{2}\right)$. Using the commutation relations (2.7) it can be shown that $\hat{a}^\dagger |n\rangle$ and $\hat{a} |n\rangle$ are also eigenstates of the operator $\hat{a}^\dagger \hat{a}$ with eigenvalues $n+1$ and $n-1$ respectively. This implies that

$$\hat{a} \left|n\right\rangle = \sqrt{n} \left|n-1\right\rangle \qquad ; \qquad \hat{a}^\dagger \left|n\right\rangle = \sqrt{n+1} \left|n+1\right\rangle . \tag{2.9}$$

These properties justify the naming of $\hat{a}$ as the *lowering operator* and of $\hat{a}^\dagger$ as the *raising operator*. Operators $\hat{a}^\dagger$ and $\hat{a}$ are also called the *creation* and *annihilation* operators since they create or annihilate an excitation of the harmonic oscillator. The *ground state* $|0\rangle$ of the oscillator is defined by $\hat{a} |0\rangle = 0$.

2.1.1 Coherent states

It is well known that the state of a system in quantum physics cannot have a precise value for non-commuting observables. In the case of the harmonic oscillator, the fact that $\hat{X}$ and $\hat{P}$ are non-commuting operators leads to the Heisenberg uncertainty relation:

$$\mathrm{Var}\, \hat{X}\, \mathrm{Var}\, \hat{P} \geq \frac{1}{4}, \tag{2.10}$$

where $\mathrm{Var}\hat{X} = \mathrm{Tr}(\hat{X}^2\rho) - [\mathrm{Tr}(\hat{X}\rho)]^2$ and $\mathrm{Var}\hat{P} = \mathrm{Tr}(\hat{P}^2\rho) - [\mathrm{Tr}(\hat{P}\rho)]^2$ are the variances of $\hat{X}$ and $\hat{P}$ in the state ρ.

The coherent state $|\alpha\rangle$ of the quantum harmonic oscillator, parameterised by the complex number α, can be defined in various equivalent ways:

1. As the eigenstates of the annihilation operator $\hat{a} |\alpha\rangle = \alpha |\alpha\rangle$;
2. As the displaced vacuum, $|\alpha\rangle = \hat{D}(\alpha) |0\rangle$, where $\hat{D}(\alpha) = e^{\alpha\hat{a}^\dagger - \alpha^* \hat{a}}$ is the *displacement operator*;
3. In terms of Fock states: $|\alpha\rangle = e^{-|\alpha|^2/2} \sum_{n=0}^{\infty} \frac{\alpha^n}{\sqrt{n!}} |n\rangle$.

The coherent states have a number of interesting properties that have led to them being regarded as "classical states" of the harmonic oscillator [Gerry & Knight (2005)]. First, the variances of the observables $\hat{X}$ and $\hat{P}$ in the coherent state are

$$\mathrm{Var}\,\hat{X} = \frac{1}{2} \quad ; \quad \mathrm{Var}\,\hat{P} = \frac{1}{2}, \tag{2.11}$$

so that

$$\mathrm{Var}\,\hat{X}\,\mathrm{Var}\,\hat{P} = \frac{1}{4}. \tag{2.12}$$

Comparing (2.12) with (2.10) shows that the coherent states are minimum uncertainty states of $\hat{X}$ and $\hat{P}$ with the property that $\mathrm{Var}\,\hat{X} = \mathrm{Var}\,\hat{P}$. Moreover, a coherent state evolving by the quantum Harmonic oscillator Hamiltonian $\hat{H}_{QHO}$ remains a coherent state throughout its evolution:

$$e^{-it\hat{H}_{QHO}}\left|\alpha\right\rangle = \left|\alpha e^{-i\omega t}\right\rangle. \tag{2.13}$$

The expectation values of operators $\hat{X}$ and $\hat{P}$ in this evolving coherent state are

$$\left\langle \alpha e^{-i\omega t}\right|\hat{X}\left|\alpha e^{-i\omega t}\right\rangle = \frac{1}{\sqrt{2}}(\alpha e^{-i\omega t} + \alpha^* e^{i\omega t}) \tag{2.14}$$

$$\left\langle \alpha e^{-i\omega t}\right|\hat{P}\left|\alpha e^{-i\omega t}\right\rangle = \frac{i}{\sqrt{2}}(\alpha^* e^{i\omega t} - \alpha e^{-i\omega t}), \tag{2.15}$$

which are also the solutions to the classical equations of motion for the coordinates $X(t)$ and $P(t)$ of an harmonic oscillator. Coherent states of light are also, in principle, easily prepared: they are the steady states of a field mode in a dissipative cavity that is driven by a classical electric field [Gerry & Knight (2005)].

2.1.2 Phase space pictures

Since the quantum harmonic oscillator cannot simultaneously have a precise value for both $\hat{X}$ and $\hat{P}$ [equation (2.10)], we cannot have a phase space picture of the harmonic oscillator as in classical physics where the state of the oscillator can have a precise value for both position and momentum. The coherent states are the closest we can get since they are minimum uncertainty states of $\hat{X}$ and $\hat{P}$ with

the property that $\mathrm{Var}\,\hat{X} = \mathrm{Var}\,\hat{P}$. This means that they are more like points in phase space (the complex α-plane) than other states. It is therefore useful to try to write other quantum states in terms of coherent states. To do this one uses the property [Gerry & Knight (2005)]:

$$\int d^2\alpha \, |\alpha\rangle \langle\alpha| = \pi. \tag{2.16}$$

Equation 2.16 shows that the sum of all projectors onto coherent states is proportional to the identity operator. Since the constant of proportionality is greater than the identity, however, the coherent state basis is said to be *overcomplete*. Using equation (2.16), any state ρ can thus be written in the form

$$\rho = \frac{1}{\pi^2} \int d^2\alpha \int d^2\beta \, \langle\alpha| \rho |\beta\rangle \, |\alpha\rangle \langle\beta| \,. \tag{2.17}$$

Since the coherent state basis is overcomplete, this decomposition is not unique. In particular, it is also possible to write the state in diagonal form in the coherent state basis [Glauber (1963); Sudarshan (1963)]:

$$\rho = \int d^2\alpha \; P(\alpha) \, |\alpha\rangle \langle\alpha| \,, \tag{2.18}$$

where normalisation of ρ implies that $\int d^2\alpha \, P(\alpha) = 1$ and $P(\alpha)$ must be real since ρ is Hermitian. Equation (2.18) is known as the *Glauber-Sudarshan P-representation*, or, more succinctly, as the P-representation for the state ρ. The function $P(\alpha)$ for a coherent state $\rho = |\alpha\rangle \langle\alpha|$ is a delta function, $P(\alpha) = \delta^2(\alpha)$. In this respect, the function $P(\alpha)$ seems to capture the idea of the coherent state as a point in classical phase space (the complex α-plane is the phase space of the quantum harmonic oscillator [Gerry & Knight (2005)]). The P-function for a thermal state with an average excitation number $\langle \hat{a}^\dagger \hat{a} \rangle = \bar{n}$ is a Gaussian $P(\alpha) = \frac{1}{\pi\bar{n}} e^{-|\alpha|^2/\bar{n}}$, reflecting the statistical uncertainty of the the thermal state. In these cases the P-function can be interpreted as a phase space probability distribution. However, the P-function cannot always be interpreted as a probability distribution since it can take negative values (examples are given in the next section). Moreover, the P-function can even be a derivative of a δ-function – a distribution that is even more singular than a δ-function and only makes sense as an integrand [Gerry & Knight (2005)]. In fact, a widely used classification

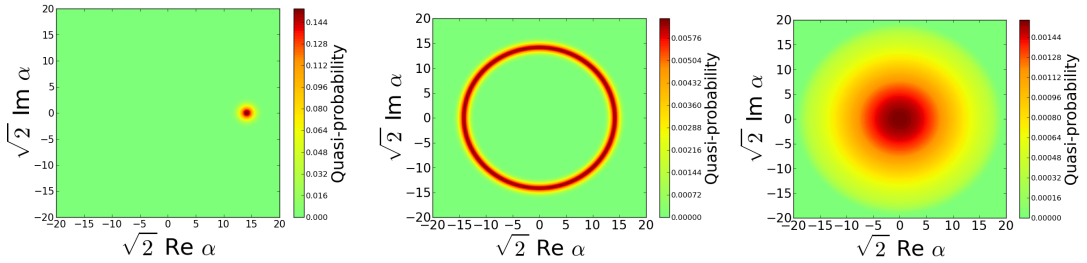

Figure 2.1: Left: Q-function for coherent state with $\alpha = 10$. Middle: Q-function for $n = 100$ Fock state. Right: Q-function for $\bar{n} = 100$ thermal state. In each case the average excitation number is $\langle \hat{a}^\dagger \hat{a} \rangle = 100$.

of classical and non-classical states is that classical states are those whose P-functions can be interpreted as probability distributions, and non-classical states are those whose P-functions cannot be interpreted as probability distributions. Hillery (1985) showed that by this criteria coherent states are the only classical pure states. From (2.18) it is clear that any mixed state ρ that is classical is a statistical mixture of coherent states. Since the P-function is not always a true probability distribution it is sometimes called a "quasi-probability" distribution.

Because the P-function is highly singular for some states it is often difficult to manipulate in calculation (or even to find numerically). An alternative is the *Husimi Q-representation*. The Q-function is defined as

$$Q(\alpha) = \frac{1}{\pi} \langle \alpha | \rho | \alpha \rangle . \tag{2.19}$$

Since ρ is a positive operator we have $Q(\alpha) \geq 0$ for any value of α. Also, the factor of π^{-1} ensures that

$$\int d^2\alpha \, Q(\alpha) = 1. \tag{2.20}$$

The Q-function is clearly more like a probability distribution than the P-function. In figure 2.1 we plot the Q-functions for a coherent state, for a Fock state, and for a thermal state. The Q-function has the advantage of being easy to calculate. It does not, however, have a useful criteria to classify classical and non-classical states, as for the P-function.

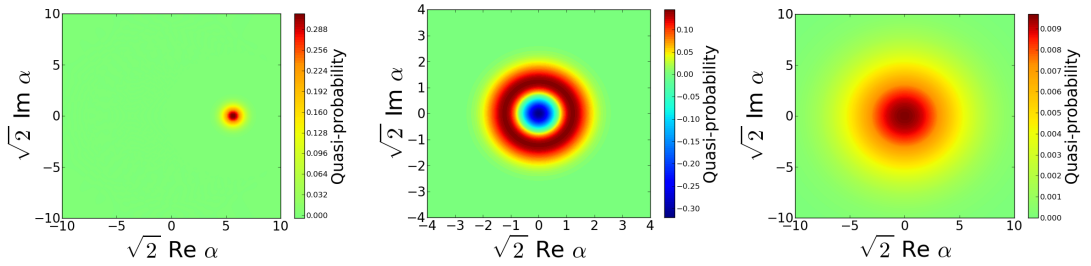

Figure 2.2: Left: Wigner function for coherent state with $\alpha = 4$. Middle: Wigner function for the $n = 1$ Fock state. Blue indicates negative regions of quasi-probability. Right: Wigner function for $\bar{n} = 16$ thermal state.

A middle ground between the P-function and the Q-function is the *Wigner function*. It can be defined as:

$$W(\alpha) = \frac{1}{\pi^2} \int d^2\beta \, e^{\beta^*\alpha - \beta\alpha^*} \mathrm{Tr}\left[\rho \, e^{\beta\hat{a}^\dagger - \beta^*\hat{a}}\right]. \tag{2.21}$$

The Wigner function has the property that $\int d^2\alpha \, W(\alpha) = 1$, but – like the P-function – can have negative regions. The Wigner function is never singular so that it is easier to calculate than the P-function. Moreover, it gives a way of distinguishing (some) non-classical states from classical states: a state ρ is non-classical if its Wigner function is negative [Kenfack & Życzkowski (2004)]. The converse is not true, i.e., some non-classical states (by the P-function criterion) have Wigner functions that are positive everywhere (e.g. some squeezed states, to be discussed in the next section) [Hudson (1974)].

In figure 2.2 we plot the Wigner functions for a coherent state, a Fock state and a thermal state. For the Fock state the Wigner function has some negative regions, indicating that the Fock state is a non-classical state.

Interestingly, the Q-function, the Wigner function and the P-function are all special cases of a more general function $R_s(\alpha)$ introduced by Cahill & Glauber (1969):

$$R_s(\alpha) = \frac{1}{\pi^2} \int d^2\beta \, e^{\beta^*\alpha - \beta\alpha^*} \mathrm{Tr}\left[\rho \, e^{\beta\hat{a}^\dagger - \beta^*\hat{a} + s|\beta|^2/2}\right]. \tag{2.22}$$

This is the Q-function for $s = -1$, the Wigner function for $s = 0$, and the P-function for $s = 1$.

2.1.3 Non-classical oscillator states

In this section we introduce some important non-classical states of the harmonic oscillator. These states are all non-classical by the P-function criterion since their P functions are either negative or more singular than a δ-function.

Quadrature squeezed states

The coherent state is a minimum uncertainty state $\operatorname{Var}\hat{X}\operatorname{Var}\hat{P} = 1/4$ with $\operatorname{Var}\hat{X} = \operatorname{Var}\hat{P} = 1/2$. The coherent state has the same uncertainty $\operatorname{Var}\hat{X}_\theta = 1/2$ for any choice of quadrature,

$$\hat{X}_\theta = \hat{X}\cos\theta + \hat{P}\sin\theta, \tag{2.23}$$

where θ is known as the *quadrature angle*. Any state for which the uncertainty in some quadrature is less than that of a coherent state is called a *squeezed state* [Lvovsky *et al.* (2013)]. The squeezing is quantified by

$$\chi^2 = 2\min_{\theta\in(0,2\pi)}\operatorname{Var}\hat{X}_\theta, \tag{2.24}$$

so that $\chi^2 = 1$ for a coherent state and $\chi^2 < 1$ for a squeezed state. Mathematically, the uncertainty $\operatorname{Var}\hat{X}_\theta$ of a state in the $\hat{X}_\theta$ quadrature can be decreased by a factor of $e^{-2|\eta|}$ by acting on it with the *squeezing operator*:

$$S(\eta) = \exp\left[\left(\eta\hat{a}^2 - \eta^*\hat{a}^{\dagger 2}\right)/2\right], \tag{2.25}$$

where $\eta = |\eta|e^{2i\theta}$ is the squeezing parameter. The state $S(\eta)\left|\alpha\right\rangle$, for example, is a squeezed state since we have $\operatorname{Var}\hat{X}_\theta = \frac{e^{-2|\eta|}}{2}$ and $\chi^2 = e^{-2|\eta|}$, indicating squeezing for $|\eta| > 0$.

Squeezing is best visualised by plotting the Wigner function or Q-function of a state. In figure 2.3 we plot the Wigner function for the vacuum $\left|0\right\rangle$ and the squeezed vacuum $S(\eta)\left|0\right\rangle$, for $\theta = 0$ (squeezed in the position quadrature) and $|\eta| = 1$. Although squeezed coherent states have Wigner distributions that are positive everywhere, they are widely regarded as non-classical states since their P-functions include derivatives of δ-functions [Gerry & Knight (2005)].

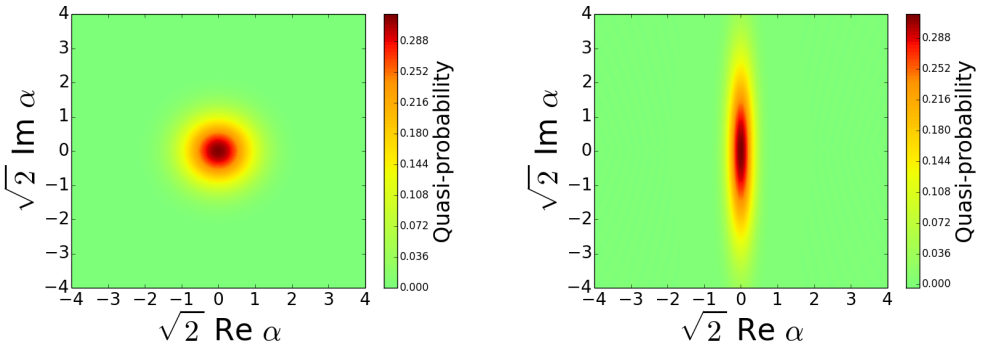

Figure 2.3: Left: Wigner function for the vacuum. Right: Wigner function for the squeezed vacuum with $\eta = 1$.

Number squeezed states

States that have less uncertainty in their photon number distribution than a coherent state are *number squeezed states* [Mandel (1979)]. Since the photon number distribution for a coherent state is Poissonian, these states are also sometimes said to have *sub-Poissonian* number statistics. The variance of the photon number distribution for a coherent state is $\mathrm{Var}(\hat{a}^\dagger\hat{a}) = \langle \hat{a}^\dagger\hat{a} \rangle$ so that a state is number squeezed if

$$\mathrm{Var}(\hat{a}^\dagger\hat{a}) < \langle \hat{a}^\dagger\hat{a} \rangle . \tag{2.26}$$

Number squeezing can thus be quantified by[1]

$$\chi'^2_n = \frac{\mathrm{Var}(\hat{a}^\dagger\hat{a})}{\langle \hat{a}^\dagger\hat{a} \rangle}. \tag{2.28}$$

(This quantity is primed because it is not our final version of the number squeezing parameter.) For the coherent state we have $\chi'^2_n = 1$. For $0 \leq \chi'^2_n < 1$ the state

[1]The standard measure of number squeezing is the *Mandel Q-parameter*, Q_M [Mandel (1979)] (nothing to do with the Husimi Q-function of section 2.1.2) and is related to χ'^2_n by an added constant:

$$Q_M = \chi'^2_n - 1. \tag{2.27}$$

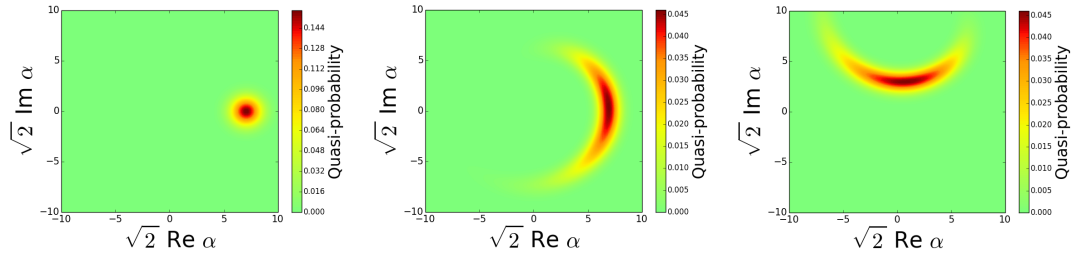

Figure 2.4: Left: the Q-function for a spin coherent state. Middle: the Q-function for a number squeezed "crescent state" with the same amplitude. Right: A displaced crescent state.

is sub-Poissonian and for $\chi'^2_n > 1$ the state is super-Poissonian. The archetypal number squeezed states are *crescent states*. An example is plotted in figure 2.4. The most number squeezing is for Fock states, for which $\chi'^2_n = 0$. We notice, however, that for the vacuum we have $\chi'^2_n = 0/0$ and the number squeezing parameter is undefined.

If a crescent state (or a Fock state) is displaced so that its arc is no longer centred at the vacuum [see figure 2.4], the parameter χ'^2_n no longer reflects the squeezing of the state. To take this into account, we modify the definition of the number squeezing parameter so that it is minimised over all possible choices of 'arc centre'. Our adjusted measure of number squeezing is:

$$\chi''^2_n = \min_{\alpha\in\mathbb{C}} \frac{\mathrm{Var}[(\hat{a}^\dagger + \alpha^*)(\hat{a} + \alpha)]}{\langle(\hat{a}^\dagger + \alpha^*)(\hat{a} + \alpha)\rangle}. \tag{2.29}$$

This has introduced a problem, however: just as χ'^2_n is undefined for the vacuum state, for any coherent state χ''^2_n is not well defined for all parameters in the minimisation. In other words, there is some α in the minimisation that gives $\chi''^2_n = 0/0$. Our final modification is to add a small constant ϵ to the numerator and denominator of χ''^2_n and to take the $\epsilon \to 0$ limit after the minimisation[1]:

$$\chi^2_n = \lim_{\epsilon\to 0} \min_{\alpha\in\mathbb{C}} \frac{\mathrm{Var}[(\hat{a}^\dagger + \alpha^*)(\hat{a} + \alpha)] + \epsilon}{\langle(\hat{a}^\dagger + \alpha^*)(\hat{a} + \alpha)\rangle + \epsilon}. \tag{2.30}$$

[1]We are not aware of any references that suggest (2.29) or (2.30) as measures of number squeezing.

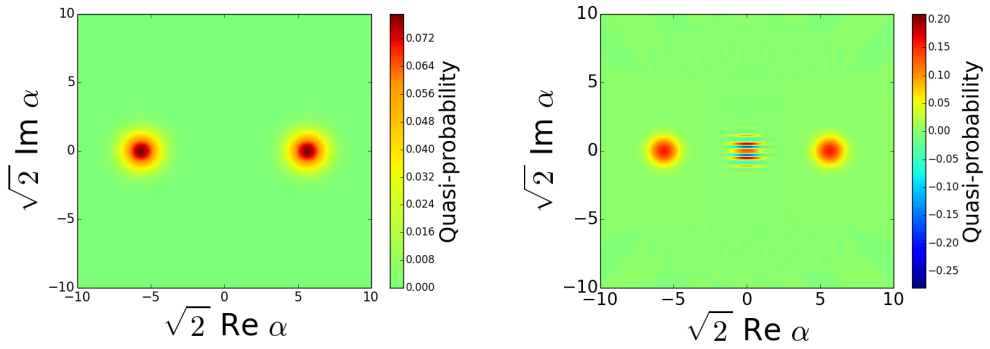

Figure 2.5: Q-function (left) and Wigner function (right) for the cat state $\frac{1}{\sqrt{2(1+e^{-2|\alpha|^2})}}(|\alpha\rangle + |-\alpha\rangle)$ with $\alpha = 4$.

This is our final number squeezing parameter. It gives $\chi_n^2 = 1$ for coherent states, $0 \leq \chi_n^2 < 1$ for number squeezed states and displaced number squeezed states, and is well defined for all states.

Schrödinger cat states

Another interesting class of non-classical states are superpositions of coherent states, sometimes called *Schrödinger cat states* or just *cat states* [Gerry & Knight (2005)]. In figure 2.5 we plot the Q-function and the Wigner function for the cat state:

$$\frac{1}{\sqrt{2(1+e^{-2|\alpha|^2})}}(|\alpha\rangle + |-\alpha\rangle)\,, \tag{2.31}$$

with $\alpha = 4$. The obvious difference between the two phase space plots is that the Wigner function has interference fringes between the two coherent state components while the Q function does not. In fact, the Q-function for a Schrödinger cat state (2.31) is almost indistinguishable from the Q-function for the mixed state $\rho = \frac{1}{2}(|\alpha\rangle\langle\alpha| + |-\alpha\rangle\langle-\alpha|)$. The Wigner function interference fringes have negative regions, indicating that the Schrödinger cat state is non-classical.

Also of interest are "multiple" cat states, superpositions of more than two coherent states [Dalvit *et al.* (2006); Lee *et al.* (2014); Munro *et al.* (2002); Toscano

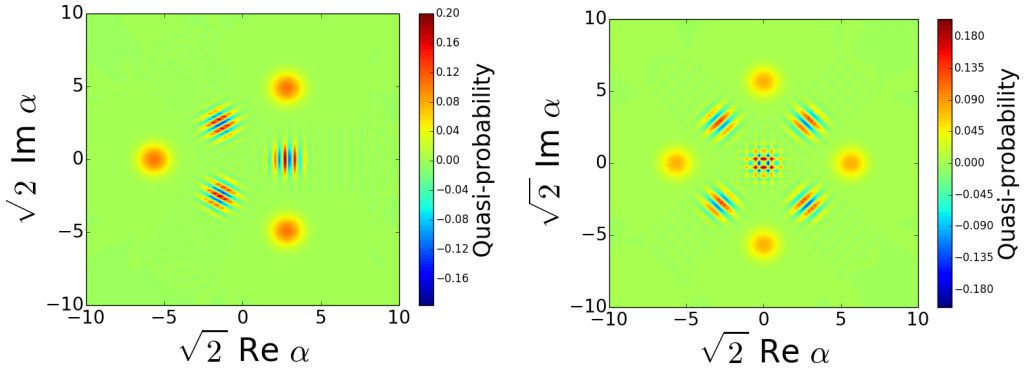

Figure 2.6: Wigner functions for multiple-cat states. Left: A superposition of three coherent states $\mathcal{N}(\left|\alpha e^{i\pi/3}\right\rangle + |\alpha e^{i\pi}\rangle + \left|\alpha e^{-i\pi/3}\right\rangle)$ where $\mathcal{N}$ is for normalisation. Right: A superposition of four coherent states, $\mathcal{N}(|\alpha\rangle + |i\alpha\rangle + |-\alpha\rangle + |-i\alpha\rangle)$. For both plots $\alpha = 4$.

et al. (2006); Zurek (2001)]. For example, we plot in figure 2.6 the Wigner functions for superpositions of 3 and 4 coherent states arranged symmetrically around the vacuum.

2.2 A system of N spin-1/2 particles

A single spin-1/2 particle is one of the simplest quantum systems. Its state space $\mathcal{H} = \mathbb{C}^2$ is two dimensional. The Pauli σ-operators are operators on this space that obey the commutation relations

$$[\hat{\sigma}_x, \hat{\sigma}_y] = 2i\hat{\sigma}_z \quad ; \quad [\hat{\sigma}_y, \hat{\sigma}_z] = 2i\hat{\sigma}_x \quad ; \quad [\hat{\sigma}_z, \hat{\sigma}_x] = 2i\hat{\sigma}_y. \tag{2.32}$$

In the basis that diagonalises $\hat{\sigma}_z$, the matrix form of these operators is:

$$\hat{\sigma}_x = \begin{pmatrix} 0 & 1 \\ 1 & 0 \end{pmatrix} ; \quad \hat{\sigma}_y = \begin{pmatrix} 0 & -i \\ i & 0 \end{pmatrix} ; \quad \hat{\sigma}_z = \begin{pmatrix} 1 & 0 \\ 0 & -1 \end{pmatrix}. \tag{2.33}$$

Our notation for eigenstates of the σ-operators is as follows:

$$\hat{\sigma}_x |{\rightarrow}\rangle = |{\rightarrow}\rangle \quad ; \quad \hat{\sigma}_x |{\leftarrow}\rangle = -|{\leftarrow}\rangle ; \tag{2.34}$$

$$\hat{\sigma}_y |{\boxtimes}\rangle = |{\boxtimes}\rangle \quad ; \quad \hat{\sigma}_y |{\odot}\rangle = -|{\odot}\rangle ; \tag{2.35}$$

$$\hat{\sigma}_z |{\uparrow}\rangle = |{\uparrow}\rangle \quad ; \quad \hat{\sigma}_z |{\downarrow}\rangle = -|{\downarrow}\rangle . \tag{2.36}$$

The symbols $\boxtimes$ and $\odot$ are meant to represent an arrow pointing into the page and out of the page, respectively. It is easily shown that the eigenstates of $\hat{\sigma}_x$ and $\hat{\sigma}_y$ can be written in terms of $|{\uparrow}\rangle$ and $|{\downarrow}\rangle$ as:

$$|{\rightarrow}\rangle = \frac{1}{\sqrt{2}} \left(|{\uparrow}\rangle + |{\downarrow}\rangle \right) \quad ; \quad |{\boxtimes}\rangle = \frac{1}{\sqrt{2}} \left(|{\uparrow}\rangle + i\,|{\downarrow}\rangle \right) \quad ; \tag{2.37}$$

$$|{\leftarrow}\rangle = \frac{1}{\sqrt{2}} \left(|{\uparrow}\rangle - |{\downarrow}\rangle \right) \quad ; \quad |{\odot}\rangle = \frac{1}{\sqrt{2}} \left(|{\uparrow}\rangle - i\,|{\downarrow}\rangle \right) . \tag{2.38}$$

Any linear operator on the space of the spin-1/2 particle can be written as a linear combination of the Pauli σ-operators $\hat{\sigma}_x$, $\hat{\sigma}_y$, $\hat{\sigma}_z$ and the identity operator $\hat{\mathbb{I}}_2 = \begin{pmatrix} 1 & 0 \\ 0 & 1 \end{pmatrix}$. In particular, the density operator for the state of a spin-1/2 particle can be written in terms of these four operators:

$$\rho = \frac{1}{2} \left(\mathbb{I}_2 + \vec{r}.\vec{\hat{\sigma}} \right) , \tag{2.39}$$

where $\vec{r} = (r_x, r_y, r_z)$ is a real vector in three dimensions with $|\vec{r}| \leq 1$ and $\vec{\hat{\sigma}} = (\hat{\sigma}_x, \hat{\sigma}_y, \hat{\sigma}_z)$ [Nielsen & Chuang (2000)]. The state of a spin-1/2 particle can thus be visualised as a three dimensional vector $\vec{r}$. This is the *Bloch sphere representation* of the state. Pure states have $|\vec{r}| = 1$ and live on the surface of the sphere. Mixed states have $|\vec{r}| < 1$ and live in the interior.

A system of two spin-1/2 particles has a four dimensional state space $\mathcal{H} = \mathbb{C}^2 \otimes \mathbb{C}^2$ (already too many degrees of freedom for a Bloch ball-like visualisation). A basis for this space is, for example, the states $|{\uparrow\uparrow}\rangle$, $|{\uparrow\downarrow}\rangle$, $|{\downarrow\uparrow}\rangle$, $|{\downarrow\downarrow}\rangle$. An alternative basis is composed of the *singlet state*

$$\frac{1}{\sqrt{2}} \left(|{\uparrow\downarrow}\rangle - |{\downarrow\uparrow}\rangle \right) , \tag{2.40}$$

(which is antisymmetric under exchange of the two spins) and the *triplet states*

$$|\uparrow\uparrow\rangle \quad ; \quad \frac{1}{\sqrt{2}}\left(|\uparrow\downarrow\rangle + |\downarrow\uparrow\rangle\right) \quad ; \quad |\downarrow\downarrow\rangle\,, \tag{2.41}$$

(which are symmetric under exchange of the two spins).

A system of N spin-1/2 particles has state space $\mathcal{H} = \mathbb{C}^2 \otimes ... \otimes \mathbb{C}^2 = (\mathbb{C}^2)^{\otimes N}$ with 2^N complex degrees of freedom. We define the collective spin operators

$$\hat{J}_x = \frac{1}{2}\sum_{i=1}^{N} \hat{\sigma}_x^{(i)} \quad ; \quad \hat{J}_y = \frac{1}{2}\sum_{i=1}^{N} \hat{\sigma}_y^{(i)} \quad ; \quad \hat{J}_z = \frac{1}{2}\sum_{i=1}^{N} \hat{\sigma}_z^{(i)}, \tag{2.42}$$

as well as the total spin operator

$$\hat{J}^2 = \hat{J}_x^2 + \hat{J}_y^2 + \hat{J}_z^2. \tag{2.43}$$

The commutation relations for the sigma operators imply the following commutation relations:

$$\left[\hat{J}_\mu, \hat{J}_\nu\right] = i\epsilon^{\mu\nu\rho}\hat{J}_\rho \qquad ; \qquad \left[\hat{J}^2, \hat{J}_\mu\right] = 0, \tag{2.44}$$

where $\epsilon^{\mu\nu\rho}$ is the antisymmetric tensor with $\epsilon^{xyz} = 1$.

Dicke states of the N spin system are the simultaneous eigenstates of the commuting operators $\hat{J}^2$ and $\hat{J}_z$, denoted by $|j,m\rangle_N$ where

$$\hat{J}^2\,|j,m\rangle_N = j(j+1)\,|j,m\rangle_N\,, \tag{2.45}$$

$$\hat{J}_z\,|j,m\rangle_N = m\,|j,m\rangle_N \tag{2.46}$$

for $j \in \left\{0, 1, ..., \frac{N}{2}\right\}$ if N is even, $j \in \left\{\frac{1}{2}, \frac{3}{2}, ..., \frac{N}{2}\right\}$ if N is odd, and $m \in \{-j, -j+1, .., j\}$. The subscript N on the ket here and throughout indicates a state of an N spin system.

As with the quantum harmonic oscillator, we can introduce operators

$$\hat{J}_\pm = \hat{J}_x \pm i\hat{J}_y, \tag{2.47}$$

that have the effect of raising or lowering the m label of the Dicke state:

$$\hat{J}_\pm\,|j,m\rangle_N = \sqrt{j(j+1) - m(m\pm 1)}\,|j,m\pm 1\rangle_N\,. \tag{2.48}$$

The raising and lowering operators obey the following commutation relations

$$\left[\hat{J}_-, \hat{J}_+\right] = -2\hat{J}_z \quad ; \quad \left[\hat{J}_z, \hat{J}_\pm\right] = \pm\hat{J}_\pm \quad ; \quad \left[\hat{J}^2, \hat{J}_\pm\right] = 0. \tag{2.49}$$

If $N > 2$ the states $|j,m\rangle_N$ are not a complete basis for the N spin system, as can be seen from the fact that there are only $\sum_{j=0}^{N/2}(2j+1) = \left(\frac{N}{2}+1\right)^2 < 2^N$ of these states. A further label $\vec{k}$ is needed. But these $\vec{k}$'s then only label degenerate copies of the space spanned by the states $|j,m\rangle_N$ for any fixed value of j [Arecchi *et al.* (1972)]. The degeneracy of the j subspace is given by the combinatorial factor [Arecchi *et al.* (1972); Wesenberg & Mølmer (2002)]

$$\nu(j,N) = \binom{N}{\frac{N}{2}-j} - \binom{N}{\frac{N}{2}-j-1} \qquad \text{with} \quad \binom{N}{-1} = 0, \tag{2.50}$$

which gives total dimension

$$\sum_{j=0}^{N/2} \nu(j,N)(2j+1) = 2^N. \tag{2.51}$$

This represents a decomposition of the state space of the N spin-1/2 particles into a direct sum of $2j+1$ dimensional subspaces $\mathbb{C}^{2j+1}$ where $0 \le j \le \frac{N}{2}$:

$$\mathcal{H} = \bigoplus_{j=0}^{N/2} \nu(N,j)\mathbb{C}^{2j+1}, \tag{2.52}$$

where each $2j+1$ dimensional subspace can be thought of as the state space of a single spin-j particle. Depending on the problem being considered, this decomposition of the state space of the N spins may be more convenient than the tensor product decomposition $\mathcal{H} = (\mathbb{C}^2)^{\otimes N}$.

The $j = \frac{N}{2}$ subspace is an $N+1$ dimensional subspace of the whole 2^N dimensional state space. Restriction to this subspace is a significant reduction in dimension when $N \gg 1$. States in this eigenspace are totally symmetric with respect to exchange of any two spins. In particular, the $j = \frac{N}{2}$ Dicke states are totally symmetric:

$$\left|\frac{N}{2}, m\right\rangle_N = \binom{N}{\frac{N}{2}+m}^{-1/2} \sum_{\text{permutations}} \left|\downarrow^{\otimes(\frac{N}{2}-m)}\uparrow^{\otimes(\frac{N}{2}+m)}\right\rangle, \tag{2.53}$$

where we have used the notation

$$\left|\downarrow^{\otimes N}\right\rangle = |\underbrace{\downarrow ... \downarrow}_{N \text{ times}}\rangle = \underbrace{|\downarrow\rangle \otimes ... \otimes |\downarrow\rangle}_{N \text{ times}}. \tag{2.54}$$

These $N+1$ states ($m \in \{-\frac{N}{2}, .., \frac{N}{2}\}$) are a basis for the $j = \frac{N}{2}$ eigenspace (this is true only for this eigenspace, the one associated with the maximal value of j). We will find it useful to define the operator:

$$\hat{a}_\uparrow^\dagger \hat{a}_\uparrow \equiv \frac{N}{2} + \hat{J}_z, \tag{2.55}$$

whose eigenstates in the symmetric subspace are the Dicke states and whose eigenvalue is the number of spins up:

$$\hat{a}_\uparrow^\dagger \hat{a}_\uparrow \left|\frac{N}{2}, m\right\rangle_N = \left(\frac{N}{2} + m\right) \left|\frac{N}{2}, m\right\rangle_N. \tag{2.56}$$

Similarly, the operator

$$\hat{a}_\downarrow^\dagger \hat{a}_\downarrow \equiv \frac{N}{2} - \hat{J}_z, \tag{2.57}$$

has the same eigenstates but its eigenvalue is the number of spins down:

$$\hat{a}_\downarrow^\dagger \hat{a}_\downarrow \left|\frac{N}{2}, m\right\rangle_N = \left(\frac{N}{2} - m\right) \left|\frac{N}{2}, m\right\rangle_N. \tag{2.58}$$

The reason for this $\hat{a}_\uparrow$, $\hat{a}_\downarrow$ notation will be made clear later in section 2.3.

In this thesis we often confine ourselves to a j-subspace of the spin system. When this is the $j = \frac{N}{2}$ subspace it will sometimes be convenient to shift the label of the Dicke states $\left|\frac{N}{2}, m\right\rangle_N = \left|\frac{N}{2}, n - \frac{N}{2}\right\rangle_N$. In this case we drop the redundant $j = \frac{N}{2}$ label for the Dicke state, $\left|\frac{N}{2}, n - \frac{N}{2}\right\rangle_N \equiv |n\rangle_N$. The N subscript distinguishes the Dicke state $|n\rangle_N$ from the harmonic oscillator Fock state $|n\rangle$.

2.2.1 Spin coherent states

In this section we follow the notation of Arecchi *et al.* (1972). *Spin coherent state* are simultaneous eigenstates of $\hat{J}^2$ and $\vec{r}.\vec{\hat{J}}$ with eigenvalues $j(j+1)$ and j respectively where $\vec{r}$ is a unit vector in three dimensions and $\vec{\hat{J}} = (\hat{J}_x, \hat{J}_y, \hat{J}_z)$ is the vector whose x, y and z components are the collective spin operators. In a given j-subspace a spin coherent state is thus specified by the vector $\vec{r} = (r_x, r_y, r_z)$ so

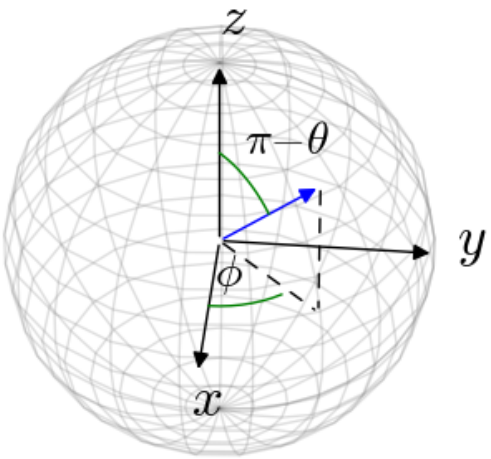

Figure 2.7: Spherical coordinates for the unit vector, $\vec{r}$, in blue.

that we can write it as $|j,\vec{r}\rangle_N$ and we can, roughly speaking, visualise it as a point on a unit sphere specified by the vector $\vec{r}=(r_x,r_y,r_z)$. In spherical coordinates, $\vec{r}=(\sin\theta\cos\phi,\sin\theta\sin\phi,-\cos\theta)$ where θ and ϕ are the polar and azimuthal angles respectively (see figure 2.7). With this parameterisation we write the spin coherent state as $|j,(\theta,\phi)\rangle_N$. The spin coherent can also be thought of as a displacement of some reference spin coherent state. This displacement is achieved by a unitary operator $R(\theta,\phi)=e^{-i\theta\vec{J}.\vec{n}}$ which rotates the reference spin coherent state by an angle θ about an axis specified by the unit vector $\vec{n}$. If we take the Dicke state $|j,-j\rangle_N$ (which is also a spin coherent state) as our reference state and $\vec{n}=(\sin\phi,-\cos\phi,0)$ to be in the xy-plane, then

$$\begin{aligned} |j,(\theta,\phi)\rangle_N &= R(\theta,\phi)\,|j,-j\rangle_N && (2.59)\\ &= e^{-i\theta(J_x\sin\phi-J_y\cos\phi)}\,|j,-j\rangle_N = e^{\tau J_+-\tau^* J_-}\,|j,-j\rangle_N\,, && (2.60)\end{aligned}$$

where $\tau=\frac{\theta}{2}e^{-i\phi}$. The spin coherent state can also be written in terms of the Dicke states:

$$|j,(\theta,\phi)\rangle_N=\sum_{m=-j}^{j}\binom{2j}{m+j}^{1/2}\left(\cos\frac{\theta}{2}\right)^{j-m}\left(e^{-i\phi}\sin\frac{\theta}{2}\right)^{j+m}|j,m\rangle_N\,. \qquad (2.61)$$

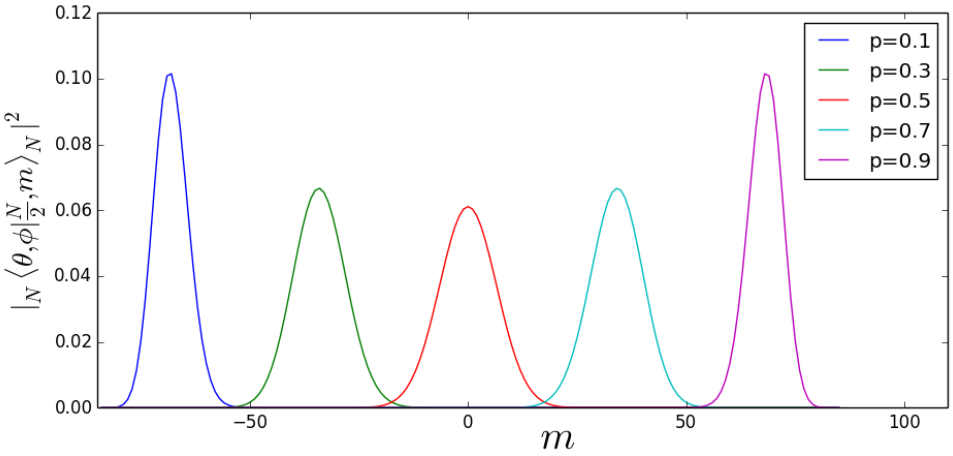

Figure 2.8: The distribution of Dicke states $\left|\frac{N}{2},m\right\rangle_N$ for the spin coherent state $\left|\frac{N}{2},(\theta,\phi)\right\rangle_N$ for different values of $p=\sin^2\frac{\theta}{2}$. ($N=170$.)

For a spin coherent state the distribution of Dicke states is binomial:

$$|_N\langle j,(\theta,\phi)|j,m\rangle_N|^2=\binom{2j}{j+m}p^{j+m}(1-p)^{j-m}, \tag{2.62}$$

where $p=\sin^2\frac{\theta}{2}$. This distribution is plotted in figure 2.8 for various values of p.

An alternative parameterisation of the spin coherent state that is useful is found by stereographic projection of the sphere. If we project from the north pole (the state corresponding to $\theta=\pi$) onto a complex plane through the equator (see figure 2.9), then the spherical coordinates (θ,ϕ) are related to the stereographic coordinates $\zeta\in\mathbb{C}$ by the transformation[1]:

$$\zeta=e^{-i\phi}\tan\frac{\theta}{2}. \tag{2.63}$$

With this parameterisation, we write the spin coherent state as $|j,\zeta\rangle_N$. Rewriting equation (2.61) in terms of ζ gives:

$$|j,\zeta\rangle_N=\sum_{m=-j}^{j}\binom{2j}{j+m}^{1/2}\frac{1}{\left(1+|\zeta|^2\right)^j}\zeta^{j+m}\,|j,m\rangle_N\,. \tag{2.64}$$

[1]The stereographic projection is defined at every point on the sphere except the projection point, in this case, the north pole.

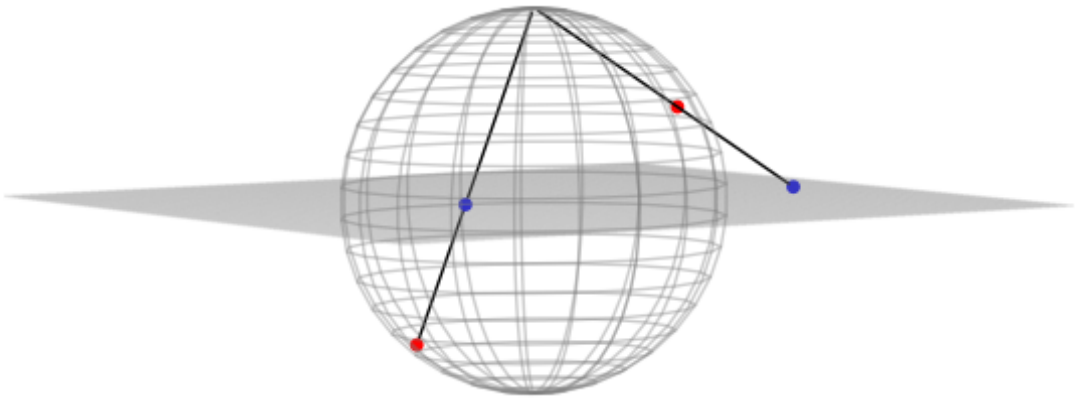

Figure 2.9: Stereographic projection of two points on the sphere (in red) to points on a complex plane (in blue). The plane passes through the equator of the sphere.

Various expectation values of collective spin operators in the spin coherent state $|j,\zeta\rangle_N$ are given in appendix A.1.

Spin coherent states in the $j = \frac{N}{2}$ symmetric subspace have the property that they are separable states of the N spins. To see this we write the rotation operator in equation (2.60) as

$$R(\theta,\phi) = e^{-i\theta\left(\hat{J}_x \sin\phi - \hat{J}_y \cos\phi\right)} = \left[\cos\frac{\theta}{2} + \left(e^{-i\phi}\hat{\sigma}_+ - e^{i\phi}\hat{\sigma}_-\right)\sin\frac{\theta}{2}\right]^{\otimes N}. \tag{2.65}$$

Operating on the reference state $\left|\frac{N}{2},-\frac{N}{2}\right\rangle_N \equiv |\downarrow\rangle^{\otimes N}$ results in the state

$$\left|\frac{N}{2},(\theta,\phi)\right\rangle_N = \left[\cos\frac{\theta}{2}|\downarrow\rangle + e^{-i\phi}\sin\frac{\theta}{2}|\uparrow\rangle\right]^{\otimes N}, \tag{2.66}$$

or, in stereographic coordinates,

$$\left|\frac{N}{2},\zeta\right\rangle_N = \left[\frac{|\downarrow\rangle + \zeta|\uparrow\rangle}{\sqrt{1+|\zeta|^2}}\right]^{\otimes N}. \tag{2.67}$$

As we did for the Dicke states, we drop the redundant $\frac{N}{2}$ spin coherent state label when we are in the $j = \frac{N}{2}$ subspace:

$$\left|\frac{N}{2},(\theta,\phi)\right\rangle_N \equiv |\theta,\phi\rangle_N \quad ; \qquad \left|\frac{N}{2},\zeta\right\rangle_N \equiv |\zeta\rangle_N \,. \tag{2.68}$$

Spin coherent states in the symmetric subspace are easily prepared in principle. Suppose, for example, that the bare Hamiltonian for the spin sytem is $\hat{H}_0 = \omega \hat{J}_z$. By cooling the system it will relax to its ground state, the spin coherent state $|\downarrow\rangle^{\otimes N}$. From this state any other spin coherent state can be generated by applying the same rotation to each of the spins [equation (2.65)]. This can be achieved by an external classical magnetic field $\vec{B}$ [Arecchi *et al.* (1972)]. To see this, we note that the Hamiltonian for the N spin system in a uniform magnetic field is $\hat{H}_B = -\gamma \vec{B} \cdot \hat{\vec{J}}$ where γ is the gyromagnetic ratio of the spins. By choosing an appropriate magnetic field $\vec{B}$, the state $|\downarrow\rangle^{\otimes N}$ will evolve by the total Hamiltonian $\hat{H} = \omega \hat{J}_z - \gamma \vec{B} \cdot \hat{\vec{J}}$ to the desired spin coherent state, at which time we switch off the interaction with the magnetic field. For example, if we want to prepare the spin coherent state $|\theta,\phi\rangle_N$, we can apply the magnetic field:

$$\vec{B} = \begin{pmatrix} -B\sin\phi \\ B\cos\phi \\ \omega/\gamma \end{pmatrix}. \tag{2.69}$$

This leads to the Hamiltonian

$$\hat{H} = \omega \hat{J}_z - \gamma \vec{B} \cdot \hat{\vec{J}} = B\sin\phi\, \hat{J}_x - B\cos\phi\, \hat{J}_y. \tag{2.70}$$

From equation (2.65) we see that evolving for a time $t = \theta/B$ leads to the spin coherent state $|\theta,\phi\rangle_N$.

Alternatively, by applying a strong magnetic field $\gamma|\vec{B}| \gg \omega$ in the direction of the spin coherent state that we are trying to generate, the Hamiltonian is

$$\hat{H} = \omega \hat{J}_z - \gamma \vec{B} \cdot \hat{\vec{J}} \approx -\gamma \vec{B} \cdot \hat{\vec{J}}. \tag{2.71}$$

The ground state of this approximate Hamiltonian is a spin coherent state in the direction of the magnetic field so that this state can be prepared by cooling the system. We note, however, that if the parameter ω in the bare Hamiltonian $\hat{H}_0 = \omega \hat{J}_z$ is very large, then we require a very large magnetic field for the condition $\gamma|\vec{B}| \gg \omega$ to be satisfied. Similarly, if we want to generate the spin coherent state by rotation of the spin by Hamiltonian (2.70), then the magnetic field (2.69) will be very large if ω is a large parameter.

2.2.2 Spin phase space pictures

In section 2.1.2 we saw that there are quasi-probability distributions that give a convenient representation of the state of a quantum harmonic oscillator. Similarly, we can visualise states of the spin system (restricted to a particular j-subspace) with phase space plots [Agarwal (1981)].

Just like the harmonic oscillator coherent states, the spin coherent states form an overcomplete basis:

$$\int d\Omega \left|j,(\theta,\phi)\right\rangle_N \left\langle j,(\theta,\phi)\right| = \frac{4\pi}{2j+1}, \tag{2.72}$$

where $d\Omega = \sin\theta\, d\theta\, d\phi$. It follows that an arbitrary state ρ can be written in the spin coherent state basis. It is also possible to write the state ρ diagonally in the spin coherent state basis, the *spin P-representation* of the state [Arecchi *et al.* (1972)]:

$$\rho = \int d\Omega\, P(\theta,\phi) \left|j,(\theta,\phi)\right\rangle_N \left\langle j,(\theta,\phi)\right|, \tag{2.73}$$

for some fixed value of j, although the function $P(\theta,\phi)$ is not uniquely determined for each state ρ. In fact, $P(\theta,\phi)$ can always be chosen to be a smooth function (in contrast with the harmonic oscillator P-function) [Arecchi *et al.* (1972); Giraud *et al.* (2008)]. The classical and non-classical states can be categorised by a spin P-function criterion analogous to the harmonic oscillator: a state ρ of a spin-j is classical if it can be written in the form of equation (2.73) with $P(\theta,\phi)$ non-negative (i.e., as a statistical mixture of spin coherent states). Otherwise the state is non-classical [Giraud *et al.* (2008)].

In this thesis we prefer to use the spin Q-function or the spin Wigner function. There are various definitions for the spin Wigner function of a spin-j particle. We choose [Agarwal (1981); Dowling *et al.* (1994)]:

$$W(\theta,\phi) = \sum_{k=0}^{2j} \sum_{q=-k}^{k} Y_{kq}(\theta,\phi)\rho_{kq}, \tag{2.74}$$

where Y_{kq} are the spherical harmonics and $\rho_{kq} = \mathrm{Tr}\left[\rho\, \hat{T}^{\dagger}_{kq}\right]$ are the expansion coefficients of ρ in terms of the multipole operators $\hat{T}_{kq}$, defined as

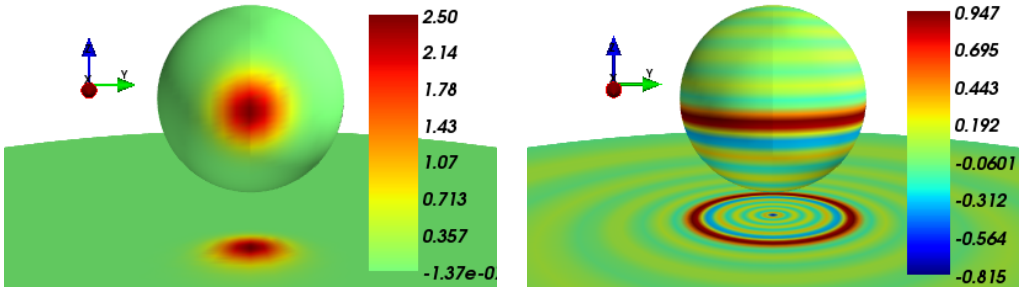

Figure 2.10: Left: The spin Wigner function $W(\theta,\phi)$ and its stereographic projection $W(\zeta)$ for the spin coherent state $|{\rightarrow}\rangle^{\otimes N}$ with $N = 20$. Right: The spin Wigner function for the Dicke state $\left|\frac{N}{2},m\right\rangle_N$ with $N = 20$ and $m = -1$.

$$\hat{T}_{kq} = \sum_{m=-j}^{j}\sum_{m'=-j}^{j}(-1)^{k+m+m'}\sqrt{\frac{2k+1}{2j+1}}\left\langle j,-m\right|\left\langle k,q|j,-m'\right\rangle\left|j,m\right\rangle\left\langle j,m'\right|, \quad (2.75)$$

where $\langle j,-m|\langle k,q|j,-m'\rangle$ are Clebsch-Gordon coefficients. The stereographic projection $W(\zeta)$ of the spin Wigner function is found via the transformation $\zeta = e^{-i\phi}\tan\frac{\theta}{2}$. In section 2.1.2 we saw that negativity of the Wigner function for a state of the harmonic oscillator indicates non-classicality of the state. Unfortunately, there is no analogous criterion for the spin Wigner function.

For a fixed value of j the *spin Q-function* is defined analogously to the harmonic oscillator Q-function. In spherical coordinates it is:

$$Q(\theta,\phi) = \frac{2j+1}{4\pi}\,{}_N\left\langle j,(\theta,\phi)\right|\rho\left|j,(\theta,\phi)\right\rangle_N, \quad (2.76)$$

and in stereographic coordinates:

$$Q(\zeta) = \frac{2j+1}{4\pi}\,{}_N\left\langle j,\zeta\right|\rho\left|j,\zeta\right\rangle_N. \quad (2.77)$$

The spin Q-function is always non-negative $[Q(\theta,\phi) \geq 0]$ and it normalises to unity $[\int d\Omega Q(\theta,\phi) = 1]$. In figure 2.11 we plot the spin Q-functions for a spin coherent state and for a Dicke state.

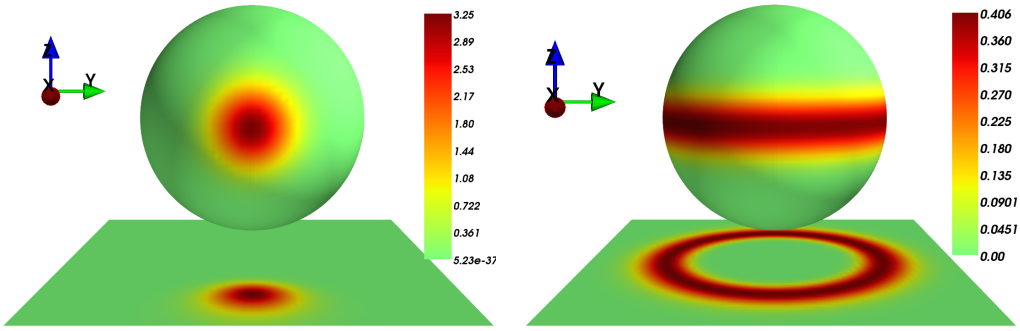

Figure 2.11: Left: The spin Q-function $Q(\theta, \phi)$ and its stereographic projection $Q(\zeta)$ for the spin coherent state $|{\rightarrow}\rangle^{\otimes N}$ with $N = 40$. Right: The spin Q-function for the Dicke state $\left|\frac{N}{2}, m\right\rangle_N$ with $N = 40$ and $m = 0$.

2.2.3 Non-classical spin states

Although there is no straightforward classification of non-classical states based on the spin Wigner function, certain states can be regarded as non-classical in an operational sense: they can give an improvement over "classical" limits for measurement precision. This will be discussed in more detail in the next chapter. For now we give some of the properties of the spin states that are analogous to the non-classical states of the harmonic oscillator that were introduced in section 2.1.3.

Spin squeezed states

Each of the commutation relations $\left[\hat{J}_\mu, \hat{J}_\nu\right] = i\epsilon^{\mu\nu\rho}\hat{J}_\rho$ for the collective spin operators [equation (2.44)] allow us to derive a different uncertainty relation:

$$\operatorname{Var} \hat{J}_\mu \operatorname{Var} \hat{J}_\nu \geq \frac{\left|\left\langle \hat{J}_\rho \right\rangle\right|^2}{4}. \tag{2.78}$$

In each of these inequalities the quantity on the right hand side depends on the state of the spin-j particle. In this respect, the uncertainty relation is a little more complicated than $\operatorname{Var} \hat{X} \operatorname{Var} \hat{P} \geq \frac{1}{4}$ for the harmonic oscillator. For the harmonic oscillator, squeezed states were defined [in equation (2.24)] as those that have a variance in some quadrature that is less than that of a coherent state, i.e., less

than 1/2. We cannot define spin squeezed states in the same way since we can always choose a collective spin operator $\vec{r}\cdot\hat{\vec{J}}$ for which the spin coherent state is an eigenstate with zero uncertainty. This problem is easily overcome by defining the mean spin direction

$$\vec{r}_m = \frac{\left\langle \hat{\vec{J}} \right\rangle}{\left| \left\langle \hat{\vec{J}} \right\rangle \right|} = \frac{\left(\left\langle \hat{J}_x \right\rangle, \left\langle \hat{J}_y \right\rangle, \left\langle \hat{J}_z \right\rangle \right)}{\sqrt{\left\langle \hat{J}_x \right\rangle^2 + \left\langle \hat{J}_y \right\rangle^2 + \left\langle \hat{J}_z \right\rangle^2}}, \tag{2.79}$$

and considering only the uncertainties of spin operators $\hat{J}_{\vec{r}_m^\perp} = \vec{r}_m^\perp \cdot \hat{\vec{J}}$ where $\vec{r}_m^\perp$ is a unit vector perpendicular to the mean spin direction. A spin coherent state $|j,(\theta,\phi)\rangle_N$ then has the same variance, $\mathrm{Var}\, \hat{J}_{\vec{r}_m^\perp} = \frac{j}{2}$ for any choice of $\vec{r}_m^\perp$. A state in the j-subspace is spin squeezed if it has a variance smaller than $j/2$ for some operator $\hat{J}_{\vec{r}_m^\perp}$. Spin squeezing can then be quantified [Kitagawa & Ueda (1993)] by:

$$\chi_s^2 = \frac{2}{j} \min_{\vec{r}_m^\perp} \mathrm{Var}\, \hat{J}_{\vec{r}_m^\perp}, \tag{2.80}$$

where the minimisation is over all possible directions $\vec{r}_m^\perp$. For a spin coherent state $|j,(\theta,\phi)\rangle_N$ we have $\chi_s^2 = 1$. If $\chi_s^2 < 1$ the state is spin squeezed. To illustrate spin squeezing we plot in figure 2.12 the Q-functions for a spin coherent state and a spin squeezed state.

The spin squeezing parameter χ_s^2 is not the only measure of spin squeezing. Later, in section 3.2, we give another measure that is directly related to metrology.

Dicke squeezed states

States ρ that have less uncertainty in their Dicke state distribution ${}_N\langle j,m|\rho|j,m\rangle_N$ than a spin coherent state we call *Dicke squeezed states*. A Dicke state is the ideal example since it has no uncertainty in its Dicke state distribution. The spin squeezing parameter χ_s^2 cannot detect this kind of squeezing since we have $\chi_s^2 \geq 1$ for the Dicke state $|j,m\rangle_N$ (with equality only for the spin coherent states $|j,\pm j\rangle_N$). We would thus like to find a Dicke spin squeezing parameter that is analogous to the number squeezing parameter for the harmonic oscillator. To do this we follow the same procedure as in section 2.1.3.

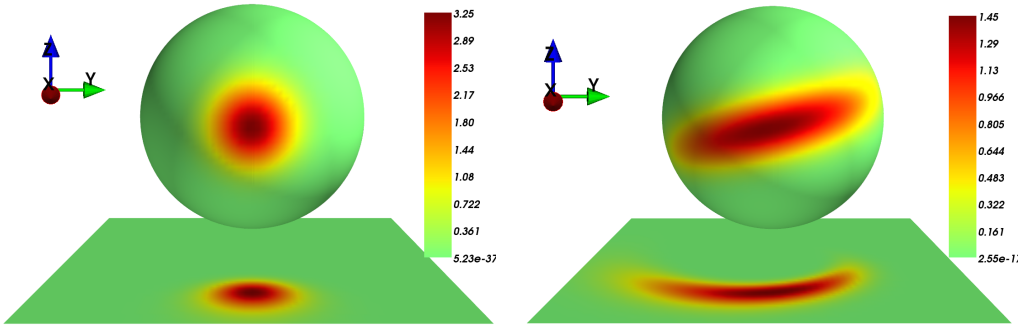

Figure 2.12: Left: The Q-function for an $N = 40$ spin coherent state. The Q-function is symmetric around the mean spin direction (the direction of the positive x-axis). Right: The Q-function for a spin squeezed state. The minimum variance orthogonal to the mean spin direction is less than that of the spin coherent state.

We first consider Dicke squeezing in the z-direction. We notice that for any spin coherent state we have the identity

$$2j \operatorname{Var} \hat{J}_z = j^2 - \left\langle \hat{J}_z \right\rangle^2, \tag{2.81}$$

(This is easily shown via the expectation values and variances given in appendix A.1.) We could define Dicke squeezed states as those states for which

$$2j \operatorname{Var} \hat{J}_z < j^2 - \left\langle \hat{J}_z \right\rangle^2, \tag{2.82}$$

and the Dicke squeezing parameter as [Raghavan *et al.* (2001)]

$$\chi'^2_D = \frac{2j \operatorname{Var} \hat{J}_z}{j^2 - \left\langle \hat{J}_z \right\rangle^2}. \tag{2.83}$$

This is analogous to χ'^2_n for the harmonic oscillator [equation (2.28)]. It gives $\chi'^2_D = 1$ for a spin coherent state, $0 \leq \chi'^2_D < 1$ for Dicke squeezed states and its smallest value $\chi'^2_D = 0$ for Dicke states. It is, however, undefined for the states $|j, \pm j\rangle_N$. Moreover, χ'^2_D does not detect the squeezing of rotated Dicke states, for example, simultaneous eigenstates of $\hat{J}_x$ and $\hat{J}^2$. Replacing the operator $\hat{J}_z$ with $\hat{J}_{\vec{r}} = \hat{\vec{J}} \cdot \vec{r}$ and minimising over all possible directions $\vec{r}$ gives a rotationally invariant measure but introduces the problem that for spin coherent states the

measure is not well defined for all parameters of the minimisation (i.e., for spin coherent states there is always some direction $\vec{r}$ for which ${\chi'}^2_D = 0/0$). As for the harmonic oscillator, this can be overcome by adding a small positive number ϵ to the numerator and denominator and taking the $\epsilon \to 0$ limit after the minimisation:

$${\chi''}^2_D = \lim_{\epsilon\to 0} \min_{\vec{r}} \frac{2j \operatorname{Var} \hat{J}_{\vec{r}} + \epsilon}{j^2 - \left\langle \hat{J}_{\vec{r}} \right\rangle^2 + \epsilon}. \tag{2.84}$$

The squeezing parameter ${\chi''}^2_D$ is, however, difficult to calculate, since the numerator and denominator both depend on the parameter that is being minimised. In practice, it is convenient to let $\epsilon = \left\langle \hat{J}_{\vec{r}} \right\rangle^2$ and to discard the $\epsilon \to 0$ limit. This gives [Ma *et al.* (2011)]

$$\chi^2_D = \frac{1}{j^2} \min_{\vec{r}} \left[2j \operatorname{Var} \hat{J}_{\vec{r}} + \left\langle \hat{J}_{\vec{r}} \right\rangle^2 \right]. \tag{2.85}$$

We have $\chi^2_D = 1$ for spin coherent states, $0 \leq \chi^2_D < 1$ for squeezed states and $\chi^2_D = m^2/j^2$ for Dicke states $|j, m\rangle_N$.

GHZ States

The Greenberger-Horne-Zeilinger (GHZ) states in the $\hat{\sigma}_x$, $\hat{\sigma}_y$, $\hat{\sigma}_z$ bases are,

$$\left|GHZ^x_\pm\right\rangle_N = \frac{1}{\sqrt{2}} \left(|\rightarrow\rangle^{\otimes N} \pm |\leftarrow\rangle^{\otimes N} \right), \tag{2.86}$$

$$\left|GHZ^y_\pm\right\rangle_N = \frac{1}{\sqrt{2}} \left(|\boxtimes\rangle^{\otimes N} \pm |\odot\rangle^{\otimes N} \right), \tag{2.87}$$

$$\left|GHZ^z_\pm\right\rangle_N = \frac{1}{\sqrt{2}} \left(|\uparrow\rangle^{\otimes N} \pm |\downarrow\rangle^{\otimes N} \right), \tag{2.88}$$

respectively where $|\rightarrow\rangle$ and $|\leftarrow\rangle$ are the eigenstates of $\hat{\sigma}_x$ and $|\boxtimes\rangle$ and $|\odot\rangle$ are the eigenstates of $\hat{\sigma}_y$ [as defined in equations (2.34) and (2.35)]. More generally, a GHZ state in an arbitrary direction $\vec{r}$ is the superposition of antipodal spin coherent states:

$$\left|GHZ^{\vec{r}}_\pm\right\rangle_N = \frac{1}{\sqrt{2}} \left(\left|\frac{N}{2}, \zeta\right\rangle_N \pm \left|\frac{N}{2}, -\frac{1}{\zeta^*}\right\rangle_N \right), \tag{2.89}$$

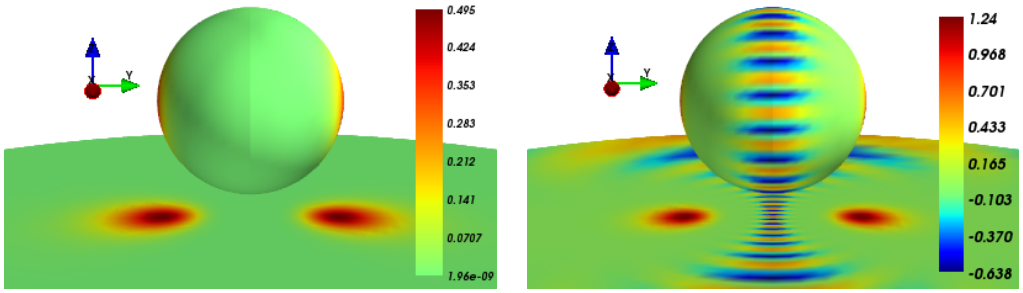

Figure 2.13: Left: The spin Q-function for the GHZ state $|GHZ^y_+\rangle_N$. Right: The spin Wigner function for $|GHZ^y_+\rangle_N$. $(N = 20)$

where ζ specifies the direction in stereographic coordinates.

In figure 2.13 we plot the spin Q-function and the spin Wigner function for the state $|GHZ^y_+\rangle_N$.

Spin Cat States

We define the spin cat state as

$$|\mathcal{Z}_\pm(\zeta)\rangle_N \equiv \mathcal{N}_\pm \left(|j,\zeta\rangle_N \pm |j,-\zeta\rangle_N\right), \tag{2.90}$$

where $\mathcal{N}_\pm = (2 \pm 2K^N)^{-1/2}$ is for normalisation with $K = \frac{1-|\zeta|^2}{1+|\zeta|^2}$. As $|\zeta|$ ranges from 0 to 1, the spin cat state $|\mathcal{Z}_+(\zeta)\rangle_N$ goes from a spin coherent state to a spin cat state composed of two orthogonal components. For $j = N/2$, for example, we have

$$|\mathcal{Z}_+(0)\rangle_N = |\downarrow\rangle^{\otimes N} \tag{2.91}$$

$$|\mathcal{Z}(1)\rangle_N = |GHZ^x\rangle_N = \frac{1}{\sqrt{2}}\left(|\rightarrow\rangle^{\otimes N} + |\leftarrow\rangle^{\otimes N}\right) \tag{2.92}$$

so that $|\mathcal{Z}(0)\rangle_N$ is a separable state of the N spins and $|\mathcal{Z}(1)\rangle_N$ is a maximally entangled GHZ state. In figure 2.14 we plot the spin Q-function and the spin Wigner function for the spin cat state $|\mathcal{Z}_+(\zeta)\rangle_N$ for $j = N/2$ and $\zeta = i/2$.

Also of interest are *multiple cat states*: superpositions of more than two spin coherent states. For example, the spin Q-functions for a three and four component multiple cat state are plotted in figure 2.15.

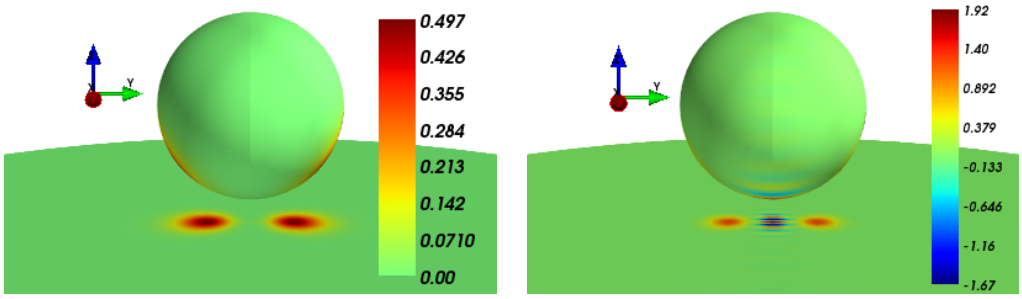

Figure 2.14: Left: Q-function for the spin cat state $|\mathcal{Z}_+(\zeta)\rangle_N$. Right: Spin Wigner function for $|\mathcal{Z}_+(\zeta)\rangle_N$. ($N = 20$, $\zeta = i/2$.)

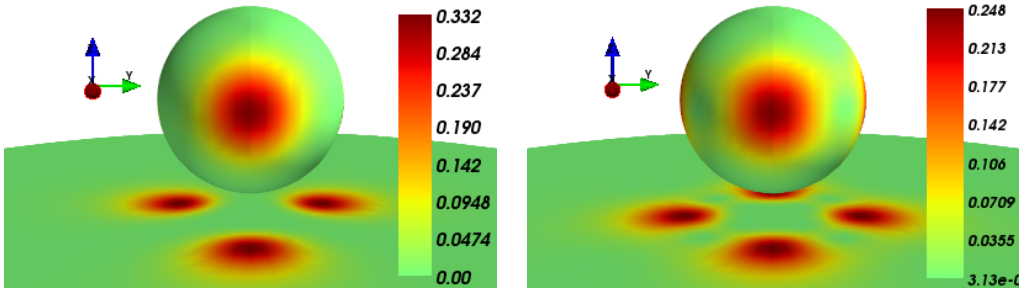

Figure 2.15: Left: Q-function for a superposition of three spin coherent states $\mathcal{N}\left(|\zeta\rangle_N + \left|\zeta e^{2\pi i/3}\right\rangle_N + \left|\zeta e^{-2\pi i/3}\right\rangle_N\right)$. Right: A superposition of four spin coherent states $\mathcal{N}\left(|\zeta\rangle_N + |i\zeta\rangle_N + |-\zeta\rangle_N + |-i\zeta\rangle_N\right)$. ($N = 20$, $\zeta = 1$.)

2.3 The bosonic limit

It is clear from the above sections that there are many similarities between the quantum harmonic oscillator and the j-subspace of a spin system. In this section we elaborate on the correspondence between the two systems and show that they are identical in a certain limit, the *bosonic limit* of the spin system.

The j-subspace of a spin system and the harmonic oscillator differ fundamentally in the property that the spin has a finite [$(2j+1)$-dimensional] state space while the harmonic oscillator has an infinite dimensional state space. The two systems can only be identical to each other in the $j \to \infty$ limit so that the state spaces of both systems are both infinite dimensional. If both systems have the same dimension all that remains is to find the relations between the states and observables of each system. Below we consider $j = \frac{N}{2}$, the symmetric subspace of the spin system.

From equations (2.46) and (2.48) the $\hat{J}_\pm$ and $\hat{J}_z$ operators, restricted to the $j = \frac{N}{2}$ subspace, can be written as

$$\hat{J}_+ = \sum_{n=0}^{N} \sqrt{(n+1)(N-n)}\, |n+1\rangle_N \langle n|_N \,, \tag{2.93}$$

$$\hat{J}_- = \sum_{n=0}^{N} \sqrt{n(N-n+1)}\, |n-1\rangle_N \langle n|_N \,, \tag{2.94}$$

$$\hat{J}_z + \frac{N}{2} = \sum_{n=0}^{N} n\, |n\rangle_N \langle n|_N \,, \tag{2.95}$$

where we've shifted the label of the Dicke state $\left|\frac{N}{2}, m\right\rangle_N = \left|\frac{N}{2}, n - \frac{N}{2}\right\rangle_N$ and dropped the redundant $N/2$ labels: $\left|\frac{N}{2}, n - \frac{N}{2}\right\rangle_N \equiv |n\rangle_N$. Defining

$$\hat{a}_\uparrow = \sum_{n=0}^{N} \sqrt{n}\, |n-1\rangle_N \langle n|_N \,, \tag{2.96}$$

$$\hat{a}_\uparrow^\dagger = \sum_{n=0}^{N-1} \sqrt{n+1}\, |n+1\rangle_N \langle n|_N \,, \tag{2.97}$$

allows us to rewrite equations (2.93), (2.94) and (2.95) as

$$\frac{\hat{J}_+}{\sqrt{N}} = \hat{a}_\uparrow^\dagger \sqrt{1 - \frac{\hat{a}_\uparrow^\dagger \hat{a}_\uparrow}{N}}, \tag{2.98}$$

$$\frac{\hat{J}_-}{\sqrt{N}} = \sqrt{1 - \frac{\hat{a}_\uparrow^\dagger \hat{a}_\uparrow}{N}}\, \hat{a}_\uparrow, \tag{2.99}$$

$$\hat{J}_z = \hat{a}_\uparrow^\dagger \hat{a}_\uparrow - \frac{N}{2}. \tag{2.100}$$

These are known as the *Holstein-Primakoff transformations* [Holstein & Primakoff (1940)]. Taking the $N \to \infty$ limit gives:

$$\lim_{N\to\infty} \frac{\hat{J}_+}{\sqrt{N}} = \lim_{N\to\infty} \hat{a}_\uparrow^\dagger = \hat{a}^\dagger, \tag{2.101}$$

$$\lim_{N\to\infty} \frac{\hat{J}_-}{\sqrt{N}} = \lim_{N\to\infty} \hat{a}_\uparrow = \hat{a}, \tag{2.102}$$

$$\lim_{N\to\infty} \left(\hat{J}_z + \frac{N}{2}\right) = \lim_{N\to\infty} \hat{a}_\uparrow^\dagger \hat{a}_\uparrow = \hat{a}^\dagger \hat{a}. \tag{2.103}$$

The right hand sides of equations (2.101), (2.102), (2.103) of are exactly the harmonic oscillator creation, annihilation, and number operators respectively. These operators obey the bosonic commutation relation $\left[\hat{a}, \hat{a}^\dagger\right] = 1$. When N is finite, however, we have

$$\left[\frac{\hat{J}_-}{\sqrt{N}}, \frac{\hat{J}_+}{\sqrt{N}}\right] = \hat{\mathbb{I}} - \frac{2\,\hat{a}_\uparrow^\dagger \hat{a}_\uparrow}{N}. \tag{2.104}$$

If we want $\left[\frac{\hat{J}_-}{\sqrt{N}}, \frac{\hat{J}_+}{\sqrt{N}}\right] \approx \hat{\mathbb{I}}$ we need the $\frac{\hat{a}_\uparrow^\dagger \hat{a}_\uparrow}{N}$ to be negligible. The operator $\hat{a}_\uparrow^\dagger \hat{a}_\uparrow$ was defined in equation (2.56). It counts the number of spins up in the N spin state. Roughly speaking, $\frac{\hat{a}_\uparrow^\dagger \hat{a}_\uparrow}{N}$ is negligible if the number of spins up in the N spin system is small compared to N. We remind the reader that we have restricted to the $j = N/2$ symmetric subspace here. More generally the condition is that $\frac{\hat{a}_\uparrow^\dagger \hat{a}_\uparrow}{j}$ should be negligible in each j subspace. If j is a small number, then this is a difficult condition to satisfy.

Another interesting aspect of the similarity between these systems is that the spin coherent state can reduce to the coherent state in the $N \to \infty$ [Arecchi

et al. (1972); Radcliffe (1971)]. To see this we first scale the spin coherent state parameter $\zeta \to \zeta/\sqrt{N}$. The spin coherent state can then be written as

$$\begin{aligned}\left|\frac{\zeta}{\sqrt{N}}\right\rangle_N &= \sum_{n=0}^{N} \frac{1}{\left(1+\frac{|\zeta|^2}{N}\right)^{N/2}} \sqrt{\binom{N}{n}} \left(\frac{\zeta}{\sqrt{N}}\right)^n |n\rangle_N \\ &= \sum_{n=0}^{N} \left[\binom{N}{n}(1-p)^{N-n}p^n\right]^{1/2} e^{-i\phi n} |n\rangle_N ,\end{aligned}$$

where $p \equiv \frac{|\zeta|^2/N}{1+|\zeta|^2/N}$. The term in the square brackets is the binomial distribution. The *Poisson Limit Theorem* [Papoulis & Pillai (2002)] says that under certain conditions the binomial distribution tends to a Poissonian distribution in the $N \to \infty$ limit. More precisely, if $N \to \infty$ and $p \to 0$ such that $Np \to \lambda$, then $\binom{N}{n}(1-p)^{N-n}p^n \to e^{-\lambda}\frac{\lambda^n}{n!}$ in this limit. For our $p = \frac{|\zeta|^2/N}{1+|\zeta|^2/N}$, it is clear that when $N \to \infty$ we have $p \to 0$ and $Np \to |\zeta|^2$, as required, so that

$$\lim_{N\to\infty}\left|\frac{\zeta}{\sqrt{N}}\right\rangle_N = \sum_{n=0}^{\infty}\left[e^{-|\zeta|^2}\frac{|\zeta|^{2n}}{n!}\right]^{1/2} e^{-i\phi n}|n\rangle \tag{2.105}$$

$$= e^{-|\zeta|^2/2}\sum_{n=0}^{\infty}\frac{\zeta^n}{\sqrt{n!}}|n\rangle \tag{2.106}$$

$$= |\zeta\rangle . \tag{2.107}$$

In the last line we have dropped the N subscript in the state $|\zeta\rangle_N$ to indicate that this is a coherent state of the harmonic oscillator with complex amplitude ζ rather than a spin coherent state of the N spin system. We have also identified the Dicke state $\lim_{N\to\infty}|n\rangle_N$ with the Fock state $|n\rangle$. When N is finite the spin coherent state $\left|\frac{\zeta}{\sqrt{N}}\right\rangle_N$ is well approximated by the coherent state $|\zeta\rangle$ when $|\zeta| \ll \sqrt{N}$, as illustrated in figure 2.16.

There is no unique way to get the coherent state as a limit of the spin coherent state. For example, instead of transforming $\zeta \to \zeta/\sqrt{N}$ and taking $N \to \infty$, we could have started by writing the spin coherent state in spherical coordinates as a rotation of the reference state $|\downarrow\rangle^{\otimes N}$:

$$|\theta,\phi\rangle_N = e^{\tau\hat{J}_+ - \tau^*\hat{J}_-}|\downarrow\rangle^{\otimes N} , \tag{2.108}$$

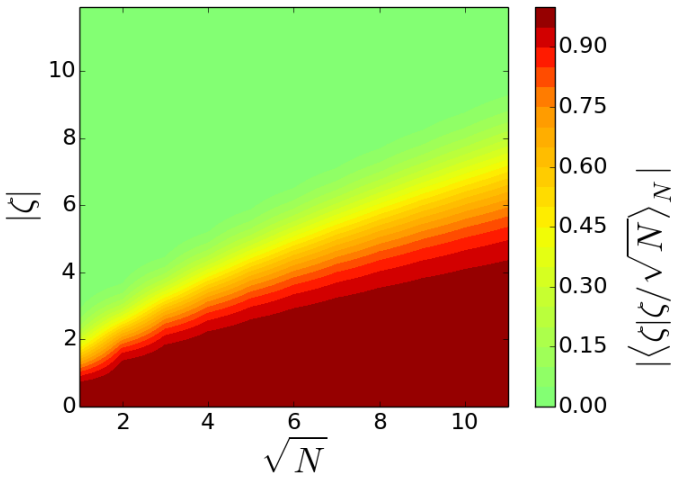

Figure 2.16: (colour online). The fidelity of the spin coherent state $\left|\frac{\zeta}{\sqrt{N}}\right\rangle_N$ against the oscillator coherent state $|\zeta\rangle$. When $|\zeta| \ll \sqrt{N}$ the fidelity is close to unity.

where $\tau = \frac{\theta}{2}e^{-i\phi}$ [see equation (2.60)]. In this case, transforming $\theta \to \theta/\sqrt{N}$ and taking $N \to \infty$ gives the bosonic coherent state as a result of (2.101) and (2.102), i.e.,

$$\lim_{N\to\infty}\left|\frac{\theta}{\sqrt{N}},\phi\right\rangle_N = \lim_{N\to\infty} e^{(\tau\hat{J}_+ - \tau^*\hat{J}_-)/\sqrt{N}}\,|\downarrow\rangle^{\otimes N} = e^{\tau\hat{a}^\dagger - \tau^*\hat{a}}\,|0\rangle = |\tau\rangle\,, \qquad (2.109)$$

where in the second equality we have identified the state $|\downarrow\rangle^{\otimes N}$ with the vacuum $|0\rangle$ of the harmonic oscillator.

Finally, we finally mention an alternative correspondence between the two systems. The ground state $|0\rangle$ of the harmonic oscillator is defined by the property $\hat{a}\,|0\rangle = 0$. In our discussion above, the corresponding ground state for the spin system is $|\downarrow\rangle^{\otimes N}$ with $\hat{J}_-\,|\downarrow\rangle^{\otimes N} = 0$, but we also have a "roof state" $|\uparrow\rangle^{\otimes N}$ with the property $\hat{J}_+\,|\uparrow\rangle^{\otimes N} = 0$. Instead of $\hat{a}_\uparrow$ and $\hat{a}_\uparrow^\dagger$ we could have defined the raising and lowering operators

$$\hat{a}_{\downarrow} = \sum_{n=0}^{N} \sqrt{N-n}\, |n+1\rangle_N \langle n|_N \,, \tag{2.110}$$

$$\hat{a}_{\downarrow}^{\dagger} = \sum_{n=1}^{N} \sqrt{N-n+1}\, |n-1\rangle_N \langle n|_N \,. \tag{2.111}$$

Taking the $N \to \infty$ limit of these operators gives an alternative bosonic limit with the state $|\uparrow\rangle^{\otimes N}$ corresponding to the harmonic oscillator ground state.

Chapter 3

Motivation: Quantum Metrology

Quantum metrology – one aspect of the emerging field of quantum technologies – is the study of making very precise measurement of certain physical parameters by exploiting non-classical states [e.g., Giovannetti *et al.* (2004, 2011); Lee *et al.* (2002)]. In this chapter we discuss quantum metrology, focussing on the example of estimating an unknown magnetic field with an N spin system. We start, in section 3.1, with the problem of estimating the magnetic field using a spin coherent state, a "classical" state. Then, in section 3.2, we show that using non-classical states can give a significant improvement in measurement precision. In section 3.3 we discuss the ultimate limit to the precision of a magnetic field measurement. Finally, in the last section, 3.4, we consider the problem of estimating an unknown magnetic field for which the direction is also unknown, a problem that – to our knowledge – has not been studied for an N spin system.

3.1 The standard quantum limit

Suppose that we have N identical copies of a spin-1/2 particle, each in the arbitrary pure state

$$|\zeta\rangle = \frac{|\downarrow\rangle + \zeta\,|\uparrow\rangle}{\sqrt{1+|\zeta|^2}}, \tag{3.1}$$

with an *unknown* value of ζ. In other words, we have a spin coherent state

$$|\zeta\rangle_N = \left(\frac{|\downarrow\rangle + \zeta\,|\uparrow\rangle}{\sqrt{1+|\zeta|^2}}\right)^{\otimes N}. \tag{3.2}$$

As discussed at the end of section 2.2.1, such states of the N spin system are easily prepared, in principle. We would like to estimate the probability $p = \frac{|\zeta|^2}{1+|\zeta|^2}$ that a spin is up, assuming that we are constrained to measurements of each individual spin in the $\hat{\sigma}_z = |\uparrow\rangle\langle\uparrow| - |\downarrow\rangle\langle\downarrow|$ basis. To find our estimate p^{est} we perform the measurement of the z-component of the spin on each of the N copies and – given that we get outcome "up" r times – say that:

$$p^{est} = \text{frequency of outcome "up"} = \frac{r}{N}. \tag{3.3}$$

We estimate the probability by the frequency of outcomes.

If $N = 1$, we find that either the spin is up in which case we estimate $p^{est} = 1$, or that the spin is down from which we estimate $p^{est} = 0$. Clearly, with a single spin we can't say much about the value of p. We must do the measurement on more spins to improve our estimate. For $N = 2$, our measurement of the state

$$|\zeta\rangle_2 = \left(\frac{|\downarrow\rangle + \zeta\,|\uparrow\rangle}{\sqrt{1+|\zeta|^2}}\right)^{\otimes 2}, \tag{3.4}$$

is represented by the observable

$$\hat{M}_2 \equiv |\uparrow\uparrow\rangle\langle\uparrow\uparrow| + \frac{1}{2}|\uparrow\downarrow\rangle\langle\uparrow\downarrow| + \frac{1}{2}|\downarrow\uparrow\rangle\langle\downarrow\uparrow| + 0\,|\downarrow\downarrow\rangle\langle\downarrow\downarrow| \tag{3.5}$$

$$= \frac{1}{4}\left(2\mathbb{I}_4 + \hat{\sigma}_z \otimes \mathbb{I}_2 + \mathbb{I}_2 \otimes \hat{\sigma}_z\right). \tag{3.6}$$

The eigenstates of $\hat{M}_2$ are the possible outcomes of the measurement, and the corresponding eigenvalues are the estimates p^{est} attached to that outcome, i.e., the relative frequencies r/N of outcome "up" . With probability p^2 we'll get "up" twice and estimate $p^{est} = 1$. With probability $(1-p)^2$ we'll get "down" twice and estimate $p^{est} = 0$. With probability $2p(1-p)$ we'll get "up" once and "down" once and we'll say that $p^{est} = 1/2$. Again, we cannot be very confident in our

estimate: our expected result (the weighted average over all possible measurement outcomes) is $\langle p^{est} \rangle = \left\langle \hat{M}_2 \right\rangle = p^2 + p(1-p) = p$ but with standard deviation

$$\delta p^{est} \equiv \sqrt{\langle (p^{est} - \langle p^{est} \rangle)^2 \rangle} = \sqrt{\mathrm{Var} \hat{M}_2} = \sqrt{p(1-p)/2}. \tag{3.7}$$

In general, this standard deviation is relatively large. For $p = 0.5$, for example, $\delta p^{est} = 1/2\sqrt{2} \approx 0.35$.

More generally, performing the measurement on N spins, we measure the spin coherent state

$$|\zeta\rangle_N = \left(\frac{|\downarrow\rangle + \zeta |\uparrow\rangle}{\sqrt{1 + |\zeta|^2}} \right)^{\otimes N}, \tag{3.8}$$

with measurement observable

$$\hat{M}_N = \sum_{r=0}^{N} \frac{r}{N} \hat{P}_r, \tag{3.9}$$

(the eigenvalues of $\hat{M}_N$ are $\frac{r}{N}$, the relative frequencies) where the projectors $\hat{P}_r$ are defined as

$$\hat{P}_r = \sum_{perms} |\uparrow\rangle \langle\uparrow|^{\otimes r} \otimes |\downarrow\rangle \langle\downarrow|^{\otimes (N-r)}. \tag{3.10}$$

The probability of finding that a fraction $\frac{r}{N}$ of the spins are "up" is the expectation value of the projector $\hat{P}_r$:

$$\langle P_r \rangle = \binom{N}{r} p^r (1-p)^{N-r}. \tag{3.11}$$

This is the binomial coefficient. If N is big and if p is not too close to zero (or not too close to unity) we can approximate the binomial distribution (3.11) as a Gaussian [Hunter *et al.* (1978)]:

$$\langle P_r \rangle = \binom{N}{r} p^r \, (1-p)^{N-r} \tag{3.12}$$

$$\overset{N\gg 1}{\approx} \frac{1}{\sqrt{2\pi N p(1-p)}} \exp\left[-\frac{(r-Np)^2}{2Np(1-p)}\right] \tag{3.13}$$

$$= \frac{1}{\sqrt{2\pi N p(1-p)}} \exp\left[-\frac{N\left(\frac{r}{N}-p\right)^2}{2p(1-p)}\right]. \tag{3.14}$$

From the last expression (3.14) we can see that the probability of obtaining the outcome corresponding to $p^{est} = r/N$ is small unless $r/N \approx p$.

The measurement observable $\hat{M}_N$ can be rewritten as

$$\hat{M}_N = \frac{1}{2N}\left(N + \sum_{i=1}^{N} \hat{\sigma}_z^{(i)}\right) = \frac{1}{2} + \frac{1}{N}\hat{J}_z, \tag{3.15}$$

so that our measurement is essentially a measurement of $\hat{J}_z$, the total z-component of spin of the combined system of N spins. The expectation value of our estimate (the average over all possible measurement outcomes) is

$$\left\langle p^{est} \right\rangle = \left\langle \hat{M}_N \right\rangle = p, \tag{3.16}$$

so that, on average, our estimate gives the actual value of p. The standard deviation

$$\delta p^{est} = \sqrt{\langle (p^{est} - \langle p^{est} \rangle)^2 \rangle} = \sqrt{\mathrm{Var}\hat{M}_N} = \sqrt{\frac{p(1-p)}{N}}, \tag{3.17}$$

is proportional to $N^{-1/2}$, so using more spins in our ensemble decreases the uncertainty in our estimate of p. This $N^{-1/2}$ scaling is known as the *standard quantum limit* [Giovannetti *et al.* (2004, 2011); Lee *et al.* (2002)].

This type of procedure – estimating probabilities from relative frequencies of measurement outcomes – is very important in quantum physics. Also important is the situation where we are interested in estimating some parameter λ on which the probabilities depend. If we know how $p(\lambda)$ depends on the *unknown* parameter λ then we can estimate this parameter as

$$\lambda^{est} = \lambda(p^{est}). \tag{3.18}$$

To find the uncertainty in the estimate we expand $p(\lambda)$ around $\langle p^{est}\rangle$:

$$p(\lambda) = \langle p^{est}\rangle + \frac{dp}{d\lambda}\Big|_{p=\langle p^{est}\rangle} \left(\lambda - \langle \lambda^{est}\rangle\right) + ... \tag{3.19}$$

Rearranging, and taking the root-mean-square of both sides gives

$$\sqrt{\langle (\lambda - \langle \lambda^{est}\rangle)^2\rangle} = \frac{\sqrt{\langle (p - \langle p^{est}\rangle)^2\rangle}}{|d\,\langle p^{est}\rangle\,/d\lambda|}. \tag{3.20}$$

Substituting equation (3.18) into equation (3.20) and defining

$$\delta\lambda^{est} = \sqrt{\langle (\lambda^{est} - \langle \lambda^{est}\rangle)^2\rangle}, \tag{3.21}$$

then gives the 'propagation of error' formula:

$$\delta\lambda^{est} = \frac{\delta\, p^{est}}{|d\,\langle p^{est}\rangle\,/d\lambda|}. \tag{3.22}$$

For example, we may want to estimate $|\zeta|$ rather than $p = \frac{|\zeta|^2}{1+|\zeta|^2}$ in the state (3.2). This function $p(|\zeta|)$ is plotted in figure 3.1. In this case, our estimate for $|\zeta|$ is easily found from the expression for p. It is just

$$|\zeta|^{est} = \sqrt{\frac{p^{est}}{1 - p^{est}}}. \tag{3.23}$$

The average uncertainty in this estimate is found by equation (3.22) [see figure 3.1]:

$$\delta|\zeta|^{est} = \frac{\delta\, p^{est}}{|d\,\langle p^{est}\rangle\,/d|\zeta||} = \sqrt{\frac{p(1-p)}{N}}\frac{(1+|\zeta|^2)^2}{2|\zeta|} = \frac{1+|\zeta|^2}{2\sqrt{N}}. \tag{3.24}$$

Another, more interesting example, is when the probability p depends on some Hamiltonian parameter that we want to measure. For concreteness, consider the interaction of the N spin-1/2 particles with an *unknown* static magnetic field which we take to be in the y-direction, $\vec{B} = (0, B, 0)$. The Hamiltonian for the evolution of the spin system is $\hat{H} = -\gamma B \hat{J}_y$, where γ is the gyromagnetic ratio of our spins. We would like to estimate the magnetic field B assuming that the values of γ and the evolution time t are known. In this example we take the initial state to be

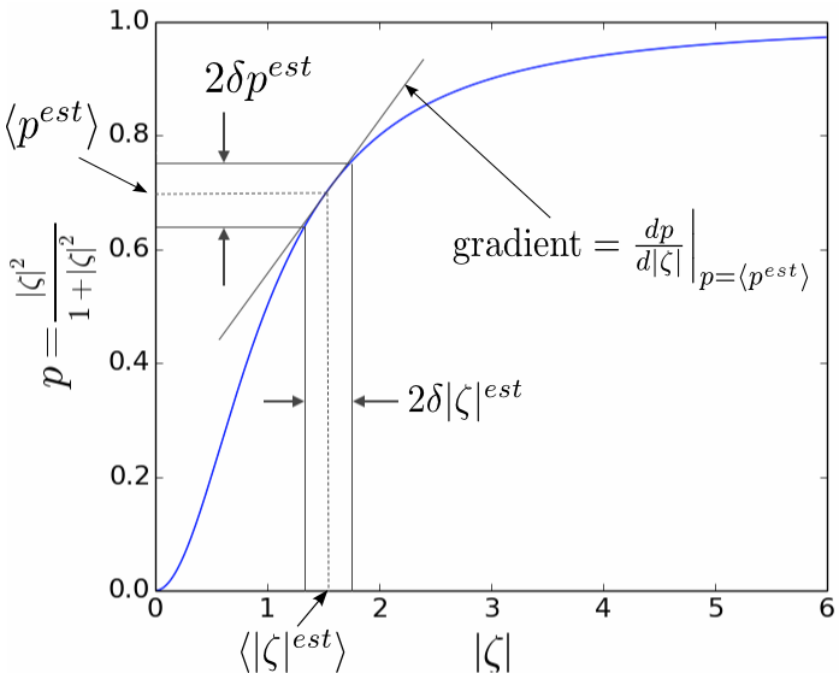

Figure 3.1: An illustration of the propagation of error formula. If the function $p(|\zeta|)$ is approximately linear in the range $\langle p^{est} \rangle \pm \delta p^{est}$, then the uncertainty $\delta|\zeta|^{est}$ is the uncertainty δp^{est}, divided by the gradient of $p(|\zeta|)$ at $p = \langle p^{est} \rangle$ [see equation (3.22)].

$$|\Psi(0)\rangle = |\rightarrow\rangle^{\otimes N} = \left(\frac{|\downarrow\rangle + |\uparrow\rangle}{\sqrt{2}}\right)^{\otimes N}, \tag{3.25}$$

an easily prepared spin coherent state (see section 2.2.1). This evolves after a time t to the state

$$|\Psi(t)\rangle = \left[\frac{\left(\cos\frac{\gamma tB}{2} - \sin\frac{\gamma tB}{2}\right)|\downarrow\rangle + \left(\cos\frac{\gamma tB}{2} + \sin\frac{\gamma tB}{2}\right)|\uparrow\rangle}{2}\right]^{\otimes N}. \tag{3.26}$$

The probability that a spin is up is

$$p = \frac{1 + \sin\gamma tB}{2}. \tag{3.27}$$

We obtain an estimate p^{est} of this probability by measuring the observable $\hat{M}_N$ for which the expectation value is $\langle p^{est}\rangle = \left\langle \hat{M}_N \right\rangle = p$ with standard deviation $\delta p^{est} = \sqrt{\mathrm{Var}\hat{M}_N} = \sqrt{\frac{p(1-p)}{N}}$. By the propagation of error formula (3.22) we find that the error in our estimate of the magnetic field B is

$$\delta B^{est} = \frac{1}{\gamma t\sqrt{N}}. \tag{3.28}$$

In the procedure above we have considered N identical measurements on an ensemble of N independent (uncorrelated) spins. We note that we could equally have thought of this as N identical consecutive measurements on a single spin. We will find it useful to distinguish these two cases and for the rest of this chapter we use upper case N to refer to the number of spins in a spatial ensemble and lower case n to refer to the number of repeated experiments in time. Above, the ensemble of N spins interacts with the magnetic field for a time t before we make our measurement. Suppose that we repeat the procedure for a total amount of time T, giving $n = T/t$ repetitions. From the analysis above, we know that these independent repetitions of the experiment decrease the uncertainty by a factor of $n^{-1/2} = (T/t)^{-1/2}$ so that the uncertainty is modified to

$$\delta B^{est} = \frac{1}{\gamma\sqrt{NtT}}, \tag{3.29}$$

or,

$$\delta B^{est}\sqrt{T} = \frac{1}{\gamma\sqrt{Nt}}. \tag{3.30}$$

Since the quantity on the left hand side of equation (3.30) has units of

$$\text{magnetic field} \times \sqrt{\text{time}}, \tag{3.31}$$

precision of magnetic field measurements is often quoted in units of $\mathrm{T}/\sqrt{\mathrm{Hz}}$ (Tesla per root Hertz).

From equation (3.28) we see the $N^{-1/2}$ standard quantum limit scaling: the precision is increased by increasing the number of spins in our ensemble. The precision of our estimate is also better for bigger values of the gyromagnetic ratio γ and for longer evolution time t. This is reasonable because for larger values of γ the spin is more strongly coupled to the magnetic field and as the evolution time increases, a small difference between two nearby values of magnetic field is accentuated. However, we have not included the effects of decoherence in the above analysis. If this is included, the interaction time t cannot be arbitrarily large, since information about the magnetic field contained in the state of the spin system will be lost to decoherence. There is, it turns out, an optimal exposure time t as discussed by Chin *et al.* (2012); Huelga *et al.* (1997); Jones *et al.* (2009); Matsuzaki *et al.* (2011). This optimal time finds the right balance between the benefit of a long sensing time and the destructive effects of decoherence as the system evolves.

3.2 A quantum advantage

The problem of estimating the probability p in the previous section was "classical" in the sense that it is the same for N identical and independent measurements of any binary probabilistic event. For example, the above analysis would be the same if we were trying to estimate the probability p of obtaining "heads" in N coin tosses (or trying to estimate a parameter λ on which that probability depends). The error is a result of the statistics of identical, independent events. It is possible, however, to improve the precision beyond the standard quantum limit $N^{-1/2}$ scaling. This is achieved by preparing an initial state with quantum

correlations between the spins so that they are *no longer independent* of each other. Below – staying with the problem of estimating a magnetic field B – we give some examples of states that give a "quantum advantage".

Spin squeezed states

Again, we have N spin-1/2 particles in an unknown static magnetic field $\vec{B} = (0, B, 0)$ so that the spins evolve by the Hamiltonian $\hat{H} = -\gamma B \hat{J}_y$. We would like to estimate B by a measurement of each spin in the $\hat{\sigma}_z$ basis. As mentioned in the previous section, this is essentially a measurement of the collective spin operator $\hat{J}_z$. In the Heisenberg picture, the operator $\hat{J}_z$ evolves to

$$\hat{J}_z(t) = \hat{J}_z \cos \gamma B t + \hat{J}_x \sin \gamma B t. \tag{3.32}$$

A measurement of this operator at time t thus has expectation value

$$\left\langle \hat{J}_z(t) \right\rangle = \left\langle \hat{J}_z \right\rangle \cos \gamma B t + \left\langle \hat{J}_x \right\rangle \sin \gamma B t, \tag{3.33}$$

and variance

$$\begin{aligned} \mathrm{Var}(\hat{J}_z(t)) &= \mathrm{Var}(\hat{J}_z) \cos^2(\gamma B t) + \mathrm{Var}(\hat{J}_x) \sin^2(\gamma B t) \\ &\quad + 2 \,\mathrm{Cov}(\hat{J}_x, \hat{J}_z) \cos(\gamma B t) \sin(\gamma B t), \end{aligned} \tag{3.34}$$

where

$$\mathrm{Cov}(\hat{J}_x, \hat{J}_z) = \left\langle \frac{\hat{J}_x \hat{J}_z + \hat{J}_z \hat{J}_x}{2} \right\rangle - \left\langle \hat{J}_x \right\rangle \left\langle \hat{J}_z \right\rangle, \tag{3.35}$$

is the *covariance* of $\hat{J}_x$ and $\hat{J}_z$. By the propagation of error formula (3.22), the expected error in our estimate for B is

$$\delta B^{est} = \frac{\sqrt{\mathrm{Var} \hat{J}_z(t)}}{\left| d \left\langle \hat{J}_z(t) \right\rangle / d\, B \right|} \tag{3.36}$$

$$= \frac{\sqrt{\mathrm{Var}(\hat{J}_z) \cos^2(\gamma B t) + \mathrm{Var}(\hat{J}_x) \sin^2(\gamma B t) + 2 \,\mathrm{Cov}(\hat{J}_x, \hat{J}_z) \cos(\gamma B t) \sin(\gamma B t)}}{\left| -\gamma t \left\langle \hat{J}_z \right\rangle \sin(\gamma B t) + \gamma t \left\langle \hat{J}_x \right\rangle \cos(\gamma B t) \right|}. \tag{3.37}$$

For simplicity, we assume that $\gamma Bt \ll 1$ so that $\cos(\gamma Bt) \approx 1$ and $\sin(\gamma Bt) \approx 0$. This is a reasonable approximation because we are often interested in estimating small magnetic fields B. In this case we find [Ma *et al.* (2011); Wineland *et al.* (1994)]:

$$\delta B^{est} = \frac{\sqrt{\mathrm{Var}\hat{J}_z}}{\gamma t \left|\left\langle \hat{J}_x \right\rangle\right|}. \tag{3.38}$$

If we can keep $\left|\left\langle \hat{J}_x \right\rangle\right|$ close to its maximum value while $\mathrm{Var}\hat{J}_z$ is decreased, the precision is improved. This is essentially what spin squeezing gives us: $\left|\left\langle \hat{J}_x \right\rangle\right|$ takes its maximum value for the spin coherent state $|{\rightarrow}\rangle^{\otimes N}$ or for the spin coherent state $|{\leftarrow}\rangle^{\otimes N}$, and a spin squeezed state can have a similar value of $\left|\left\langle \hat{J}_x \right\rangle\right|$ but with a variance $\mathrm{Var}\hat{J}_z$ that is less than that of a spin coherent state.

If instead the state of the spin system has its mean spin in an arbitrary direction $\vec{r}_m = \mathrm{Tr}\left[\rho\vec{\hat{J}}\right] / \left|\left\langle \vec{\hat{J}} \right\rangle\right|$ (where $\left|\left\langle \vec{\hat{J}} \right\rangle\right|$ is the length of the mean spin vector) and the measurement of a collective spin operator $\hat{J}_{\vec{r}_m^{\perp}}$ is in some orthogonal direction $\vec{r}_m^{\perp}$, and the magnetic field $\vec{B}$ in a direction orthogonal to both $\vec{r}_m$ and $\vec{r}_m^{\perp}$, then the same analysis can be applied. To find the best precision we minimise over all possible measurement directions $\vec{r}_m^{\perp}$, which gives:

$$\delta|\vec{B}|^{est} = \frac{\min_{\vec{r}_m^{\perp}} \sqrt{\mathrm{Var}\hat{J}_{\vec{r}_m^{\perp}}}}{\gamma t \left|\left\langle \vec{\hat{J}} \right\rangle\right|}. \tag{3.39}$$

For a spin coherent state, we have

$$\delta|\vec{B}|^{est}_{\mathrm{scs}} = \frac{1}{\gamma t\sqrt{N}}. \tag{3.40}$$

Based on the above arguments, Wineland *et al.* (1994) introduced an operational measure of spin squeezing: For a state ρ of a spin system, their spin squeezing parameter, χ_R^2, is the ratio of the precision (3.39) that can be achieved with the state ρ, to the precision (3.40) that can be obtained with a spin coherent state:

$$\chi_R^2 = \left(\frac{\delta|\vec{B}|^{est}}{\delta|\vec{B}|^{est}_{\text{scs}}}\right)^2 = \frac{N \min_{\vec{r}_m^\perp} \text{Var}\hat{J}_{\vec{r}_m^\perp}}{\left|\left\langle \hat{\vec{J}} \right\rangle\right|^2}. \tag{3.41}$$

This quantifies the amount of spin squeezing in the state that is useful in the magnetic field sensing protocol described above. The subscript R indicates that this quantity was derived by Wineland *et al.* (1994) in the context of Ramsey interferometry. It is convenient to write equation (3.39) in terms of this squeezing parameter:

$$\delta|\vec{B}|^{est} = \frac{\chi_R}{\gamma t\sqrt{N}}. \tag{3.42}$$

By comparing equation (3.42) and equation (3.40), it is clear that the precision of the magnetic field measurement can be improved by a factor of χ_R by squeezing the initial state.

The Wineland *et al.* (1994) squeezing parameter χ_R^2 is related to the Kitagawa & Ueda (1993) squeezing parameter χ_s^2 that was mentioned in section 2.2.3 [Ma *et al.* (2011)]:

$$\chi_R^2 = \left(\frac{N/2}{\left|\left\langle \vec{J} \right\rangle\right|}\right)^2 \chi_s^2. \tag{3.43}$$

We note we always have $\left|\left\langle \vec{J} \right\rangle\right| \leq N/2$ so that $\chi_s^2 \leq \chi_R^2$. Both spin squeezing parameters give the same value, $\chi_R^2 = \chi_s^2 = 1$, for spin coherent states (since $\left|\left\langle \vec{J} \right\rangle\right| = N/2$), but it is possible to have $\chi_s^2 < 1$ and $\chi_R^2 > 1$. This indicates that some spin squeezed states do not give an improvement in precision in the magnetic field sensing protocol described above.

GHZ states

In the previous examples we have restricted our measurement of the spin system to a measurement of collective spin operator $\hat{J}_z$ (or of a rotated spin operator $\hat{J}_{\vec{r}^\perp}$). What if we allow ourselves the freedom to perform any measurement? What other states can give better precision in estimating the magnetic field?

Consider the initial state

$$|\Psi(0)\rangle = |GHZ^y_+\rangle_N = \frac{1}{\sqrt{2}}\left(|\boxtimes\rangle^{\otimes N} + |\odot\rangle^{\otimes N}\right), \tag{3.44}$$

a GHZ state in the y-direction. We plotted its spin Wigner function in figure 2.13. Intuitively, this state can be used to estimate a magnetic field more precisely than a spin coherent state because the interference fringes in this spin Wigner plot have a finer structure than the coherent state 'blobs'. This means that a smaller rotation of the whole state can be detected by some measurement that can distinguish states with rotated interference fringes [Toscano *et al.* (2006)]. After interacting with the magnetic field $\vec{B} = (0, B, 0)$ for a time t the state of the spin system is

$$|\Psi(t)\rangle = \frac{1}{\sqrt{2}}\left(e^{it\gamma BN/2}|\boxtimes\rangle^{\otimes N} + e^{-it\gamma BN/2}|\odot\rangle^{\otimes N}\right). \tag{3.45}$$

We notice that the phase that is accumulated has a factor of N compared to the separable state case, equation (3.26). We also notice that for any interaction time, t, the state $|\Psi(t)\rangle$ is in the two dimensional subspace spanned by the states $|\boxtimes\rangle^{\otimes N}$ and $|\odot\rangle^{\otimes N}$. In fact, it evolves in a path around the equator of the Bloch sphere whose north and south poles are the states $|\otimes\rangle^{\otimes N}$ and $|\odot\rangle^{\otimes N}$. With this evolution the state oscillates between the orthonormal states $|GHZ^y_+\rangle_N = \frac{1}{\sqrt{2}}\left(|\boxtimes\rangle^{\otimes N} + |\odot\rangle^{\otimes N}\right)$ and $|GHZ^y_-\rangle_N = \frac{1}{\sqrt{2}}\left(|\boxtimes\rangle^{\otimes N} - |\odot\rangle^{\otimes N}\right)$. In terms of the spin Wigner function, this evolution only changes the interference fringes. The projector onto the initial state:

$$\hat{M}_{GHZ} = |GHZ^y_+\rangle_N \langle GHZ^y_+|_N, \tag{3.46}$$

is an appropriate measurement observable [Huelga *et al.* (1997)]. Roughly speaking, this measurement checks for rotation of the interference fringes from the initial state $|GHZ^y_+\rangle_N$ of the N spin system.

It is difficult to implement such an N spin measurement in practice. Since the evolving state of the spin system is in a two-dimensional subspace of the whole 2^N dimensional state space, however, we can, in principle, map the N spin state onto a single qubit over which we may have more control [Huelga *et al.* (1997)].

The expectation value of this measurement is $\left\langle \hat{M}_{GHZ} \right\rangle = \frac{1+\cos(t\gamma BN)}{2}$ and its standard deviation is $\sqrt{\mathrm{Var}\hat{M}_{GHZ}} = \frac{1}{2}\left|\sin(t\gamma BN)\right|$. The precision of our estimate of B is thus

$$\delta B^{est} = \frac{\sqrt{\mathrm{Var}\hat{M}_{GHZ}}}{\left| d\left\langle \hat{M}_{GHZ} \right\rangle / d\, B \right|} = \frac{1}{t\gamma N}. \tag{3.47}$$

Although there are N spins in our ensemble there are just two outcomes in the measurement of the observable $\hat{M}_{GHZ}$ on our N spin system: either we find that the N spin system is in the state $\left|GHZ_{+}^{y}\right\rangle_{N}$, or it is not. Just as the outcome of a single coin toss can not tell us anything about whether the coin is fair or biased, the outcome of a single measurement of $\hat{M}_{GHZ}$ does not give enough information to estimate the magnetic field B[1]. We must repeat the measurement. Suppose that we repeat for a total amount of time T, giving $n = T/t$ repetitions. This decreases the uncertainty by a factor of $n^{-1/2}$ so that equation (3.47) is modified to

$$\delta B^{est}\sqrt{T} = \frac{1}{\gamma N\sqrt{t}}. \tag{3.48}$$

The N^{-1} scaling in this precision is known as the *Heisenberg limit* and is a factor of $N^{-1/2}$ smaller than in the example of the uncorrelated particles in equation (3.30). We will see in the next section that for the problem of estimating a magnetic field, this is the ultimate limit to precision scaling.

To convey the potential of quantum metrology at the Heisenberg limit, we suppose, for example, that we want measure the magnetic field with system of 10^6 spins. If it takes each run $t = 90$ seconds to achieve a given level of precision δB_y^{est} at the Heisenberg limit (3.47), then it takes $1000\,t \approx 1$ day to achieve the same level of precision at the standard quantum limit (3.28) [Gross (2010)].

[1]The standard deviation of a single measurement is $\sqrt{\mathrm{Var}\hat{M}_{GHZ}} = \frac{1}{2}\left|\sin(t\gamma BN)\right| = \sqrt{\langle M_{GHZ}\rangle\left(1-\langle M_{GHZ}\rangle\right)}$.

3.3 Ultimate limits to precision

In the previous section we saw that by correlating the N spins we can beat the standard quantum limit precision scaling. A natural question to ask is: what is the best possible precision for our estimate of the magnetic field? In this section we see that the ultimate limit to precision is given by the *quantum Cramer-Rao lower bound*, which depends on a quantity known as the *quantum Fisher information* [Paris (2009); Wiseman & Milburn (2010)].

Again, we suppose that initial state $\rho(0)$ evolves by the Hamiltonian $\hat{H} = -\gamma B \hat{J}_y$ and that we want to estimate B. Usually we think of the evolving state as:

$$\rho(t) = e^{it\gamma B\hat{J}_y}\rho(0)e^{-it\gamma B\hat{J}_y}, \tag{3.49}$$

parameterised by the time t for a fixed value of the magnetic field B. However, since the unknown magnetic field B is the parameter that we are trying to estimate, we instead view this as:

$$\rho(B) = e^{it\gamma B\hat{J}_y}\rho(0)e^{-it\gamma B\hat{J}_y}, \tag{3.50}$$

parameterised by B at some fixed value of time. In general, the dependence of ρ on B need not be of the form (3.50) but can be any arbitrary path $\rho(B)$ through the state space of the system.

A general measurement of the state $\rho(B)$ is a *positive-operator valued measure* (POVM) [Nielsen & Chuang (2000)]. A POVM is a set of positive operators $\{\hat{\mathcal{M}}_i\}$ whose sum is the identity operator on the state space of the system:

$$\sum_i \hat{\mathcal{M}}_i = \hat{\mathbb{I}}. \tag{3.51}$$

Each of the operators $\hat{\mathcal{M}}_i$ corresponds to a possible measurement outcome labelled by the index i that has a probability $p_i(B) = \mathrm{Tr}\left[\hat{\mathcal{M}}_i\,\rho(B)\right]$. Property (3.51) ensures that these probabilities add to unity. We assume that we repeat the measurements of the POVM $\{\hat{\mathcal{M}}_i\}$ n times. We label the result of the first measurement as x_1, the result of the second measurement as x_2, and so on, up

to the n'th measurement result x_n. Our full list of measurement results can then be written as a vector,

$$\hat{x} = (x_1, x_2, ..., x_n). \tag{3.52}$$

An *estimator* for the parameter B is a function $B^{est}(\vec{x})$ that takes the measurement results $\vec{x}$ as its input and gives an estimate for the magnetic field as output[1]. An estimator is called *unbiased* if

$$\sum_{\vec{x}} B^{est}(\vec{x}) p_{x_1}(B) p_{x_2}(B) ... p_{x_n}(B) = B, \tag{3.53}$$

that is, if on average it gives the actual value of the parameter we are trying to estimate.

To derive a lower bound for the precision of our measurement of B, we first take the derivative of both sides of equation (3.53) with respect to the parameter B, giving:

$$\sum_i B^{est} \frac{dp_i(B)}{dB} = 1. \tag{3.54}$$

Now, since

$$\sum_i p_i(B) = 1 \quad \Rightarrow \quad \sum_i \frac{dp_i(B)}{dB} = 0, \tag{3.55}$$

we have

$$B \sum_i \frac{dp_i(B)}{dB} = 0. \tag{3.56}$$

Subtracting equation (3.56) from equation (3.54) gives:

$$\sum_i \left(B^{est} - B\right) \frac{dp_i(B)}{dB} = 1. \tag{3.57}$$

We rewite this as

[1] For example, in equation (3.3) our estimator for the probability p was $p^{est} = \frac{r}{n}$, the relative frequency of obtaining the outcome "up" in n spin measurements. This is an example of an unbiased estimator.

$$\sum_i \left(B^{est} - B\right) \sqrt{p_i(B)} \frac{1}{\sqrt{p_i(B)}} \frac{dp_i(B)}{dB} = 1, \tag{3.58}$$

before applying the Cauchy-Schwartz inequality [Apostol (1969)] to obtain the *Cramer-Rao lower bound* [Cramér (1999)]:

$$1 \leq \left[\sum_i \left(B^{est} - B\right)^2 p_i(B)\right] \left[\sum_i \frac{1}{p_i(B)} \left(\frac{dp_i(B)}{dB}\right)^2\right]. \tag{3.59}$$

Defining the *(classical) Fisher information* as

$$F\left[\rho(B), \{\mathcal{M}_i\}\right] = \sum_i \frac{1}{p_i(B)} \left(\frac{dp_i(B)}{dB}\right)^2, \tag{3.60}$$

we can rewrite this as

$$\delta B^{est} \geq \frac{1}{\sqrt{F}}. \tag{3.61}$$

The Cramer-Rao lower bound tells us that the uncertainty in our estimate of B is bounded from below by $F^{-1/2}$.

The classical Fisher information (3.60) depends on the state $\rho(B)$ and also on the measurement POVM $\{\mathcal{M}_i\}$. Choosing a different POVM will, in general, give a different classical Fisher information and a different lower bound for the precision. The *quantum Fisher information* is the classical Fisher information maximised over all possible choices of POVM:

$$\mathcal{F}[\rho(B)] = \max_{\{\mathcal{M}_i\}} F\left[\rho(B), \{\mathcal{M}_i\}\right]. \tag{3.62}$$

The *quantum* Cramer-Rao lower bound is then:

$$\delta B^{est} \geq \frac{1}{\sqrt{\mathcal{F}}}. \tag{3.63}$$

This is the ultimate lower bound for the precision in our estimate of B.

Interestingly, despite the maximisation in (3.62), it is possible to write down useful formulas for the quantum Fisher information $\mathcal{F}$ for some special cases. For example, if the dependence of the parameter of interest, B on the state ρ is of the form:

$$\rho(B) = e^{-i\hat{G}B}\rho(0)e^{i\hat{G}B}, \tag{3.64}$$

for some Hermitian operator $\hat{G}$ (i.e., the parameter dependence is generated by a unitary transformation) then the quantum Fisher information can be written in a convenient form. Writing the operator $\hat{G}$ as a subscript for $\mathcal{F}$ in this case, we have [Paris (2009)]:

$$\mathcal{F}_{\hat{G}}\left[\rho(0)\right] = 2\sum_{i\neq j}\frac{(\alpha_i-\alpha_j)^2}{\alpha_i+\alpha_j}\left|\langle\phi_j|\,\hat{G}\,|\phi_i\rangle\right|^2, \tag{3.65}$$

where α_i and $|\phi_i\rangle$ are the eigenvalues and eigenstates of the initial density operator:

$$\rho(0) = \sum_i \alpha_i\,|\phi_i\rangle\,\langle\phi_i|\,. \tag{3.66}$$

We note that the quantum Fisher information (3.65) in this case is independent of B, the parameter of interest. It only depends on the initial state $\rho(0)$ and the operator $\hat{G}$ that generates the unitary transformation. It is known that for a mixed state $\rho(0)$ we have [Tóth & Petz (2013); Wiseman & Milburn (2010)],

$$\mathcal{F}_{\hat{G}}\left[\rho(0)\right] \leq 4\mathrm{Var}\left(\hat{G}\right) = 4\langle \mathrm{Tr}\left[\rho(0)\hat{G}^2\right] - \left(\mathrm{Tr}\left[\rho(0)\hat{G}\right]\right)^2\rangle. \tag{3.67}$$

If the initial state $\rho(0) = |\Psi(0)\rangle\,\langle\Psi(0)|$ is pure, then we have equality in (3.67):

$$\mathcal{F}_{\hat{G}}\left[|\Psi(0)\rangle\right] = 4\mathrm{Var}\left(\hat{G}\right). \tag{3.68}$$

In this case, the pure state that maximises the quantum Fisher information is the state that maximises the variance of the operator $\hat{G}$. This is

$$|\Psi\rangle = \frac{1}{\sqrt{2}}\left(|g_{min}\rangle + e^{i\phi}\,|g_{max}\rangle\right), \tag{3.69}$$

where $|g_{min}\rangle$ and $|g_{max}\rangle$ are the eigenstates of $\hat{G}$ associated with the minimum and maximum eigenvalues, respectively, and ϕ is an arbitrary phase. In equation (3.50) we see that the evolution of the spin system in the magnetic field $\vec{B} = (0, B, 0)$ leads to a state of the form (3.64), with $\hat{G} = t\gamma\hat{J}_y$. In this case, the GHZ state,

$$|GHZ^{y}_{\pm}\rangle_N = \frac{1}{\sqrt{2}}\left(|\boxtimes\rangle^{\otimes N} \pm |\odot\rangle^{\otimes N}\right), \tag{3.70}$$

gives the maximum possible value of the quantum Fisher information:

$$\mathcal{F}_{\hat{G}} = t^2\gamma^2N^2. \tag{3.71}$$

From the quantum Cramer-Rao bound, the Heisenberg limit for precision of our estimate of the magnetic field B is thus:

$$\delta B^{est} \geq \frac{1}{t\gamma N}. \tag{3.72}$$

In the derivation of the Cramer-Rao bound (3.63) above we defined the Fisher information without giving any explanation of its meaning. Below, following an argument by Wootters (1981), we give an interpretation of the Fisher information by relating it to the notion of *statistical distance*.

Statistical distance and Fisher information

To investigate the idea of statistical distance between quantum states, we first consider a POVM with just two elements $\mathcal{M}_0$ and $\mathcal{M}_1$ corresponding to two possible measurement outcomes, 0 and 1, say, with probabilities $p(B)$ and $1-p(B)$ respectively. In section 3.1 we saw that for n repetitions of such a measurement the probability of obtaining the outcome 0 a total of r times is a binomial distribution which, for $n \gg 1$, can be approximated as the Gaussian distribution [see equation (3.14)]:

$$\langle P_r\rangle \propto \exp\left[-\frac{n\left[\frac{r}{n}-p(B)\right]^2}{2p(B)[1-p(B)]}\right], \tag{3.73}$$

with average value $p(B)$ and standard deviation

$$\delta p(B) = \sqrt{\frac{p(B)[1-p(B)]}{n}}. \tag{3.74}$$

Two probability distributions $p(B')$ and $p(B'')$ are said to be *distinguishable in n measurements* if [Wootters (1981)]:

$$|p(B') - p(B'')| \geq \delta p(B') + \delta p(B''), \tag{3.75}$$

that is, if their regions of uncertainty do not overlap. The *(classical) statistical distance* between the two probability distributions is then defined as [Wootters (1981)]:

$$\mathcal{D}_{cl}[\rho(B'), \rho(B''), \{\mathcal{M}_i\}] = \lim_{n\to\infty} \frac{1}{\sqrt{n}} \times \Big[\text{maximum number of mutually distinguishable (in } n \text{ measurements) distributions between } p(B') \text{ and } p(B'')\Big]. \tag{3.76}$$

Taking the limit of an infinite number of measurements ($n \to \infty$) makes the statistical distance independent of the number of measurements n. Since the uncertainty (3.74) scales as $n^{-1/2}$, however, the factor of $n^{-1/2}$ in definition (3.76) is needed so that the statistical distance is finite in the $n \to \infty$ limit. The statistical distance (3.76) depends on the two states $\rho(B')$ and $\rho(B'')$ and on the POVM $\{\mathcal{M}_i\}$, but for simplicity, we write this as:

$$\mathcal{D}_{cl}[\rho(B'), \rho(B''), \{\mathcal{M}_i\}] \equiv \mathcal{D}_{cl}\left(B', B''\right). \tag{3.77}$$

Using equations (3.74) and (3.75) the statistical distance can be written more explicitly as

$$\mathcal{D}_{cl}\left(B', B''\right) = \int_{p(B')}^{p(B'')} \frac{d\,p(B)}{2\,\delta p(B)} \tag{3.78}$$

$$= \int_{p(B')}^{p(B'')} \frac{d\,p(B)}{2\sqrt{p(B)[1-p(B)]}} \tag{3.79}$$

$$= \int_{B'}^{B''} dB \frac{|d\,p(B)/dB|}{2\sqrt{p(B)[1-p(B)]}}, \tag{3.80}$$

where $dp(B) = p(B + dB) - p(B)$ and in the last line we have rewritten the integral in terms of the parameter B.

More generally, for a POVM with m outcomes the probability of obtaining r_i occurrences of the outcome $i \in \{1, 2, ..., m\}$ in n measurements is a multinomial

distribution, which for $n \gg 1$ can be approximated as a multivariate Gaussian distribution [Gut (2009)]:

$$\langle P_{r_1 r_2 \ldots r_m} \rangle \propto \exp\left[-\frac{n}{2} \sum_{i=1}^{m} \frac{\left[\frac{r_i}{n} - p_i(B)\right]^2}{p_i(B)} \right]. \tag{3.81}$$

(This probability is very small unless $r_i/n \approx p_i(B)$.) Again, following Wootters (1981), we define the *region of uncertainty* around the point $\vec{p} = (p_1, p_2, ..., p_n)$ in probability space to be the set of all points $\frac{\vec{r}}{n} = \left(\frac{r_1}{n}, \frac{r_2}{n}, ..., \frac{r_m}{n}\right)$ for which the exponent in (3.81) has absolute value less than $\frac{1}{2}$[1]. In other words, this is the set of all points $\frac{\vec{r}}{n} = \left(\frac{r_1}{n}, \frac{r_2}{n}, ..., \frac{r_n}{n}\right)$ for which

$$\sqrt{\frac{n}{2} \sum_{i=1}^{m} \frac{\left[\frac{r_i}{n} - p_i(B)\right]^2}{p_i(B)}} < \frac{1}{\sqrt{2}}. \tag{3.82}$$

The distributions

$$\vec{p}(B') = (p_1(B'), p_2(B'), ..., p_m(B')) \tag{3.83}$$

and

$$\vec{p}(B'') = (p_1(B''), p_2(B''), ..., p_m(B'')) \tag{3.84}$$

are then said to be *distinguishable in n measurements* if their regions of uncertainty do not overlap. As n increases and the regions of uncertainty shrink, this is the case if and only if:

$$\sqrt{\frac{n}{2} \sum_{i=1}^{m} \frac{(\delta p_i)^2}{p_i}} > \frac{1}{\sqrt{2}} + \frac{1}{\sqrt{2}}, \tag{3.85}$$

or,

$$\frac{\sqrt{n}}{2} \sqrt{\sum_{i=1}^{m} \frac{(\delta p_i)^2}{p_i}} > 1, \tag{3.86}$$

[1] Choosing $\frac{1}{2}$ here instead of some other number gives agreement with the previous example where $m = 2$.

where $\delta p_i = p_i(B'') - p_i(B')$. For this more general case, the statistical distance between the two probability distributions is defined as:

$$\mathcal{D}_{cl}\left(B', B''\right) = \lim_{n\to\infty} \frac{1}{\sqrt{n}} \times \Big[\text{maximum number of mutually distinguishable (in } n \text{ measurements) distributions between } \vec{p}(B') \text{ and } \vec{p}(B'') \text{ along the path in probability space parameterised by } B\Big]. \tag{3.87}$$

From equation (3.86), this can be written more explicitly as

$$\mathcal{D}_{cl}\left(B', B''\right) = \int_{\vec{p}(B')}^{\vec{p}(B'')} \frac{1}{2}\sqrt{\sum_{i=1}^{m} \frac{(dp_i)^2}{p_i(B)}} \tag{3.88}$$

$$= \frac{1}{2}\int_{B'}^{B''} dB \left\{\sum_{i=1}^{m} \frac{1}{p_i(B)}\left[\frac{d\,p_i(B)}{dB}\right]^2\right\}^{1/2}, \tag{3.89}$$

where $dp_i = p_i(B + dB) - p_i(B)$. The quantity in curly brackets is exactly the classical Fisher information defined in equation (3.60). From (3.89), we can see that the classical Fisher information is proportional to the square of the rate of change of the statistical distance along the path $\vec{p}(B)$ in probability space parameterised by B_y:

$$F = 4\left(\frac{d\mathcal{D}_{cl}}{dB}\right)^2. \tag{3.90}$$

Above, we found the statistical distance between the quantum states $\rho(B')$ and $\rho(B'')$ assuming that we were constrained to a fixed measurement POVM. Choosing a different POVM will, in general, give a different statistical distance between the two states. Maximising the statistical distance over all possible choices of POVM gives the *quantum statistical distance* [Braunstein & Caves (1994)]:

$$\mathcal{D}_q\left[\rho(B'), \rho(B'')\right] = \max_{\{\mathcal{M}_i\}} \mathcal{D}_{cl}\left[\rho(B'), \rho(B''), \{\mathcal{M}_i\}\right]. \tag{3.91}$$

It depends only on the two states $\rho(B')$ and $\rho(B'')$. From (3.89), we can see that the quantum Fisher information can be written as:

$$\mathcal{F} = 4\left(\frac{d\mathcal{D}_q}{dB}\right)^2. \tag{3.92}$$

This gives a nice interpretation of the quantum Fisher information: it is proportional to the square of the rate of change of the quantum statistical distance. Since the precision of an estimate of B depends crucially on how well we can distinguish two nearby values B' and B'' of the magnetic field, which in turn depends on how well we can distinguish the quantum states $\rho(B')$ and $\rho(B'')$, it is not surprising that this quantity should relate to the optimum precision of our estimate of B.

3.4 Estimating a magnetic field with unknown direction

In our previous examples of estimation of a magnetic field, we have assumed that the orientation of the magnetic field is in the y-direction, $\vec{B} = (0, B_y, 0)$. What if, not only the magnitude, but also the orientation of the magnetic field is unknown? In this case the Hamiltonian for the evolution of our spin system is

$$\hat{H} = -\gamma \vec{B} \cdot \hat{\vec{J}}. \tag{3.93}$$

In this section we consider the problem of which initial state of our system of N spins we should prepare to get the best possible precision in estimating $|\vec{B}|$.

If, by chance, it turns out that the magnetic field is $\vec{B} = (0, B_y, 0)$ then, from equation (3.68) above, the GHZ state

$$|GHZ^y_{\pm}\rangle_N = \frac{1}{\sqrt{2}}\left(|\boxtimes\rangle^{\otimes N} + |\odot\rangle^{\otimes N}\right), \tag{3.94}$$

has quantum Fisher information,

$$\mathcal{F} = 4\mathrm{Var}\left[\gamma t \hat{J}_y\right] = \gamma^2 t^2 N^2, \tag{3.95}$$

so that we can, in principle, estimate B_y at the Heisenberg limit. If, however the magnetic field is $\vec{B} = (B_x, 0, 0)$ then, again from equation (3.68), we find

that preparing the spins in the state $|GHZ_{\pm}^{y}\rangle_N$ can, at best, give precision at the standard quantum limit since the quantum Fisher information is:

$$\mathcal{F} = 4\mathrm{Var}\left[\gamma t \hat{J}_x\right] = \gamma^2 t^2 N. \tag{3.96}$$

In general, if $\vec{B} = (B_x, B_y, B_z)$ then the state $\left|GHZ_{\pm}^{\vec{B}/|\vec{B}|}\right\rangle_N$ aligned with the magnetic field has quantum Fisher information $\mathcal{F} = \gamma^2 t^2 N^2$, but preparation of this state requires that we know the direction $\vec{B}/|\vec{B}|$. Since we have assumed that this direction is unknown, we cannot prepare this optimum state and choosing an arbitrary GHZ state for our initial state leaves us open to a "worst case scenario" where precision of our estimate is no better than the standard quantum limit.

As another example, we assume that the initial state of the N spins is the spin coherent state $|{\rightarrow}\rangle^{\otimes N}$. In this case, if $\vec{B} = (0, B_y, B_z)$ the magnetic field can be measured with precision at the standard quantum limit because $\mathcal{F} = \gamma^2 t^2 N$. However, if $\vec{B} = (B_x, 0, 0)$ then we have $\mathcal{F} = 0$ and the same state is useless for estimating the magnetic field because as the system evolves all information about the field is contained in a physically inaccessible global phase: $e^{it\gamma B_x \hat{J}_x}|{\rightarrow}\rangle^{\otimes N} = e^{it\gamma B_x N/2}|{\rightarrow}\rangle^{\otimes N}$. Again, preparation of the appropriate spin coherent state requires that we know the orientation of the field and choosing an arbitrary spin coherent state leaves us open to the "worst case scenario" where we cannot estimate $|\vec{B}|$ at all.

Our question is whether we can improve on the "worst case scenario" by choosing a different initial state: Is there some state that we can prepare without knowing the orientation of the magnetic field with which we can we recover the N^2 scaling of the quantum Fisher information for *any* orientation of the magnetic field? A similar problem has been studied by Toscano *et al.* (2006) and Dalvit *et al.* (2006) for an harmonic oscillator.

We begin by noticing that the state of the spin system at a fixed time t,

$$\rho(B_x, B_y, B_z) = e^{it\gamma\vec{B}\cdot\hat{\vec{J}}}\rho(0)e^{-it\gamma\vec{B}\cdot\hat{\vec{J}}}, \tag{3.97}$$

depends on the three unknown parameters B_x, B_y and B_z, the magnetic fields in the x, y and z directions, respectively. On first sight, it seems that our problem is

one of multi-parameter estimation [Paris (2009)] rather than just single parameter estimation, since the parameter we are trying to estimate is

$$|\vec{B}| = \sqrt{B_x^2 + B_y^2 + B_z^2}, \tag{3.98}$$

a combination of the three unknown parameters B_x, B_y and B_z. However, in spherical coordinates the magnetic field $\vec{B}$ can be written as

$$\vec{B} = \begin{pmatrix} B_x \\ B_y \\ B_z \end{pmatrix} = \begin{pmatrix} |\vec{B}| \sin\theta_1 \cos\theta_2 \\ |\vec{B}| \sin\theta_1 \sin\theta_2 \\ |\vec{B}| \cos\theta_1 \end{pmatrix}, \tag{3.99}$$

so that we can express our state (3.97) in terms of these spherical coordinates:

$$\rho(|\vec{B}|, \theta_1, \theta_2) = e^{it\gamma\vec{B}\cdot\hat{\vec{J}}} \rho(0) e^{-it\gamma\vec{B}\cdot\hat{\vec{J}}}. \tag{3.100}$$

Written in this way, we see that estimation of $|\vec{B}|$ need not be a multi-parameter problem. Moreover, if we define the Hermitian operator

$$\hat{G}(\theta_1, \theta_2) \equiv t\gamma \left(\sin\theta_1 \cos\theta_2 \ \hat{J}_x + \sin\theta_1 \sin\theta_2 \ \hat{J}_y + \cos\theta_1 \ \hat{J}_z \right), \tag{3.101}$$

then we have:

$$\rho(|\vec{B}|, \theta_1, \theta_2) = e^{i|\vec{B}|\hat{G}(\theta_1,\theta_2)} \rho(0) e^{-i|\vec{B}|\hat{G}(\theta_1,\theta_2)}. \tag{3.102}$$

Now the dependence of $\rho(|\vec{B}|, \theta_1, \theta_2)$ on the parameter of interest $|\vec{B}|$ is generated by the unitary transformation[1] (3.102). From equation (3.65), we know that for states of the form (3.102) the quantum Fisher information with respect to the parameter $|\vec{B}|$ depends only on the initial state $\rho(0)$ and on the generator $\hat{G}$. Substituting $\hat{G}(\theta_1, \theta_2)$ into the expression (3.65) for the quantum Fisher information, we find that

[1] We note that this is possible for the parameter $|\vec{B}|$ but that the dependence of ρ on any of the other parameters (θ_1, θ_2, B_x, B_y, B_z) is, in general, not generated by a unitary transformation.

$$\begin{aligned}\mathcal{F}_{\hat{G}} &= t^2\gamma^2\Big[\sin^2\theta_1\cos^2\theta_2\mathcal{F}_{\hat{J}_x}+\sin^2\theta_1\sin^2\theta_2\mathcal{F}_{\hat{J}_y}+\cos^2\theta_1\mathcal{F}_{\hat{J}_z}\\ &\quad +2\sin^2\theta_1\cos\theta_2\sin\theta_2\mathcal{F}_{\hat{J}_x,\hat{J}_y}+2\sin\theta_1\cos\theta_1\cos\theta_2\mathcal{F}_{\hat{J}_x,\hat{J}_z}\\ &\quad +2\sin\theta_1\cos\theta_1\sin\theta_2\mathcal{F}_{\hat{J}_y,\hat{J}_z}\Big],\end{aligned} \tag{3.103}$$

where we define[1]:

$$\mathcal{F}_{\hat{J}_\mu,\hat{J}_\nu}=2\sum_{i\neq j}\frac{(\alpha_i-\alpha_j)^2}{\alpha_i+\alpha_j}\left(\frac{\langle\phi_j|\,\hat{J}_\mu\,|\phi_i\rangle\,\langle\phi_i|\,\hat{J}_\nu\,|\phi_j\rangle+\langle\phi_j|\,\hat{J}_\nu\,|\phi_i\rangle\,\langle\phi_i|\,\hat{J}_\mu\,|\phi_j\rangle}{2}\right). \tag{3.104}$$

As we have already mentioned, the state that maximises the quantum Fisher information (3.103) is the appropriate GHZ state. Another way of saying this is that

$$\max_{\rho(0)}\max_{\theta_1,\theta_2}\mathcal{F}_{\hat{G}(\theta_1,\theta_2)}[\rho(0)]=t^2\gamma^2N^2. \tag{3.105}$$

However, preparation of this state requires knowledge of the orientation of the magnetic field. We would like to find a state that is independent of all unknown parameters and that gives the best quantum Fisher information in the "worst case scenario". In other words, we would like to know the state $\rho(0)$ that maximises the quantity

$$\min_{\theta_1,\theta_2}\mathcal{F}_{\hat{G}(\theta_1,\theta_2)}\left[\rho(0)\right]. \tag{3.106}$$

Looking at (3.103) it is not obvious what this state might be. We approach this problem by first writing the *quantum Fisher information matrix*:

$$\mathbb{F}=\begin{pmatrix}\mathcal{F}_{\hat{J}_x} & \mathcal{F}_{\hat{J}_x,\hat{J}_y} & \mathcal{F}_{\hat{J}_x,\hat{J}_z}\\ \mathcal{F}_{\hat{J}_y,\hat{J}_x} & \mathcal{F}_{\hat{J}_y} & \mathcal{F}_{\hat{J}_y,\hat{J}_z}\\ \mathcal{F}_{\hat{J}_z,\hat{J}_x} & \mathcal{F}_{\hat{J}_z,\hat{J}_y} & \mathcal{F}_{\hat{J}_z}\end{pmatrix}, \tag{3.107}$$

whose diagonal elements are found by equation (3.65) and the off-diagonal elements by equation (3.104)[2].

[1] If the state $\rho(0)$ is pure, then the quantity in equation (3.104) reduces to the covariance, $\mathcal{F}_{\hat{J}_\mu,\hat{J}_\nu}=\mathrm{Cov}\left[\hat{J}_\mu,\hat{J}_\nu\right]$, [see equation (3.35)].

[2] If the state $\rho(0)$ is pure then the quantum Fisher information matrix reduces to the *covariance matrix*, with variances on the diagonals and covariances on the off-diagonals.

Since the quantum Fisher information matrix is real ($\mathbb{F} = \mathbb{F}^*$) and symmetric ($\mathbb{F} = \mathbb{F}^T$). It follows that for any state $\rho(0)$ there is some orthogonal matrix,

$$\mathbb{Q} = \begin{pmatrix} q_{11} & q_{12} & q_{13} \\ q_{21} & q_{22} & q_{23} \\ q_{31} & q_{32} & q_{33} \end{pmatrix}, \qquad \mathbb{Q}\mathbb{Q}^T = \mathbb{Q}^T\mathbb{Q} = 1, \tag{3.108}$$

that diagonalises $\mathbb{F}$, i.e., the transformed matrix $\mathbb{Q}\mathbb{F}\mathbb{Q}^T$ is diagonal. Using the notation

$$\text{diag}\begin{pmatrix} a \\ b \\ c \end{pmatrix} = \begin{pmatrix} a & 0 & 0 \\ 0 & b & 0 \\ 0 & 0 & c \end{pmatrix}, \tag{3.109}$$

we find from equations (3.107) and (3.108) that the diagonal elements of $\mathbb{Q}\mathbb{F}\mathbb{Q}^T$ are:

$$\mathbb{Q}\mathbb{F}\mathbb{Q}^T = \text{diag}\begin{pmatrix} q_{11}^2\mathcal{F}_{\hat{J}_x} + q_{12}^2\mathcal{F}_{\hat{J}_y} + q_{13}^2\mathcal{F}_{\hat{J}_z} + 2q_{11}q_{12}\mathcal{F}_{\hat{J}_x,\hat{J}_y} + 2q_{11}q_{13}\mathcal{F}_{\hat{J}_x,\hat{J}_z} + 2q_{12}q_{13}\mathcal{F}_{\hat{J}_y,\hat{J}_z} \\ q_{21}^2\mathcal{F}_{\hat{J}_x} + q_{22}^2\mathcal{F}_{\hat{J}_y} + q_{23}^2\mathcal{F}_{\hat{J}_z} + 2q_{21}q_{22}\mathcal{F}_{\hat{J}_x,\hat{J}_y} + 2q_{21}q_{23}\mathcal{F}_{\hat{J}_x,\hat{J}_z} + 2q_{22}q_{23}\mathcal{F}_{\hat{J}_y,\hat{J}_z} \\ q_{31}^2\mathcal{F}_{\hat{J}_x} + q_{32}^2\mathcal{F}_{\hat{J}_y} + q_{33}^2\mathcal{F}_{\hat{J}_z} + 2q_{31}q_{32}\mathcal{F}_{\hat{J}_x,\hat{J}_y} + 2q_{31}q_{33}\mathcal{F}_{\hat{J}_x,\hat{J}_z} + 2q_{32}q_{33}\mathcal{F}_{\hat{J}_y,\hat{J}_z} \end{pmatrix}. \tag{3.110}$$

Now, using equation (3.65) we notice that these diagonal elements can be rewritten as

$$\mathbb{Q}\mathbb{F}\mathbb{Q}^T = \text{diag}\begin{pmatrix} \mathcal{F}_{\hat{J}'_1} \\ \mathcal{F}_{\hat{J}'_2} \\ \mathcal{F}_{\hat{J}'_3} \end{pmatrix}, \tag{3.111}$$

where

$$\hat{J}'_1 = q_{11}\hat{J}_x + q_{12}\hat{J}_y + q_{13}\hat{J}_z \tag{3.112}$$

$$\hat{J}'_2 = q_{21}\hat{J}_x + q_{22}\hat{J}_y + q_{23}\hat{J}_z \tag{3.113}$$

$$\hat{J}'_3 = q_{31}\hat{J}_x + q_{32}\hat{J}_y + q_{33}\hat{J}_z, \tag{3.114}$$

or, equivalently,

$$\begin{pmatrix} \hat{J}'_1 \\ \hat{J}'_2 \\ \hat{J}'_3 \end{pmatrix} = \mathbb{Q} \begin{pmatrix} \hat{J}_x \\ \hat{J}_y \\ \hat{J}_z \end{pmatrix}. \tag{3.115}$$

Since $\mathbb{Q}$ is an orthogonal matrix, this just corresponds to a rotation of the spin operators $\hat{J}_x$, $\hat{J}_y$ and $\hat{J}_z$. Rewriting $\hat{G}$ in terms of these new operators, we have

$$\hat{G} = t\gamma \left(\sin\theta'_1 \cos\theta'_2 \ \hat{J}'_1 + \sin\theta'_1 \sin\theta'_2 \ \hat{J}'_2 + \cos\theta'_1 \ \hat{J}'_3 \right), \tag{3.116}$$

for some new unknown angles θ'_1 and θ'_2 that depend on θ_1, θ_2 and the elements of $\mathbb{Q}$. The upshot is that – in terms of these new observables and new unknown parameters – the quantum Fisher information is

$$\mathcal{F}_{\hat{G}} = t^2\gamma^2 \left(\sin^2\theta'_1 \cos^2\theta'_2 \ \mathcal{F}_{\hat{J}'_1} + \sin^2\theta'_1 \sin^2\theta'_2 \ \mathcal{F}_{\hat{J}'_2} + \cos^2\theta'_1 \ \mathcal{F}_{\hat{J}'_3} \right), \tag{3.117}$$

a linear combination of the quantum Fisher information of each of the rotated operators $\hat{J}'_1$, $\hat{J}'_2$ and $\hat{J}'_3$. Comparision with (3.103) shows that the effect of the transformation has been to get rid of the "covariance" terms like (3.104). This makes the minimisation in equation (3.106) easier. Without loss of generality, we can assume that[1]

$$\mathcal{F}_{\hat{J}'_1} \geq \mathcal{F}_{\hat{J}'_2} \geq \mathcal{F}_{\hat{J}'_3}. \tag{3.118}$$

Now the minimum of $\mathcal{F}_{\hat{G}}$ (3.117) is achieved when θ'_1 is an integer multiple of π:

$$\min_{\theta'_1,\theta'_2} \mathcal{F}_{\hat{G}} = t^2\gamma^2 \mathcal{F}_{\hat{J}'_3}. \tag{3.119}$$

Finally, for any state $\rho(0)$ we now have:

[1] We are free to shuffle the rows of $\mathbb{Q}$ to guarantee this.

$$\min_{\theta_1',\theta_2'} \mathcal{F}_{\hat{G}} = t^2\gamma^2 \mathcal{F}_{\hat{J}_3'} \tag{3.120}$$

$$\leq t^2\gamma^2 \frac{\mathcal{F}_{\hat{J}_1'} + \mathcal{F}_{\hat{J}_2'} + \mathcal{F}_{\hat{J}_3'}}{3} \tag{3.121}$$

$$\leq \frac{4t^2\gamma^2}{3}\left(\mathrm{Var}\hat{J}_1' + \mathrm{Var}\hat{J}_2' + \mathrm{Var}\hat{J}_3'\right) \tag{3.122}$$

$$\leq \frac{2Nt^2\gamma^2}{3}\left(\frac{N}{2}+1\right). \tag{3.123}$$

The first inequality follows from equation (3.118): the smallest of three numbers cannot be greater than the mean of the three numbers. The second inequality (3.122) follows from equation (3.67) and the third inequality is based on:

$$\mathrm{Var}\hat{J}_1' + \mathrm{Var}\hat{J}_2' + \mathrm{Var}\hat{J}_3' \leq \frac{N}{2}\left(\frac{N}{2}+1\right), \tag{3.124}$$

a well known relation for a system of N spin-1/2 particles [Tóth *et al.* (2007)].

Equality in the first inequality (3.121) can be achieved only if

$$\mathcal{F}_{\hat{J}_1'} = \mathcal{F}_{\hat{J}_2'} = \mathcal{F}_{\hat{J}_3'}. \tag{3.125}$$

In this case, since $\mathbb{Q}\mathbb{F}\mathbb{Q}^T$ is proportional to the identity matrix, we see from equation (3.111) that the quantum Fisher information matrix $\mathbb{F}$ with the original operators $\hat{J}_x$, $\hat{J}_y$ and $\hat{J}_z$ must also be proportional to the identity matrix. In other words, it is diagonal:

$$\mathbb{F} = \begin{pmatrix} \mathcal{F}_{\hat{J}_x} & 0 & 0 \\ 0 & \mathcal{F}_{\hat{J}_y} & 0 \\ 0 & 0 & \mathcal{F}_{\hat{J}_z} \end{pmatrix}, \tag{3.126}$$

with

$$\mathcal{F}_{\hat{J}_x} = \mathcal{F}_{\hat{J}_y} = \mathcal{F}_{\hat{J}_z}. \tag{3.127}$$

Substituting into equation (3.103) gives:

$$\min_{\theta_1,\theta_2} \mathcal{F}_{\hat{G}} = \mathcal{F}_{\hat{G}} = t^2\gamma^2\mathcal{F}_{\hat{J}_x} = t^2\gamma^2\mathcal{F}_{\hat{J}_y} = t^2\gamma^2\mathcal{F}_{\hat{J}_z}. \tag{3.128}$$

We have equality in the second inequality (3.122) if and only if the state $\rho(0)$ is pure. Combining this and condition (3.127) tells us that the states that give the best "worst case" precision will be pure states with the property that

$$\mathrm{Var}\hat{J}_x = \mathrm{Var}\hat{J}_y = \mathrm{Var}\hat{J}_z, \tag{3.129}$$

giving

$$\min_{\theta_1,\theta_2} \mathcal{F}_{\hat{G}} = \mathcal{F}_{\hat{G}}\left[|\Psi(0)\rangle\right] = 4t^2\gamma^2\mathrm{Var}\hat{J}_x = 4t^2\gamma^2\mathrm{Var}\hat{J}_y = 4t^2\gamma^2\mathrm{Var}\hat{J}_z. \tag{3.130}$$

The third inequality in (3.123) then indicates that for states of this kind we have

$$\min_{\theta_1,\theta_2} \mathcal{F}_{\hat{G}} = \mathcal{F}_{\hat{G}}\left[|\Psi(0)\rangle\right] \leq \frac{2N}{3}\left(\frac{N}{2}+1\right). \tag{3.131}$$

In figure 3.2 we compare the scaling of this upper bound to the Heisenberg limit (3.105) when the direction of the magnetic field is known. Unsurprisingly, the upper bound (3.131) is smaller than the Heisenberg limit. However, it scales as N^2 so that a significant improvement over the standard quantum limit is still possible, in principle. Also in figure 3.2 we plot $\min_{\theta_1,\theta_2} \mathcal{F}_{\hat{G}}$ for the state

$$|\Psi_6(0)\rangle = \mathcal{N}\left(|{\rightarrow}\rangle^{\otimes N} + |{\leftarrow}\rangle^{\otimes N} + |{\odot}\rangle^{\otimes N} + |{\otimes}\rangle^{\otimes N} + |{\uparrow}\rangle^{\otimes N} + |{\downarrow}\rangle^{\otimes N}\right) \tag{3.132}$$

$$= \mathcal{N}\left(\left|GHZ^x_+\right\rangle_N + \left|GHZ^y_+\right\rangle_N + \left|GHZ^z_+\right\rangle_N\right), \tag{3.133}$$

where $\mathcal{N}$ is for normalisation. (The subscript on the state $|\Psi_6(0)\rangle$ is because it is a superposition of six spin coherent states.) This state satisfies condition (3.129). Figure 3.2 shows for $N > 4$, the "worst case" quantum Fisher information for this state is at the upper limit. To our knowledge, this result has not been presented before.

In figure 3.3 we plot the spin Wigner function for this state. Intuitively, its quantum Fisher information is high, even in the worst case when the magnetic field direction is unknown, because there are some interference fringes with a fine structure that can distinguish small rotations about *any* axis. For comparison, the spin Wigner function for the GHZ state $\left|GHZ^y_+\right\rangle_N$ (plotted in figure 2.13) has interference fringes that can only detect small small rotations about the y-axis.

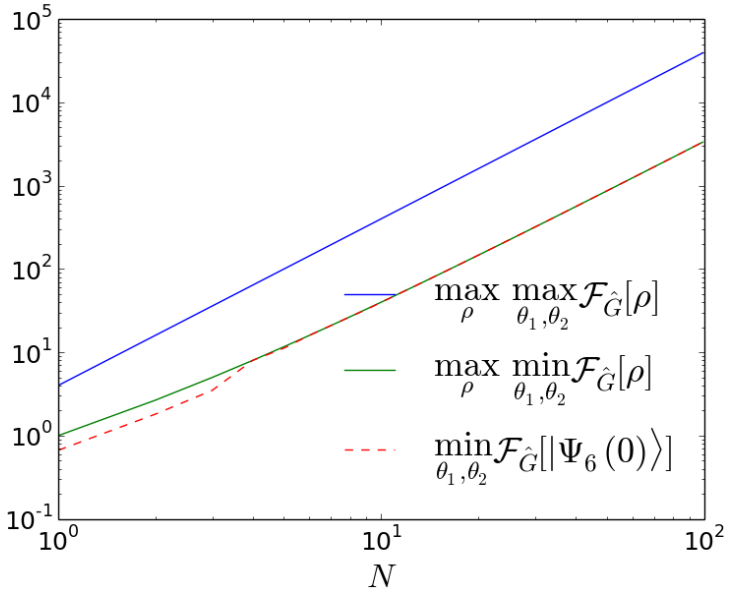

Figure 3.2: The blue line is the quantum Fisher information assuming that we know the orientation of the magnetic field $\vec{B}$ and that we can prepare the optimum GHZ state. The green line is the upper bound to the quantum Fisher information in the "worst case scenario" . The dashed red line is the quantum Fisher information for the state $|\Psi_6(0)\rangle$ [equation (3.133)]. We see that $|\Psi_6(0)\rangle$ reaches the maximum for $N > 4$. (We have set $t\gamma = 1$ in this plot.)

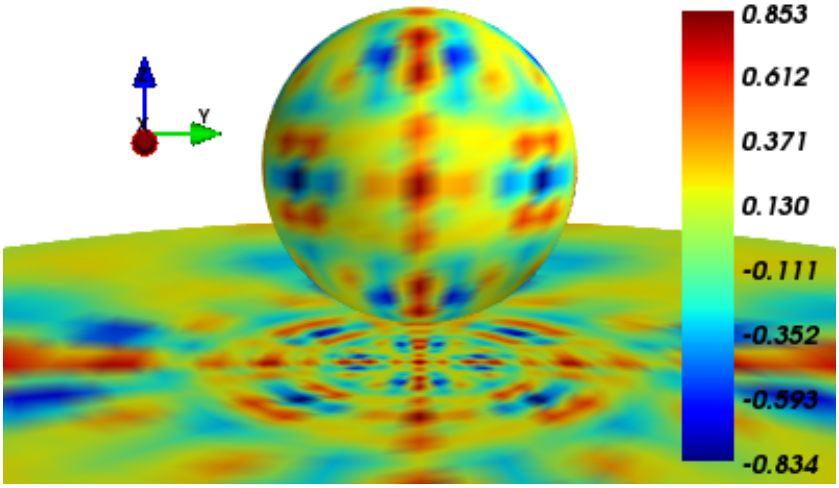

Figure 3.3: The spin Wigner function for the state $|\Psi_6(0)\rangle$ [equation (3.133)]. For a magnetic field in any direction, there are interference fringes with fine structure that allow us to distinguish small rotations. (N=20.)

Similarly, a superposition of just two GHZ states:

$$|\Psi_4(0)\rangle = \mathcal{N}\left(\left|GHZ^x_{\pm}\right\rangle_N + \left|GHZ^y_{\pm}\right\rangle_N\right), \tag{3.134}$$

can detect small rotations if the magnetic field is in the xy-plane. Such a state would be useful for estimating magnetic fields with unknown direction in two dimensions. Later, in chapter 6 we show states like (3.134) can be generated by interacting the N spin system with a single spin.

An interesting problem would be to find the states that give the best possible precision in estimation of the direction of the magnetic field [i.e., the angles θ_1 and θ_2 in equation (3.99)]. A device that estimates this direction could be called a "quantum compass". We will address this problem in future work.

Chapter 4

The Spin Star Model

The spin star model – introduced by Hutton & Bose (2004) – is composed of N spin-1/2 particles interacting with a single spin-1/2 particle in a 'star topology' (see figure 4.1). The interactions with the central spin are through Heisenberg XX couplings of equal strength and there are no direct interactions between the outer spins:

$$\hat{H}_{SS} = \frac{\Omega}{2}\hat{\sigma}_z + \frac{\omega}{2}\sum_{i=1}^{N}\hat{\sigma}_z^{(i)} + \lambda\sum_{i=1}^{N}\left(\hat{\sigma}_+^{(i)}\hat{\sigma}_- + \hat{\sigma}_-^{(i)}\hat{\sigma}_+\right) \tag{4.1}$$

$$= \frac{\Omega}{2}\hat{\sigma}_z + \omega\hat{J}_z + \lambda\left(\hat{J}_+\hat{\sigma}_- + \hat{J}_-\hat{\sigma}_+\right), \tag{4.2}$$

where $\hat{J}_\pm = \sum_{i=1}^{N}\hat{\sigma}_\pm^{(i)}$ and i labels the N outer spins.

The spin star Hamiltonian (4.2) is highly symmetric. Since

$$\left[\hat{H}_{SS}, \hat{J}^2\right] = 0, \tag{4.3}$$

the total angular momentum of the outer spins is conserved. The operator $\hat{M} = \hat{J}_z + \frac{1}{2}\hat{\sigma}_z$ also commutes with the Hamiltonian:

$$\left[\hat{H}_{SS}, \hat{M}\right] = 0. \tag{4.4}$$

Although $\hat{M}$ can have negative and half-integer eigenvalues, we can interpret it as the "total excitation number" operator for the whole $N+1$ spin system (if,

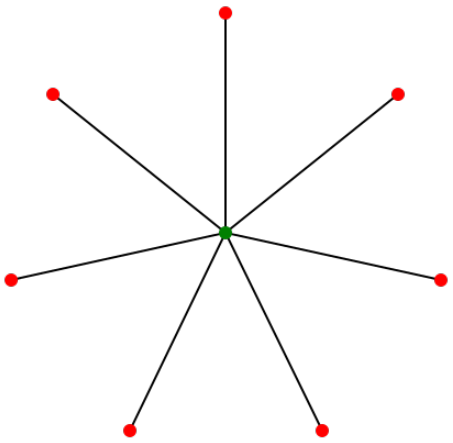

Figure 4.1: (colour online). Schematic of the spin star interaction: N outer spins (in red) interact equally with a central spin (in green) but not among themselves.

for example, $\left\langle \hat{M} \right\rangle = 0$ then on average there are as many spins 'up' as there are 'down' in the combined $N+1$ spin system). The commutation relation (4.4) then tells us that this excitation number is conserved as the system evolves. Also, since the the coupling of the central spin to each of the outer spins has the same strength, the Hamiltonian is symmetric under exchange of any two of the outer spins.

Hutton & Bose (2004) studied ground state entanglement between the spins when $\Omega = \omega$. As an application, they proposed this as a way of sharing entanglement between spins at nodes of a quantum network. Multipartite entanglement between the spins at thermal equilibrium was investigated by Anza *et al.* (2010); Militello & Messina (2011).

The spin star Hamiltonian has also been studied from the point of view of the N outer spins as an environment for the central spin [Breuer *et al.* (2004)]. Since the reduced dynamics of the central spin can be solved exactly but cannot be treated in the Markovian approximation, the spin star model is useful for testing the validity of various non-Markovian approximation methods [Breuer & Petruccione (2007)]. In that case the reduced state of the central spin is of primary interest. Here, we are interested in the unitary evolution of the whole $N+1$ spin system. This is also the focus of the paper by El-Orany & Abdalla

(2011), who solved the Heisenberg equations of motion for various operators of the spin star model. They identified several regimes of collapse and revival by plotting the expectation value $\langle\sigma_z\rangle$ for the central spin, but gave little physical explanation or intuition for their results.

The spin star model is interesting because its dynamics can be solved exactly but still include many non-trivial quantum phenomena. Moreover, it may be possible to engineer the spin star Hamiltonian. An understanding of its dynamics is thus important for possible applications in quantum technologies. In section 4.1 of this chapter we briefly consider some candidate systems for physical implementation of $\hat{H}_{SS}$. In section 4.2 we find the eigenstates and eigenvalues of $\hat{H}_{SS}$ and write down the time evolved state for an arbitrary separable initial state. This exact solution does not, however, give much insight into the dynamics of the spin star model.

In section 4.3 we derive an effective Hamiltonian that is valid when the central spin and the outer spins are far off-resonance ($|\Omega-\omega| \gg \lambda N$). This effective Hamiltonian has a term proportional to $\hat{J}_z^2$ which, as we will see in later chapters, is very interesting from the point of view of generating non-classical states. It is known that one obtains a similar $\hat{J}_z^2$ term in the dispersive limit of N spins interacting with a harmonic oscillator [Bennett *et al.* (2013)], but – to our knowledge – the effective Hamiltonian (4.54) for the interaction of N spins with a single spin has not been presented elsewhere.

In section 4.4 we derive another effective Hamiltonian, this time valid on-resonance and for initial spin coherent states. This result was included in our publication Dooley & Spiller (2014).

4.1 Candidates for implementation

There are examples of highly symmetric molecules that consist of N spins equally coupled to a central spin in a spin star geometry (figure 4.1). The trimethyl phosphite molecule, for instance, has nine ^1H spins, all equally coupled to a single ^{31}P spin [Jones *et al.* (2009)]. The tetramethylsilane molecule has twelve ^1H spins equally coupled to a single ^{21}S spin [Simmons *et al.* (2010)]. Using NMR techniques, entangled states of both of these molecules have been generated for

use as magnetic field sensors [Jones *et al.* (2009); Simmons *et al.* (2010)]. A limitation of such implementations, however, is that the number of outer spins N cannot be very large: even if such symmetric molecules could be engineered for arbitrary N, the dipole-dipole interaction has a strong dependence on the distance between the spins so that as N is increased it becomes more and more difficult to maintain equal, strong coupling of each outer spin to the central spin without interaction among the outer spins. Even though there are restrictions on the value of N in this implementation, it is worth noting that interesting revival phenomena may be observed in the spin star model even for small values of N. This is discussed in more detail in chapter 6.

Our outer spins can, however, be qubits of any kind. Interestingly, the $\lambda(\sigma_+\sigma_- + \sigma_-\sigma_+)$ coupling can be achieved between superconducting qubits. Two superconducting phase qubits can be coupled by a $\lambda(\sigma_+\sigma_- + \sigma_-\sigma_+)$ interaction by connecting them via a capacitor [McDermott *et al.* (2005); Neeley *et al.* (2010)], or two flux qubits coupled via mutual inductance can interact by $\lambda(\sigma_+\sigma_- + \sigma_-\sigma_+)$ [Niskanen *et al.* (2007)]. Our interaction Hamiltonian (4.2) is composed of N such equal interactions with the central spin. Again, however, it may be difficult in practice to design a spin star system with large value of N since these interactions depend on the qubits being attached to each other.

It has been proposed [Tsomokos *et al.* (2008)] that the spin star Hamiltonian can be implemented for large values of N with a superconducting system. A collection of superconducting qubits coupled resonantly to an harmonic oscillator circuit element interact in a star geometry with the oscillator at the centre of the star. By adding a non-linearity to the oscillator circuit element it can act as a qubit with just two effective levels and all other level separations detuned. Experiments demonstrations of similar proposals have already been made with three or four superconducting qubits coupled to a superconducting resonator [DiCarlo *et al.* (2010); Reed *et al.* (2012)].

Perhaps most promisingly, the spin star Hamiltonian may be implemented for a superconducting flux qubit interacting with a thin layer of nitrogen vacancy (NV) centres in diamond [Marcos *et al.* (2010); Twamley & Barrett (2010)]. In this case, the superconducting qubit is the central 'spin' whose basis states are the persistent current rotating clockwise or anti-clockwise in a superconducting

ring. The current in either state generates a magnetic field that couples with the spin degrees of freedom of the ground state manifold of each NV centre. For many NV centres in a thin layer, the coupling with the flux qubit is approximately the same for each spin. Also, the coupling between NV centres is negligible. Rabi oscillations between the state $\left|\frac{N}{2}, -\frac{N}{2}\right\rangle|\uparrow\rangle$ and the state $\left|\frac{N}{2}, 1-\frac{N}{2}\right\rangle|\downarrow\rangle$ for such an interaction have been observed experimentally for $N \sim 10^7$ [Saito *et al.* (2013); Zhu *et al.* (2011, 2014)]. We will discuss this implementation in more detail later in chapter 7.

4.2 Exact solution

Eigenstates and eigenvalues

In order to solve the dynamics of the spin star model we first find the eigenstates and eigenvalues of the Hamiltonian

$$\hat{H}_{SS} = \omega \hat{J}_z + \frac{\Omega}{2}\hat{\sigma}_z + \lambda\left(\hat{J}_+\hat{\sigma}_- + \hat{J}_-\hat{\sigma}_+\right). \tag{4.5}$$

These were first presented by Hutton & Bose (2004) for the resonant case ($\Omega = \omega$).

We rewrite the Hamiltonian as

$$\hat{H} = \omega \hat{M} + \frac{\Delta}{2}\hat{\sigma}_z + \lambda\left(\hat{J}_+\hat{\sigma}_- + \hat{J}_-\hat{\sigma}_+\right), \tag{4.6}$$

where $\Delta = \Omega - \omega$ and $\hat{M} = \hat{J}_z + \frac{\hat{\sigma}_z}{2}$ has eigenstates and eigenvalues

$$\hat{M}\left|j,m\right\rangle_N|\uparrow\rangle = \left(m+\frac{1}{2}\right)\left|j,m\right\rangle_N|\uparrow\rangle, \tag{4.7}$$

$$\hat{M}\left|j,m\right\rangle_N|\downarrow\rangle = \left(m-\frac{1}{2}\right)\left|j,m\right\rangle_N|\downarrow\rangle. \tag{4.8}$$

As previously mentioned, although $\hat{M}$ can have negative and half-integer eigenvalues, we can interpreted it as the "total excitation number" operator. It commutes with the total Hamiltonian (4.6) so that $\hat{M}$ and $\hat{H}$ share a set of eigenstates. The most general form of an eigenstate $|\psi_m^{\pm}\rangle$ of $\hat{M}$ that has eigenvalue $m - \frac{1}{2}$ is,

$$\left|\psi^-_{-j}\right\rangle = |j,-j\rangle_N |\downarrow\rangle , \tag{4.9}$$

$$\left|\psi^+_m\right\rangle = \cos\Theta_m |j,m\rangle_N |\downarrow\rangle + e^{-i\Phi_m}\sin\Theta_m |j,m-1\rangle_N |\uparrow\rangle , \tag{4.10}$$

$$(\text{for } -j+1 \le m \le j)$$

$$\left|\psi^-_m\right\rangle = \sin\Theta_m |j,m\rangle_N |\downarrow\rangle - e^{-i\Phi_m}\cos\Theta_m |j,m-1\rangle |\uparrow\rangle , \tag{4.11}$$

$$(\text{for } -j+1 \le m \le j)$$

$$\left|\psi^+_{j+1}\right\rangle = |j,j\rangle_N |\uparrow\rangle , \tag{4.12}$$

where Θ_m and Φ_m are arbitrary angles. The states $\left|\psi^-_{-j}\right\rangle$ and $\left|\psi^+_{j+1}\right\rangle$ are already eigenstates of the spin star Hamiltonian, with eigenvalues $-\omega j - \Omega/2$ and $\omega j + \Omega/2$ respectively, but the states $|\psi^\pm_m\rangle$ are not, in general, eigenstates of $\hat{H}_{SS}$. However, we can find values of Θ_m and Φ_m for which $|\psi^\pm_m\rangle$ are eigenstates of $\hat{H}_{SS}$. Operating on the states $|\psi^\pm_m\rangle$ by $\hat{H}_{SS}$ gives

$$\begin{aligned}
\hat{H}_{SS}\left|\psi^+_m\right\rangle &= \omega\left(m-\frac{1}{2}\right)\left|\psi^+_m\right\rangle + \\
&+\left(\lambda\sqrt{j(j+1)-m(m-1)}e^{-i\Phi_m}\tan\Theta_m - \frac{\Delta}{2}\right)\cos\Theta_m |j,m\rangle |\downarrow\rangle + \\
&+\left(\lambda\sqrt{j(j+1)-m(m-1)}e^{i\Phi_m}\arctan\Theta_m + \frac{\Delta}{2}\right)e^{-i\Phi_m}\sin\Theta_m |j,m-1\rangle |\uparrow\rangle
\end{aligned} \tag{4.13}$$

$$\begin{aligned}
\hat{H}_{SS}\left|\psi^-_n\right\rangle &= \omega\left(m-\frac{1}{2}\right)\left|\psi^-_m\right\rangle + \\
&+\left(-\lambda\sqrt{j(j+1)-m(m-1)}e^{-i\Phi_m}\arctan\Theta_m - \frac{\Delta}{2}\right)\sin\Theta_m |j,m\rangle |\downarrow\rangle + \\
&+\left(-\lambda\sqrt{j(j+1)-m(m-1)}e^{i\Phi_m}\tan\Theta_m + \frac{\Delta}{2}\right)\left(-e^{-i\Phi_m}\cos\Theta_m\right)|j,m-1\rangle |\uparrow\rangle .
\end{aligned} \tag{4.14}$$

For $|\psi^\pm_m\rangle$ to be eigenstates of $\hat{H}_{SS}$ we require

$$\lambda\sqrt{j(j+1)-m(m-1)}e^{-i\Phi_m}\tan\Theta_m - \frac{\Delta}{2} = \\ = \lambda\sqrt{j(j+1)-m(m-1)}e^{i\Phi_m}\arctan\Theta_m + \frac{\Delta}{2}, \tag{4.15}$$

$$\lambda\sqrt{j(j+1)-m(m-1)}e^{-i\Phi_m}\arctan\Theta_m + \frac{\Delta}{2} = \\ = \lambda\sqrt{j(j+1)-m(m-1)}e^{i\Phi_m}\tan\Theta_m - \frac{\Delta}{2}. \tag{4.16}$$

So that the eigenvalues are real we need $\Phi_m = 0$. Defining

$$\mu_m = \sqrt{\Delta^2 + 4\lambda^2[j(j+1)-m(m-1)]}, \tag{4.17}$$

equations (4.15) and (4.16) are both solved for

$$\Phi_m = 0, \tag{4.18}$$

$$\tan\Theta_m = \sqrt{\frac{\mu_m+\Delta}{\mu_m-\Delta}}. \tag{4.19}$$

From this expression for $\tan\Theta_m$ we can find $\sin\Theta_m$ and $\cos\Theta_m$:

$$\cos\Theta_m = \sqrt{\frac{\mu_m-\Delta}{2\mu_m}} \quad ; \quad \sin\Theta_m = \sqrt{\frac{\mu_m+\Delta}{2\mu_m}}. \tag{4.20}$$

By substituting (4.19) into the eigenvalue equations (4.13) and (4.14) we can also obtain the eigenvalues of $\hat{H}_{SS}$. In summary, we find that:

$$\hat{H}_{SS}\left|\psi_m^{\pm}\right\rangle = E_m^{\pm}\left|\psi_m^{\pm}\right\rangle, \tag{4.21}$$

where for $-j < m \leq j$:

$$\left|\psi_m^{+}\right\rangle = \sqrt{\frac{\mu_m-\Delta}{2\mu_m}}\left|j,m\right\rangle_N\left|\downarrow\right\rangle + \sqrt{\frac{\mu_m+\Delta}{2\mu_m}}\left|j,m-1\right\rangle_N\left|\uparrow\right\rangle, \tag{4.22}$$

$$\left|\psi_m^{-}\right\rangle = \sqrt{\frac{\mu_m+\Delta}{2\mu_m}}\left|j,m\right\rangle_N\left|\downarrow\right\rangle - \sqrt{\frac{\mu_m-\Delta}{2\mu_m}}\left|j,m-1\right\rangle_N\left|\uparrow\right\rangle, \tag{4.23}$$

$$E_m^{\pm} = \omega\left(m-\frac{1}{2}\right) \pm \frac{1}{2}\mu_m. \tag{4.24}$$

For $m = -j$ we have only the minus eigenstate:

$$\left|\psi^-_{-j}\right\rangle = \left|j, -j\right\rangle_N \left|\downarrow\right\rangle \qquad ; \qquad E^-_{-j} = -\omega j - \frac{\Omega}{2}, \tag{4.25}$$

and for $m = j + 1$ we have only the plus eigenstate:

$$\left|\psi^+_{j+1}\right\rangle = \left|j, j\right\rangle_N \left|\uparrow\right\rangle \qquad ; \qquad E^+_{j+1} = \omega j + \frac{\Omega}{2}. \tag{4.26}$$

We will see in the next chapter that the spin star Hamiltonian reduces to the Jaynes-Cummings Hamiltonian in the bosonic limit. We expect, therefore, that the eigenstates and eigenvalues above reduce to the Jaynes-Cummings expressions in that limit. Indeed, changing the labelling from m to n (where $m = n - j$), transforming the coupling parameter $\lambda \to \lambda/\sqrt{2j}$ and taking the $j \to \infty$ limit gives back the Jaynes-Cummings model eigenstates and eigenvalues [given in the next chapter in equations (5.3), (5.4) and (5.5)].

Exact solution

Rearranging equations (4.22) and (4.23) for the spin star Hamiltonian eigenstates we can write

$$\left|j, m\right\rangle_N \left|\downarrow\right\rangle = \sqrt{\frac{\mu_m - \Delta}{2\mu_m}} \left|\psi^+_m\right\rangle + \sqrt{\frac{\mu_m + \Delta}{2\mu_m}} \left|\psi^-_m\right\rangle, \tag{4.27}$$

$$\left|j, m-1\right\rangle_N \left|\uparrow\right\rangle = \sqrt{\frac{\mu_m + \Delta}{2\mu_m}} \left|\psi^+_m\right\rangle - \sqrt{\frac{\mu_m - \Delta}{2\mu_m}} \left|\psi^-_m\right\rangle. \tag{4.28}$$

An arbitrary separable state of the system can then be written as

$$\left|\Psi(0)\right\rangle = \left(\sum_{m=-j}^{j} C_m \left|j, m\right\rangle\right) \left(C_\uparrow \left|\uparrow\right\rangle + C_\downarrow \left|\downarrow\right\rangle\right) \tag{4.29}$$

$$\begin{aligned} &= \sum_{m=-j+1}^{j} \left[\left(C_m C_\downarrow \sqrt{\frac{\mu_m - \Delta}{2\mu_m}} + C_{m-1} C_\uparrow \sqrt{\frac{\mu_m + \Delta}{2\mu_m}} \right) \left|\psi^+_m\right\rangle + \right. \\ &\quad \left. + \left(C_m C_\downarrow \sqrt{\frac{\mu_m + \Delta}{2\mu_m}} - C_{m-1} C_\uparrow \sqrt{\frac{\mu_m - \Delta}{2\mu_m}} \right) \left|\psi^-_m\right\rangle \right] + \\ &\quad + C_{-j} C_\downarrow \left|\psi^-_{-j}\right\rangle + C_j C_\uparrow \left|\psi^+_{j+1}\right\rangle. \end{aligned} \tag{4.30}$$

Since this is expressed in terms of the eigenstates of the spin star Hamiltonian it is straightforward to write down the state of the system at arbitrary time:

$$\begin{aligned}|\Psi(t)\rangle &= \sum_{m=-j+1}^{j}\Bigg[\left(C_mC_\downarrow\sqrt{\frac{\mu_m-\Delta}{2\mu_m}}+C_{m-1}C_\uparrow\sqrt{\frac{\mu_m+\Delta}{2\mu_m}}\right)e^{-itE_m^+}\left|\psi_m^+\right\rangle+\\ &+\left(C_mC_\downarrow\sqrt{\frac{\mu_m+\Delta}{2\mu_m}}-C_{m-1}C_\uparrow\sqrt{\frac{\mu_m-\Delta}{2\mu_m}}\right)e^{-itE_m^-}\left|\psi_m^-\right\rangle\Bigg]+\\ &+C_{-j}C_\downarrow e^{-itE_{-j}^-}\left|\psi_{-j}\right\rangle+C_jC_\uparrow e^{-itE_{j+1}^+}\left|\psi_{j+1}\right\rangle. \end{aligned} \tag{4.31}$$

Returning to the Dicke basis of the N spin system, we can rewrite this concisely as

$$|\Psi(t)\rangle=\sum_{m=-j}^{j}|j,m\rangle_N\left(f_m^\Delta(t)\left|\uparrow\right\rangle+g_m^\Delta(t)\left|\downarrow\right\rangle\right), \tag{4.32}$$

by defining

$$\begin{aligned}f_m^\Delta(t) &= e^{-itE_{m+1}^+}\left(C_{m+1}C_\downarrow\frac{\sqrt{\mu_{m+1}^2-\Delta^2}}{2\mu_{m+1}}+C_mC_\uparrow\frac{\mu_{m+1}+\Delta}{2\mu_{m+1}}\right)\\ &\quad -e^{-itE_{m+1}^-}\left(C_{m+1}C_\downarrow\frac{\sqrt{\mu_{m+1}^2-\Delta^2}}{2\mu_{m+1}}-C_mC_\uparrow\frac{\mu_{m+1}-\Delta}{2\mu_{m+1}}\right), \end{aligned} \tag{4.33}$$

$$\begin{aligned}g_m^\Delta(t) &= e^{-itE_m^+}\left(C_mC_\downarrow\frac{\mu_m-\Delta}{2\mu_m}+C_{m-1}C_\uparrow\frac{\sqrt{\mu_m^2-\Delta^2}}{2\mu_m}\right)\\ &\quad +e^{-itE_m^-}\left(C_mC_\downarrow\frac{\mu_m+\Delta}{2\mu_m}-C_{m-1}C_\uparrow\frac{\sqrt{\mu_m^2-\Delta^2}}{2\mu_m}\right). \end{aligned} \tag{4.34}$$

The reduced state of the single central spin, and the reduced state of the N outer spins are easily expressed in terms of these functions $f_m^\Delta(t)$ and $g_m^\Delta(t)$. However, the functions $f_m^\Delta(t)$ and $g_m^\Delta(t)$ are complicated and do not give much intuition for the dynamics of the spin star model.

Interaction picture

It is often convenient to work in an interaction picture defined by separation of the Hamiltonian (4.2) into a bare term $\omega\hat{M}$ and an interaction term $\hat{H}_{SS}^{int}=$

$\frac{\Delta}{2}\hat{\sigma}_z + \lambda\left(\hat{J}_-\hat{\sigma}_+ + \hat{J}_+\hat{\sigma}_-\right)$:

$$\hat{H}_{SS} = \omega\hat{M} + \hat{H}_{SS}^{int}. \tag{4.35}$$

In a rotating frame of reference (interaction picture) the Hamiltonian is:

$$\hat{H}_{SS}^{I} = e^{i\omega\hat{M}}\hat{H}_{SS}^{int}e^{-i\omega\hat{M}} = \frac{\Delta}{2}\hat{\sigma}_z + \lambda\left(\hat{J}_-\hat{\sigma}_+ + \hat{J}_+\hat{\sigma}_-\right), \tag{4.36}$$

and the state of the system is

$$\left|\Psi^I(t)\right\rangle = e^{i\omega\hat{M}}\left|\Psi(t)\right\rangle, \tag{4.37}$$

where the superscript I indicates that we are in the interaction picture. Mathematically speaking, if we set $\omega = 0$ and $\Omega = \Delta$ in the full (Schrödinger picture) spin star Hamiltonian (4.5) we end up with the interaction picture Hamiltonian (4.36). It follows that the eigenstates and eigenvalues of (4.36) can be easily obtained from the general expressions [(4.22), (4.23) and (4.24)] by setting $\omega = 0$ and $\Omega = \Delta$. In this case the eigenstates are unchanged and the eigenvalues are

$$E_m^{I,\pm} = \pm\frac{1}{2}\sqrt{\Delta^2 + 4\lambda^2[j(j+1) - m(m-1)]}. \tag{4.38}$$

If we further assume that the the outer spins and the central spin are on resonance ($\Delta = 0$), the interaction picture Hamiltonian is $\hat{H}_{SS}^{I} = \lambda\left(\hat{J}_-\hat{\sigma}_+ + \hat{J}_+\hat{\sigma}_-\right)$ and its eigenstates take the simple form:

$$\left|\psi_{-j}^{I,-}\right\rangle = \left|j,-j\right\rangle\left|\downarrow\right\rangle \tag{4.39}$$

$$\left|\psi_{j+1}^{I,+}\right\rangle = \left|j,j\right\rangle\left|\uparrow\right\rangle \tag{4.40}$$

$$\left|\psi_{m}^{I,\pm}\right\rangle = \frac{1}{\sqrt{2}}\left(\left|j,m\right\rangle\left|\downarrow\right\rangle \pm \left|j,m-1\right\rangle\left|\uparrow\right\rangle\right), \tag{4.41}$$

with eigenvalues

$$E_m^{I,\pm} = \pm\lambda\sqrt{j(j+1) - m(m-1)}. \tag{4.42}$$

In this case the time evolved state in the interaction picture is

$$\left|\Psi^I(t)\right\rangle = \sum_{m=-j}^{j}\left|j,m\right\rangle_N\left(f_m^{(0)}(t)\left|\uparrow\right\rangle + g_m^{(0)}(t)\left|\downarrow\right\rangle\right), \tag{4.43}$$

where

$$\begin{aligned} f_m^{(0)}(t) &= C_m C_\uparrow \cos\left(\lambda t\sqrt{j(j+1)-m(m+1)}\right) - \\ &\quad -iC_{m+1}C_\downarrow \sin\left(\lambda t\sqrt{j(j+1)-m(m+1)}\right), \qquad (4.44) \\ g_m^{(0)}(t) &= C_m C_\downarrow \cos\left(\lambda t\sqrt{j(j+1)-m(m-1)}\right) - \\ &\quad -iC_{m-1}C_\uparrow \sin\left(\lambda t\sqrt{j(j+1)-m(m-1)}\right). \qquad (4.45) \end{aligned}$$

As an example, if the N qubit system is initially in a Dicke state $|j,m\rangle_N$ we see that the system evolves to:

$$\begin{aligned} \left|\Psi^I(t)\right\rangle &= |j,m\rangle_N \left[C_\uparrow \cos\left(\lambda t\sqrt{j(j+1)-m(m+1)}\right)|\uparrow\rangle \right. \\ &\quad \left. +C_\downarrow \cos\left(\lambda t\sqrt{j(j+1)-m(m-1)}\right)|\downarrow\rangle\right] \\ &\quad -iC_\downarrow |j,m-1\rangle_N \sin\left(\lambda t\sqrt{j(j+1)-m(m-1)}\right)|\uparrow\rangle \\ &\quad -iC_\uparrow |j,m+1\rangle_N \sin\left(\lambda t\sqrt{j(j+1)-m(m+1)}\right)|\downarrow\rangle. \qquad (4.46) \end{aligned}$$

If we further suppose that $C_\uparrow = 1$ and $C_\downarrow = 0$, then the system oscillates sinusoidally between the states $|j,m\rangle_N|\uparrow\rangle$ and $|j,m+1\rangle_N|\downarrow\rangle$ with frequency $\lambda\sqrt{j(j+1)-m(m+1)}$:

$$\begin{aligned} \left|\Psi^I(t)\right\rangle &= \cos\left(\lambda t\sqrt{j(j+1)-m(m+1)}\right)|j,m\rangle_N|\uparrow\rangle \\ &\quad -i\sin\left(\lambda t\sqrt{j(j+1)-m(m+1)}\right)|j,m+1\rangle_N|\downarrow\rangle. \qquad (4.47) \end{aligned}$$

This is the spin system analogue of the Jaynes-Cummings Rabi oscillations [equation (5.15)]. In this example it is easy to understand the dynamics of the spin star model but we are especially interested in the situation where the N qubit system is initially in a spin coherent state. In this case the dynamics are more complex and the exact expression (4.32) does not give much insight into the evolution of the system. In the next two sections we derive two effective Hamiltonians that help us to understand the dynamics in different parameter regimes.

4.3 Effective Hamiltonian: Large Detuning

If the detuning Δ is large we can approximate the eigenstates (4.22), (4.23) and eigenvalues (4.24), giving an effective Hamiltonian for the system.

The eigenstates and eigenvalues both depend on the quantity

$$\mu_m = \sqrt{\Delta^2 + 4\lambda^2[j(j+1) - m(m-1)]}, \tag{4.48}$$

which was defined in equation (4.17). When

$$\Delta \gg 2\lambda\sqrt{j(j+1) - \langle m^2\rangle + \langle m\rangle}, \tag{4.49}$$

where $\langle m\rangle = \left\langle \hat{J}_z \right\rangle$ and $\langle m^2\rangle = \left\langle \hat{J}_z^2 \right\rangle$ are the average values of m and m^2 in the initial state, we can expand the square root. This gives:

$$\mu_m \approx \Delta + \frac{2\lambda^2}{\Delta}\left[j(j+1) - m(m-1)\right]. \tag{4.50}$$

If the detuning Δ is large enough, we can say that $\mu_m \approx \Delta$ so that the eigenstates are

$$\left|\psi_m^+\right\rangle \approx |j, m-1\rangle\,|\uparrow\rangle \tag{4.51}$$

$$\left|\psi_m^-\right\rangle \approx |j, m\rangle\,|\downarrow\rangle\,. \tag{4.52}$$

In this case, the Hamiltonian is diagonal in the Dicke basis of the N spins and in the $\hat{\sigma}_z$ basis of the single spin. Substituting equation (4.50) into the expression for the eigenvalues of the spin star Hamiltonian gives

$$E_m^{\pm} \approx \omega\left(m - \frac{1}{2}\right) \pm \frac{\Delta}{2} \pm \frac{\lambda^2}{\Delta} j(j+1) \mp \frac{\lambda^2}{\Delta} m(m-1). \tag{4.53}$$

Since the state $|j, m\rangle\,|\uparrow\rangle$ is an eigenstate with eigenvalue E_{m+1}^+ and $|j, m\rangle\,|\downarrow\rangle$ is an eigenstate with eigenvalue E_m^- we can write an effective Hamiltonian for the spin star model:

$$\hat{H}_{SS}^{\Delta} = \left(\omega - \frac{\lambda^2}{\Delta}\right)\hat{J}_z + \frac{\Omega}{2}\hat{\sigma}_z + \frac{\lambda^2}{\Delta}\left(\hat{J}^2 - \hat{J}_z^2\right) \otimes \hat{\sigma}_z. \tag{4.54}$$

The Δ superscript in $\hat{H}_{SS}^{\Delta}$ is meant to indicate that this is the effective Hamiltonian for large detuning. The $\hat{J}_z^2 \otimes \hat{\sigma}_z$ term here is interesting since it can generate spin squeezing and multiple cat states of the N spin system (we discuss this in more detail in chapter 7).

Interestingly, following a different method, the effective Hamiltonian (4.54) can be derived without the need to diagonalise the spin star Hamiltonian [Gerry & Knight (2005); Klimov & Sanchez-Soto (2000)]. To see this, we do a unitary transformation of the spin star Hamiltonian, $e^{\hat{R}}\hat{H}_{SS}e^{-\hat{R}}$, where we define

$$\hat{R} = \frac{\lambda}{\Delta}\left(\hat{J}_-\hat{\sigma}_+ - \hat{J}_+\hat{\sigma}_-\right). \tag{4.55}$$

Expanding the exponentials, we find that

$$e^{\hat{R}}\hat{H}_{SS}e^{-\hat{R}} = \hat{H}_{SS} + \left[\hat{R}, \hat{H}_{SS}\right] + \frac{1}{2}\left[\hat{R}, \left[\hat{R}, \hat{H}_{SS}\right]\right] + \cdots \tag{4.56}$$

When $\Delta \gg N\lambda$, the operator $\hat{R}$ is small so that higher order terms in the sum (4.56) can be ignored. Keeping only the terms up to order $\mathcal{O}(\lambda/\Delta)$ gives

$$e^{\hat{R}}\hat{H}_{SS}e^{-\hat{R}} \approx \left(\omega - \frac{\lambda^2}{\Delta}\right)\hat{J}_z + \frac{\Omega}{2}\hat{\sigma}_z + \frac{\lambda^2}{\Delta}\left(\hat{J}^2 - \hat{J}_z^2\right) \otimes \hat{\sigma}_z. \tag{4.57}$$

This is the same as our effective Hamiltonian (4.54).

We close this section by taking the bosonic limit of Hamiltonian (4.54) for later reference. Writing $\hat{J}_z = \hat{a}^\dagger\hat{a} - j$ [see equation (2.100)], transforming $\lambda \to \lambda/\sqrt{2j}$ and taking the $j \to \infty$ limit gives (up to an added scalar):

$$\hat{H}_{JC}^{\Delta} = \omega\,\hat{a}^\dagger\hat{a} + \left(\frac{\Omega}{2} + \frac{\lambda^2}{2\Delta}\right)\hat{\sigma}_z + \frac{\lambda^2}{\Delta}\hat{a}^\dagger\hat{a} \otimes \hat{\sigma}_z. \tag{4.58}$$

In the next chapter we will see that this is the *dispersive limit* of the *Jaynes-Cummings model* for the interaction of an harmonic oscillator and a two-level system. We note that there is an interesting difference between our effective Hamiltonian (4.54) and its bosonic limit (4.58): although the oscillator analogue of the operator $\hat{J}_z^2$ is the operator $(\hat{a}^\dagger\hat{a})^2$, there are no non-linear terms like $(\hat{a}^\dagger\hat{a})^2$ in the dispersive limit of the Jaynes-Cummings model.

4.4 Effective Hamiltonian: On resonance and initial spin coherent state

In this section we derive an effective Hamiltonian for the spin star model with zero detuning ($\Delta = 0$), assuming that the N spin system is initially in a spin coherent state.

On resonance and in the interaction picture the spin star Hamiltonian is:

$$\hat{H}_{SS}^{I} = \lambda \left(\hat{J}_{-}\hat{\sigma}_{+} + \hat{J}_{+}\hat{\sigma}_{-} \right). \tag{4.59}$$

The unitary time evolution operator is thus

$$\hat{U}(t) = e^{-it\hat{H}_{SS}^{I}} = e^{-it\lambda\left(\hat{J}_{-}\hat{\sigma}_{+}+\hat{J}_{+}\hat{\sigma}_{-}\right)}. \tag{4.60}$$

Expanding the exponential as a Taylor series, and using the identities $\hat{\sigma}_{+}\hat{\sigma}_{+} = \hat{\sigma}_{-}\hat{\sigma}_{-} = 0$ and $\hat{\sigma}_{+}\hat{\sigma}_{-} = |\uparrow\rangle\langle\uparrow|$ and $\hat{\sigma}_{-}\hat{\sigma}_{+} = |\downarrow\rangle\langle\downarrow|$, gives

$$\hat{U}(t) = \sum_{k=0}^{\infty} \frac{(-it\lambda)^{k}}{k!} \left(\hat{J}_{-}\hat{\sigma}_{+} + \hat{J}_{+}\hat{\sigma}_{-} \right)^{k} = \tag{4.61}$$

$$= \sum_{k=0}^{\infty} \frac{(-it\lambda)^{k}}{k!} \left(\underbrace{\hat{J}_{-}\hat{J}_{+}\hat{J}_{-}...}_{k} \otimes \underbrace{\hat{\sigma}_{+}\hat{\sigma}_{-}\hat{\sigma}_{+}...}_{k} + \underbrace{\hat{J}_{+}\hat{J}_{-}\hat{J}_{+}...}_{k} \otimes \underbrace{\hat{\sigma}_{-}\hat{\sigma}_{+}\hat{\sigma}_{-}...}_{k} \right) = \tag{4.62}$$

$$= \sum_{k=0,\,(k\ \text{even}\ )}^{\infty} \frac{(-it\lambda)^{k}}{k!} \left[\left(\hat{J}_{-}\hat{J}_{+} \right)^{k/2} |\uparrow\rangle\langle\uparrow| + \left(\hat{J}_{+}\hat{J}_{-} \right)^{k/2} |\downarrow\rangle\langle\downarrow| \right] -$$
$$-i \sum_{k=0,\,(k\ \text{odd}\ )}^{\infty} \frac{(-i)^{k-1}(t\lambda)^{k}}{k!} \left[\hat{J}_{+} \left(\hat{J}_{-}\hat{J}_{+} \right)^{\frac{(k-1)}{2}} |\uparrow\rangle\langle\downarrow| + \hat{J}_{-} \left(\hat{J}_{+}\hat{J}_{-} \right)^{\frac{(k-1)}{2}} |\downarrow\rangle\langle\uparrow| \right] \tag{4.63}$$

$$= \cos\left(\lambda t \sqrt{\hat{J}_{-}\hat{J}_{+}} \right) |\uparrow\rangle\langle\uparrow| + \cos\left(\lambda t \sqrt{\hat{J}_{+}\hat{J}_{-}} \right) |\downarrow\rangle\langle\downarrow| -$$
$$-i \sin\left(\lambda t \sqrt{\hat{J}_{+}\hat{J}_{-}} \right) \left(\hat{J}_{+}\hat{J}_{-} \right)^{-1/2} \hat{J}_{+} |\downarrow\rangle\langle\uparrow| -$$
$$-i \sin\left(\lambda t \sqrt{\hat{J}_{-}\hat{J}_{+}} \right) \left(\hat{J}_{-}\hat{J}_{+} \right)^{-1/2} \hat{J}_{-} |\uparrow\rangle\langle\downarrow| . \tag{4.64}$$

For convenience we choose the initial spin coherent state $|j,\zeta\rangle_N$ of the N spins to be symmetric with respect to exchange of spins, i.e. with $j = N/2$ and we write $\left|\frac{N}{2},\zeta\right\rangle_N = |\zeta\rangle_N$. The initial state of the combined system is then

$$|\Psi(0)\rangle = |\zeta\rangle_N \otimes \left(\alpha \left|D_+^\phi(0)\right\rangle + \beta \left|D_-^\phi(0)\right\rangle\right), \tag{4.65}$$

where the central spin is in an arbitrary pure state written here in terms of the orthonormal basis states

$$\left|D_\pm^\phi(0)\right\rangle = \frac{1}{\sqrt{2}}\left(|\downarrow\rangle \pm e^{-i\phi}|\uparrow\rangle\right). \tag{4.66}$$

These states depend on the phase ϕ of the spin coherent state parameter $\zeta = |\zeta|e^{-i\phi}$. They are sometimes called "semi-classical eigenstates" [Gea-Banacloche (1991)] because they are eigenstates of $\hat{H}_{SS}^I = \lambda\left(\hat{J}_-\hat{\sigma}_+ + \hat{J}_+\hat{\sigma}_-\right)$ if we replace the operators $\hat{J}_\pm$ with their expectation values in the initial spin coherent state of the N spins. We consider separately the evolution of the two orthonormal states $|\Psi^\pm(0)\rangle = |\zeta\rangle_N \left|D_\pm^\phi(0)\right\rangle$ by our Hamiltonian since the evolution of an arbitrary initial state (4.65) is just a superposition of these two solutions. Depending on whether the initial state of the qubit is $\left|D_+^\phi(0)\right\rangle$ or $\left|D_-^\phi(0)\right\rangle$ we write this unitary operator as $\hat{U}^+(t)$ or $\hat{U}^-(t)$, i.e. $\hat{U}(t) = \hat{U}^+(t) + \hat{U}^-(t)$ with $\hat{U}^\pm(t) \equiv U(t)\left|D_\pm^\phi(0)\right\rangle\left\langle D_\pm^\phi(0)\right|$. From (4.64) we find that

$$\begin{aligned}
\hat{U}^\pm(t) \;=\; & \left[\frac{1}{\sqrt{2}}\cos\left(\lambda t\sqrt{\hat{J}_+\hat{J}_-}\right)|\downarrow\rangle \mp \right. \\
& \mp i\frac{e^{-i\phi}}{\sqrt{2}}\sin\left(\lambda t\sqrt{\hat{J}_+\hat{J}_-}\right)\left(\hat{J}_+\hat{J}_-\right)^{-1/2}\hat{J}_+|\downarrow\rangle \\
& \pm\frac{e^{-i\phi}}{\sqrt{2}}\cos\left(\lambda t\sqrt{\hat{J}_-\hat{J}_+}\right)|\uparrow\rangle - \\
& \left. -\frac{i}{\sqrt{2}}\sin\left(\lambda t\sqrt{\hat{J}_-\hat{J}_+}\right)\left(\hat{J}_-\hat{J}_+\right)^{-1/2}\hat{J}_-|\uparrow\rangle\right]\left\langle D_\pm^\phi\right|.
\end{aligned} \tag{4.67}$$

This is still an exact expression that does not give much insight into the features of the system as it evolves in time. We now use the approximation that for $1/\sqrt{N} \ll |\zeta| \ll \sqrt{N}$ the spin coherent state $|\zeta\rangle_N$ is an approximate eigenstate of

the operators $\left(\hat{J}_-\hat{J}_+\right)^{-1/2}\hat{J}_-$ and $\left(\hat{J}_+\hat{J}_-\right)^{-1/2}\hat{J}_+$ with eigenvalues $e^{-i\phi}$ and $e^{i\phi}$ respectively. (The proof of this, which we published in Dooley & Spiller (2014), is given in appendix A.2.) This approximation is valid for all times and has an error of leading order $\frac{|\zeta|^2}{N}+\frac{1}{N|\zeta|^2}$ in the sense that $\left(\hat{J}_-\hat{J}_+\right)^{-1/2}\hat{J}_-\left|\zeta\right\rangle_N = e^{-i\phi}\left|\zeta\right\rangle_N+\left|\delta\psi\right\rangle$ with $|\langle\delta\psi|\delta\psi\rangle|^2 \sim \mathcal{O}\left(\frac{|\zeta|^2}{N}+\frac{1}{N|\zeta|^2}\right)$ (see appendix A.2 for details). It allows us to replace the operator $\left(\hat{J}_-\hat{J}_+\right)^{-1/2}\hat{J}_-$ with the complex number $e^{-i\phi}$ and to replace the operator $\left(\hat{J}_+\hat{J}_-\right)^{-1/2}\hat{J}_+$ with $e^{i\phi}$ in equation (4.67) above. This gives:

$$\hat{U}^{\pm}(t) \approx \left[\frac{1}{\sqrt{2}}e^{\mp i\lambda t\sqrt{\hat{J}_+\hat{J}_-}}\left|\downarrow\right\rangle \pm \frac{e^{-i\phi}}{\sqrt{2}}e^{\mp i\lambda t\sqrt{\hat{J}_-\hat{J}_+}}\left|\uparrow\right\rangle\right]\left\langle D_\pm^\phi\right|. \tag{4.68}$$

Now, using the identities $\hat{J}_+\hat{J}_- = \hat{J}^2-\hat{J}_z^2+\hat{J}_z$ and $\hat{J}_-\hat{J}_+ = \hat{J}^2-\hat{J}_z^2-\hat{J}_z$ and noticing that

$$e^{\mp i\lambda t\sqrt{\hat{J}^2-\hat{J}_z^2+\hat{J}_z}}\left|\downarrow\right\rangle = e^{\mp i\lambda t\sqrt{\hat{J}^2-\hat{J}_z^2-\hat{J}_z\otimes\hat{\sigma}_z}}\left|\downarrow\right\rangle, \tag{4.69}$$

$$e^{\mp i\lambda t\sqrt{\hat{J}^2-\hat{J}_z^2-\hat{J}_z}}\left|\uparrow\right\rangle = e^{\mp i\lambda t\sqrt{\hat{J}^2-\hat{J}_z^2-\hat{J}_z\otimes\hat{\sigma}_z}}\left|\uparrow\right\rangle, \tag{4.70}$$

we can write (4.68) as

$$\hat{U}^{\pm}(t) = e^{\mp i\lambda t\sqrt{\hat{J}^2-\hat{J}_z^2-\hat{J}_z\otimes\hat{\sigma}_z}}\left|D_\pm^\phi\right\rangle\left\langle D_\pm^\phi\right|. \tag{4.71}$$

In other words, the effective Hamiltonian given the initial state $\left|\Psi^{\pm}(0)\right\rangle = \left|\zeta\right\rangle_N\left|D_\pm^\phi\right\rangle$ is

$$\hat{H}_{SS}^{\pm} = \pm\lambda\sqrt{\hat{J}^2-\hat{J}_z^2-\hat{J}_z\otimes\hat{\sigma}_z}. \tag{4.72}$$

If the initial state of the N spins is a spin coherent state $\left|j,\zeta\right\rangle_N$ with arbitrary choice of j, we arrive at the same effective Hamiltonian (4.72). Since we have chosen the initial spin coherent state to be in the $j = N/2$ subspace it is an eigenstate of $\hat{J}^2$ with eigenvalue $\frac{N}{2}\left(\frac{N}{2}+1\right)$ so that we can also write (4.72) as

$$\hat{H}_{SS}^{\pm} = \pm\lambda\sqrt{\left(\hat{a}_\downarrow^\dagger\hat{a}_\downarrow+\left|\downarrow\right\rangle\left\langle\downarrow\right|\right)\left(\hat{a}_\uparrow^\dagger\hat{a}_\uparrow+\left|\uparrow\right\rangle\left\langle\uparrow\right|\right)}, \tag{4.73}$$

where $\hat{a}_\uparrow^\dagger \hat{a}_\uparrow = \frac{N}{2} + \hat{J}_z = \sum_{i=1}^N |\uparrow_i\rangle \langle\uparrow_i|$ and $\hat{a}_\downarrow^\dagger \hat{a}_\downarrow = \frac{N}{2} - \hat{J}_z = \sum_{i=1}^N |\downarrow_i\rangle \langle\downarrow_i|$ are as defined earlier in equations 2.96 and 2.97.

The Hamiltonian (4.73) has an interesting symmetry beyond that of our starting Hamiltonian, $\hat{H}_{SS}^I = \lambda\left(\hat{J}_-\hat{\sigma}_+ + \hat{J}_+\hat{\sigma}_-\right)$: while $\hat{H}_{SS}^I$ is symmetric only with respect to exchange of *outer* spins, $\hat{H}_{SS}^\pm$ is symmetric with respect to exchange of *any* two spins (but only if the initial state of the central spin is $\left|D_\pm^\phi(0)\right\rangle$). Also, unlike our starting Hamiltonian $\hat{H}_{SS}^I = \lambda\left(\hat{J}_-\hat{\sigma}_+ + \hat{J}_+\hat{\sigma}_-\right)$ the effective Hamiltonian $\hat{H}_{SS}^\pm$ is diagonal in the Dicke state basis of the N qubits, in the sense that $\left\langle \frac{N}{2}, m\right| \hat{H}_{SS}^\pm \left|\frac{N}{2}, m'\right\rangle \propto \delta_{mm'}$.

For $N \gg 1$, the restriction $1/\sqrt{N} \ll |\zeta| \ll \sqrt{N}$ on our initial spin coherent state is not at all severe. We also note that – unlike the effective Hamiltonian for large detuning (4.54) – our on-resonance effective Hamiltonian (4.72) is valid for all times. On the other hand, the effective Hamiltonian for large detuning, is not restricted to initial spin coherent states.

In the remaining chapters we use the effective Hamiltonians derived in this chapter to better understand the dynamics of the spin star model.

Chapter 5

The Jaynes-Cummings Approximation

In this chapter we investigate the dynamics of the spin star model in the bosonic approximation (see section 2.3), that is, when the number of excitations in the system is small compared to the total number of spins.

This parameter regime is of interest because in some setups low excitation numbers may be easier to access experimentally than high excitation of the spin system. For example, if the spin coherent state $|\downarrow\rangle^{\otimes N}$ is easily prepared, e.g., by cooling the spin system, then any other spin coherent states can be generated by applying a uniform external magnetic field to the spin system for a fixed time [see equation (2.65)]. If there are constraints on the power of the external field that can be applied, then it may be possible only to generate spin coherent states with low spin excitation, i.e., in the bosonic approximation (this was discussed briefly at the end of section 2.2.1).

The bosonic approximation is also of interest because in this parameter regime the dynamics of the system resembles the Jaynes-Cummings model for the interaction of an harmonic oscillator with a two-level system. Since the Jaynes-Cummings is very well understood we can look to the Jaynes-Cummings model for ideas for generating non-classical states of the N spin system. Some if these ideas might be easier to implement in spin systems than for other implementations of the Jaynes-Cummings model (e.g., an electromagnetic field mode interacting

with a two-level atom) since different implementations have different decoherence mechanisms.

We begin this chapter by reviewing the Jaynes-Cummings model, including the phenomenon of collapse and revival, and the generation of harmonic oscillator cat states. Then in section 5.2 we consider the analogous dynamics for the spin star model. The results presented here were published in Dooley *et al.* (2013).

5.1 The Jaynes-Cummings Model

In this section we review the Jaynes-Cummings model for the interaction of a harmonic oscillator and a two-level system. This model was first introduced to describe the interaction of a two-level atom with a mode of the electromagnetic field [Jaynes & Cummings (1963)]. Since then it has been implemented experimentally for various systems, e.g. an effective two-level atom in a microwave cavity [Brune *et al.* (1996)] and an ion in a harmonic trap [Meekhof *et al.* (1996)]. It has the advantage that its eigenvalues and eigenstates can be found, so that given the initial conditions the state of the system at any later time can be calculated.

The Jaynes-Cummings Hamiltonian is [Jaynes & Cummings (1963)]:

$$\hat{H}_{JC} = \frac{\Omega}{2}\hat{\sigma}_z + \omega\left(\hat{a}^\dagger\hat{a} + \frac{1}{2}\right) + \lambda\left(\hat{a}\,\hat{\sigma}_+ + \hat{a}^\dagger\hat{\sigma}_-\right). \tag{5.1}$$

We denote its eigenvalues and eigenstates by $\hat{H}_{JC}\left|\psi_n^\pm\right\rangle = E_n^\pm\left|\psi_n^\pm\right\rangle$. These eigenvalues and eigenstates, can be determined in the same way as for the spin star model in section 4.2. Defining the detuning $\Delta = \Omega - \omega$ and the *Rabi frequency*, $\mu_n = \sqrt{\Delta^2 + 4\lambda^2 n}$ one finds that [Gerry & Knight (2005)]

$$\left|\psi_0\right\rangle = \left|0\right\rangle\left|\downarrow\right\rangle \qquad ; \qquad E_0 = -\frac{\Delta}{2}, \tag{5.2}$$

for $n = 0$, and:

$$\left|\psi_n^+\right\rangle = \sqrt{\frac{\mu_n - \Delta}{2\mu_n}}\left|n\right\rangle\left|\downarrow\right\rangle + \sqrt{\frac{\mu_n + \Delta}{2\mu_n}}\left|n-1\right\rangle\left|\uparrow\right\rangle, \tag{5.3}$$

$$\left|\psi_n^-\right\rangle = \sqrt{\frac{\mu_n + \Delta}{2\mu_n}}\left|n\right\rangle\left|\downarrow\right\rangle - \sqrt{\frac{\mu_n - \Delta}{2\mu_n}}\left|n-1\right\rangle\left|\uparrow\right\rangle, \tag{5.4}$$

$$E_n^{\pm} = \omega n \pm \frac{1}{2}\mu_n, \tag{5.5}$$

for $n \geq 1$. Rearranging equations (5.3) and (5.4) we can write

$$\left|n\right\rangle\left|\downarrow\right\rangle = \sqrt{\frac{\mu_n - \Delta}{2\mu_n}}\left|\psi_n^+\right\rangle + \sqrt{\frac{\mu_n + \Delta}{2\mu_n}}\left|\psi_n^-\right\rangle, \tag{5.6}$$

$$\left|n-1\right\rangle\left|\uparrow\right\rangle = \sqrt{\frac{\mu_n + \Delta}{2\mu_n}}\left|\psi_n^+\right\rangle - \sqrt{\frac{\mu_n - \Delta}{2\mu_n}}\left|\psi_n^-\right\rangle. \tag{5.7}$$

Given (5.6) and (5.7) and the initial state in the Fock basis, we can find the state at any later time, following the same procedure as in section 4.2 for the spin star model. However, the most general form of the exact solution is unwieldy and does not give much intuition for the dynamics of the system. Such an intuition can be provide by a combination of numerics and approximations. We see this in the next sections, both for large detuning (section 5.1.1) and on-resonance (section 5.1.2).

5.1.1 The dispersive limit

When $\Delta \gg \lambda$ we can derive an effective Hamiltonian for the Jaynes-Cummings model in the same way as in section 4.3 for the spin star Hamiltonian. Defining the "small" operator $\hat{R} = \frac{\lambda}{\Delta}\left(\hat{a}\hat{\sigma}_+ - \hat{a}^\dagger\hat{\sigma}_-\right)$, we find that

$$e^{\hat{R}}\hat{H}_{JC}e^{-\hat{R}} = \hat{H}_{JC} + \left[\hat{R}, \hat{H}_{JC}\right] + \frac{1}{2}\left[\hat{R}, \left[\hat{R}, \hat{H}_{JC}\right]\right] + \cdots \tag{5.8}$$

$$\approx \omega\,\hat{a}^\dagger\hat{a} + \left(\frac{\Omega}{2} + \frac{\lambda^2}{2\Delta}\right)\hat{\sigma}_z + \frac{\lambda^2}{\Delta}\hat{a}^\dagger\hat{a}\otimes\hat{\sigma}_z. \tag{5.9}$$

This is known as the *dispersive limit* of the Jaynes-Cummings model [Gerry & Knight (2005)]. Hamiltonian (5.9) is identical to Hamiltonian (4.58), the bosonic limit of the corresponding approximation for the spin star model.

The most interesting part in (5.9) is the third term, $\frac{\lambda^2}{\Delta}\hat{a}^\dagger\hat{a}\otimes\hat{\sigma}_z$. We can isolate this term by rotating to an interaction picture with respect to the bare Hamiltonian $\omega\,\hat{a}^\dagger\hat{a} + \left(\frac{\Omega}{2} + \frac{\lambda^2}{2\Delta}\right)\hat{\sigma}_z$. The interaction picture Hamiltonian is then

$$\hat{H}_{JC}^{I,\Delta} = \frac{\lambda^2}{\Delta}\hat{a}^\dagger\hat{a}\otimes\hat{\sigma}_z, \tag{5.10}$$

where the superscript I indicates that we are in the interaction picture. If the oscillator is initially in the coherent state $|\alpha\rangle$ and the atom in the excited state $|\uparrow\rangle$, then the system evolves to:

$$|\alpha\rangle\,|\uparrow\rangle \to \left|\alpha e^{-it\lambda^2/\Delta}\right\rangle|\uparrow\rangle\,. \tag{5.11}$$

This is a separable state of the atom-oscillator system that can be easily visualised in phase space: the initial oscillator coherent state simply rotates clockwise around the origin in phase space. Similarly, if the oscillator is initially in the coherent state $|\alpha\rangle$ and the atom in the ground state $|\downarrow\rangle$, then the system evolves to:

$$|\alpha\rangle\,|\downarrow\rangle \to \left|\alpha e^{it\lambda^2/\Delta}\right\rangle|\downarrow\rangle\,. \tag{5.12}$$

In this case the coherent state rotates anti-clockwise in phase space. If the initial state of the atom is a superposition of $|\uparrow\rangle$ and $|\downarrow\rangle$ then the atom and the oscillator become entangled [in a superposition of (5.11) and (5.12)], but are periodically separable at integer multiples of the time $t_r = \pi\Delta/\lambda^2$ when the counter-rotating coherent states $\left|\alpha e^{-it\lambda^2/\Delta}\right\rangle$ and $\left|\alpha e^{it\lambda^2/\Delta}\right\rangle$ overlap in phase space.

5.1.2 On resonance

Separating the full Jaynes-Cummings Hamiltonian (5.1) into a "bare" Hamiltonian, $\hat{H}_0 = \omega\left(\hat{a}^\dagger\hat{a} + \frac{1}{2} + \frac{\hat{\sigma}_z}{2}\right)$ and an interaction Hamiltonian $\hat{H}_{JC}^{int} = \frac{\Delta}{2}\hat{\sigma}_z + \lambda\left(\hat{a}\,\hat{\sigma}_+ + \hat{a}^\dagger\hat{\sigma}_-\right)$, we can transform to the interaction picture:

$$\hat{H}_{JC}^{I} = e^{i\omega t\hat{H}_0}\hat{H}_{JC}^{int}e^{-i\omega t\hat{H}_0} = \frac{\Delta}{2}\hat{\sigma}_z + \lambda\left(\hat{a}\,\hat{\sigma}_+ + \hat{a}^\dagger\hat{\sigma}_-\right). \tag{5.13}$$

The resonance condition for the Jaynes-Cummings Hamiltonian is that $\Omega = \omega$ or, since $\Delta = \Omega - \omega$, that the detuning Δ is zero. In this case, the Hamiltonian in the interaction picture takes a simple form:

$$\hat{H}^I_{JC} = \lambda\,(\hat{a}\,\hat{\sigma}_+ + \hat{a}^\dagger\hat{\sigma}_-). \tag{5.14}$$

We note that, mathematically, this interaction Hamiltonian can be obtained from the full Hamiltonian (5.1) by setting $\Omega = \omega = 0$. It follows that the eigenstates and eigenvalues of $\hat{H}^I_{JC}$ can be obtained by simply setting $\Omega = \omega = 0$ in equations (5.3), (5.4) and (5.5) above. We assume the resonance condition and we work in the interaction picture for the remainder of this section.

If the initial state of the system is $|\psi(0)\rangle = |n\rangle\,|\uparrow\rangle$ we find from equation (5.7) that the system evolves to

$$\left|\psi^I(t)\right\rangle = \cos\left(\lambda t\sqrt{n+1}\right)|n\rangle\,|\uparrow\rangle - i\sin\left(\lambda t\sqrt{n+1}\right)|n+1\rangle\,|\downarrow\rangle \tag{5.15}$$

where the superscript I indicates that the state $\left|\psi^I(t)\right\rangle = e^{i\omega t\hat{H}_0}\,|\psi(t)\rangle$ is in the interaction picture. The state $\left|\psi^I(t)\right\rangle$ oscillates between the orthogonal states $|n\rangle\,|\uparrow\rangle$ and $|n+1\rangle\,|\downarrow\rangle$. The expectation value $\langle\hat{\sigma}_z(t)\rangle$, sometimes called the "atomic inversion", oscillates sinusoidally at the (on resonance) Rabi frequency $\mu_{n+1} = 2\lambda\sqrt{n+1}$:

$$\langle\hat{\sigma}_z(t)\rangle = \cos\left(2\lambda t\sqrt{n+1}\right). \tag{5.16}$$

These oscillations are called *Rabi oscillations* [Gerry & Knight (2005)]. Even for an harmonic oscillator initially in its vacuum state ($n = 0$) there are *vacuum Rabi oscillations*, plotted in figure 5.1. The green line in figure 5.1 shows the *linear entropy* of the two-level atom, defined as

$$S_L(\rho_A) = 1 - \mathrm{Tr}\left[\rho_A^2\right], \tag{5.17}$$

where ρ_A is the reduced state of the atom. Since the combined oscillator-atom system is in a pure state, it quantifies the entanglement between the oscillator and the two level system.

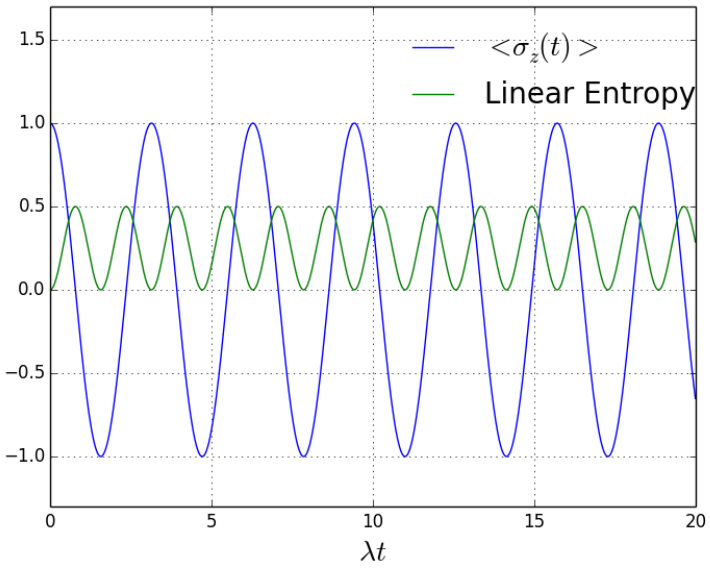

Figure 5.1: Rabi oscillations (blue) and atomic linear entropy (green) for initial state $|n\rangle|\uparrow\rangle$ with $n = 0$.

If the oscillator is initially in a coherent state and the atom in its excited state, the state of the system after time t is:

$$\left|\psi^I(t)\right\rangle = \sum_{n=0}^{\infty} C_n \left(\cos\lambda t\sqrt{n+1}\,|n\rangle\,|\uparrow\rangle - i\sin\lambda t\sqrt{n+1}\,|n+1\rangle\,|\downarrow\rangle\right), \tag{5.18}$$

a superposition of the solutions (5.15) for every value of n, weighted by the coherent state amplitudes $C_n = e^{-|\alpha|^2/2}\alpha^n/\sqrt{n!}$. The atomic inversion is

$$\langle\hat{\sigma}_z(t)\rangle = \sum_{n=0}^{\infty} |C_n|^2 \cos 2\lambda t\sqrt{n+1}, \tag{5.19}$$

a superposition of Rabi oscillations with frequencies weighted by the Poisson distribution $|C_n|^2$. For $\alpha = 4$ the atomic inversion is plotted in figure 5.2. There are three timescales that encapsulate the key features of the atomic inversion in figure 5.2. These are [Gerry & Knight (2005)]:

- The *Rabi time*, $\lambda t_R \approx \frac{\pi}{|\alpha|}$: the period of the Rabi oscillations,

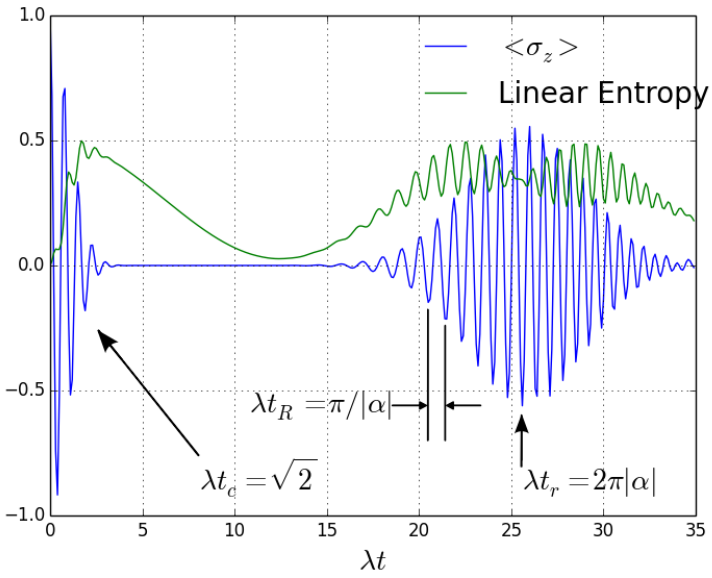

Figure 5.2: Collapse and revival of Rabi oscillations (blue) and atomic linear entropy (green) for initial state $|\alpha\rangle\,|\uparrow\rangle$ with $\alpha = 4$.

- The *collapse time*, $\lambda t_c \approx \sqrt{2}$: the decay time for the initial (Gaussian) collapse of the Rabi oscillations,
- The *revival time*, $\lambda t_r \approx 2\pi|\alpha|$: the time at which the Rabi oscillations revive to a peak.

This is the well known phenomenon of "collapse and revival" of Rabi oscillations in the resonant Jaynes-Cummings model. The timescales above can be found by approximating the expression for the atomic inversion (5.19) [Gerry & Knight (2005)]. We do not give the details of this approximation because we find these timescales by a different argument below.

Also of interest is the linear entropy of the atom, the green line in figure 5.2. We see that the linear entropy rises sharply as the Rabi oscillations decay, showing that the atom and the oscillator become entangled. Then, at about half the revival time the linear entropy dips almost to zero indicating that the oscillator and atom are close to a separable state.

Gea-Banacloche (1990, 1991) has made an insightful analysis of the resonant Jaynes-Cummings model for an initial coherent state $|\alpha\rangle$. He has shown that when $|\alpha|^2 \gg 1$, there are two initially orthogonal atomic states,

$$\left|D_{\pm}^{\phi}(0)\right\rangle = \frac{1}{\sqrt{2}}\left(|\downarrow\rangle \pm e^{-i\phi}\,|\uparrow\rangle\right), \tag{5.20}$$

that – to a good approximation – evolve without entangling with the harmonic oscillator. In equation (5.20), ϕ is the phase of the coherent state amplitude $\alpha = |\alpha|e^{-i\phi}$. We remind the reader that in the previous chapter [equation (4.66)] we already defined the state $\left|D_{\pm}^{\phi}(0)\right\rangle$ in the context of the spin star model (although there ϕ is the phase of the spin coherent state amplitude $\zeta = |\zeta|e^{-i\phi}$). For the Jaynes-Cummings model these states $\left|D_{\pm}^{\phi}(0)\right\rangle$ are eigenstates of the "semi-classical" Hamiltonian

$$\hat{H}_{\alpha} = \langle\alpha|\,\hat{H}_{JC}^{I}\,|\alpha\rangle = \lambda(\alpha\hat{\sigma}_{+} + \alpha^{*}\hat{\sigma}_{-}), \tag{5.21}$$

that is obtained by replacing the creation and annihilation operators in $\hat{H}_{JC}^{I}$ with their expectation values for the initial coherent state. The evolving separable state is [Gea-Banacloche (1991)]:

$$\left|D_{\pm}^{\phi}(0)\right\rangle|\alpha\rangle \rightarrow |\Phi_{\pm}(t)\rangle\left|D_{\pm}^{\phi}(t)\right\rangle, \tag{5.22}$$

where

$$|\Phi_{\pm}(t)\rangle = e^{\mp i\lambda t\sqrt{\hat{a}^{\dagger}\hat{a}}}\,|\alpha\rangle \tag{5.23}$$

$$\left|D_{\pm}^{\phi}(t)\right\rangle = e^{\mp i\lambda t\frac{|\uparrow\rangle\langle\uparrow|}{2|\alpha|}}\left|D_{\pm}^{\phi}(0)\right\rangle = \frac{1}{\sqrt{2}}\left(|\downarrow\rangle \pm e^{\mp\frac{i\lambda t}{2|\alpha|}}e^{-i\phi}\,|\uparrow\rangle\right). \tag{5.24}$$

To get a clearer idea of the evolution of the oscillator states $|\Phi_{\pm}(t)\rangle = e^{\mp i\lambda t\sqrt{\hat{a}^{\dagger}\hat{a}}}\,|\alpha\rangle$ we expand the operators $\sqrt{\hat{a}^{\dagger}\hat{a}}$ around their average values in the initial coherent state $|\alpha\rangle$[1] [Robinett (2004)]. This is a useful step because the initial coherent state number distribution is narrowly peaked around its average value and, since the number operator $\hat{a}^{\dagger}\hat{a}$ commutes with the evolution Hamiltonian $\sqrt{\hat{a}^{\dagger}\hat{a}}$, this

[1] We note that the evolution by the non-linear Hamiltonian in (5.23) has also been studied – in a slightly different way – by Gilchrist *et al.* (2003).

property of the number distribution stays fixed throughout the evolution. Writing $\sqrt{\hat{a}^\dagger\hat{a}} = \sqrt{\langle\hat{a}^\dagger\hat{a}\rangle + (\hat{a}^\dagger\hat{a} - \langle\hat{a}^\dagger\hat{a}\rangle)}$ and expanding, we find that

$$\sqrt{\hat{a}^\dagger\hat{a}} = \langle\hat{a}^\dagger\hat{a}\rangle^{1/2} + \frac{\Delta(\hat{a}^\dagger\hat{a})}{2\langle\hat{a}^\dagger\hat{a}\rangle^{1/2}} - \frac{\Delta(\hat{a}^\dagger\hat{a})^2}{8\langle\hat{a}^\dagger\hat{a}\rangle^{3/2}} + ..., \tag{5.25}$$

where we have defined $\Delta(\hat{a}^\dagger\hat{a}) = \hat{a}^\dagger\hat{a} - \langle\hat{a}^\dagger\hat{a}\rangle$. Since the expectation value $\langle\hat{a}^\dagger\hat{a}\rangle = |\alpha|^2$ and the operator $\Delta(\hat{a}^\dagger\hat{a})$ is of the order $\sqrt{\mathrm{Var}(\hat{a}^\dagger\hat{a})} = |\alpha|$, higher order terms in (5.25) are of the order $|\alpha|^{-3}$ and can be ignored when $|\alpha| \gg 1$. Since each of the terms in the expansion (5.25) commute with each other, their effect on the evolution can be considered separately. Each of these terms corresponds to dynamics on a different timescale. If the atom is initially in the state $|D_+(0)\rangle$ or the state $|D_-(0)\rangle$, then the first term just gives a global phase factor that can be ignored:

$$e^{\mp i\lambda t\langle\hat{a}^\dagger\hat{a}\rangle^{1/2}}|\alpha\rangle = e^{\mp i\lambda t|\alpha|}|\alpha\rangle \sim |\alpha\rangle\,. \tag{5.26}$$

If, however, the atom is initially is a superposition of $|D_+(0)\rangle$ and $|D_-(0)\rangle$, this will be an oscillating relative phase. The period of this oscillation is $t_R = \frac{\pi}{\lambda|\alpha|}$, exactly the Rabi period in figure 5.2.

If the atom is initially in the state $|D_+(0)\rangle$, the second term in (5.25) causes the coherent state to evolve clockwise in phase space:

$$e^{-it\lambda\Delta(\hat{a}^\dagger\hat{a})/(2|\alpha|)}|\alpha\rangle = e^{it\lambda|\alpha|/2}\left|\alpha e^{-it\lambda/(2|\alpha|)}\right\rangle, \tag{5.27}$$

as shown in figure 5.3. If the atom is initially in the state $|D_-(0)\rangle$ the coherent state rotates in the opposite direction:

$$e^{it\lambda\Delta(\hat{a}^\dagger\hat{a})/(2|\alpha|)}|\alpha\rangle = e^{-it\lambda|\alpha|/2}\left|\alpha e^{it\lambda/(2|\alpha|)}\right\rangle. \tag{5.28}$$

The collapse in Rabi oscillation and the concurrent increase in entanglement can be understood as occurring when these counter-rotating wave packets become distinguishable from one another. This distinguishability can be quantified by the overlap [Gerry & Knight (2005)]:

$$\left|\langle\alpha e^{-it\lambda/(2|\alpha|)}|\alpha e^{it\lambda/(2|\alpha|)}\rangle\right| = e^{-2|\alpha|\sin\frac{t\lambda}{2|\alpha|}}. \tag{5.29}$$

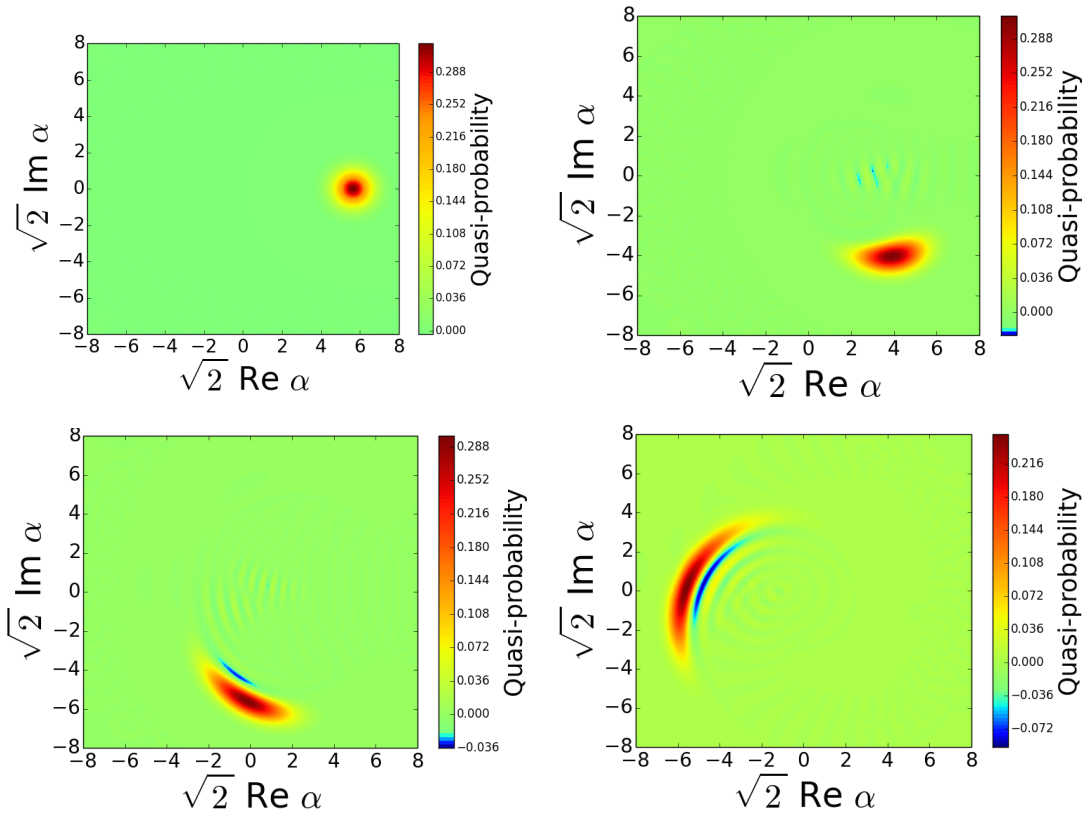

Figure 5.3: Wigner functions for the initial state $|\alpha\rangle \left|D_+^\phi(0)\right\rangle$ (with $\alpha = 4$) evolving by Jaynes-Cummings Hamiltonian at various times. Top left: $t = 0$, the coherent state $|\alpha\rangle$ with $\alpha = 4$. Top right: $t = t_r/4$. Bottom left: $t = t_r/2$. Bottom right: $t = t_r$.

For short times we can approximate $\sin \frac{t\lambda}{2|\alpha|} \approx \frac{t\lambda}{2|\alpha|}$ so that

$$\left|\langle \alpha e^{-it\lambda/(2|\alpha|)} | \alpha e^{it\lambda/(2|\alpha|)} \rangle\right| \approx e^{-t\lambda}. \tag{5.30}$$

By setting the exponent in (5.30) equal to $\sqrt{2}$ we find that the characteristic time of this decay is $t_c = \sqrt{2}/\lambda$. The revival comes about when the counter-rotating wave packets overlap again in phase space. From equations (5.27) and (5.28), this happens at the time $t_r = 2\pi|\alpha|/\lambda$, as illustrated in figure 5.2.

We see in figure 5.3 that as the coherent state rotates in phase space it become distorted. This is primarily due to the third term in (5.25). The distortion creates a "crescent" shape that is reminiscent of the number squeezed states introduced in section 2.1.3. In equation (2.30) we introduced the quantity,

$$\chi_n^2 = \lim_{\epsilon \to 0} \min_{\alpha' \in \mathbb{C}} \frac{\mathrm{Var}[(\hat{a}^\dagger + \alpha'^*)(\hat{a} + \alpha')] + \epsilon}{\langle (\hat{a}^\dagger + \alpha'^*)(\hat{a} + \alpha') \rangle + \epsilon}, \tag{5.31}$$

to quantify number squeezing. The minimisation over the primed parameter α' is necessary to detect the number squeezing of displaced "crescent" states. In figure 5.4 we plot

$$\frac{\mathrm{Var}[(\hat{a}^\dagger + \alpha'^*)(\hat{a} + \alpha')]}{\langle (\hat{a}^\dagger + \alpha'^*)(\hat{a} + \alpha') \rangle} \tag{5.32}$$

for initial state $|\alpha\rangle\,|D_+(0)\rangle$ evolving by the on-resonance Jaynes-Cummings Hamiltonian (see figure 5.3 for the corresponding Wigner functions). We plot this against time on the horizontal axis and against a range of (real) values of α' on the vertical axis. We see that for no displacement ($\alpha' = 0$) the amount of number squeezing achieved is small. (Up to an added constant, this corresponds to the usual Mandel Q-parameter for the state [see equation 2.28].) By displacing the state, however, a significant amount of number squeezing is revealed (the green area in figure 5.4). This was first pointed out by Dutra *et al.* (1994)[1].

Finally, we consider the evolution of the atom in equation (5.24). At a time $t_a = \pi|\alpha|/\lambda$, which is equal to half the revival time ($t_a = t_r/2$) we notice that $|D_+(t)\rangle$ and $|D_-(t)\rangle$ coincide [Gea-Banacloche (1991)]:

[1] In Dutra *et al.* (1994), however, they do not use a number squeezing measure like (5.31). Instead they use the usual Mandel Q-parameter to measure number squeezing, but achieve the displacement α' by driving the atom with an external electromagnetic field of amplitude α'. For the Jaynes-Cummings model, both this approach and the one presented here are equivalent.

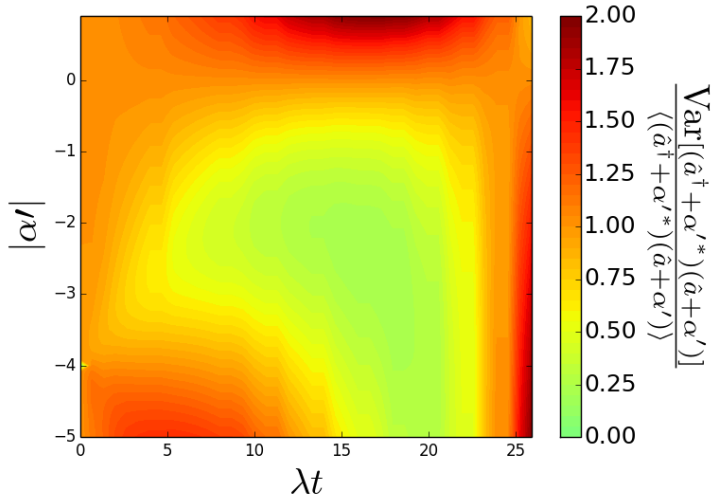

Figure 5.4: The number squeezing (5.32) for the initial state $|\alpha\rangle\,|D_+(0)\rangle$ (with $\alpha = 4$) evolving by the Jaynes-Cummings Hamiltonian. Low values (green areas) correspond to significant number squeezing. We see that for no displacement ($\alpha' = 0$) the amount of number squeezing achieved is small. By displacing the state ($\alpha' \neq 0$), however, a significant amount of number squeezing is revealed (the green area).

$$|D_+(t_a)\rangle = |D_-(t_a)\rangle = \frac{1}{\sqrt{2}}\left(|{\downarrow}\rangle - ie^{-i\phi}\,|{\uparrow}\rangle\right). \tag{5.33}$$

This is sometimes called the *attractor state* of the atom [Shore & Knight (1993)] and it is independent of the initial atom state. Since any pure state of the qubit can be written as a superposition of $|D_+(0)\rangle$ and $|D_-(0)\rangle$, it follows that any initial atom state will converge to the attractor state at $t_a = \pi|\alpha|/\lambda$. This explains the dip in qubit entropy at half the revival time in figure 5.2 (the green line). Since the state of the composite atom-oscillator system is pure at all times, the field must also be in a pure state at t_a. The quantum information in the initial state of the atom has been "swapped" into the state of the oscillator at this time. In particular, for an initial atom state that is an equal superposition of $|D_+(0)\rangle$ and $|D_-(0)\rangle$, the field at the attractor time $t_a = t_r/2$ is in the cat state [Bužek *et al.* (1992); Gea-Banacloche (1991)]

$$\mathcal{N}(|\Phi_+(t_a) + |\Phi_-(t_a)\rangle\rangle), \tag{5.34}$$

where $|\Phi_\pm(t)\rangle$ is defined in equation (5.23) and $\mathcal{N}$ is for normalisation (since $|\Phi_+(t_a)\rangle$ and $|\Phi_-(t_a)\rangle$ are not orthogonal). The Wigner function for this state is shown in figure 5.5.

5.2 The JC approximation of the spin star model

The spin star Hamiltonian (4.2),

$$\hat{H}_{SS} = \frac{\Omega}{2}\hat{\sigma}_z + \omega\hat{J}_z + \lambda\left(\hat{J}_+\hat{\sigma}_- + \hat{J}_-\hat{\sigma}_+\right), \tag{5.35}$$

is superficially similar to the Jaynes-Cummings Hamiltonian (5.1). If we consider only the part of $\hat{H}_{SS}$ that acts on the symmetric subspace ($j = N/2$) of the outer spins, then by applying the Holstein-Primakoff transformations [(2.98), (2.99) and (2.100)], the Hamiltonian can be written as

$$\hat{H}_{SS} = \frac{\Omega}{2}\hat{\sigma}_z + \omega\left(\hat{a}_\uparrow^\dagger\hat{a}_\uparrow - \frac{N}{2}\right) + \lambda\sqrt{N}\left(\hat{a}_\uparrow^\dagger\sqrt{1 - \frac{\hat{a}_\uparrow^\dagger\hat{a}_\uparrow}{N}}\,\hat{\sigma}_- + \sqrt{1 - \frac{\hat{a}_\uparrow^\dagger\hat{a}_\uparrow}{N}}\hat{a}_\uparrow\,\hat{\sigma}_+\right). \tag{5.36}$$

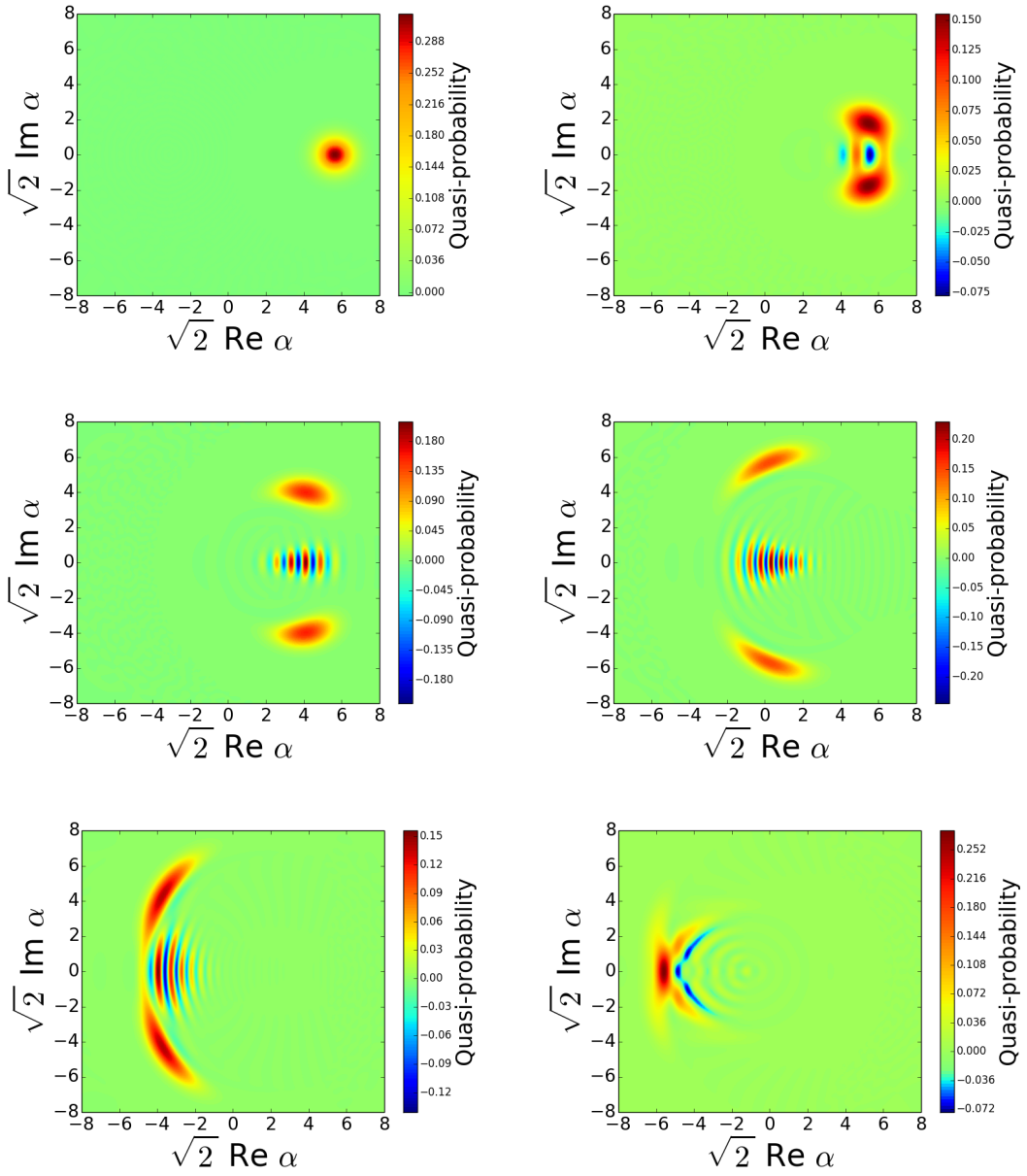

Figure 5.5: Harmonic oscillator Wigner functions for the initial state $|\alpha\rangle\,|\uparrow\rangle$ (with $\alpha = 4$) evolving by Jaynes-Cummings Hamiltonian at various times. Top left: $t = 0$, the coherent state $|\alpha\rangle$ with $\alpha = 4$. Top right: $t = t_r/10$. Middle left: $t = t_r/4$. Middle right: $t = t_r/2$. Bottom left: $t = 3t_r/4$. Bottom right: $t = t_r$.

Roughly speaking, when $N \gg 1$ and when the number of excitations in the spin system is small, the $\hat{a}_\uparrow^\dagger \hat{a}_\uparrow / N$ term can be ignored [see section 2.3] so that

$$\hat{H}_{SS} \approx \frac{\Omega}{2}\hat{\sigma}_z + \omega\, \hat{a}_\uparrow^\dagger \hat{a}_\uparrow + \lambda\sqrt{N}\left(\hat{a}_\uparrow^\dagger\, \hat{\sigma}_- + \hat{a}_\uparrow\, \hat{\sigma}_+\right), \tag{5.37}$$

where we have also dropped a constant term $\omega N/2$ since it only contributes a physically irrelevant global phase factor. In this approximation, equation (5.37) is essentially the Jaynes-Cummings Hamiltonian, but with the coupling λ enhanced by a factor of $\sqrt{N}$ due to collective coupling of the outer spins to the central spin. If we scale the coupling parameter $\lambda \to \lambda/\sqrt{N}$ and take the $N \to \infty$ limit, then the spin star Hamiltonian (5.36) corresponds exactly to the Jaynes-Cummings Hamiltonian. We recall (from section 2.3) that a spin coherent state $\left|\frac{\zeta}{\sqrt{N}}\right\rangle_N$ is identical to an oscillator coherent state of amplitude ζ in the $N \to \infty$ limit. Since we always assume an initial spin coherent state $|\zeta\rangle_N$, transforming $\lambda \to \lambda/\sqrt{N}$ and $\zeta \to \zeta/\sqrt{N}$ and taking $N \to \infty$ gives the Jaynes-Cummings limit throughout this chapter. If N is finite and if the terms $\hat{a}_\uparrow^\dagger \hat{a}_\uparrow / N$ in (5.36) are important, however, the analogy with the Jaynes-Cummings model breaks down. In the next chapter we discuss this regime of dynamics in more detail. Below, we determine the evolution of the spin star model in the Jaynes-Cummings approximation, including modifications to the Rabi frequency and revival time due to the finite number of spins. We also make use of the correspondence with the Jaynes-Cummings model to propose that Dicke squeezed states and spin cat states can be generated in this parameter regime.

5.2.1 Dynamics

On-resonance and for initial state $|\zeta\rangle_N \left|D_\pm^\phi(0)\right\rangle$ with $1/\sqrt{N} \ll |\zeta| \ll \sqrt{N}$ we have the effective Hamiltonian (4.73):

$$\hat{H}_{SS}^\pm = \pm\lambda\sqrt{\left(\hat{a}_\downarrow^\dagger \hat{a}_\downarrow + |\downarrow\rangle\langle\downarrow|\right)\left(\hat{a}_\uparrow^\dagger \hat{a}_\uparrow + |\uparrow\rangle\langle\uparrow|\right)}, \tag{5.38}$$

derived in the previous chapter. Below, we also suppose that $|\zeta| \ll 1$ so that the N spin system is in the bosonic approximation (section 2.3). In this parameter regime we expect the dynamics to resemble the Jaynes-Cummings model. In

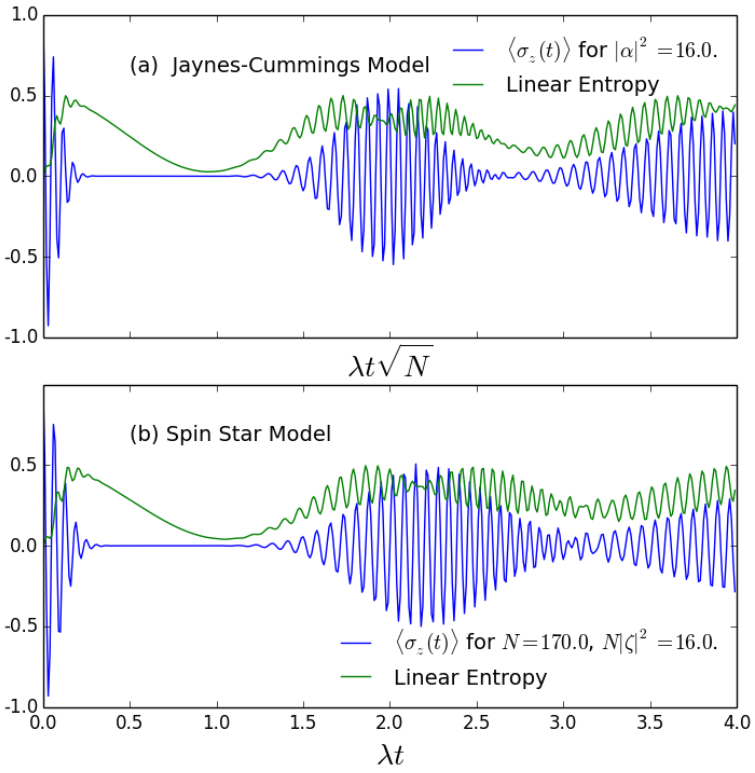

Figure 5.6: When $|\zeta| \ll 1$, the spin star system evolves like the Jaynes-Cummings model. Here we see collapse and revival of $\langle\sigma_z(t)\rangle$ (blue line) in (a) the JC model, and (b) the spin star model ($N = 170$).

figure 5.6(a) we plot the expectation value $\langle\hat{\sigma}_z(t)\rangle$ for the Jaynes-Cummings model with initial coherent state amplitude $\alpha = 4$. Next to this in figure 5.6(b) we show the corresponding plot in the spin star model with $|\zeta| \ll 1$ (we've chosen an initial spin coherent state with $\zeta = \alpha/\sqrt{N}$ for a convenient comparison with the Jaynes-Cummings model picture). The similarities between the two plots are clear. There are, however, small differences, for example, in the revival times, because N is finite.

In appendix A.3 we show that if we expand the square roots $\sqrt{\hat{a}_\downarrow^\dagger\hat{a}_\downarrow + |\downarrow\rangle\langle\downarrow|}$ and $\sqrt{\hat{a}_\uparrow^\dagger\hat{a}_\uparrow + |\uparrow\rangle\langle\uparrow|}$ in the effective Hamiltonian (5.38) around the expectation values $\left\langle\hat{a}_\downarrow^\dagger\hat{a}_\downarrow\right\rangle$ and $\left\langle\hat{a}_\uparrow^\dagger\hat{a}_\uparrow\right\rangle$ respectively, then in the bosonic approximation ($|\zeta| \ll$

1) and for times satisfying

$$\lambda t \ll 2\pi/|\zeta| \quad ; \quad \lambda t \ll 2\pi\sqrt{N}|\zeta|^3, \tag{5.39}$$

this Hamiltonian can be approximated as

$$\hat{H}_{SS}^{\pm} \approx \pm\lambda \left[\frac{N|\zeta|}{1+|\zeta|^2} + \frac{1}{2|\zeta|} |\uparrow\rangle\langle\uparrow| + \frac{1-|\zeta|^2}{2|\zeta|}\Delta(\hat{a}_\uparrow^\dagger \hat{a}_\uparrow) - \frac{1+|\zeta|^2}{8N|\zeta|^3}[\Delta(\hat{a}_\uparrow^\dagger \hat{a}_\uparrow)]^2 \right], \tag{5.40}$$

where again we have defined $\Delta(\hat{a}_\uparrow^\dagger \hat{a}_\uparrow) = \hat{a}_\uparrow^\dagger \hat{a}_\uparrow - \left\langle \hat{a}_\uparrow^\dagger \hat{a}_\uparrow \right\rangle$. The initial state $|\Psi^{\pm}(0)\rangle = |\zeta\rangle_N \left| D_{\pm}^{\phi}(0) \right\rangle$ evolves by this Hamiltonian to

$$\left|\Psi^{\pm}(t)\right\rangle \approx \left|\Phi^{\pm}(t)\right\rangle_N \left| D_{\pm}^{\phi}(t) \right\rangle, \tag{5.41}$$

where:

$$\begin{aligned} \left|\Phi^{\pm}(t)\right\rangle_N &= \exp\left[\mp it\lambda \frac{N|\zeta|}{1+|\zeta|^2}\right] \exp\left[\mp it\lambda \frac{1-|\zeta|^2}{2|\zeta|}\Delta(\hat{a}_\uparrow^\dagger \hat{a}_\uparrow)\right] \\ &\quad \otimes \exp\left[\pm it\lambda \frac{1+|\zeta|^2}{8N|\zeta|^3}(\Delta \hat{a}_\uparrow^\dagger \hat{a}_\uparrow)^2\right] |\zeta\rangle_N, \end{aligned} \tag{5.42}$$

$$\left| D_{\pm}^{\phi}(t) \right\rangle = \frac{1}{\sqrt{2}} \left(|\downarrow\rangle \pm e^{-i\phi} e^{\mp \frac{i\lambda t}{2|\zeta|}} \right). \tag{5.43}$$

This is a separable state of the system. We first consider the state (5.42) of the N spin system. Since each of the three exponentials in (5.42) commute with each other, their effects on the evolution can be considered separately. These three exponentials correspond to dynamics on three different timescales. When the initial state is $|\zeta\rangle_N \left| D_{+}^{\phi}(0) \right\rangle$ or $|\zeta\rangle_N \left| D_{-}^{\phi}(0) \right\rangle$ the first exponential just gives a global phase factor that can be ignored. However, if the initial state of the central spin is a superposition of $\left| D_{+}^{\phi}(0) \right\rangle$ and $\left| D_{-}^{\phi}(0) \right\rangle$ the opposite sign in each case mean that it is a relative phase factor that cannot be ignored. The oscillation of this relative phase has the period

$$t_R = \frac{\pi(1+|\zeta|^2)}{\lambda N|\zeta|}. \tag{5.44}$$

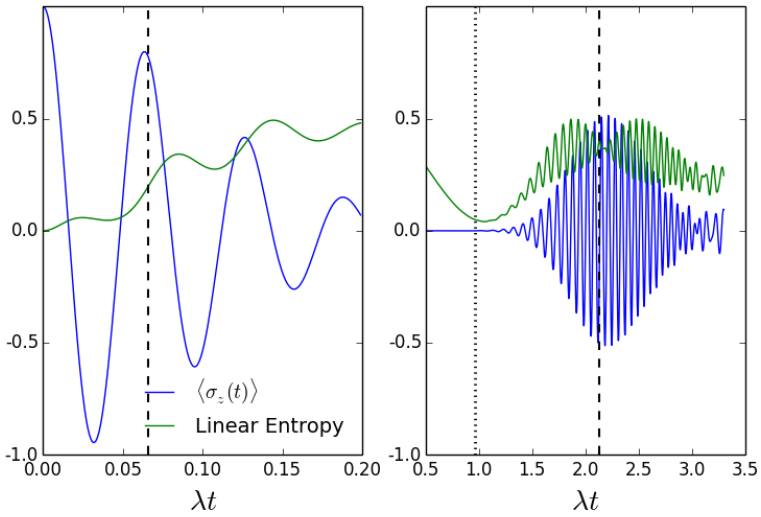

Figure 5.7: Left: the first few Rabi oscillations of figure 5.6(b). The vertical dashed line is at $t_R = \frac{\pi(1+|\zeta|^2)}{\lambda N|\zeta|}$. We see that this accurately predicts the Rabi time. Right: The revival region of figure 5.6(b). The vertical dashed line is plotted at $t_r = \frac{2\pi|\zeta|}{\lambda(1-|\zeta|^2)}$ and the dotted line is at $t_a = \pi|\zeta|/\lambda$.

Since $1/\sqrt{N} \ll |\zeta| \ll 1$ this is a very short time[1]. Further investigation is left as future work. In figure 5.7 we plot a magnified version of the first few Rabi oscillations of figure 5.6(b). We find that equation (5.44) accurately predicts the Rabi time. Taking the Jaynes-Cummings limit by transforming $\zeta \to \zeta/\sqrt{N}$ and $\lambda \to \lambda/\sqrt{N}$ and taking $N \to \infty$, we find that t_R is the Rabi period of the Jaynes-Cummings model.

If the central spin is initially in the state $\left|D^{\phi}_{\pm}(0)\right\rangle$ then the second exponential causes the spin coherent state to rotate in phase space:

$$\exp\left[\mp it\lambda\frac{1-|\zeta|^2}{2|\zeta|}\Delta(\hat{a}^{\dagger}_{\uparrow}\hat{a}_{\uparrow})\right]|\zeta\rangle_N = e^{\mp it\lambda\frac{1-|\zeta|^2}{2|\zeta|}\langle\hat{a}^{\dagger}_{\uparrow}\hat{a}_{\uparrow}\rangle}\left|\zeta e^{\mp it\lambda\frac{1-|\zeta|^2}{2|\zeta|}}\right\rangle_N. \tag{5.45}$$

The revival occurs when the counter-rotating states overlap again in phase space at the time:

[1]The N^{-1} scaling of t_R is interesting because estimation at the Heisenberg limit can often be traced back to some oscillation with a period that scales as N^{-1}, compared to $N^{-1/2}$ for the standard quantum limit [see section (3.2)].

$$t_r = \frac{2\pi|\zeta|}{\lambda(1-|\zeta|^2)}. \tag{5.46}$$

Since $\frac{t_r}{t_R} = \frac{2N|\zeta|^2}{1-|\zeta|^4} \approx 2N\,|\zeta|^2$ and $1 \ll \sqrt{N}|\zeta|$, this is much longer than t_R, the Rabi period. We notice that, unlike the Rabi period t_R, this revival time t_r cannot be decreased by increasing the number of outer spins, N (the revival time t_r is independent of N). In figure 5.7 we see that that t_r does indeed accurately predict the revival of Rabi oscillations. Again, transforming $\zeta \to \zeta/\sqrt{N}$ and $\lambda \to \lambda/\sqrt{N}$ and taking $N \to \infty$ of t_r gives the revival time for the Jaynes-Cummings model.

The third exponential in (5.42) corresponds to dynamics on a slower timescale and results in a distortion of the evolving spin coherent states. Since the analogous evolution for the Jaynes-Cummings model generates number squeezing, here we anticipate that for the spin star model this will be Dicke squeezing of the N spin state. To see this we plot in figure 5.8 the Dicke squeezing parameter χ_D^2, for initial state $|\zeta\rangle_N \left|D_+^\phi(0)\right\rangle$ [as defined in equation (2.85)]. For comparison, we also plot in figure 5.8 the squeezing parameter χ_s^2 [defined in equation (2.80)]. We see that $\chi_D^2 \leq \chi_s^2$ and that there are regions of time when $\chi_D^2 < 1 < \chi_s^2$, indicating that it is important to choose the appropriate measure to detect the spin squeezing in this parameter regime.

Next we consider the state (5.43) of the central spin. At $t_a = \pi|\zeta|/\lambda$ the states $\left|D_+^\phi(t_a)\right\rangle$ and $\left|D_-^\phi(t_a)\right\rangle$ coincide:

$$\left|D_\pm^\phi\left(t_a\right)\right\rangle = \frac{1}{\sqrt{2}}\left(|\downarrow\rangle - ie^{-i\phi}\,|\uparrow\rangle\right). \tag{5.47}$$

Following the terminology for the Jaynes-Cummings model, we call this the "attractor state" and the time t_a the "attractor time". In figure 5.7 we see that t_a accurately predicts the time when the linear entropy of the central spin dips to a minimum. The attractor time is approximately equal to half the revival time, $t_r = \frac{2\pi|\zeta|}{\lambda(1-|\zeta|^2)} \approx 2\pi|\zeta|/\lambda$. When the central spin is in the attractor state the combined system is (approximately) in a separable state, regardless of the initial state, with the quantum information from the initial state "swapped" into the state of the N outer spins. We see below that a judicious choice of initial state of the central spin leads to a spin cat state of the outer spins at the attractor time.

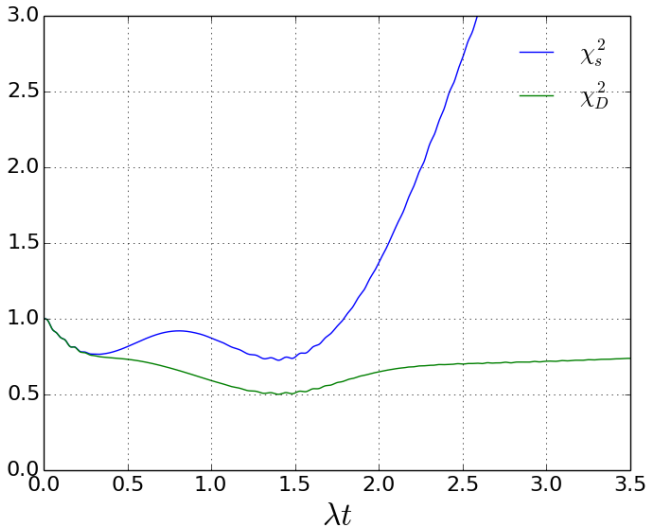

Figure 5.8: Spin squeezing for initial state $|\zeta\rangle_N \left|D_+^\phi(0)\right\rangle$ [with $N = 170$ and $\zeta = 4/\sqrt{N}$, the same parameters as in figure 5.6(b)]. We see Dicke squeezing $\chi_D^2 < 1$ even at times when $\chi_s^2 > 1$.

If we choose the initial state of the central spin to be

$$|\downarrow\rangle = \frac{1}{\sqrt{2}}\left(\left|D_+^\phi(0)\right\rangle + \left|D_-^\phi(0)\right\rangle\right), \tag{5.48}$$

then from equation (5.42) we see that the state of the N spin system at the attractor time, $t_a = \pi|\zeta|/\lambda$ is:

$$|\psi_\zeta\rangle \equiv \mathcal{N}\left(\left|\Phi^+(t_a)\right\rangle + \left|\Phi^-(t_a)\right\rangle\right). \tag{5.49}$$

The $\mathcal{N}$ has been introduced to maintain normalisation since $|\Phi^+(t_a)\rangle$ and $|\Phi^-(t_a)\rangle$ are, in general, not orthogonal to each other and the ζ subscript in the state $|\psi_\zeta\rangle$ indicates that this state at time t_a depends on the initial coherent state $|\zeta\rangle_N$.

Figure 5.9 shows $\sqrt{\langle\psi_\zeta|\,\rho_N(t_a)\,|\psi_\zeta\rangle}$, the fidelity of $|\psi_\zeta\rangle$ with respect to $\rho_N(t_a)$, the (exact) reduced state of the N outer spins at t_a, plotted against $|\zeta|^2$ for various values of N. As expected (given the correspondence between the spin star model and the Jaynes-Cummings model) the fidelity is high when $1/N \ll |\zeta|^2 \ll 1$ and when $N \gg 1$. At $N = 100$ and $|\zeta|^2 = 0.06$, for example, the fidelity at t_a is high

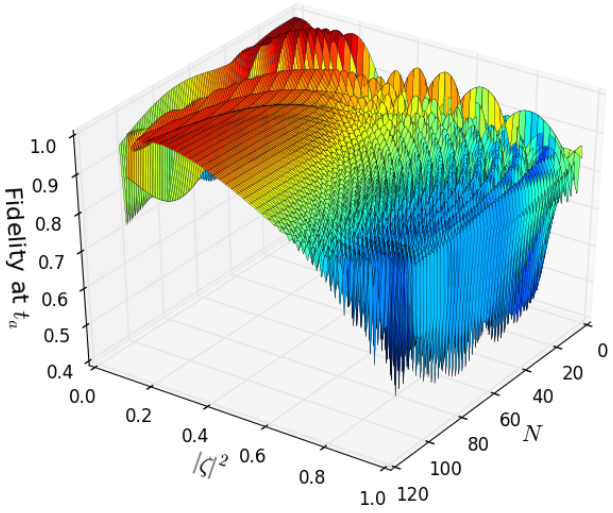

Figure 5.9: The fidelity $\sqrt{\langle\psi_\zeta|\,\rho_N(t_a)\,|\psi_\zeta\rangle}$. Red indicates areas of high fidelity. Fidelity is high when $1/N \ll |\zeta|^2 \ll 1$, but also around $|\zeta|^2 \approx 0.5$ for certain small values of N.

(~ 0.96). This is telling us that the state of the outer spins is close to the cat state $|\psi_\zeta\rangle$ at the attractor time.

Interestingly, figure 5.9 shows that this domain of high fidelity includes relatively small values of N. At $N = 40$, for example, $F \sim 0.93$ at t_a for $|\zeta|^2 = 0.16$. To see that this is indeed a cat state, we plot in figure 5.12(d) its spin Wigner function. We see two crescent shapes with interference fringes between them – clearly a cat state, although not quite a superposition of spin coherent states.

Also of interest in figure 5.9 are the ripples in the fidelity outside of our $1/N \ll |\zeta|^2 \ll 1$ parameter regime, for example, for low N around $|\zeta|^2 \approx 0.5$. A cross section of figure 5.9 at $|\zeta|^2 = 0.5$ is plotted in figure 5.10 (the blue line). These ripples are peaked for certain small values of N. At $N = 12$, for example, the fidelity with respect to the spin cat state $|\psi_\zeta\rangle$ is ~ 0.91 at t_a. Figure 5.12(b) shows the spin Wigner function of this state.

Figure 5.11 shows $\sqrt{\langle\psi_\zeta|\,\rho_N(t)\,|\psi_\zeta\rangle}$, the fidelity of $|\psi_\zeta\rangle$ against $\rho_N(t)$, the (exact) reduced N spin state, plotted against time for $N = 12, 40, 70, 100$. Fidelity at t_a, marked by a black dot, is high in each case. As explained above, however, although the $N = 12$ fidelity is high, it is in a different domain of high fidelity than $N = 40, 70, 100$.

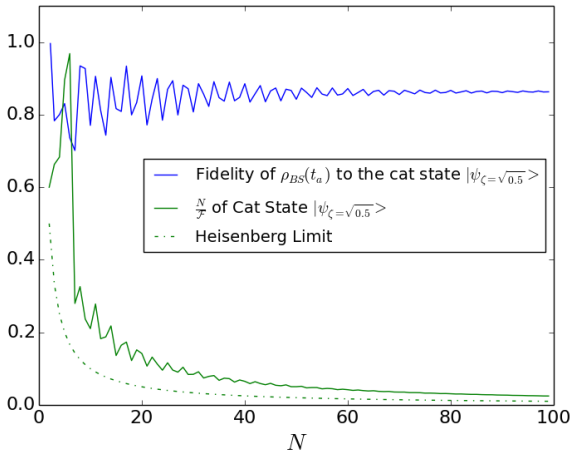

Figure 5.10: The green line shows $N/\mathcal{F}$ for the cat state $\left|\psi_{\zeta=\sqrt{0.5}}\right\rangle$ (the cross section of figure 5.13 at $|\zeta|^2 = 0.5$). A value less than unity indicates that the state is capable of magnetic field sensing below the standard quantum limit ($N/\mathcal{F} = 1$). The blue line shows fidelity of the exact state $\rho_{BS}(t_a)$ (for $\zeta = \sqrt{0.5}$) with respect to the cat state $\left|\psi_{\zeta=\sqrt{0.5}}\right\rangle$ (this is the cross section of figure 5.9 at $|\zeta|^2 = 0.5$). We see that peaks of fidelity (the blue line) coincide with troughs of $N/\mathcal{F}$ (the green line). This tells us that cat states that can be generated with high fidelity are useful for quantum enhanced magnetic field sensing.

In figure 5.11 the fidelity oscillates very quickly (with the Rabi period t_R) indicating that this method of generating a cat state is sensitive to the interaction time. However, any physical realisation for which there is control at the Rabi period time scale should have sufficient time resolution to identify the time(s) at which a cat is generated. Figure 5.9, on the other hand, shows that fidelity is not very sensitive to the initial spin coherent state parameter $|\zeta|$ when $1/N \ll |\zeta|^2 \ll 1$.

A superposition of spin coherent states can be used to sense magnetic fields with a precision better than the standard quantum limit. Although our spin cat state $|\psi_\zeta\rangle$ is not a perfect superposition of spin coherent states, the spin Wigner function in figure 5.12(d) shows that it is still a superposition of two distinct wave packets with interference fringes between them, so we expect that it also gives an advantage in magnetic field sensing. If the spin system interacts with a magnetic field $\vec{B} = B_y$, via the Hamiltonian $\hat{H} = -\gamma B_y \hat{J}_y$ then the best achievable precision

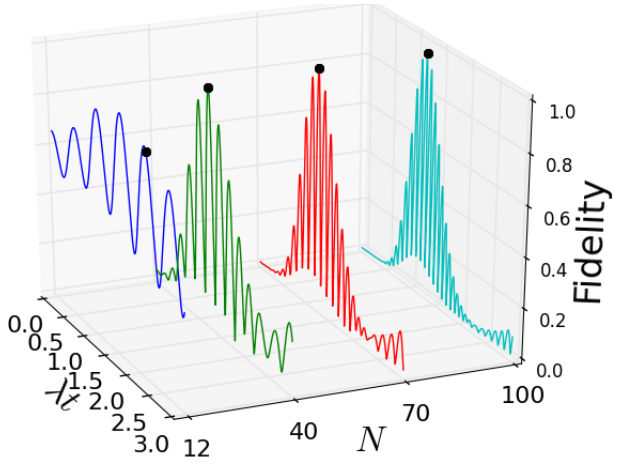

Figure 5.11: Fidelity at t_a is marked by a black dot. The fidelity around t_a is highly oscillatory. The spin Wigner functions at the times marked by the black dot are plotted in figure 5.12 for $N = 12$ and $N = 40$. (Blue line: $N = 12$, $|\zeta|^2 = 0.5$; Green line: $N = 40$, $|\zeta|^2 = 0.16$; Red line: $N = 70$, $|\zeta|^2 = 0.16$; Cyan line: $N = 100$, $|\zeta|^2 = 0.16$.)

in our estimate is $(\delta B_y)^2 \geq 1/\mathcal{F}$ where $\mathcal{F}$ is the quantum Fisher information (see section 3.3). For ease of comparison between different values of N we quantify precision by $N(\delta B_y)^2 \geq N/\mathcal{F}$. Given that our N spin system evolves unitarily and is initially in pure state $|\psi_\zeta\rangle$ we can write the quantum Fisher information as

$$\mathcal{F} = 4\gamma^2 t^2 \left(\Delta \hat{J}_y\right)^2 = 4\gamma^2 t^2 \left(\langle\psi_\zeta| \hat{J}_y^2 |\psi_\zeta\rangle - \langle\psi_\zeta| \hat{J}_y |\psi_\zeta\rangle^2\right). \tag{5.50}$$

In figure 5.13 we plot $N/\mathcal{F}$ against $|\zeta|^2$ for different values of N up to $N = 100$. If $\zeta = 0$, our state $|\psi_{\zeta=0}\rangle$ is just a spin coherent state and $N/F = 1$, the standard quantum limit. The Heisenberg limit, $N/\mathcal{F} = 1/N$, is marked in figure 5.13 by a black line for each N (the grid under the coloured contour plot). We see that, especially for large N, our cat state $|\psi_\zeta\rangle$ can allow for magnetic field sensing significantly beating the standard quantum limit, even in the $1/N \ll |\zeta|^2 \ll 1$ regime in which the cat state emerges from the collapse and revival dynamics.

Also in figure 5.13, we notice the ripples in $N/\mathcal{F}$ at $|\zeta|^2 \approx 0.5$. These ripples are most pronounced for small values of N. The green line in figure 5.10 shows the cross section of figure 5.13 at $|\zeta|^2 = 0.5$. We see that even for moderate values

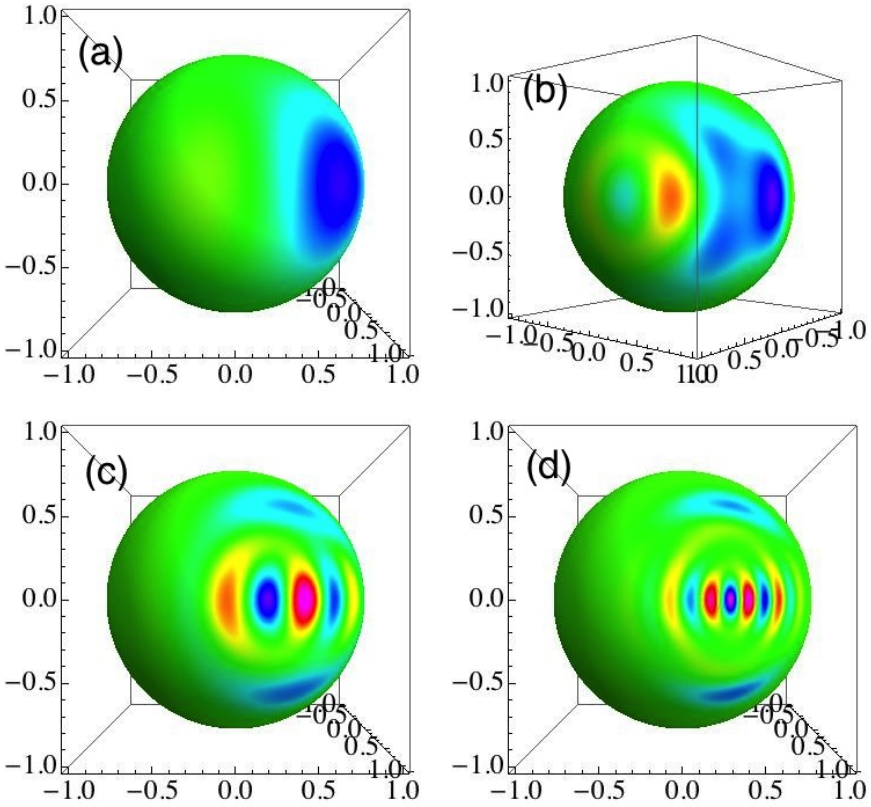

Figure 5.12: Spin Wigner functions of $\rho_N(t_a)$, the exact reduced N spin state at t_a. (a) $N = 5$; (b) $N = 12$, $\zeta = 0.5$; (c) $N = 20$, $|\zeta|^2 = 0.16$; (d) $N = 40$, $|\zeta|^2 = 0.16$. This figure is reproduced from Dooley *et al.* (2013) (Copyright 2013 by the American Physical Society).

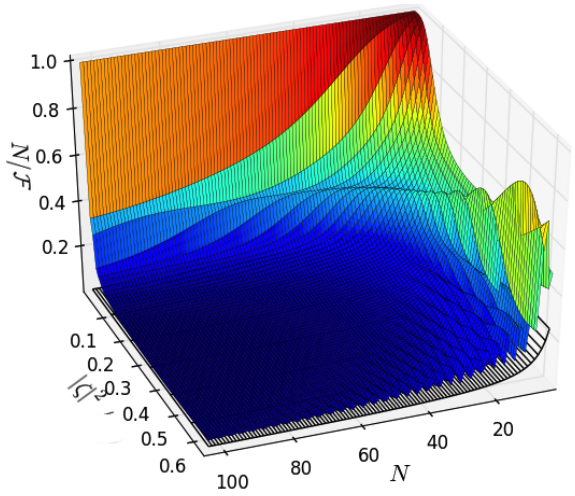

Figure 5.13: At $|\zeta|^2 = 0$ we have $N/\mathcal{F} = 1$, corresponding to the standard quantum limit. The Heisenberg limit, $N/\mathcal{F} = 1/N$ is marked by the black grid under the coloured surface. ($\gamma t = 1$.)

of N, cat states that are useful for magnetic field sensing can be generated with high fidelity. This is of interest for implementations of the spin star model where the number of outer spins N, is limited.

In summary, we have shown that there is a parameter regime where the spin star model can be approximated by the Jaynes-Cummings model. We have identified the timescales of the collapse and revival dynamics and spin cat state generation, including corrections due to the finiteness of N, the number of outer spins. In the next chapter we investigate the dynamics beyond the Jaynes-Cummings approximation for the spin star model.

Chapter 6

Beyond the Jaynes-Cummings Approximation – I

In this chapter we investigate some of the features of the on-resonance spin star model beyond the bosonic approximation assumed in the previous chapter.

6.1 Fractional Revival

As discussed in section 5.1, the phrase "collapse and revival" in the Jaynes-Cummings model refers to the collapse and revival of the oscillations of the expectation value $\langle\hat{\sigma}_z(t)\rangle$. More generally, collapse and revival is the feature of quantum systems whereby the initial wave packet collapses as it evolves, but at a later time returns (either exactly or approximately) to the initial state: the revival. We see this in the resonant Jaynes-Cummings model because for any initial atom state the initial coherent state of the oscillator returns (approximately) to another coherent state at the revival time, as illustrated in figure 5.5.

Fractional revival is an additional effect where at a rational fraction of the revival time the state of the system is made up of a number of superposed, displaced copies of the initial wave packet. This phenomenon is well known and well investigated, both theoretically [Averbukh & Perelman (1989); Robinett (2004)] and experimentally [Greiner *et al.* (2002)], for systems with infinite-dimensional Hilbert space, but less well studied for finite-dimensional systems. In the previous chapter it was shown that the resonant spin star model exhibits Jaynes-

Cummings-like collapse and revival for a particular class of initial spin coherent states of the N outer spins (even for moderate values of N). In this chapter we show that the same system with a different class of initial spin coherent states also exhibits *fractional revivals*. The transition from one regime of collapse and revival (Jaynes-Cummings like) to the other (with fractional revival) is made by changing the initial spin-coherent state parameter, something that is in principle very straightforward in the state preparation. We suggest that fractional revivals and the associated multiple cat states could be observed in this model even for systems of few spins. We published these results in Dooley & Spiller (2014). We introduce the phenomenon of fractional revival by giving some examples in the following subsections.

6.1.1 The Kerr Hamiltonian

The Kerr Hamiltonian for an oscillator is

$$\hat{H}_k = \lambda_k \hat{a}^{\dagger 2}\hat{a}^2 = \lambda_k \left[(\hat{a}^\dagger \hat{a})^2 - \hat{a}^\dagger \hat{a}\right]. \tag{6.1}$$

For an initial coherent state the system evolves to

$$|\Psi_k(t)\rangle = e^{-it\lambda_k\left[(\hat{a}^\dagger\hat{a})^2-\hat{a}^\dagger\hat{a}\right]}|\alpha\rangle = e^{-|\alpha|^2/2}\sum_{n=0}^{\infty}\frac{\alpha^n e^{-it\lambda_k n(n-1)}}{\sqrt{n!}}|n\rangle. \tag{6.2}$$

After evolution for a time $T_k = \pi/\lambda_k$, the oscillator is again in the initial state, $|\Psi_k(T_k)\rangle = |\alpha\rangle$ since at this time the phase in the exponential on the right hand side of (6.2) is an integer multiple of $2\pi i$ for any value of n [Yurke & Stoler (1986)]. This corresponds to a revival of the initial state of the system. At half the revival time, $t = T_k/2$, the oscillator is in a superposition of two coherent states; a cat state [Yurke & Stoler (1986)]. To see this, we note that at this time the exponential on the right hand side of (6.2) is

$$e^{-it\pi n(n-1)/2} = \begin{cases} i^n & : \quad n \text{ even} \\ i^{n-1} & : \quad n \text{ odd} \end{cases} \tag{6.3}$$

This gives:

$$|\Psi_k(T_k/2)\rangle = e^{-|\alpha|^2/2}\sum_{n\ even}\frac{(i\alpha)^n}{\sqrt{n!}}|n\rangle - ie^{-|\alpha|^2/2}\sum_{n\ odd}\frac{(i\alpha)^n}{\sqrt{n!}}|n\rangle \tag{6.4}$$

$$= \frac{1}{\sqrt{2}}\left(e^{-i\pi/4}|i\alpha\rangle + e^{i\pi/4}|-i\alpha\rangle\right). \tag{6.5}$$

More generally, it was shown by Gantsog & Tanas (1991) and by Tara *et al.* (1993) that for coprime integers p and q, the state at a time $\frac{p}{q}T_k$ will be in a superposition of q coherent states (a multiple cat state):

$$\left|\Psi_k\left(\frac{p}{q}T_k\right)\right\rangle = \begin{cases} \sum_{l=0}^{q-1} c_l\left|\alpha e^{i\pi(2l+1)/q}\right\rangle & : \quad n \text{ even} \\ \sum_{l=0}^{q-1} c_l\left|\alpha e^{2\pi i l/q}\right\rangle & : \quad n \text{ odd} \end{cases} \tag{6.6}$$

In figure 6.1 we plot the state $\left|\Psi_k\left(\frac{p}{q}T_k\right)\right\rangle$ for different values of p and q. Interestingly, there has been a recent experimental demonstration of fractional revival with this kind of Kerr non-linearity for a superconducting microwave resonator [Kirchmair *et al.* (2013)].

6.1.2 The Jaynes-Cummings Hamiltonian

The resonant Jaynes-Cummings model for an initial coherent state also seems to have a limited form of fractional revival: for a judiciously chosen initial atom state, at half the revival time the oscillator is (approximately) in a superposition of two coherent states [Bužek *et al.* (1992); Gea-Banacloche (1991)] as shown in figure 5.5. However, this cat state generation is really due to the conditional evolution of the oscillator rather than fractional revival. This is because there are two orthogonal initial atom states that result in two different effective Hamiltonians, $\hat{H}_{JC}^{\pm} = \pm\lambda\sqrt{\hat{a}^\dagger\hat{a}}$, for the oscillator evolution [see equations (5.22) and (5.23)]. Starting in a superposition of these two atom states leads to Schrödinger-cat states of the oscillator. At no time is the oscillator composed of more than two distinct coherent states.

It is possible to see fractional revival and multiple cat states (with more than two components) in the Jaynes-Cummings model, but this requires sub-Poissonian number statistics for the initial state [Averbukh (1992); Góra & Jedrzejek (1993)] (i.e., a non-classical, number-squeezed initial state). In this case

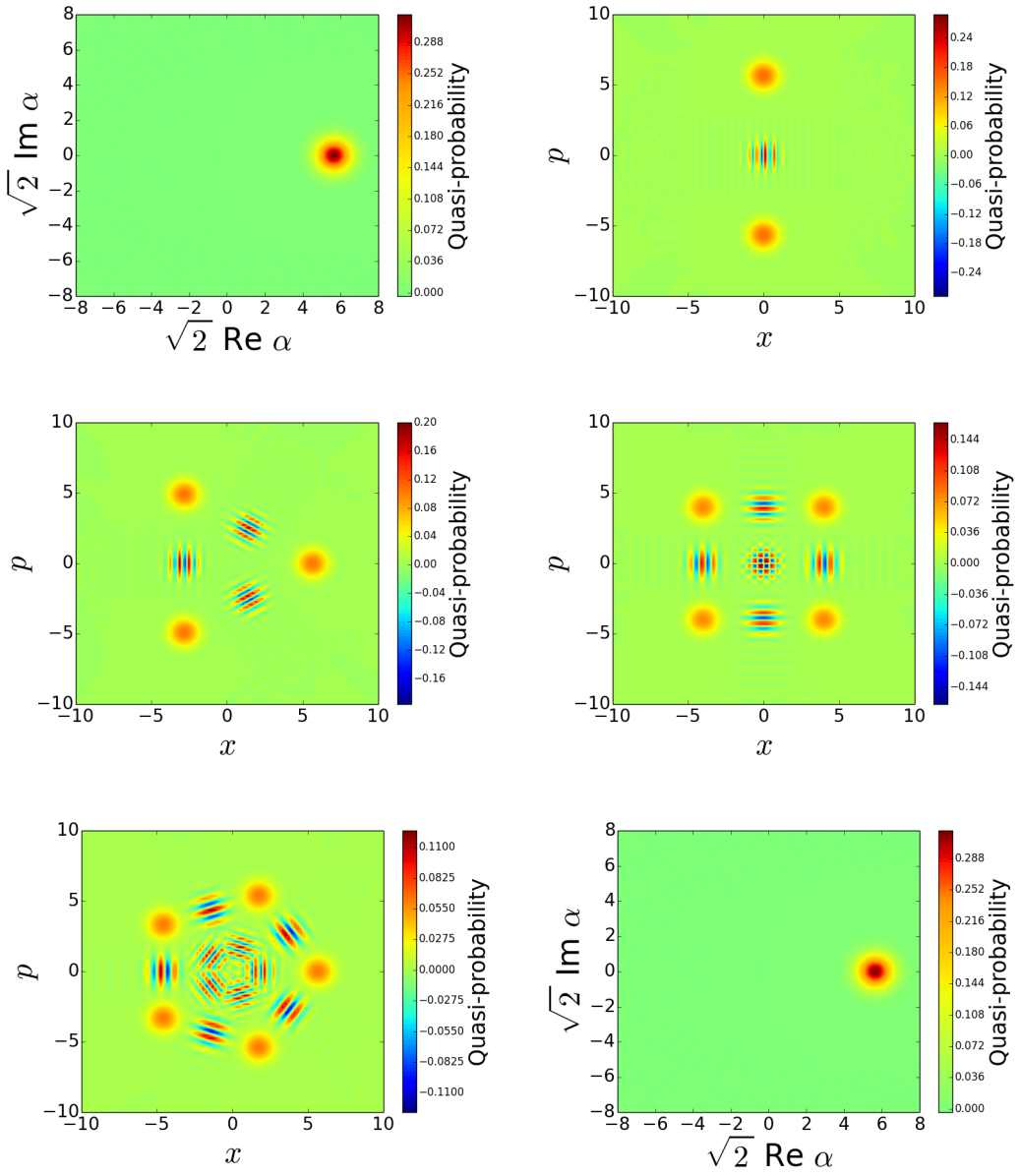

Figure 6.1: Wigner functions for the state of the oscillator evolving by the Kerr Hamiltonian at various times. Top left: $t = 0$. Top right: $t = T_k/2$. Middle left: $t = 2T_k/3$. Middle right: $t = 3T_k/4$. Bottom left: $t = 4T_k/5$. Bottom right: $t = T$. Initial state $|\alpha\rangle$ with $\alpha = 4$.

one finds the usual collapse and revival, but also "super-revivals" at longer times, and multiple cat states at rational fractions of the "super-revival" time [Góra & Jedrzejek (1993)]. This kind of fractional revival is different to the Kerr-type fractional revivals since they come *after* the first revival. Kerr-type fractional revivals, on the other hand, appear *before* the first revival.

6.1.3 The one-axis-twisting Hamiltonian

Agarwal *et al.* (1997) and Chumakov *et al.* (1999) have studied the evolution of an N spin system in a "finite Kerr medium" analogous to the Kerr evolution above for the oscillator. The Hamiltonian for this model, also called the *one-axis twisting* model [Kitagawa & Ueda (1993)], is

$$\hat{H}_{oat} = \lambda_{oat} \hat{J}_z^2. \tag{6.7}$$

An initial spin coherent state $|\zeta\rangle_N$ evolves by the one-axis twisting Hamiltonian to:

$$|\Psi_{oat}(t)\rangle = e^{-it\lambda_{oat}\hat{J}_z} |\zeta\rangle_N = \sum_{m=-N/2}^{N/2} \binom{N}{\frac{N}{2}+m}^{1/2} \frac{\zeta^{\frac{N}{2}+m} e^{-it\lambda_{oat}m^2}}{\sqrt{1+|\zeta|^2}^N} \left|\frac{N}{2}, m\right\rangle_N . \tag{6.8}$$

If N is even then m takes integer values. In this case we have a revival $|\Psi_{oat}(T_{oat})\rangle = |\zeta\rangle_N$ at time $T_{oat} = 2\pi/\lambda_{oat}$ since at this time we have $e^{-it\lambda_{oat}m^2} = 1$ for any value of m. At half of this time $t = T_{oat}/2$ we have $e^{-it\lambda_{oat}m^2} = (-1)^m$ so that $|\Psi_{oat}(T_{oat}/2)\rangle = (-1)^{N/2} |-\zeta\rangle_N$, an "anti-revival". At a quarter of the revival time, $t = T_{oat}/4$, we have $e^{-it\lambda_{oat}m^2} = 1$ if m is even and $e^{-it\lambda_{oat}m^2} = -i$ is m is odd. The N spin state at this time is thus:

$$|\Psi_{oat}(T_{oat}/4)\rangle = \sum_{m\ even} \binom{N}{\frac{N}{2}+m}^{1/2} \frac{\zeta^{\frac{N}{2}+m}}{\sqrt{1+|\zeta|^2}^N} \left|\frac{N}{2}, m\right\rangle_N \tag{6.9}$$

$$-i \sum_{m\ odd} \binom{N}{\frac{N}{2}+m}^{1/2} \frac{\zeta^{\frac{N}{2}+m}}{\sqrt{1+|\zeta|^2}^N} \left|\frac{N}{2}, m\right\rangle_N \tag{6.10}$$

$$= \frac{1}{\sqrt{2}} \left(e^{-i\pi/4} |\zeta\rangle_N + e^{i\pi/4} |-\zeta\rangle_N\right), \tag{6.11}$$

a spin cat state. This fractional revival behaviour closely resembles the Kerr Hamiltonian fractional revival. Similarly to the Kerr Hamiltonian, it can be shown that at rational fractions $t = \frac{p}{2q}T_{oat}$ of the revival time (where p and q are mutually prime numbers) there are fractional revivals where the spin system is in a multiple cat state. To see this we first notice that in the Dicke state expansion of a spin coherent state [equation (2.61)] the phase in the exponential is linear in the Dicke state index, m. In the evolved state $|\Psi_{oat}(t)\rangle$ [equation (6.8)], however, the phase in the exponential is quadratic in m. If we want to write $|\Psi_{oat}(t)\rangle$ as a superposition of spin coherent states we must somehow convert this quadratic exponent to a linear exponent. Following Averbukh & Perelman (1989), we do this by writing the exponential $e^{-it\lambda_{oat}m^2}$ at a time $t = \frac{p}{2q}T_{oat}$ in terms of its discrete Fourier transform. This is a useful step because $e^{-it\lambda_{oat}m^2} = e^{-i\pi pm^2/q}$ is periodic in m with period q (still assuming that N is even and that m takes integer values) so that it can be decomposed as a finite sum of exponentials that have exponents linear in m. We find that:

$$\exp\left[\frac{-i\pi pm^2}{q}\right] = \frac{1}{\sqrt{2q}}\sum_{l=0}^{2q-1}\mathcal{F}_l\,\exp\left[\frac{-i\pi lm}{q}\right], \tag{6.12}$$

where

$$\mathcal{F}_l = \frac{1}{\sqrt{2q}}\sum_{m=0}^{2q-1}\exp\left[\frac{-i\pi pm^2}{q}\right]\exp\left[\frac{\pi ilm}{q}\right], \tag{6.13}$$

is the discrete Fourier transform of $e^{-i\pi pm^2/q}$. Substituting (6.12) into (6.8) now allows us to write the state $|\Psi_{oat}(pT_{oat}/2q)\rangle$ as a superposition of spin coherent states:

$$|\Psi_{oat}(pT_{oat}/2q)\rangle = \frac{1}{\sqrt{2q}}\sum_{l=0}^{2q-1}\mathcal{F}_l\,e^{i\pi lN/2q}\left|\zeta e^{i\pi l/q}\right\rangle_N. \tag{6.14}$$

The discrete Fourier transform $\mathcal{F}_l$ is, in general, difficult to calculate, but it is possible to write down a closed formula for the sum in equation (6.13). From Bernt & Evans (1981), we quote the following result:

$$\sum_{k=0}^{|c|-1}e^{i\pi(ak^2+bk)/c} = \left|\frac{c}{a}\right|^{1/2}e^{i\pi(|ac|-b^2)/(4ac)}\sum_{k=0}^{|a|-1}e^{-i\pi(ck^2+bk)/a}, \tag{6.15}$$

where a, b and c are integers with $ac \neq 0$ and $ac + b$ is even. Applying this to (6.13) and, for simplicity, taking $p = 1$ and q to be an even number, we find that $\mathcal{F}_l$ vanishes for odd values of l and

$$\mathcal{F}_l = (1 - i) \exp\left[\frac{i\pi l^2}{4q}\right] \tag{6.16}$$

when $l = 2l'$ is even. For this particular example, we then have:

$$\left|\Psi_{oat}\left(\frac{T_{oat}}{2q}\right)\right\rangle = \frac{1}{\sqrt{q}} \sum_{l'=0}^{q-1} e^{i\pi l'^2/q} e^{i\pi l'^2/q} \left|\zeta e^{2\pi i l'/q}\right\rangle_N . \tag{6.17}$$

This is superposition of q spin coherent states distributed uniformly in the phase of the spin coherent state parameter ζ. Similar expressions can be derived for other values of p and q.

This type of evolution is the basis of several proposals to generate cat states of various finite-dimensional systems [Ferrini *et al.* (2008); Gerry (1998)]. We note, however, that the primary focus of study of the one-axis twisting Hamiltonian is the generation of spin squeezed states. We discuss this in more detail in the next chapter.

6.2 The spin star model

On-resonance and for initial state $|\Psi^{\pm}(0)\rangle = |\zeta\rangle_N \left|D^{\phi}_{\pm}(0)\right\rangle$ with $1/\sqrt{N} \ll |\zeta| \ll \sqrt{N}$ we have the effective Hamiltonian (4.72):

$$\hat{H}^{\pm}_{SS} = \pm\lambda\sqrt{\hat{J}^2 - \hat{J}_z^2 - \hat{J}_z \otimes \hat{\sigma}_z}. \tag{6.18}$$

In appendix A.3.2 we show that for $N \gg 1$ this Hamiltonian can be further approximated as:

$$\hat{H}^{\pm}_{SS} \approx \pm\lambda\left(\sqrt{\hat{J}^2} + \frac{1}{8\sqrt{\hat{J}^2}} - \frac{\left(\hat{J}_z + \frac{\hat{\sigma}_z}{2}\right)^2}{2\sqrt{\hat{J}^2}}\right), \tag{6.19}$$

when $|\zeta| \approx 1$ (or, in spherical coordinates for the initial spin coherent state, $\theta \approx \pi/2$) and $\lambda t \ll N$. In figure 6.2 we plot $|\langle\tilde{\Psi}^{+}(t)|\Psi^{+}(t)\rangle|$, the fidelity of

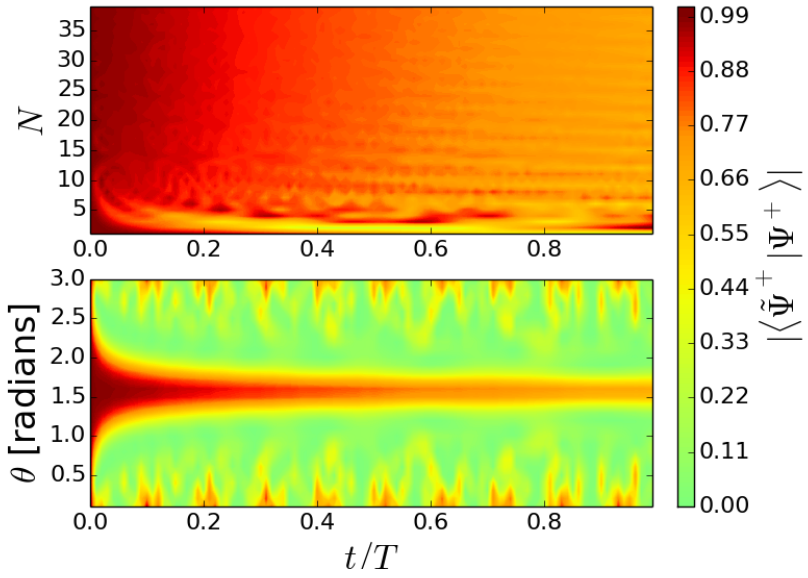

Figure 6.2: Top: Fidelity of the approximation $\left|\tilde{\Psi}^+\right\rangle$ with respect to the exact state $|\Psi^+\rangle$, plotted against N and t/T for initial spin coherent state with $\theta = \pi/2$ and $\phi = 0$. Bottom: Fidelity plotted against θ and t/T with $N = 40$ and $\phi = 0$. For $\theta \approx \pi/2$ (or $|\zeta| \approx 1$) and $\lambda t \ll N$ (or $t \ll T$) the fidelity is high (red). This figure is reproduced from Dooley & Spiller (2014) (copyright 2014 by the American Physical Society).

the state $|\Psi^+(t)\rangle = e^{-it\hat{H}_{SS}}|\Psi^+(0)\rangle$ [evolving by the full spin star Hamiltonian (4.2)] with respect to the approximate state $\left|\tilde{\Psi}^+(t)\right\rangle$ [evolving by the effective Hamiltonian (6.19)]. The tilde above Ψ indicates approximation. We plot this fidelity against time for various initial values of θ and N. The time axis is scaled by $T = \frac{2\pi}{\lambda}\sqrt{\frac{N}{2}\left(\frac{N}{2}+1\right)}$ because this turns out to be the revival time, as we will see in the next section. Figure 6.2 shows that our approximation is good in the parameter regimes of interest ($\theta \approx \pi/2$ and $t \ll T$).

If the initial state is either $|\Psi^+(0)\rangle$ or $|\Psi^-(0)\rangle$ then (since both $|\Psi^+(0)\rangle$ and $|\Psi^-(0)\rangle$ are eigenstates of $\hat{J}^2$) the first two terms of (6.19) just give a global phase factor that can be ignored. If the initial state is a superposition of $|\Psi^+(0)\rangle$ and $|\Psi^-(0)\rangle$ then the first two terms cannot be ignored since they give a quickly oscillating relative phase factor. The last term of (6.19) is proportional to $\left(\hat{J}_z + \frac{\sigma_z}{2}\right)^2$.

This is a one-axis twisting term for the combined $(N+1)$-spin system.

Previous examples of finite-dimensional systems whose Hamiltonians include one-axis twisting terms are: a collection of two-level atoms interacting with a far detuned field mode [Agarwal *et al.* (1997); Klimov & Saavedra (1998)]; Bose-Einstein condensates in a double-well potential [Milburn *et al.* (1997)]; molecular nano-magnets [Wernsdorfer (2008)]; a collection of NV centers coupled to the vibrational mode of a diamond resonator [Bennett *et al.* (2013)]. Here we have shown that the one-axis-twisting Hamiltonian can also be an effective Hamiltonian in the resonant spin star model. We note, however, that the coupling parameter λ is weakened by a factor of $1/(2\sqrt{\hat{J}})$ for the one-axis-twisting term in (6.19).

6.2.1 Fractional revivals, multiple cat states and quantum carpets

We know from section 6.1.3 that the one-axis twisting Hamiltonian $\hat{H}_{oat} = \lambda_{oat}\hat{J}_z^2$ generates multiple cat states. Since our effective Hamiltonian (6.19) has a term proportional to $\left(\hat{J}_z + \frac{\hat{\sigma}_z}{2}\right)^2$ we expect that this generates multiple cat states of the combined $N+1$ spin system. In this section [following the method of analysis of Averbukh & Perelman (1989); Robinett (2004)] we investigate the details of this evolution. We take the initial state to be $|\Psi^{\pm}(0)\rangle = |\theta,\phi\rangle_N \left|D_{\pm}^{\phi}(0)\right\rangle$, with $\theta = \pi/2$ for the spin coherent state.

The system evolves by the Hamiltonian (6.19) to the state

$$\left|\tilde{\Psi}^{\pm}(t)\right\rangle = \sum_{m=-\frac{N}{2}}^{N/2} \frac{C_m}{\sqrt{2}} \left|\frac{N}{2}, m\right\rangle \left(F_m^{\pm}(t)\,|\downarrow\rangle \pm e^{-i\phi} G_m^{\pm}(t)\,|\uparrow\rangle\right), \tag{6.20}$$

where, again, the tilde above Ψ indicates approximation and where we define

$$F_m^{\pm}(t) = \exp\left[\mp it\lambda\left(\sqrt{\frac{N}{2}\left(\frac{N}{2}+1\right)} - \frac{m(m-1)}{2\sqrt{\frac{N}{2}\left(\frac{N}{2}+1\right)}}\right)\right], \tag{6.21}$$

$$G_m^{\pm}(t) = \exp\left[\mp it\lambda\left(\sqrt{\frac{N}{2}\left(\frac{N}{2}+1\right)} - \frac{m(m+1)}{2\sqrt{\frac{N}{2}\left(\frac{N}{2}+1\right)}}\right)\right]. \tag{6.22}$$

The C_m in equation (6.20) are the expansion coefficients of the spin coherent state $|\theta,\phi\rangle_N$ in the Dicke basis [see equation (2.64)]. So that we can eventually arrive at a more useful expression for $\left|\tilde{\Psi}(t)\right\rangle$ we now consider some properties of these functions $F_m^{\pm}(t)$ and $G_m^{\pm}(t)$. First, when N is an even number both $F_m^{\pm}(t)$ and $G_m^{\pm}(t)$ are periodic in time with period $T = \frac{2\pi}{\lambda}\sqrt{\frac{N}{2}\left(\frac{N}{2}+1\right)}$. To see this note that when N is even both $\frac{N}{2}\left(\frac{N}{2}+1\right)$ and $m(m\pm 1)$ are even integers so that $F_m^{\pm}(T)$ and $G_m^{\pm}(T)$ are exponentials whose phases are integer multiples of 2π. Since $F_m^{\pm}(t)$ and $G_m^{\pm}(t)$ are periodic in time we have $\left|\tilde{\Psi}^{\pm}(t+T)\right\rangle = \left|\tilde{\Psi}^{\pm}(t)\right\rangle$: the system returns to its initial state after period T. Similarly, when N is an odd number we have $\left|\tilde{\Psi}^{\pm}(t+2T)\right\rangle = \left|\tilde{\Psi}^{\pm}(t)\right\rangle$ and the state has a revival time of $2T$.

Focussing on the case when N is even, we now consider times $t = \frac{pT}{q}$ where p and q are coprime integers, i.e., rational fractions of the revival time. Then $F_m^{\pm}(pT/q)$ and $G_m^{\pm}(pT/q)$ are both either periodic functions of the discrete variable m with period q if q is odd, or anti-periodic functions of m with (anti-) period q if q is even:

$$F_m^{\pm} = F_{m+q}^{\pm}\,; \quad G_m^{\pm} = G_{m+q}^{\pm} \quad (q\,\text{odd}), \tag{6.23}$$

$$F_m^{\pm} = -F_{m+q}^{\pm}\,; \quad G_m^{\pm} = -G_{m+q}^{\pm} \quad (q\,\text{even}). \tag{6.24}$$

Either way, this means that we can write $F_m^{\pm}(pT/q)$ and $G_m^{\pm}(pT/q)$ in terms of their discrete Fourier transforms,

$$\mathcal{F}_l^{\pm} = \frac{1}{\sqrt{q}}\sum_{m=0}^{q-1} F_m^{\pm}\, e^{i\phi_l m}\,; \quad \mathcal{G}_l^{\pm} = \frac{1}{\sqrt{q}}\sum_{m=0}^{q-1} G_m^{\pm}\, e^{i\phi_l m}, \tag{6.25}$$

where we define

$$\phi_l \equiv \begin{cases} 2\pi l/q & \text{if } q \text{ is odd,} \\ \pi(2l+1)/q & \text{if } q \text{ is even.} \end{cases} \tag{6.26}$$

The inverse transform is

$$F_m^{\pm} = \frac{1}{\sqrt{q}}\sum_{l=0}^{q-1} \mathcal{F}_l^{\pm}\, e^{-i\phi_l m}\,; \quad G_m^{\pm} = \frac{1}{\sqrt{q}}\sum_{l=0}^{q-1} \mathcal{G}_l^{\pm}\, e^{-i\phi_l m}. \tag{6.27}$$

As in section (6.1.3) for the N spin one-axis twisting Hamiltonian, the advantage of writing the functions in terms of their discrete Fourier transforms is

that the phases in the exponentials $F_m^{\pm}$ and $G_m^{\pm}$ are now linear in m rather than quadratic in m. Substituting (6.21) and (6.22) into (6.25) and using the fact that $e^{i\phi_l m}F_m^{\pm}(pT/q)$ and $e^{i\phi_l m}G_m^{\pm}(pT/q)$ are periodic in m, it is not difficult to show that

$$\mathcal{G}_l^{\pm} = e^{-i\phi_l}\mathcal{F}_l^{\pm}. \tag{6.28}$$

Substituting (6.27) and (6.28) into our expression (6.20) allows us to write the state $\left|\tilde{\Psi}^{\pm}(t)\right\rangle$ as:

$$\begin{aligned}\left|\tilde{\Psi}^{\pm}(pT/q)\right\rangle = \frac{1}{\sqrt{q}}\sum_{l=0}^{q-1}\mathcal{F}_l^{\pm}e^{i\phi_l N/2}\left|\frac{\pi}{2},\phi+\phi_l\right\rangle_N \\ \otimes\frac{1}{\sqrt{2}}\left(|{\downarrow}\rangle \pm e^{-i(\phi+\phi_l)}|{\uparrow}\rangle\right).\end{aligned} \tag{6.29}$$

This is a superposition of q terms involving spin-coherent states $\left|\frac{\pi}{2},\phi+\phi_l\right\rangle_N$ of the N-qubit system distributed uniformly in the azimuthal Bloch sphere angle ϕ. Expression (6.29) indicates that the system undergoes fractional revivals at times $t = pT/q$ since it shows that the state at that time is a superposition of displaced copies of the initial wave packet.

The explicit value of $\mathcal{F}_l^{\pm}$ is

$$\mathcal{F}_l^{\pm} = e^{\mp\frac{i2\pi p}{q}\frac{N}{2}\left(\frac{N}{2}+1\right)}\frac{1}{\sqrt{q}}\sum_{m=0}^{q-1}e^{i\left[\phi_l m\pm\frac{p}{q}\pi m(m-1)\right]}. \tag{6.30}$$

Using equation (6.15), the sum in (6.30) can be calculated for various values of p and q. For simplicity we take $p = 1$. In this case:

$$\mathcal{F}_l^{\pm} = e^{\mp\frac{i2\pi}{q}\frac{N}{2}\left(\frac{N}{2}+1\right)}e^{\pm i\frac{\pi}{4}}e^{\mp\frac{i\pi}{4}\frac{(2l\mp1)^2}{q}} \quad (q\text{ odd}), \tag{6.31}$$

$$\mathcal{F}_l^{\pm} = e^{\mp\frac{i2\pi}{q}\frac{N}{2}\left(\frac{N}{2}+1\right)}e^{\pm i\frac{\pi}{4}}e^{\mp\frac{i\pi}{4}\frac{(2l\mp1+1)^2}{q}} \quad (q\text{ even}). \tag{6.32}$$

The initial state $|\Psi^+(0)\rangle = \left|\frac{\pi}{2},\phi\right\rangle_N\left|D_+^{\phi}(0)\right\rangle$ is a spin-coherent state of the combined $(N+1)$-qubit system:

$$\left|\Psi^+(0)\right\rangle = \left[\frac{1}{\sqrt{2}}\left(|{\downarrow}\rangle + e^{-i\phi}|{\uparrow}\rangle\right)\right]^{\otimes(N+1)}. \tag{6.33}$$

In this case (ignoring global phase factors) the evolved state takes a particularly straightforward form:

$$\left|\tilde{\Psi}^+(T/q)\right\rangle \overset{(q\text{ odd})}{=} \frac{1}{\sqrt{q}}\sum_{l=0}^{q-1} e^{i\phi_l N/2} e^{-i\pi l(l-1)/q} \left|\frac{\pi}{2}, \phi+\phi_l\right\rangle_{N+1}, \tag{6.34}$$

$$\left|\tilde{\Psi}^+(T/q)\right\rangle \overset{(q\text{ even})}{=} \frac{1}{\sqrt{q}}\sum_{l=0}^{q-1} e^{i\phi_l N/2} e^{-i\pi l^2/q} \left|\frac{\pi}{2}, \phi+\phi_l\right\rangle_{N+1}. \tag{6.35}$$

This is a superposition of spin coherent states of the $N+1$ qubit system uniformly spaced around the equator of the Bloch sphere. This is consistent with the results of Agarwal *et al.* (1997) and Chumakov *et al.* (1999) for the evolution of a spin-coherent state by a the one-axis twisting Hamiltonian. Taking $q = 2$, for example, $\left|\tilde{\Psi}^+(T/2)\right\rangle$ is a GHZ state of the $N+1$ qubits. To visualize such states we plot in Fig. 6.3 the spin Q function

$$Q(\theta,\phi) = \left|\langle\Psi^+(t)|\theta,\phi\rangle_{N+1}\right|^2, \tag{6.36}$$

of the exact state $|\Psi^+(t)\rangle$ at various times for $N = 100$ and for the initial state $|\Psi^+(0)\rangle = \left[\frac{1}{\sqrt{2}}(|\uparrow\rangle + |\downarrow\rangle)\right]^{\otimes N+1}$. For very short times the initial spin-coherent state evolves to a spin-squeezed state [Kitagawa & Ueda (1993); Ma *et al.* (2011)], as shown in figure 6.3(b). At later times we see multiple-cat states [figures 6.3(c),(d),(e)].

Since the operator $J_z + \frac{\sigma}{2}$ commutes with our Hamiltonian (6.19), we know that it (and its powers) are conserved quantities of the system. This means that if the Q function is initially a narrow distribution at the equator of the sphere, the Q function is constrained to the equator at all times, as seen in Fig. 6.3. This suggests a concise visualization of the system dynamics by plotting $Q\left(\frac{\pi}{2},\phi\right)$ as a function of time and of ϕ (ignoring the variation in the polar angle θ that plays a less interesting role). The resulting pattern is shown in Fig. 6.4. Such patterns are know as "quantum carpets" [Berry *et al.* (2001); Kaplan *et al.* (2000)]. At times $t = pT/q$ that are rational fractions of the period T we see bright spots at the values of ϕ where there are spin coherent states.

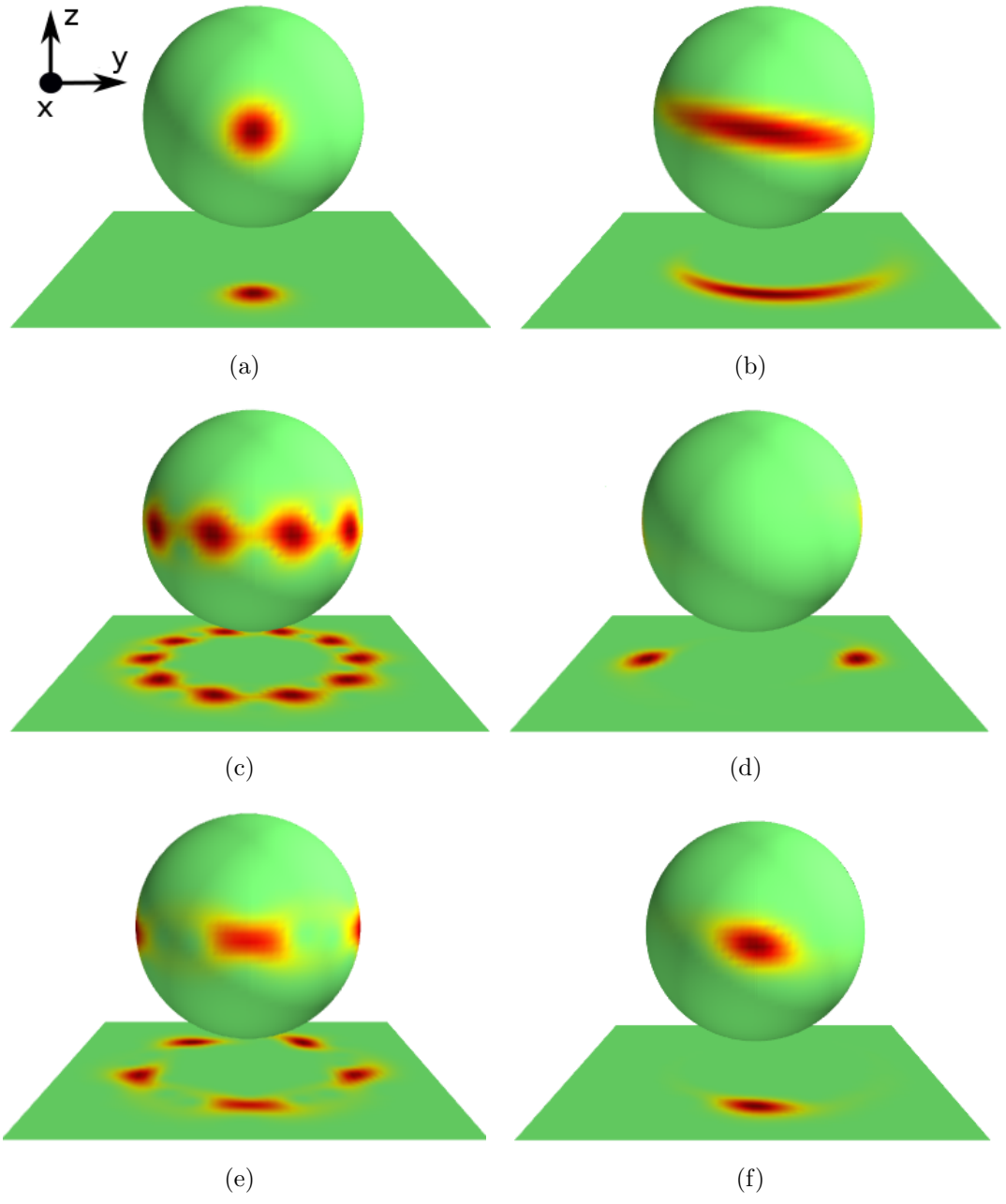

Figure 6.3: Q functions [Eq. (6.36)] and their stereographic projections at various times for the (exact) state $|\Psi^+(t)\rangle$ with $N = 100$. (a) The initial state $|\Psi^+(0)\rangle = \left[\frac{1}{\sqrt{2}}\left(|\uparrow\rangle + |\downarrow\rangle\right)\right]^{\otimes N+1}$, a spin-coherent state. (b) The state $|\Psi^+(T/50)\rangle$. (c) The state $|\Psi^+(T/10)\rangle$. (d) The state $|\Psi^+(T/2)\rangle$, a GHZ state. (e) The state $|\Psi^+(4T/5)\rangle$. (f) The state $|\Psi^+(T)\rangle$ at the revival time. This figure is reproduced from Dooley & Spiller (2014) (copyright 2014 by the American Physical Society).

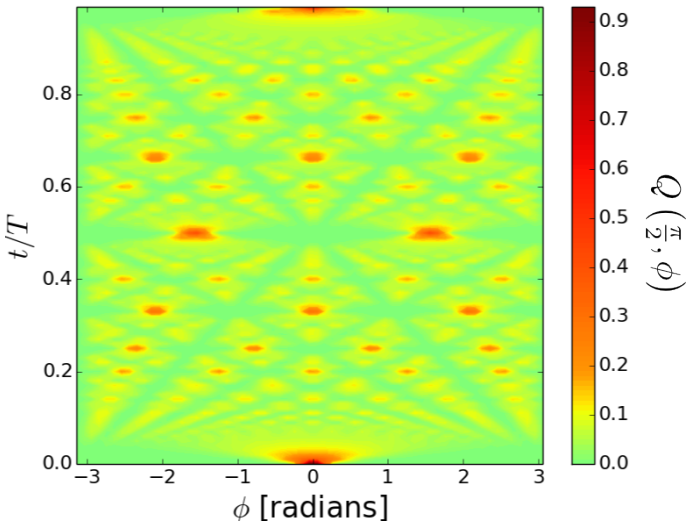

Figure 6.4: Plotted is $Q\left(\frac{\pi}{2},\phi\right)$, the Q-function slice at $\theta = \pi/2$. Here $N = 168$. We see a "quantum carpet." This figure is reproduced from Dooley & Spiller (2014) (copyright 2014 by the American Physical Society).

Small N

Our approximations require that the initial spin coherent state parameter is $|\zeta| \approx 1$ (or $\theta \approx \pi/2$), and also that $N \gg 1$ and $\lambda t \ll N$ (or, $t \ll T$). As illustrated in figure 6.2, the fidelity of the exact state to the approximate state gets worse as N gets small or as t gets close to T. Our Q-function plots show, however, that the qualitative features of the approximation are valid well outside of these parameter regimes.

In figure 6.4, for example, it is clear that the multiple-Schrödinger-cat states persist well beyond $t \ll T$. It is also clear in figures 6.3(e) and 6.3(f) where we plot the Q functions for $N = 100$ at $t = 4T/5$ and $t = T$, respectively. In figure 6.3(e) we see something qualitatively like a superposition of spin-coherent states, although the coherent states are distorted [the likely cause for the decrease in fidelity against the ideal superposition of spin-coherent states (figure 6.2)].

Similarly, although our approximation required that we assume $N \gg 1$, the Q functions in figure 6.5 show that our approximation captures the qualitative features of the exact evolution of the system for moderately small values of N. It is clear from these plots that, although they are not superpositions of perfect

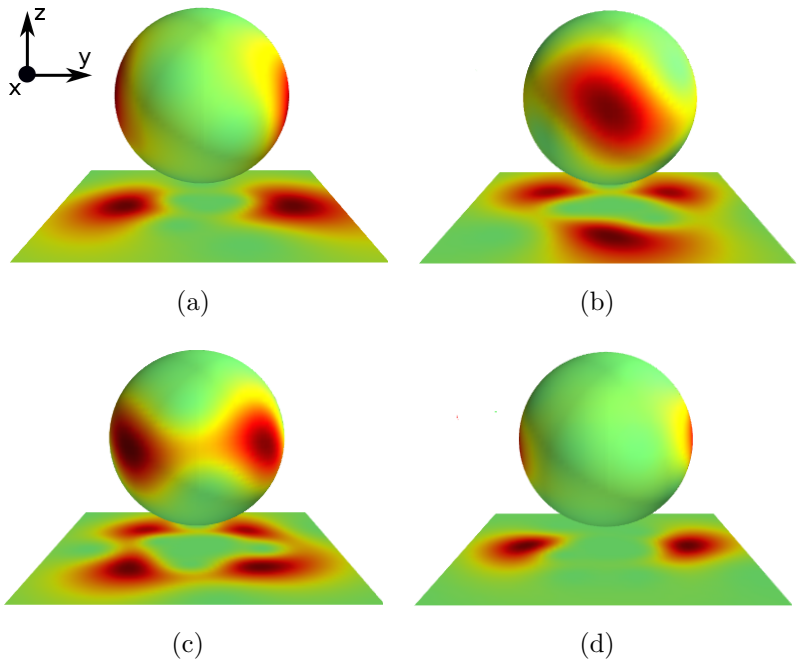

Figure 6.5: Q functions at various times and for small values of N. Each time the initial state is $|\Psi^+(0)\rangle = \left[\frac{1}{\sqrt{2}}\left(|\uparrow\rangle + |\downarrow\rangle\right)\right]^{\otimes N+1}$. (a) $|\Psi^+(T/2)\rangle$ for $N = 8$. (b) $|\Psi^+(T/3)\rangle$ for $N = 10$. (c) $|\Psi^+(T/4)\rangle$ for $N = 16$; (d) $|\Psi^+(T/2)\rangle$ for $N = 16$. This figure is reproduced from Dooley & Spiller (2014) (copyright 2014 by the American Physical Society).

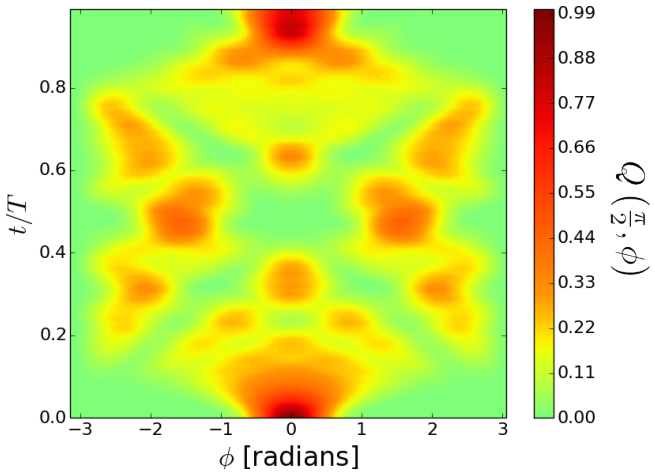

Figure 6.6: Plotted is $Q\left(\frac{\pi}{2},\phi\right)$ for $N = 16$. Even for this small value of N the "carpet" pattern is conspicuous. This figure is reproduced from Dooley & Spiller (2014) (copyright 2014 by the American Physical Society).

spin-coherent states, they are superpositions of distorted spin-coherent states, still highly non-classical states. In figure 6.6 we plot the $\theta = \pi/2$ "slice" as a function of ϕ and of t/T for $N = 16$. The "carpet" pattern, although not as sharp as in figure 6.4, is clearly recognizable. The states at $t = T/4$ and $t = T/2$ are plotted in figure 6.5(c) and 6.5(d), respectively.

The main result of this chapter has been that for an appropriate initial state the one-axis twisting Hamiltonian is an effective Hamiltonian for the resonant spin star model. This approximation is valid when $N \gg 1$, but also when N is a moderately small number. An interesting application of this result might be the observation of fractional revivals in systems of few-spins. In the next chapter we discuss the dispersive limit of the spin star model, where again the effective Hamiltonian is a one-axis twisting Hamiltonian.

Chapter 7

Beyond the Jaynes-Cummings Approximation – II

In section 4.3 we showed that, starting from the spin star Hamiltonian [equation (4.2)],

$$\hat{H}_{SS} = \frac{\Omega}{2}\hat{\sigma}_z + \omega\hat{J}_z + \lambda\left(\hat{J}_+\hat{\sigma}_- + \hat{J}_-\hat{\sigma}_+\right), \tag{7.1}$$

we can derive the effective Hamiltonian:

$$\hat{H}_{SS}^{\Delta} = \left(\omega - \frac{\lambda^2}{\Delta}\right)\hat{J}_z + \frac{\Omega}{2}\hat{\sigma}_z + \frac{\lambda^2}{\Delta}\left(\hat{J}^2 - \hat{J}_z^2\right)\otimes\hat{\sigma}_z, \tag{7.2}$$

when $\Delta = \Omega - \omega \gg N\lambda$. For convenience, we rotate to an interaction picture with respect to the bare Hamiltonian $\hat{H}_0 = \omega\left(\hat{J}_z + \frac{\hat{\sigma}_z}{2}\right)$. This gives, in place of (7.1), the Hamiltonian [see equation (4.36)]

$$\hat{H}_{SS}^{I} = \frac{\Delta}{2}\hat{\sigma}_z + \lambda\left(\hat{J}_+\hat{\sigma}_- + \hat{J}_-\hat{\sigma}_+\right), \tag{7.3}$$

and, in place of (7.2), the effective Hamiltonian:

$$\hat{H}_{SS}^{I,\Delta} = -\frac{\lambda^2}{\Delta}\hat{J}_z + \frac{\Delta}{2}\hat{\sigma}_z + \frac{\lambda^2}{\Delta}\left(\hat{J}^2 - \hat{J}_z^2\right)\otimes\hat{\sigma}_z. \tag{7.4}$$

We saw in the last chapter (section 6.1.3) that a term in the Hamiltonian proportional to $\hat{J}_z^2$ is a *one-axis twisting* term that generates multiple cat states of an N spin system. It is well known that one-axis twisting also generates spin squeezed states [Kitagawa & Ueda (1993); Ma *et al.* (2011)]. We notice that the

last term in (7.4) includes the operator $\frac{\lambda^2}{\Delta}\hat{J}_z^2 \otimes \hat{\sigma}_z$ which is a one-axis twisting term for the outer spins when the central spin is in an eigenstate of $\hat{\sigma}_z$. In this chapter we investigate the spin squeezing of the outer spins by the effective Hamiltonian (7.4).

We also consider in more detail the implementation with an ensemble of nitrogen-vacancy centres interacting with a flux qubit (this was briefly discussed at the end of section 4.1). Emphasising a particular implementation will allow us to make reasonable estimates of the various Hamiltonian parameters and to take into account realistic experimental imperfections compared to evolution by the ideal Hamiltonian (7.4). We find that these imperfections are very damaging to the amount of spin squeezing that can be generated, but that much of this damage can be mitigated by a spin echo protocol. Also, our spin squeezing is *improved* by adding flux qubit relaxation (i.e. central spin relaxation), something that may seem surprising or counter-intuitive on first sight. We conclude that significant spin squeezing of an ensemble of nitrogen-vacancy centres by interaction with a flux qubit is experimentally feasible.

7.1 An ensemble of NV centres coupled to a flux qubit

A perfect diamond crystal is a lattice of carbon atoms. A particular type of defect in this crystal structure is a *nitrogen-vacancy centre*, where one of the carbon atoms has been replaced by a nitrogen atom and in an adjacent lattice site there is a vacancy (a missing carbon atom). The nitrogen-vacancy centre is known to exist in two charge states, the neutral nitrogen-vacancy centre (NV^0) and the negatively charged nitrogen-vacancy centre (NV^-). The spin associated with the electrons in the ground state of the NV^- is a spin-1. Choosing the direction between the nitrogen atom and the vacancy to define the z-axis of our coordinate system, the Hamiltonian is [Doherty *et al.* (2012)]:

$$\hat{H}^{NV} = \left(D + d_{\parallel}E_z\right)\hat{S}_z^2 + \gamma\vec{B}\cdot\hat{\vec{S}} - d_{\perp}E_x\left(\hat{S}_x^2 - \hat{S}_y^2\right) + d_{\perp}E_y\left(\hat{S}_x\hat{S}_y + \hat{S}_y\hat{S}_x\right), \quad (7.5)$$

where $\vec{E}$ and $\vec{B}$ are external electric and magnetic fields, $\frac{D}{2\pi} \approx 2.88$ GHz is the zero-field splitting[1], γ is the gyromagnetic ratio of an NV centre, and $d_{\|}$ ($d_{\perp}$) is the ground state electric dipole moment in the direction parallel (perpendicular) to the z-axis.

In the eigenbasis $\{|1\rangle, |0\rangle, |-1\rangle\}$ of the spin-1 operator $\hat{S}_z$ we have:

$$\hat{S}_+ = |1\rangle\langle 0| + |0\rangle\langle -1| = \begin{pmatrix} 0 & 1 & 0 \\ 0 & 0 & 1 \\ 0 & 0 & 0 \end{pmatrix}, \tag{7.6}$$

$$\hat{S}_- = |0\rangle\langle 1| + |-1\rangle\langle 0| = \begin{pmatrix} 0 & 0 & 0 \\ 1 & 0 & 0 \\ 0 & 1 & 0 \end{pmatrix}, \tag{7.7}$$

$$\hat{S}_z = |1\rangle\langle 1| - |-1\rangle\langle -1| = \begin{pmatrix} 1 & 0 & 0 \\ 0 & 0 & 0 \\ 0 & 0 & -1 \end{pmatrix}, \tag{7.8}$$

$$\hat{S}_y = \frac{1}{i\sqrt{2}}\left(\hat{S}_+ - \hat{S}_-\right) = \frac{1}{i\sqrt{2}} \begin{pmatrix} 0 & 1 & 0 \\ -1 & 0 & 1 \\ 0 & -1 & 0 \end{pmatrix}, \tag{7.9}$$

$$\hat{S}_x = \frac{1}{\sqrt{2}}\left(\hat{S}_+ + \hat{S}_-\right) = \frac{1}{\sqrt{2}} \begin{pmatrix} 0 & 1 & 0 \\ 1 & 0 & 1 \\ 0 & 1 & 0 \end{pmatrix}. \tag{7.10}$$

The Hamiltonian for an ensemble of non-interacting NV centres (NVE) is just the sum of the Hamiltonians (7.5) for the individial NV centres. If we assume that the external electric field is negligible ($\vec{E} = 0$) and that the magnetic field is in the z-direction ($\vec{B} = (0, 0, B_z)$), then this is

$$\hat{H}^{NVE} = \sum_{i=1}^{N} \left(D\hat{S}_{z,i}^2 + \gamma B_{z,i}\hat{S}_{z,i} \right). \tag{7.11}$$

It is useful to split this into two parts: a "homogenous" part for which each NV centre feels a magnetic field $\bar{B}_z$ (the average of $B_{z,i}$ for each value of i), and an

[1] When there is "zero-field" ($\vec{E} = \vec{B} = 0$), the splitting between the NV centre energy levels is D, the zero-field splitting.

"inhomogeneous" part that includes the deviation of each $B_{z,i}$ from the average $\bar{B}_z$:

$$\hat{H}^{NVE} = \sum_{i=1}^{N} \left(D\hat{S}_{z,i}^2 + \gamma \bar{B}_z \hat{S}_{z,i} \right) + \hat{H}_{IB}^{NVE}, \tag{7.12}$$

where

$$\hat{H}_{IB}^{NVE} = \gamma \sum_{i=1}^{N} (B_{z,i} - \bar{B}_z) \hat{S}_{z,i}. \tag{7.13}$$

The subscript "IB" on the inhomogeneous part of the Hamiltonian stands for "inhomogeneous broadening".

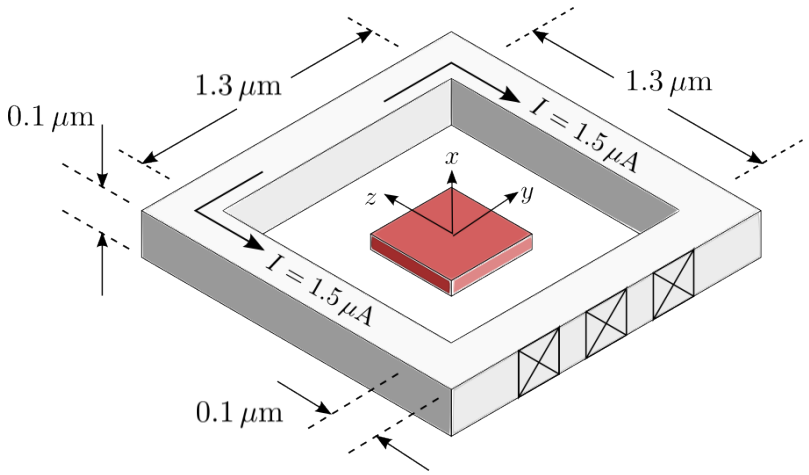

Figure 7.1: An illustration of our model. The flux qubit is in gray and the diamond containing the NV ensemble is in red.

We now consider the interaction of the NV ensemble with a flux qubit. A flux qubit is a superconducting loop interrupted by three Josephson junctions, as illustrated in figure 7.1. If the persistent current in the superconducting loop is flowing clockwise, we say that the flux qubit is in the state $|\circlearrowright\rangle$ and if the persistent current is flowing anticlockwise around the loop we say that the flux qubit is in the state $|\circlearrowleft\rangle$. We define the Pauli operator $\hat{\sigma}_x^{FQ}$ for the flux qubit to be the operator with $|\circlearrowright\rangle$ and $|\circlearrowleft\rangle$ as its eigenstates:

$$\hat{\sigma}_x^{FQ} = |\circlearrowright\rangle \langle\circlearrowright| - |\circlearrowleft\rangle \langle\circlearrowleft| . \tag{7.14}$$

By tuning the parameters of the flux qubit, the energy eigenstates can be chosen to be $|e\rangle = \frac{1}{\sqrt{2}}(|\circlearrowright\rangle + |\circlearrowleft\rangle)$ and $|g\rangle = \frac{1}{\sqrt{2}}(|\circlearrowright\rangle - |\circlearrowleft\rangle)$ with an energy splitting Ω between these two states. We define the operator $\hat{\sigma}_z^{FQ}$ to be:

$$\hat{\sigma}_z^{FQ} = |e\rangle\langle e| - |g\rangle\langle g| = |\circlearrowright\rangle\langle\circlearrowleft| + |\circlearrowleft\rangle\langle\circlearrowright|. \tag{7.15}$$

This particular configuration of the flux qubit maximises its coherence time, with the dominant form of decoherence being energy relaxation of the qubit [Yoshihara *et al.* (2006)]. The flux qubit Hamiltonian in this case is:

$$\hat{H}^{FQ} = \frac{\Omega}{2}\hat{\sigma}_z. \tag{7.16}$$

If we also take relaxation into account, the flux qubit evolves by the master equation

$$\dot{\rho} = -i\left[\hat{H}^{FQ}, \rho\right] + \frac{1}{2T_1^{FQ}}\left(\hat{\sigma}_-^{FQ}\rho\hat{\sigma}_+^{FQ} - \frac{1}{2}\rho\hat{\sigma}_+^{FQ}\hat{\sigma}_-^{FQ} - \frac{1}{2}\hat{\sigma}_+^{FQ}\hat{\sigma}_-^{FQ}\rho\right), \tag{7.17}$$

where T_1^{FQ} is the flux qubit relaxation time (the characteristic timescale for the relaxation of the flux qubit to its ground state).

Suppose that we place our NV centre ensemble in the middle of the superconducting loop of the flux qubit, with the z-axis of each NV centre in the plane of the flux qubit (see figure 7.1). Since the NV centre Hamiltonian (7.11) is symmetric around the z-axis, we are free to choose the x-axis to be perpendicular to the plane of the flux qubit, as shown in figure 7.1.

If the flux qubit is in the state $|\circlearrowright\rangle$, with the persistent current flowing clockwise, then this current generates a magnetic field at the site of each NV centre that points in the direction of the positive x-axis. Alternatively, if the flux qubit is in the state $|\circlearrowleft\rangle$ with the current flowing anti-clockwise, the magnetic field at each NV centre is in the opposite direction, pointing along the negative x-axis. The coupling between each NV centre and the magnetic field of the flux qubit is thus described by the interaction Hamiltonian,

$$\hat{H}^{int} = \sum_{i=1}^{N}\left(\sqrt{2}\lambda_i\,\hat{S}_{x,i}\otimes|\circlearrowright\rangle\langle\circlearrowright| - \sqrt{2}\lambda_i\,\hat{S}_{x,i}\otimes|\circlearrowleft\rangle\langle\circlearrowleft|\right) \tag{7.18}$$

$$= \sum_{i=1}^{N}\sqrt{2}\lambda_i\,\hat{S}_{x,i}\otimes\hat{\sigma}_x^{FQ}. \tag{7.19}$$

The coupling strength[1] $\lambda_i = \gamma|B^{FQ}_{x,i}|/\sqrt{2}$ is determined by the magnitude of the magnetic field $B^{FQ}_{x,i}$ at the i'th NV centre due to the flux qubit.

The combined Hamiltonian for the NV ensemble (7.12), the flux qubit (7.16) and the interaction (7.19) is then:

$$\begin{aligned}\hat{H}^{NVE} + \hat{H}^{FQ} + \hat{H}^{int} &= \sum_{i=1}^{N}\left(D\hat{S}^2_{z,i} + \gamma\bar{B}_{z,i}\hat{S}_{z,i}\right) + \hat{H}^{NVE}_{IB} + \frac{\Omega}{2}\hat{\sigma}_z \\ &\quad + \sum_{i=1}^{N}\sqrt{2}\lambda_i\hat{S}_{x,i}\otimes\hat{\sigma}^{FQ}_x. \end{aligned} \tag{7.20}$$

We now rotate this Hamiltonian to an interaction picture with respect to the bare Hamiltonian:

$$\hat{H}_0 = \sum_{i=1}^{N}\left(D\hat{S}^2_{z,i} + \gamma\bar{B}_z\hat{S}_{z,i}\right) + \frac{D+\gamma\bar{B}_z}{2}\hat{\sigma}^{FQ}_z. \tag{7.21}$$

The resulting interaction picture Hamiltonian is:

$$\begin{aligned}\hat{H}_I &= \hat{H}^{NVE}_{IB} + \frac{\Delta}{2}\hat{\sigma}^{FQ}_z + \sum_{i=1}^{N}\lambda_i\Big(|0_i\rangle\langle 1_i|\otimes\hat{\sigma}^{FQ}_+ + |1_i\rangle\langle 0_i|\otimes\hat{\sigma}^{FQ}_- + \\ &\quad + e^{-i2(D+\gamma\bar{B}_z)t}|0_i\rangle\langle 1_i|\otimes\hat{\sigma}^{FQ}_- + e^{i2(D+\gamma\bar{B}_z)t}|1_i\rangle\langle 0_i|\otimes\hat{\sigma}^{FQ}_+ \\ &\quad + e^{-it\gamma\bar{B}_z}|-1_i\rangle\langle 0_i|\otimes\hat{\sigma}^{FQ}_- + e^{it2\gamma\bar{B}_z}|0_i\rangle\langle -1_i|\otimes\hat{\sigma}^{FQ}_+ \\ &\quad + e^{it2D}|-1_i\rangle\langle 0_i|\otimes\hat{\sigma}^{FQ}_+ + e^{-it2D}|0_i\rangle\langle -1_i|\otimes\hat{\sigma}^{FQ}_-\Big). \end{aligned} \tag{7.22}$$

where $\Delta = \Omega - \left(D+\gamma\bar{B}_z\right)$. Now, assuming that

$$2(D+\gamma\bar{B}_z) \gg N\lambda_i, \tag{7.23}$$

$$2D \gg N\lambda_i, \tag{7.24}$$

$$2\gamma\bar{B}_z \gg N\lambda_i, \tag{7.25}$$

we can make a rotating wave approximation and throw away the quickly oscillating terms in equation (7.22). This outcome is the Hamiltonian:

[1] The factor of $2^{-1/2}$ here in the expression for λ_i and the factor of $2^{1/2}$ in equation (7.19) cancel each other, but are included for later convenience.

$$\hat{H} = \hat{H}_{IB}^{NVE} + \frac{\Delta}{2}\hat{\sigma}_z^{FQ} + \sum_{i=1}^{N} \lambda_i \Big(|0_i\rangle \langle 1_i| \otimes \hat{\sigma}_+^{FQ} + |1_i\rangle \langle 0_i| \otimes \hat{\sigma}_-^{FQ} \Big). \tag{7.26}$$

We notice that after the rotating wave approximation, the flux qubit only couples to the transition between the $|0_i\rangle$ and $|1_i\rangle$ states of each NV centre and does not interact with the $|-1_i\rangle$ state at all. If we can prepare the ensemble in the $\{|0_i\rangle, |1_i\rangle\}$ subspace of each NV centre, we can thus view it as an ensemble of spin-1/2 particles. Defining $\hat{\sigma}_{-,i}^{NV} = |0_i\rangle \langle 1_i|$ and $\hat{\sigma}_{+,i}^{NV} = |1_i\rangle \langle 0_i|$, we can rewrite (7.26) as

$$\hat{H} = \hat{H}_{IB}^{NVE} + \frac{\Delta}{2}\hat{\sigma}_z^{FQ} + \sum_{i=1}^{N} \lambda_i \Big(\hat{\sigma}_{-,i}^{NV} \otimes \hat{\sigma}_+^{FQ} + \hat{\sigma}_{+,i}^{NV} \otimes \hat{\sigma}_-^{FQ} \Big). \tag{7.27}$$

In the $\{|0_i\rangle, |1_i\rangle\}$ subspace of each NV centre, the inhomogeneous term $\hat{H}_{IB}^{NVE}$ is (after adding a term proportional to the identity operator for convenience):

$$\hat{H}_{IB}^{NVE} = \frac{\gamma}{2} \sum_{i=1}^{N} \left(B_{z,i} - \bar{B}_{z,i} \right) \hat{\sigma}_{z,i}, \tag{7.28}$$

where $\hat{\sigma}_{z,i} = |1_i\rangle \langle 1_i| - |0_i\rangle \langle 0_i|$.

At this point, we divide the last part of the above Hamiltonian into a homogenous part and an inhomogeneous part. The homogeneous part includes the average coupling of each NV centre to the flux qubit, and the inhomogenous part includes the deviations from this average:

$$\hat{H} = \hat{H}_{IB}^{NVE} + \frac{\Delta}{2}\hat{\sigma}_z^{FQ} + \bar{\lambda} \sum_{i=1}^{N} \left(\hat{\sigma}_{-,i}^{NV} \otimes \hat{\sigma}_+^{FQ} + \hat{\sigma}_{-,i}^{NV} \otimes \hat{\sigma}_-^{FQ} \right) + \hat{H}_{IC}^{int}, \tag{7.29}$$

where

$$\hat{H}_{IC}^{int} = \sum_{i=1}^{N} (\lambda_i - \bar{\lambda}) \Big(\hat{\sigma}_{-,i}^{NV} \otimes \hat{\sigma}_+^{FQ} + \hat{\sigma}_{-,i}^{NV} \otimes \hat{\sigma}_-^{FQ} \Big). \tag{7.30}$$

The subscript "IC" here stands for "inhomogeneous coupling". Now, with our usual definition $\hat{J}_\pm = \sum_{i=1}^{N} \hat{\sigma}_\pm^{NV}$ we rewrite (7.31) to give our final Hamiltonian,

$$\hat{H} = \hat{H}_{IB}^{NVE} + \frac{\Delta}{2}\hat{\sigma}_z^{FQ} + \bar{\lambda}\left(\hat{J}_- \otimes \hat{\sigma}_+^{FQ} + \hat{J}_+ \otimes \hat{\sigma}_-^{FQ}\right) + \hat{H}_{IC}^{int}. \tag{7.31}$$

Including the effect of flux qubit relaxation, our system evolves by the master equation:

$$\dot{\rho} = -i\left[\hat{H}, \rho\right] + \frac{1}{2T_1^{FQ}}\left(\hat{\sigma}_-^{FQ}\rho\hat{\sigma}_+^{FQ} - \frac{1}{2}\rho\hat{\sigma}_+^{FQ}\hat{\sigma}_-^{FQ} - \frac{1}{2}\hat{\sigma}_+^{FQ}\hat{\sigma}_-^{FQ}\rho\right). \tag{7.32}$$

7.2 Spin squeezing

If there is no inhomogeneous broadening ($\hat{H}_{IB}^{NVE} = 0$) and if each NV centre is equally coupled to the flux qubit ($\hat{H}_{IC}^{int} = 0$) then the Hamiltonian (7.31) is just the spin star Hamiltonian,

$$\hat{H}_{SS}^{I} = \frac{\Delta}{2}\hat{\sigma}_z^{FQ} + \bar{\lambda}\left(\hat{J}_- \otimes \hat{\sigma}_+^{FQ} + \hat{J}_+ \otimes \hat{\sigma}_-^{FQ}\right). \tag{7.33}$$

In the dispersive limit (when $\Delta \gg \bar{\lambda}N$) we can approximate this as [see equation (7.4)]:

$$\hat{H}_{SS}^{I,\Delta} = \frac{\Delta}{2}\hat{\sigma}_z^{FQ} - \frac{\bar{\lambda}^2}{\Delta}\hat{J}_z + \frac{\bar{\lambda}^2}{\Delta}\left(\hat{J}^2 - \hat{J}_z^2\right) \otimes \hat{\sigma}_z^{FQ}. \tag{7.34}$$

In this chapter we call this the "ideal" Hamiltonian. For clarity, we list the steps taken to get from the full Hamiltonian (7.31) to the ideal Hamiltonian (7.34):

- Inhomogeneous broadening, represented by the term $\hat{H}_{IB}^{NVE}$ in the Hamiltonian, is neglected.
- Inhomogeneous couplings, represented by the term $\hat{H}_{IC}^{int}$ in the Hamiltonian, are neglected.
- Higher order terms in the dispersive limit approximation between (7.33) and (7.34) are neglected.
- Flux qubit relaxation is neglected.

Below, we consider the "ideal" spin squeezing due to evolution of the system by (7.34). We then investigate the effect of each of the differences listed above on the spin squeezing, before looking at the spin squeezing due to the full Hamiltonian (7.31).

"Ideal" squeezing

From the ideal Hamiltonian (7.34), we can see that for a flux qubit in the ground state $|g\rangle$ or the excited state $|e\rangle$ the conditional Hamiltonian for the NV centres is

$$\hat{H}_{(g)}^{NVE} = -\frac{\Delta}{2} - \frac{\bar{\lambda}^2}{\Delta}\hat{J}_z - \frac{\bar{\lambda}^2}{\Delta}\left(\hat{J}^2 - \hat{J}_z^2\right), \tag{7.35}$$

or

$$\hat{H}_{(e)}^{NVE} = \frac{\Delta}{2} - \frac{\bar{\lambda}^2}{\Delta}\hat{J}_z + \frac{\bar{\lambda}^2}{\Delta}\left(\hat{J}^2 - \hat{J}_z^2\right), \tag{7.36}$$

respectively. We assume that the initial state of our system is,

$$|\Psi(0)\rangle = \bigotimes_{i=1}^{N}\left[\frac{1}{\sqrt{2}}\left(|1_i\rangle + |0_i\rangle\right)\right] \otimes |g\rangle\,, \tag{7.37}$$

with the flux qubit is in its ground state $|g\rangle$ and the NV ensemble in a spin coherent state. Each of the spins in this spin coherent state is an eigenstate of $\hat{\sigma}_{x,i}^{NV}$. Its spin Q-function is plotted in figure 2.11. Such a spin coherent state – with each spin on the equator of its Bloch sphere – gives us the most squeezing under one-axis twisting [Ma *et al.* (2011)]. We choose the ground state $|g\rangle$ rather than the excited state $|e\rangle$ for the flux qubit initial state because the ground state is both an eigenstate of the ideal Hamiltonian (7.34), and a steady state of the master equation (7.32) under relaxation.

In figure 7.2 we plot the spin squeezing parameter χ_R^2 as a function of time for the state $|\Psi(0)\rangle$ evolving by the ideal Hamiltonian (7.34). We remind the reader that this spin squeezing parameter was defined [in equation (3.41)] as:

$$\chi_R^2 = \frac{N \min_{\vec{r}_m^{\perp}} \mathrm{Var}\hat{J}_{\vec{r}_m^{\perp}}}{\left|\left\langle \hat{\vec{J}} \right\rangle\right|^2} \tag{7.38}$$

where $\vec{r}_m = \left\langle \vec{J} \right\rangle / \left|\left\langle \vec{J} \right\rangle\right|$ is the unit vector in the mean spin direction and $\vec{r}_m^{\perp}$ is a unit vector perpendicular to the mean spin direction. It is directly related to the usefulness of the generated state for magnetic field sensing (see section 3.2).

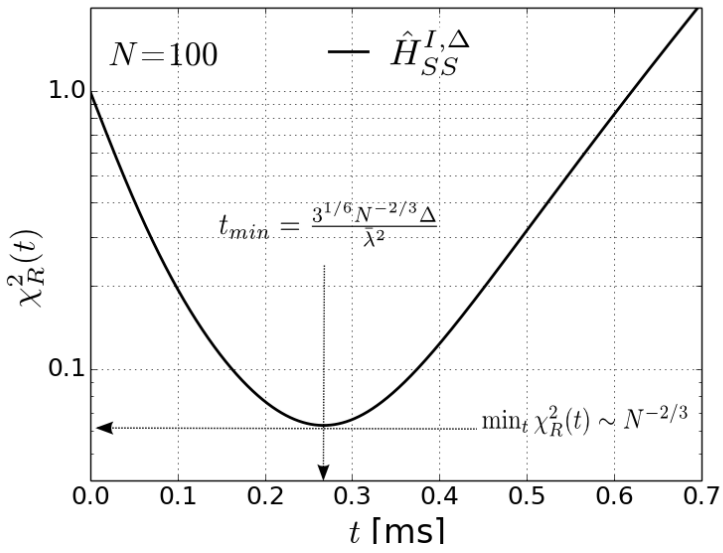

Figure 7.2: Spin squeezing of the NV ensemble for initial state (7.37) evolving by the "ideal" squeezing Hamiltonian (7.34). Here we have $N = 100$, $\bar{\lambda}/2\pi = 30$ kHz, $\Delta = 10\bar{\lambda}N$.

Figure 7.2 shows that the squeezing decreases to a minimum before increasing again. It was shown by Kitagawa & Ueda (1993); Ma *et al.* (2011) that for $N \gg 1$, this minimum comes at a time

$$t_{min} \approx \frac{3^{1/6}\Delta N^{-2/3}}{\bar{\lambda}^2}. \tag{7.39}$$

This time t_{min} scales linearly with the detuning, Δ. We would like to keep this time as short as possible to limit the effects of various types of decoherence. On the other hand, the dispersive limit approximation requires that $\Delta \gg \bar{\lambda}N$. If we decrease the detuning too much, this condition will not be satisfied. For the rest of this chapter we fix $\Delta = 10\bar{\lambda}N$ as a compromise between a well satisfied approximation condition and a reasonably short t_{min}. Substituting into equation (7.39) gives

$$t_{min} \approx \frac{12N^{1/3}}{\bar{\lambda}}. \tag{7.40}$$

It was also shown by Ma *et al.* (2011) that for $N \gg 1$ the minimum amount of

squeezing scales with N like

$$\min_t \chi_R^2(N,t) \sim N^{-2/3}. \tag{7.41}$$

This is shown in figure 7.3.

Interestingly, the spin squeezing of the NV ensemble is generated by the interaction with the flux qubit although the flux qubit is a "passive" part of the system: it remains in the ground state throughout.

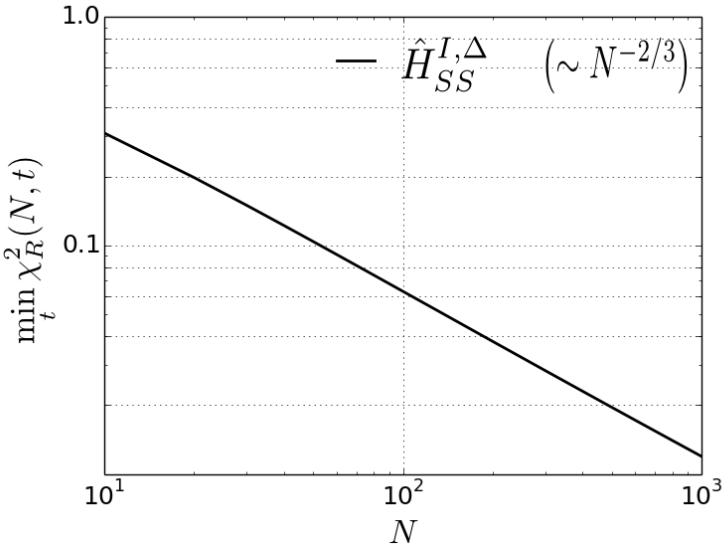

Figure 7.3: A log-log plot of the minimum spin squeezing of the NV ensemble as a function of N for the initial state (7.37) evolving by the "ideal" squeezing Hamiltonian (7.34). Here we have $\bar{\lambda}/2\pi = 30$ kHz, $\Delta = 10\bar{\lambda}N$.

We note that a similar idea has been proposed recently for the squeezing of an NV ensemble via interaction with an harmonic oscillator [Bennett *et al.* (2013)]. However, in that case the analagous effective Hamiltonian is:

$$\hat{H}_{\text{Bennett}} = \Delta\hat{a}^\dagger\hat{a} - \frac{\bar{\lambda}^2}{\Delta}\hat{J}_z - \frac{2\bar{\lambda}^2}{\Delta}\hat{J}_z \otimes \hat{a}^\dagger\hat{a} - \frac{\bar{\lambda}^2}{\Delta}\left(\hat{J}^2 - \hat{J}_z^2\right), \tag{7.42}$$

where Δ is the detuning between the NV centre energy gap and the harmonic oscillator frequency. If the harmonic oscillator is initially in the vacuum state, then this is the same as our conditional Hamiltonian (7.35) when the flux qubit

is in its ground state. In general, however, the two models are different (e.g., the conditional Hamiltonian (7.36) is different to (7.42) when the harmonic oscillator is in the first excited state).

Inhomogeneous broadening

To get an idea of the effect of inhomogeneous broadening, we briefly ignore the interaction with the flux qubit by setting $\lambda_i = 0$. In this case the NV ensemble has the Hamiltonian

$$\hat{H}_{IB}^{NVE} = \frac{g\mu_B}{2} \sum_{i=1}^{N} \left(B_{z,i} - \bar{B}_z\right) \hat{\sigma}_{z,i}, \tag{7.43}$$

and the initial spin coherent state evolves to:

$$\bigotimes_{i=1}^{N} \left[\frac{1}{\sqrt{2}} \left(|1_i\rangle + |0_i\rangle\right)\right] \longrightarrow \bigotimes_{i=1}^{N} \left[\frac{1}{\sqrt{2}} \left(e^{\frac{itg\mu_B}{2}(B_{z,i}-\bar{B}_z)} |1_i\rangle + e^{-\frac{itg\mu_B}{2}(B_{z,i}-\bar{B}_z)} |0_i\rangle\right)\right]. \tag{7.44}$$

We see that each NV centre evolves around its Bloch sphere at a different rate. In figure 7.4 we plot $\left|\left\langle \vec{\hat{J}} \right\rangle\right|$, the length of the mean spin vector of the NV ensemble, as it evolves by $\hat{H}_{IB}^{NVE}$. We see that $\left|\left\langle \vec{\hat{J}} \right\rangle\right|$ decays due to this dephasing of the spins in the ensemble.

We now turn on the interaction between the NV ensemble and the flux qubit so that the system evolves by $\hat{H}_{SS}^{I} + \hat{H}_{IB}^{NVE}$ (the ideal Hamiltonian, with inhomogeneous broadening). Again, the flux qubit relaxation can be ignored since the initial state for the flux qubit is the ground state $|g\rangle$, an eigenstate of Hamiltonian (7.34) and a steady state of the master equation (7.32). From the definition of the spin squeezing parameter (3.41):

$$\chi_R^2 = \frac{N \min_{\vec{r}^{\perp}} \mathrm{Var} \hat{J}_{\vec{r}^{\perp}}}{\left|\left\langle \vec{\hat{J}} \right\rangle\right|^2}, \tag{7.45}$$

we can see that the decay of $\left|\left\langle \vec{\hat{J}} \right\rangle\right|$ plotted in 7.4 will result in an increase in the squeezing parameter χ_R^2. This damage to the spin squeezing can, however, by compensated by a sequence of π-pulses, a *spin echo*. A π-pulse is a rotation of

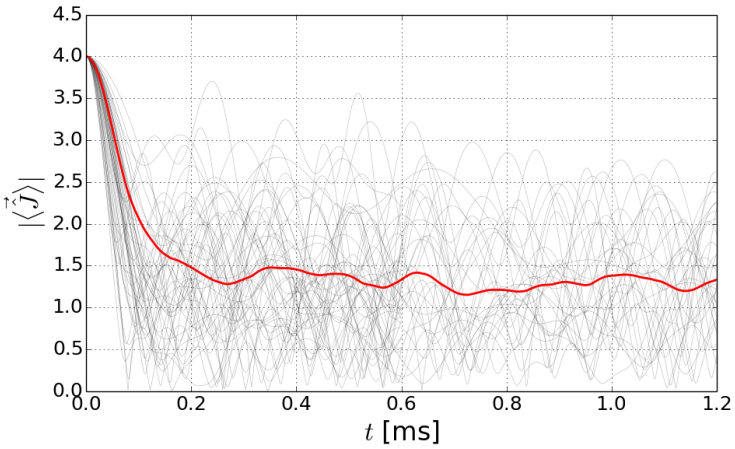

Figure 7.4: The dephasing of ($N = 8$) NV centres evolving by equation (7.44). Each black line shows a single run of the evolution for a set of values of $B_{z,i}$ randomly selected from a Gaussian distribution with standard deviation $\sigma(B_{z,i})$. The red line show the average of all the runs (a total of 50). Here we have chosen $g\mu_B\sigma(B_{z,i})/2\pi = 3$ kHz. We see that this gives a dephasing time of approximately $T_2^* \sim 100\,\mu$s, which is consistent with experimental values [Maurer *et al.* (2012)].

each of the NV centres by an angle π about the x-axis of its Bloch sphere. It is represented by the unitary operator,

$$\hat{\Pi} = \bigotimes_{i=1}^{N} e^{i\pi\hat{\sigma}_{x,i}/2} = i^N \bigotimes_{i=1}^{N} \hat{\sigma}_{x,i}. \tag{7.46}$$

We notice that this π-pulse operator commutes with our ideal Hamiltonian:

$$\left[\hat{\Pi}, \hat{H}^I_{SS}\right] = \hat{\Pi}\,\hat{H}^I_{SS} - \hat{H}^I_{SS}\,\hat{\Pi} = 0, \tag{7.47}$$

and anti-commutes with the inhomogeneous broadening Hamiltonian:

$$\{\hat{\Pi}, \hat{H}^{NVE}_{IB}\} = \hat{\Pi}\,\hat{H}^{NVE}_{IB} + \hat{H}^{NVE}_{IB}\,\hat{\Pi} = 0. \tag{7.48}$$

This means that a π-pulse at time $t/2$, and another π-pulse at time t leads to the following evolution:

$$|\Psi(t)\rangle = \hat{\Pi}\, e^{-i\frac{t}{2}\left(\hat{H}^I_{SS}+\hat{H}^{NVE}_{IB}\right)}\, \hat{\Pi}\, e^{-i\frac{t}{2}\left(\hat{H}^I_{SS}+\hat{H}^{NVE}_{IB}\right)}\, |\Psi(0)\rangle \tag{7.49}$$

$$= \hat{\Pi}\, e^{-i\frac{t}{2}\hat{H}^I_{SS}}\, e^{-i\frac{t}{2}\hat{H}^{NVE}_{IB}}\, \hat{\Pi}\, e^{-i\frac{t}{2}\hat{H}^I_{SS}}\, e^{-i\frac{t}{2}\hat{H}^{NVE}_{IB}}\, |\Psi(0)\rangle \tag{7.50}$$

$$= \hat{\Pi}\, e^{-i\frac{t}{2}\hat{H}^{NVE}_{IB}}\, \hat{\Pi}\, e^{-i\frac{t}{2}\hat{H}^{NVE}_{IB}} e^{-it\hat{H}^I_{SS}}\, |\Psi(0)\rangle \tag{7.51}$$

$$= \hat{\Pi}\, \hat{\Pi}\, e^{+i\frac{t}{2}\hat{H}^{NVE}_{IB}}\, e^{-i\frac{t}{2}\hat{H}^{NVE}_{IB}}\, e^{-it\hat{H}^I_{SS}}\, |\Psi(0)\rangle \tag{7.52}$$

$$= e^{-it\hat{H}^I_{SS}}\, |\Psi(0)\rangle\,. \tag{7.53}$$

In the second line we have used the fact that $\hat{H}^I_{SS}$ commutes with $\hat{H}^{NVE}_{IB}$ to factorise the exponential. In the third line we have used (7.47) to move the ideal evolution to the right of all other operators. In the fourth line (7.52) we have used (7.48). The final state (7.53) only includes evolution by the ideal Hamiltonian so that the effect of the π-pulse at time $t/2$ is to cancel the inhomogeneous broadening at time t.

Higher order terms

We now consider the effect of higher order terms on spin squeezing. In other words, we compare[1] the spin squeezing when the system evolves by the ideal Hamiltonian (7.34):

$$\hat{H}^{I,\Delta}_{SS} = \frac{\Delta}{2}\hat{\sigma}^{FQ}_z - \frac{\bar{\lambda}^2}{\Delta}\hat{J}_z + \frac{\bar{\lambda}^2}{\Delta}\left(\hat{J}^2 - \hat{J}^2_z\right) \otimes \hat{\sigma}^{FQ}_z, \tag{7.54}$$

to the spin squeezing when the system evolves by (7.33):

$$\hat{H}^I_{SS} = \frac{\Delta}{2}\hat{\sigma}^{FQ}_z + \bar{\lambda}\left(\hat{J}_- \otimes \hat{\sigma}^{FQ}_+ + \hat{J}_+ \otimes \hat{\sigma}^{FQ}_-\right). \tag{7.55}$$

The results are plotted against time in figure 7.5(a) for $N = 100$. The black line (slightly hidden behind the green dashed line) shows the ideal squeezing and the red line shows the effect of the higher order terms. We see that these higher order terms damage the squeezing. Interestingly, however, the dashed green line shows that adding flux qubit relaxation *improves* the spin squeezing. In figure 7.5(b) we plot the minimum squeezing as a function of N. We see that the higher order terms damage the scaling of the spin squeezing (the red line), but that adding flux qubit relaxation returns us to the ideal scaling (the dashed green line).

[1] Of course, for a fair comparison, both evolutions have the same values of $\bar{\lambda}/2\pi = 30\,\text{kHz}$ and $\Delta = 10N\bar{\lambda}$, and the same initial state (7.37).

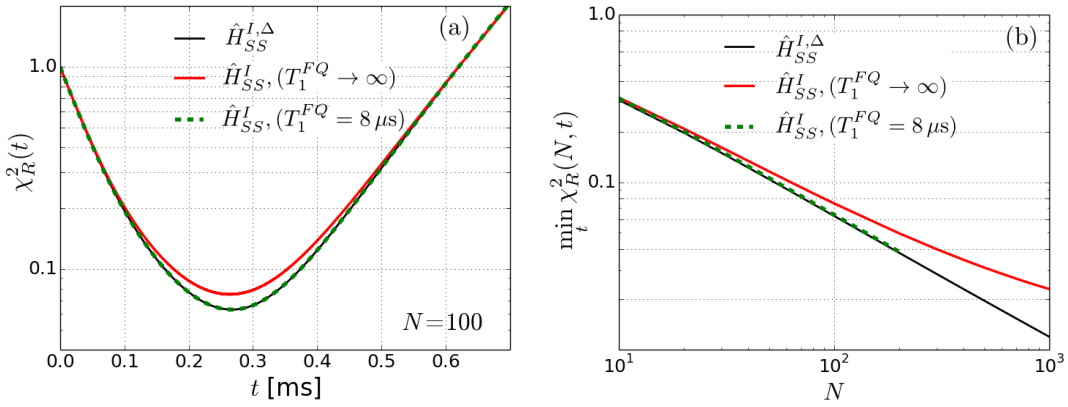

Figure 7.5: Spin squeezing including higher order terms. The black lines show ideal squeezing, the red lines show the effect of the higher order terms. The dashed green lines show that adding flux qubit relaxation returns us to the ideal squeezing.

The improvement of the spin squeezing by adding flux qubit relaxation may be surprising on first sight, since in most models decoherence is an unwanted influence on the dynamics. As a partial explanation for the improvement we plot in figure 7.6 the excitation probability of the flux qubit. In the ideal case, the flux qubit remains in the ground state $|g\rangle$ throughout the evolution (the black line). When the higher order terms are included the excitation probability is small (always below 0.01 in figure 7.6) but the oscillation indicates an exchange of energy between the NV ensemble and the flux qubit (the red line). Adding flux qubit relaxation (the dashed green line) suppresses this unwanted interaction between the flux qubit and the NV ensemble.

Now, as well as the higher order terms, we add inhomogeneous broadening. This corresponds to evolution by the Hamiltonian

$$\hat{H}_{SS}^{I} + \hat{H}_{IB}^{NVE} = \frac{\Delta}{2}\hat{\sigma}_z^{FQ} + \hat{H}_{IB}^{NVE} + \bar{\lambda}\left(\hat{J}_- \otimes \hat{\sigma}_+^{FQ} + \hat{J}_+ \otimes \hat{\sigma}_-^{FQ}\right). \tag{7.56}$$

The spin squeezing for this evolution is plotted in figure 7.7(a) for 200 runs, each run with the magnetic field $B_{z,i}$ randomly selected from a Gaussian distribution with a standard deviation $g\mu_B\sigma(B_{z,i})/2\pi = 3$ kHz. The bright red line in figure 7.7(a) shows the average of the 200 runs. As expected, the inhomogeneous broadening is very damaging to the spin squeezing. In the last section, however,

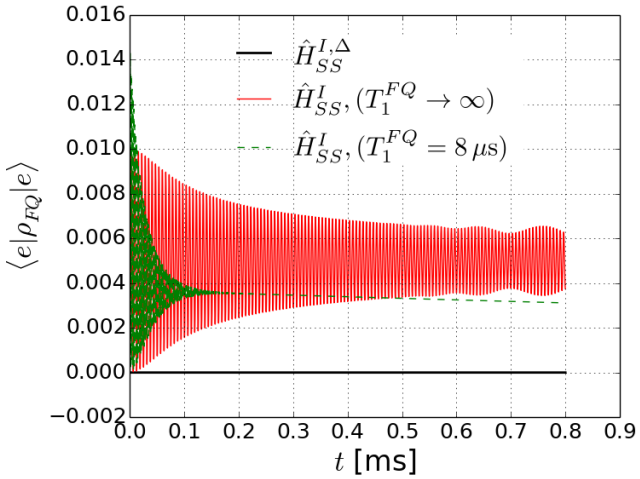

Figure 7.6: Adding flux qubit relaxation suppresses the interaction between the NV ensemble and the flux qubit.

we saw that a π-pulse at time $t/2$ can reverse the effect of the inhomogeneous broadening so that the ideal squeezing can be achieved at time t. Figure 7.7(b) shows that if the higher order terms are also included a π-pulse at time $t/2$ does improve the spin squeezing, but does not return us to the ideal squeezing at t.

Since a single π-pulse does not perfectly cancel the inhomogeneous broadening, it might turn out that a different sequence of π-pulses is more effective in improving the spin squeezing. Indeed, we see in figure 7.8(a) that adding more π-pulses allows us to achieve a better minimum spin squeezing. Figure 7.8(b) shows the scaling of this minumum squeezing with N. We see that (at least for these small values of N) the ideal scaling can be recovered. Although the three π-pulses in figure 7.8(a) give better spin squeezing than other sequences of π-pulses that we have tried numerically, some other sequence of π-pulses may improve the spin squeezing further. We intend to tackle this optimisation in future work.

We note that the effect of higher order terms was not included by Bennett *et al.* (2013) for the interaction of an NV ensemble and an harmonic oscillator.

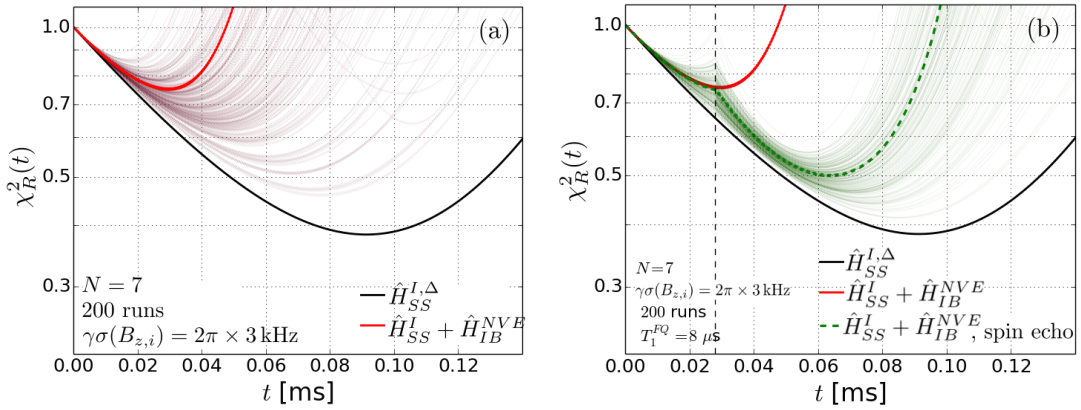

Figure 7.7: (a) Spin squeezing including higher order terms and inhomogeneous broadening. The bright red line shows the average of 200 runs, each run with the magnetic field $B_{z,i}$ randomly selected from a Gaussian distribution with a standard deviation $g\mu_B\sigma(B_{z,i})/2\pi = 3$ kHz. The individual runs are shown in light red. For comparison, the black line shows the ideal squeezing. We see that inhomogeneous broadening is very damaging to the spin squeezing. (b) Each faint green lines shows the effect of π-pulse on a single run. The dashed green line shows the average of 200 runs.

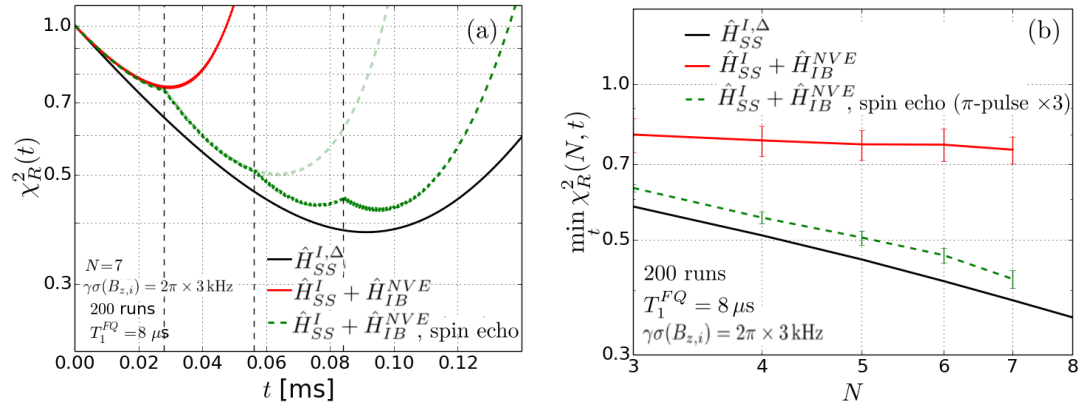

Figure 7.8: (a) Three equally spaced π-pulses allow us to achieve a better minumum squeezing than for one π-pulse [figure 7.7(b)]. (b) The scaling of the minumum squeezing is improved by the π-pulses (each point on the dashed green line corresponds to the minimum squeezing for three π-pulses where the first π-pulse is at the minimum of the red curve and the next two π-pulses are at equal time intervals after this, as in figure 7.8(a) for $N = 7$).

Inhomogeneous couplings

Finally, we also consider the effect of inhomogeneous couplings on the spin squeezing. This brings us back to the full Hamiltonian (7.31).

As explained in equation (7.19) and the surrounding text, the coupling of each NV centre to the flux qubit is $\lambda_i = \gamma |B_{x,i}^{FQ}|/\sqrt{2}$ where $B_{x,i}^{FQ}$ is the magnetic field at the i'th NV centre due to the current in the flux qubit. This magnetic field can be estimated via the Biot-Savart law:

$$\vec{B}_i^{FQ} = \frac{\mu_0}{4\pi} \int_V \frac{(\vec{J}dV) \times \vec{r}_i}{|\vec{r}_i|^3} \tag{7.57}$$

where $\mu_0 = 4\pi \times 10^{-7}\ \mathrm{T \cdot m/A}$ is the magnetic permeability of free space, $\vec{J}dV$ is the current through the volume element dV of the flux qubit, and $\vec{r}_i$ is the vector between the volume element dV and the i'th NV centre. For a flux qubit with the dimensions shown in figure 7.1, and with a uniform persistent current of $I = 1.5\,\mu\mathrm{A}$, the magnitude of the current density is $|\vec{J}| = I/A$ where A is the cross-sectional area of the flux qubit. We plot in figure 7.9 the coupling strength at each point in the interior of the flux qubit due to the magnetic field (7.57) for these parameters. We see that the coupling is relatively homogeneous across a broad region around the middle of the flux qubit. This homogeneity is an advantage of the particular setup illustrated in figure 7.1 with the NV ensemble in the middle of the flux qubit. From figure 7.9 we see that for these parameters it is reasonable to choose the couplings $\lambda_i/2\pi$ between 25 kHz and 35 kHz with an average of approximately $\bar{\lambda}/2\pi = 30\,\mathrm{kHz}$.

Putting everything together, we plot in figure 7.10(a) the spin squeezing for the full Hamiltonian (7.31), including the effect of higher order terms, inhomogeneous broadening and inhomogenous couplings selected randomly from a uniform distribution between $\lambda_i = 25\,\mathrm{kHz}$ and $\lambda_i = 35\,\mathrm{kHz}$. The red line shows the average of 200 runs. The dashed green line in figure 7.10(a) shows the average of 200 runs with a spin echo sequence consisting of three π-pulses, and also with flux qubit relaxation. The spin squeezing is significantly improved. Figure 7.10(b) shows the scaling of the spin squeezing. Even with the various imperfections included, the dashed green line shows that we can get close to the ideal scaling thanks to the spin echo and the flux qubit relaxation. We conclude that significant squeezing of the NV centres is experimentally feasible.

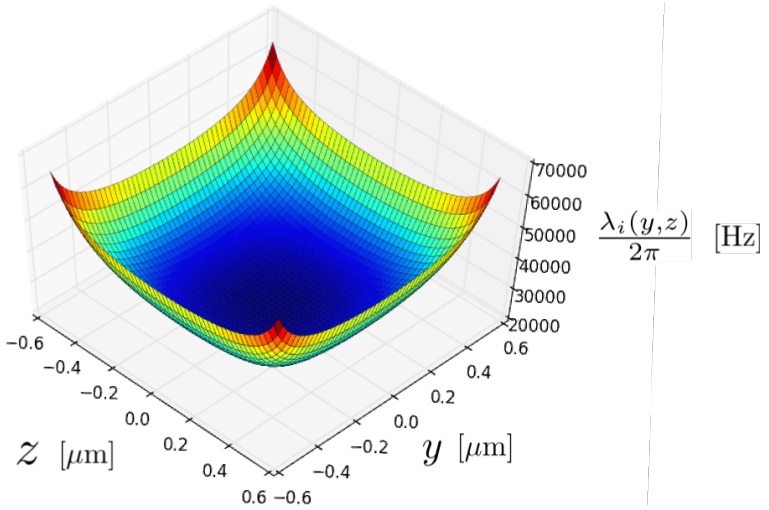

Figure 7.9: The coupling strength of the flux qubit with an NV centre at the coordinates $(0, y, z)$ in the interior of the flux qubit (where the x, y, z coordinate axes are as shown in figure 7.1). The vertical axis for the contour plot is the coupling strength $\lambda_i(y, z)/2\pi$, not the spatial coordinate x. We see that the coupling is relatively homogeneous (between $\lambda_i/2\pi \approx 25$ kHz and $\lambda_i/2\pi \approx 35$ kHz) in the middle of the flux qubit (the blue area).

The above analysis has not taken into account some other forms of decoherence, for example, NV centre dephasing due to interaction with nuclear spins in the diamond crystal lattice. The most abundant isotope of carbon is ^{12}C which has no nuclear spin. The ^{13}C isotope, however, does have nuclear spin and interaction of an NV centre with a ^{13}C nucleus results in dephasing. This dephasing can be supressed by using very pure diamond with a very low concentration of ^{13}C. Another nuclear spin that leads to dephasing of the NV centre is due to nitrogen atoms in the diamond (i.e., nitrogen atoms in place of carbon atoms). The production of NV centres requires these nitrogen atoms in the diamond lattice. It is the residual nitrogen atoms that do not form NV centres that can be a source of decoherence for the NV centres. The density of these nitrogen defects is roughly in proportion to the density of NV centres, so that this dephasing can be reduced by using a diamond sample with a low density of NV centres [Stanwix *et al.* (2010)]. However, we would like to generate a squeezed state of as many NV centres as possible, which requires either a large volume of diamond

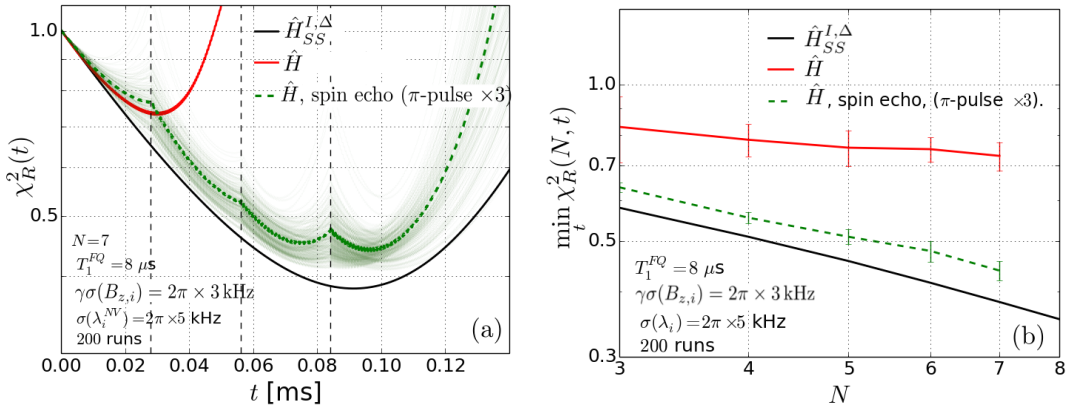

Figure 7.10: Spin squeezing by the full Hamiltonian (7.31). This includes inhomogeneous broadening, inhomogeneous coupling, and higher order terms. We see that flux qubit relaxation and a sequence of three π-pulses give a significant improvement to the spin squeezing.

(at the cost of more inhomogeneity in the couplings – see figure 7.9), or a high density (at the cost of a shorter dephasing time). In future work we will find the compromise between the density and the volume of the diamond that gives the best spin squeezing. Moreover, we note that the number of NV centres can be increased just by improving on the setup illustrated in figure 7.1. For example, we can use two flux qubits in a Helmholz coil configuration, that is, with the two flux qubits on top of each other separated by half the length of the side of one of the flux qubits. If the NV ensemble is placed between the flux qubits we can get a stronger, and more homogeneous coupling between the ensemble and the flux qubits over a larger spatial region [Scharfenberger (2014)]. This will allow us to increase the number of NV centres without increasing the density, and without sacrificing homogeneity in the coupling to the flux qubit.

Chapter 8

Conclusion

In this thesis we have shown that, starting from a spin coherent state of the outer spins, the spin star model can be used to generate a variety of non-classical states with significant potential for quantum-enhanced magnetic field sensing.

First, we have identified a parameter regime corresponding to the well-known Jaynes-Cummings model (chapter 5). Here, the evolving system can produce Dicke squeezed states and Schrödinger cat states of the outer spin system, even for modest values (~ 40) of N, the number of outer spins. Also in this parameter regime, we see collapse and revival analagous to the Jaynes-Cummings model. Future work will investigate the possibility of generating "macro-micro" entangled states between the outer spins (the "macro" system) and the central spin ("the micro" system) in the Jaynes-Cummings approximation. Preliminary numerical investigations suggest that this can be achieved in a time that becomes shorter as the number of outer spins is increased. As for the Jaynes-Cummings model (section 5.1), this is related to the collapse time, that is, the time at which the counter-rotating spin coherent states become distinguishable. Such a state – generated more quickly than a pure Schrödinger cat state of the outer spins (see section 5.2) – may also be useful for magnetic field sensing.

Also in this parameter regime, we hope to investigate the possibility of exploiting the very short Rabi period [which scales as N^{-1} – see equation (5.44) and the surrounding text] for quantum enhanced parameter estimation. Finally in the Jaynes-Cummings approximation of the spin star model, future work will explore the use of Dicke squeezed states (see figure 5.8) for quantum metrology,

a topic that has not been studied in detail until very recently [Zhang & Duan (2014)].

We have also shown that interesting non-classical states can be generated beyond the Jaynes-Cummings approximation. On resonance (chapter 6), we can generate multiple cat states of the combined $N+1$ spin system. As explained in section 3.4, such states can, in principle, give Heisenberg precision scaling in the estimation of an unknown magnetic field whose direction is also unknown, whereas (in the "worst case scenario") a GHZ state gives scaling at the standard quantum limit. We have shown that the generation of multiple cat states is associated with the phenomenon of fractional revival. Spin squeezed states can also be generated in this parameter regime. In a future work we hope to look into the practical details of this for the implementation of the spin star model with an ensemble of NV centres and a flux qubit.

In the dispersive limit of the spin star model (chapter 7) we can generate multiple cat states and spin squeezed states of the outer spins. In particular, for a system of NV centres and a flux qubit we find that, despite various realistic imperfections, the generation of spin squeezed states is feasible (section 7.2), thanks to spin echo and flux qubit relaxation. In future work we aim to improve the spin squeezing generated in this system by finding the optimal spin echo sequence and also by adding another flux qubit to the setup in a Helmholtz coil configuration (as discussed at the end of the chapter 7). More generally, we will extend the results included in this thesis to a spin star model with two central spins [Hamdouni *et al.* (2006)].

Another possible extension to the results in chapter 7 is the idea of sensing a magnetic field at the same time as squeezing. This is particularly important for our spin squeezing proposal because, as shown in equation (7.40), the time taken to generate the states with the most spin squeezing scales as $N^{1/3}$ (when the detuning is fixed at $\Delta = 10N\bar{\lambda}$). From figure 7.2 we see that for coupling $\bar{\lambda}/2\pi = 30\,\text{kHz}$ this time is of the order of hundreds of micro-seconds when $N \sim 100$. For $N \sim 10^5$, then, it is of the order of milli-seconds. This is certainly not a negligible amount of time and since the sensing time is an important resource in metrology [see equation (3.28)], it would be a more effective use of the time if we could simultaneously squeeze and sense.

From a practical perspective, each of the non-classical states mentioned above

can be generated from straightforward initial states: the central spin is initially in a pure state and the outer spins are in a spin coherent state: a separable state of its N component spins with each of the spins aligned. For some implementations, however, it may be difficult to generate some initial spin coherent states of the outer spins from the ground state $|\downarrow\rangle^{\otimes N}$. As discussed at the end of section 2.2.1, for example, this requires a very large magnetic field if the bare Hamiltonian of each of the spins has a very large energy gap. For an ensemble of NV centres this is indeed the case, since the bare Hamiltonian of the NV ensemble is [equation (7.11)]:

$$\hat{H}^{NVE} = \sum_{i=1}^{N} \left(D\hat{S}_{z,i}^2 + \gamma B_{z,i} \hat{S}_{z,i} \right), \tag{8.1}$$

with a large zero field splitting $D/2\pi \approx 2.88\,\text{GHz}$. Moreover, a very large magnetic field can damage the other component of our hybrid system, the flux qubit. For this reason, we wish to investigate another proposal for the generation of non-classical states starting from the ground state $|\downarrow\rangle^{\otimes N}$ of the outer spins. The idea is as follows: The Jaynes-Cummings Hamiltonian in a rotating frame of reference is [see equation (5.13)]:

$$\hat{H}_{JC}^{I} = \frac{\Delta}{2}\hat{\sigma}_z + \lambda\,(\hat{a}\,\hat{\sigma}_+ + \hat{a}^\dagger \hat{\sigma}_-). \tag{8.2}$$

If we drive the two-level atom with an oscillating electric field at the frequency of the rotating frame then the Hamiltonian becomes:

$$\begin{aligned}
\hat{H}_{JC}^{I,drive} &= \frac{\Delta}{2}\hat{\sigma}_z + \lambda\,(\hat{a}\,\hat{\sigma}_+ + \hat{a}^\dagger \hat{\sigma}_-) + \epsilon\hat{\sigma}_- + \epsilon^*\hat{\sigma}_+ && (8.3)\\
&= \frac{\Delta}{2}\hat{\sigma}_z + \lambda\left[\left(\hat{a} + \frac{\epsilon}{\lambda}\right)\hat{\sigma}_+ + \left(\hat{a}^\dagger + \frac{\epsilon^*}{\lambda}\right)\hat{\sigma}_-\right] && (8.4)\\
&= D^\dagger\left(\frac{\epsilon}{\lambda}\right)\hat{H}_{JC}^{I} D\left(\frac{\epsilon}{\lambda}\right), && (8.5)
\end{aligned}$$

where $D\left(\frac{\epsilon}{\lambda}\right)$ is the displacement operator for the harmonic oscillator. In the last line we see that the driven Jaynes-Cummings Hamiltonian is the same as a displacement of the standard Jaynes-Cummings Hamiltonian. Assuming that the initial state of the oscillator in this picture is the vacuum state $|0\rangle$, we are free to change the basis of our system by a displacement $D\left(\frac{\epsilon}{\lambda}\right)$, a unitary transformation.

In the new basis the Hamiltonian for the system is

$$D\left(\frac{\epsilon}{\lambda}\right)\hat{H}_{JC}^{I,drive}D^{\dagger}\left(\frac{\epsilon}{\lambda}\right)=\hat{H}_{JC}^{I}, \tag{8.6}$$

the standard Jaynes-Cummings Hamiltonian, and the initial state of the oscillator is $D\left(\frac{\epsilon}{\lambda}\right)|0\rangle=\left|\frac{\epsilon}{\lambda}\right\rangle$, a coherent state of complex amplitude $\frac{\epsilon}{\lambda}$. We see that the driven Jaynes-Cummings model with the oscillator initially in the ground state is unitarily equivalent to the standard Jaynes-Cummings model with the osillator initially in the coherent state $\left|\frac{\epsilon}{\lambda}\right\rangle$. In other words, instead of preparing a coherent state of the oscillator we may prepare the vacuum state and drive the atom. Similarly, in the Jaynes-Cummings approximation of the spin star model, instead of preparing a spin coherent state of the outer spins we can prepare the state $|\downarrow\rangle^{\otimes N}$ and drive the central spin. By increasing the amplitude of the driving field, however, we increase the parameter $|\epsilon|$ and we go beyond the Jaynes-Cummings approximation. In this case, the above analysis cannot be applied to the spin star model. Preliminary numerical investigations suggest that in this parameter regime, we can squeeze the outer spins from the initial ground state $|\downarrow\rangle^{\otimes N}$, but there is much work to be done to understand these dynamics. For the implementation of the spin star model with the NV ensemble and the flux qubit this may be particularly useful since it is easier to drive the flux qubit by a large microwave field than it is to drive the NV ensemble by a large magnetic field.

Finally, as a general problem in quantum metrology, we would like to extend the investigations of section 3.4 to find which states should be prepared to give the best precision in estimation of the *direction* (rather than the magnitude) of an unknown magnetic field (in other words, a "quantum compass").

Appendix A

A.1 Useful expressions

Here, we write down expectation values and variances of collective spin operators when the spin system is in a spin coherent state $|j,\zeta\rangle_N$.

$$\langle J_z\rangle = -j\left(\frac{1-|\zeta|^2}{1+|\zeta|^2}\right) \quad ; \quad \left\langle J_z^2\right\rangle = j^2 - \frac{2j(2j-1)\,|\zeta|^2}{\left(1+|\zeta|^2\right)^2} \tag{A.1}$$

$$\langle J_z\rangle + j = \frac{2j\,|\zeta|^2}{1+|\zeta|^2} \quad ; \quad \left\langle (J_z+j)^2\right\rangle = \frac{2j\,|\zeta|^2\left(1+2j\,|\zeta|^2\right)}{\left(1+|\zeta|^2\right)^2} \tag{A.2}$$

$$\mathrm{Var}\,(J_z+j) = \left\langle (J_z+j)^2\right\rangle - \langle (J_z+j)\rangle^2 = \frac{2j\,|\zeta|^2}{\left(1+|\zeta|^2\right)^2} = \mathrm{Var}(J_z) \tag{A.3}$$

$$\langle J_+J_-\rangle = \frac{2j\,|\zeta|^2\left(2j+|\zeta|^2\right)}{\left(1+|\zeta|^2\right)^2}\,;\ \langle J_-J_+\rangle = \frac{2j\left(1+2j\,|\zeta|^2\right)}{\left(1+|\zeta|^2\right)^2} \tag{A.4}$$

$$\langle [J_-,J_+]\rangle = 2j\left(1-\frac{2\,|\zeta|^2}{1+|\zeta|^2}\right) \approx 2j \ \text{ when } \ \frac{2\,|\zeta|^2}{1+|\zeta|^2} \ll 1 \Leftrightarrow |\zeta|^2 \ll 1 \tag{A.5}$$

$$\langle J_-\rangle = \frac{2j\zeta}{1+|\zeta|^2} \quad ; \quad \left\langle J_-^2\right\rangle = \frac{2j(2j-1)\zeta^2}{\left(1+|\zeta|^2\right)^2} \tag{A.6}$$

$$\langle J_+\rangle = \frac{2j\zeta^*}{1+|\zeta|^2} \quad ; \quad \left\langle J_+^2\right\rangle = \frac{2j(2j-1)\zeta^{*2}}{\left(1+|\zeta|^2\right)^2} \tag{A.7}$$

$$\langle J_x\rangle = \frac{j(\zeta^*+\zeta)}{1+|\zeta|^2} \quad ; \quad \mathrm{Var}\,(J_x) = \frac{j}{2}\frac{(1-\zeta^{*2}-\zeta^2+|\zeta|^4)}{\left(1+|\zeta|^2\right)^2} \tag{A.8}$$

$$\langle J_y \rangle = \frac{j(-i\zeta^* + i\zeta)}{1+|\zeta|^2} \quad ; \quad \mathrm{Var}\,(J_y) = \frac{j}{2}\frac{(1+\zeta^{*2}+\zeta^2+|\zeta|^4)}{\left(1+|\zeta|^2\right)^2} \tag{A.9}$$

A.2 The spin coherent state as an approximate eigenstate

Below we show that when

$$\frac{1}{\sqrt{2j}} \ll |\zeta| \ll \sqrt{2j} \quad \text{and} \quad 1 \ll 2j, \tag{A.10}$$

we can approximate:

$$\left(\hat{J}_-\hat{J}_+\right)^{-1/2}\hat{J}_-\left|j,\zeta\right\rangle_N \approx e^{-i\phi}\left|j,\zeta\right\rangle_N, \tag{A.11}$$

$$\left(\hat{J}_+\hat{J}_-\right)^{-1/2}\hat{J}_+\left|j,\zeta\right\rangle_N \approx e^{i\phi}\left|j,\zeta\right\rangle_N, \tag{A.12}$$

where $\zeta = |\zeta|e^{-i\phi}$. This result and its proof were included in our publication PRA2014.

The operator $\left(\hat{J}_-\hat{J}_+\right)^{-1/2}\hat{J}_-$ can be expanded in its Dicke basis to give

$$(\hat{J}_-\hat{J}_+)^{-1/2}\hat{J}_- = \sum_{m=-j}^{j-1}\left|j,m\right\rangle_N\left\langle j,m+1\right|. \tag{A.13}$$

The operator $\left(\hat{J}_+\hat{J}_-\right)^{-1/2}\hat{J}_+$ is its Hermitian conjugate:

$$(\hat{J}_+\hat{J}_-)^{-1/2}\hat{J}_+ = \hat{J}_+(\hat{J}_-\hat{J}_+)^{-1/2} = \sum_{m=-j}^{j-1}\left|j,m+1\right\rangle_N\left\langle j,m\right|. \tag{A.14}$$

Equation (A.13) is the spin system analogue of the *Susskind-Glogower phase operator* $(\hat{a}\hat{a}^\dagger)^{-1/2}\hat{a}$ [Susskind & Glogower (1964)] for the harmonic oscillator. The Susskind-Glogower operator has the property that coherent states are approximate eigenstates when $|\alpha| \gg 1$, as was shown by Loudon (1973). Below we show that this is also a good approximation for the spin analogue. We start by writing the spin coherent state in its Dicke basis:

$$|j,\zeta\rangle_N = \sum_{m=-j}^{j} C_m \,|j,m\rangle_N \tag{A.15}$$

where

$$C_m = \binom{2j}{j+m}^{1/2} \frac{\zeta^{j+m}}{\left(1+|\zeta|^2\right)^j}. \tag{A.16}$$

The operators $\left(\hat{J}_-\hat{J}_+\right)^{-1/2}\hat{J}_-$ and $\left(\hat{J}_+\hat{J}_-\right)^{-1/2}\hat{J}_+$ act on the Dicke state $|j,m\rangle_N$ as follows:

$$\left(\hat{J}_-\hat{J}_+\right)^{-1/2}\hat{J}_-\,|j,m\rangle_N = |j,m-1\rangle_N\,, \tag{A.17}$$

$$\left(\hat{J}_+\hat{J}_-\right)^{-1/2}\hat{J}_+\,|j,m\rangle_N = |j,m+1\rangle_N \tag{A.18}$$

so that we can write

$$\left(\hat{J}_-\hat{J}_+\right)^{-1/2}\hat{J}_-\,|j,\zeta\rangle_N = \sum_{m=-j}^{j-1}\left[\frac{\zeta\sqrt{j-m}}{\sqrt{j+m+1}}\right] C_m\,|j,m\rangle_N\,, \tag{A.19}$$

$$\left(\hat{J}_+\hat{J}_-\right)^{-1/2}\hat{J}_+\,|j,\zeta\rangle_N = \sum_{m=-j+1}^{j}\left[\frac{\sqrt{j+m}}{\zeta\sqrt{j-m+1}}\right] C_m\,|j,m\rangle_N\,. \tag{A.20}$$

We expand the expression in the square brackets in (A.19) around the average values of $j \pm m$:

$$\begin{aligned}\left[\frac{\zeta\sqrt{j-m}}{\sqrt{j+m+1}}\right] &= \left[\frac{\zeta\sqrt{j-\bar{m}}}{\sqrt{j+\bar{m}}}\right]\left(1-\frac{m-\bar{m}}{j-\bar{m}}\right)^{1/2}\left(1+\frac{m-\bar{m}+1}{j+\bar{m}}\right)^{-1/2}\\ &\approx \left[\frac{\zeta\sqrt{j-\bar{m}}}{\sqrt{j+\bar{m}}}\right]\left(1-\frac{m-\bar{m}}{2\,(j-\bar{m})}+\ldots\right)\left(1-\frac{m-\bar{m}+1}{2\,(j+\bar{m})}+\ldots\right).\end{aligned}$$

The average value of m with probability distribution $|C_m|^2$ is $\bar{m} = \left\langle \hat{J}_z \right\rangle = -j\left(\frac{1-|\zeta|^2}{1+|\zeta|^2}\right)$ so that

$$j-\bar{m} = \frac{2j}{1+|\zeta|^2} \quad ; \quad j+\bar{m} = \frac{2j\,|\zeta|^2}{1+|\zeta|^2} \tag{A.21}$$

and its standard deviation is $\Delta m = \Delta \hat{J}_z = \frac{\sqrt{2j}|\zeta|}{1+|\zeta|^2}$. Since $m - \bar{m}$ will be of the order of Δm we have

$$\left[\frac{\zeta\sqrt{j-m}}{\sqrt{j+m+1}}\right] \approx \frac{\zeta}{|\zeta|}\left(1+\frac{|\zeta|}{2\sqrt{2j}}+...\right)\left(1-\frac{1}{2\sqrt{2j}|\zeta|}-\frac{1}{4j\,|\zeta|^2}-\frac{1}{4j}+...\right) \tag{A.22}$$

When

$$\frac{1}{\sqrt{2j}} \ll |\zeta| \ll \sqrt{2j} \quad \text{and} \quad 1 \ll 2j, \tag{A.23}$$

we have

$$\left[\frac{\zeta\sqrt{j-m}}{\sqrt{j+m+1}}\right] \approx \frac{\zeta}{|\zeta|} = e^{-i\phi}. \tag{A.24}$$

Similarly, for the square bracket in (A.20) we have

$$\left[\frac{\sqrt{j+m}}{\zeta\sqrt{j-m+1}}\right] \approx \frac{|\zeta|}{\zeta} = e^{i\phi}. \tag{A.25}$$

Now, we'd like to show that the contributions due to the terms C_j and C_{-j} that are missing in (A.19) and (A.20) respectively are negligible. First,

$$|C_j|^2 = \left(\frac{|\zeta|^2}{1+|\zeta|^2}\right)^{2j} = \left(\frac{1}{1+\frac{1}{|\zeta|^2}}\right)^{2j}. \tag{A.26}$$

Since

$$|\zeta|^2 \ll 2j \Rightarrow \frac{1}{1+\frac{1}{|\zeta|^2}} \ll \frac{1}{1+\frac{1}{2j}} \tag{A.27}$$

we can say that

$$\left|C_{N/2}\right|^2 \ll \left(\frac{1}{1+\frac{1}{N}}\right)^N \overset{(N\gg 1)}{\approx} \frac{1}{e}. \tag{A.28}$$

Similarly, using $\frac{1}{N} \ll |\zeta|^2$,

$$\left|C_{-N/2}\right|^2 = \left(\frac{1}{1+|\zeta|^2}\right)^N \ll \left(\frac{1}{1+\frac{1}{N}}\right)^N \approx \frac{1}{e}, \tag{A.29}$$

so that both $C_{N/2}$ and $C_{-N/2}$ are negligible. Combining (A.24) and (A.28) we have

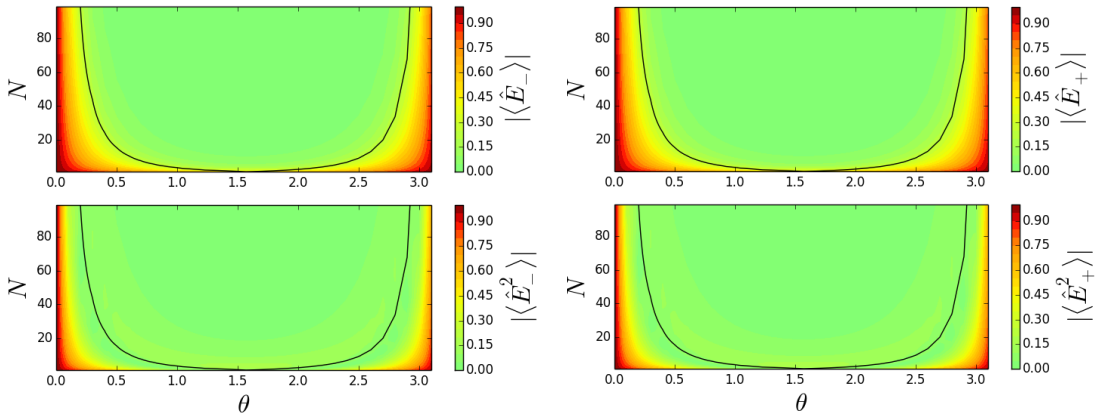

Figure A.1: Top: $\left|\langle\zeta|\,\hat{E}_\pm\,|\zeta\rangle\right|$ plotted against $\theta = 2\arctan|\zeta|$ and N. Bottom: $\left|\langle\zeta|\,\hat{E}_\pm^2\,|\zeta\rangle\right|$ plotted against θ and N (for $\phi = 0$). The black lines show $|\zeta|^2 = 1/N$ for $|\zeta| < 1$ (or $\theta < \pi/2$) and $|\zeta|^2 = N$ for $|\zeta| > 1$ (or $\theta > \pi/2$).

$$\left(\hat{J}_-\hat{J}_+\right)^{-1/2}\hat{J}_-\,|j,\zeta\rangle_N \approx e^{-i\phi}\,|j,\zeta\rangle_N\,. \tag{A.30}$$

Combining (A.25) and (A.29) we have

$$\left(\hat{J}_+\hat{J}_-\right)^{-1/2}\hat{J}_+\,|j,\zeta\rangle_N \approx e^{i\phi}\,|j,\zeta\rangle_N\,, \tag{A.31}$$

when

$$\frac{1}{\sqrt{2j}} \ll |\zeta| \ll \sqrt{2j} \quad \text{and} \quad 1 \ll 2j, \tag{A.32}$$

as required. For large j this restriction is not at all severe since a very broad range of values of ζ will satisfy condition (A.32).

We plot in figure A.1 the quantities $\left|\langle\zeta|\,\hat{E}_\pm\,|\zeta\rangle\right|$ and $\left|\langle\zeta|\,\hat{E}_\pm^2\,|\zeta\rangle\right|$ where

$$\hat{E}_- \equiv e^{-i\phi} - \left(\hat{J}_-\hat{J}_+\right)^{-1/2}\hat{J}_- \quad ; \quad \hat{E}_+ \equiv e^{i\phi} - \left(\hat{J}_+\hat{J}_-\right)^{-1/2}\hat{J}_+. \tag{A.33}$$

Since $|\left\langle \hat{E}_\pm \right\rangle|$ is small when $\frac{1}{\sqrt{N}} \ll |\zeta| \ll \sqrt{N}$ the expectation value of $\left(\hat{J}_-\hat{J}_+\right)^{-1/2}\hat{J}_-$ is close to $e^{-i\phi}$. Also, since $|\left\langle \hat{E}_\pm^2 \right\rangle|$ is small in this parameter regime the uncertainty is small. This indicates that the spin coherent state is an approximate eigenstate of $\left(\hat{J}_-\hat{J}_+\right)^{-1/2}\hat{J}_-$ and of $\left(\hat{J}_+\hat{J}_-\right)^{-1/2}\hat{J}_+$.

A.3 Approximating the Hamiltonian

On-resonance and for initial state $|\zeta\rangle_N \left|D_{\pm}^{\phi}(0)\right\rangle$ with $1/\sqrt{N} \ll |\zeta| \ll \sqrt{N}$ we have the effective Hamiltonian (4.73):

$$\hat{H}_{SS}^{\pm} = \pm\lambda\sqrt{\left(\hat{a}_{\downarrow}^{\dagger}\hat{a}_{\downarrow} + |\downarrow\rangle\langle\downarrow|\right)\left(\hat{a}_{\uparrow}^{\dagger}\hat{a}_{\uparrow} + |\uparrow\rangle\langle\uparrow|\right)}. \tag{A.34}$$

The expectation values of the operators $\hat{a}_{\downarrow}^{\dagger}\hat{a}_{\downarrow}$ and $\hat{a}_{\uparrow}^{\dagger}\hat{a}_{\uparrow}$ for the initial spin coherent state $|\zeta\rangle_N$ are

$$\left\langle \hat{a}_{\uparrow}^{\dagger}\hat{a}_{\uparrow} \right\rangle = \frac{N|\zeta|^2}{1+|\zeta|^2} \quad ; \quad \left\langle \hat{a}_{\downarrow}^{\dagger}\hat{a}_{\downarrow} \right\rangle = \frac{N}{1+|\zeta|^2}, \tag{A.35}$$

and their standard deviations are:

$$\sqrt{\mathrm{Var}\left(\hat{a}_{\uparrow}^{\dagger}\hat{a}_{\uparrow}\right)} = \sqrt{\mathrm{Var}\left(\hat{a}_{\downarrow}^{\dagger}\hat{a}_{\downarrow}\right)} = \sqrt{\mathrm{Var}\,\hat{J}_z} = \frac{\sqrt{N}|\zeta|}{1+|\zeta|^2}. \tag{A.36}$$

This means that:

$$\frac{\sqrt{\mathrm{Var}\left(\hat{a}_{\uparrow}^{\dagger}\hat{a}_{\uparrow}\right)}}{\left\langle \hat{a}_{\uparrow}^{\dagger}\hat{a}_{\uparrow} \right\rangle} = \frac{1}{|\zeta|\sqrt{N}}, \tag{A.37}$$

$$\frac{\sqrt{\mathrm{Var}\left(\hat{a}_{\downarrow}^{\dagger}\hat{a}_{\downarrow}\right)}}{\left\langle \hat{a}_{\downarrow}^{\dagger}\hat{a}_{\downarrow} \right\rangle} = \frac{|\zeta|}{\sqrt{N}}. \tag{A.38}$$

Both of these quantities are far less than unity for our initial spin coherent state parameter $\frac{1}{\sqrt{N}} \ll |\zeta| \ll \sqrt{N}$ so that the eigenvalue distributions of $\hat{a}_{\uparrow}^{\dagger}\hat{a}_{\uparrow}$ and $\hat{a}_{\downarrow}^{\dagger}\hat{a}_{\downarrow}$ are narrowly peaked around their average values. Since our effective Hamiltonian (A.34) commutes with $\hat{a}_{\uparrow}^{\dagger}\hat{a}_{\uparrow}$ and $\hat{a}_{\downarrow}^{\dagger}\hat{a}_{\downarrow}$, these distributions remain narrowly peaked throughout the evolution of the system. Defining $\Delta\hat{X} = \hat{X} - \left\langle \hat{X} \right\rangle$ for any operator $\hat{X}$ we can write the effective Hamiltonian (A.34) as:

$$\hat{H}_{SS}^{\pm} = \pm\lambda\sqrt{\left\langle \hat{a}_{\downarrow}^{\dagger}\hat{a}_{\downarrow} \right\rangle\left\langle \hat{a}_{\uparrow}^{\dagger}\hat{a}_{\uparrow} \right\rangle}\sqrt{\left(1 + \frac{|\downarrow\rangle\langle\downarrow| + \Delta(\hat{a}_{\downarrow}^{\dagger}\hat{a}_{\downarrow})}{\left\langle \hat{a}_{\downarrow}^{\dagger}\hat{a}_{\downarrow} \right\rangle}\right)\left(1 + \frac{|\uparrow\rangle\langle\uparrow| + \Delta(\hat{a}_{\uparrow}^{\dagger}\hat{a}_{\uparrow})}{\left\langle \hat{a}_{\uparrow}^{\dagger}\hat{a}_{\uparrow} \right\rangle}\right)}. \tag{A.39}$$

The operators $\frac{|\downarrow\rangle\langle\downarrow|+\Delta(\hat{a}_\downarrow^\dagger\hat{a}_\downarrow)}{\langle\hat{a}_\downarrow^\dagger\hat{a}_\downarrow\rangle}$ and $\frac{|\uparrow\rangle\langle\uparrow|+\Delta(\hat{a}_\uparrow^\dagger\hat{a}_\uparrow)}{\langle\hat{a}_\uparrow^\dagger\hat{a}_\uparrow\rangle}$ are small compared to unity when $1/\sqrt{N} \ll |\zeta| \ll \sqrt{N}$ because

$$\frac{|\downarrow\rangle\langle\downarrow|}{\left\langle\hat{a}_\downarrow^\dagger\hat{a}_\downarrow\right\rangle} \sim \mathcal{O}\left(\frac{1+|\zeta|^2}{N}\right), \tag{A.40}$$

$$\frac{\Delta(\hat{a}_\downarrow^\dagger\hat{a}_\downarrow)}{\left\langle\hat{a}_\downarrow^\dagger\hat{a}_\downarrow\right\rangle} \sim \mathcal{O}\left(\frac{\sqrt{\mathrm{Var}(\hat{a}_\downarrow^\dagger\hat{a}_\downarrow)}}{\left\langle\hat{a}_\downarrow^\dagger\hat{a}_\downarrow\right\rangle}\right) = \mathcal{O}\left(\frac{|\zeta|}{\sqrt{N}}\right), \tag{A.41}$$

$$\frac{|\uparrow\rangle\langle\uparrow|}{\left\langle\hat{a}_\uparrow^\dagger\hat{a}_\uparrow\right\rangle} \sim \mathcal{O}\left(\frac{1+|\zeta|^2}{N|\zeta|^2}\right), \tag{A.42}$$

$$\frac{\Delta(\hat{a}_\uparrow^\dagger\hat{a}_\uparrow)}{\left\langle\hat{a}_\uparrow^\dagger\hat{a}_\uparrow\right\rangle} \sim \mathcal{O}\left(\frac{\sqrt{\mathrm{Var}(\hat{a}_\uparrow^\dagger\hat{a}_\uparrow)}}{\left\langle\hat{a}_\uparrow^\dagger\hat{a}_\uparrow\right\rangle}\right) = \mathcal{O}\left(\frac{1}{|\zeta|\sqrt{N}}\right). \tag{A.43}$$

This allows us to expand the square roots in the Hamiltonian (A.34) in powers of these small operators. Keeping terms to second order gives:

$$\hat{H}_{SS}^{\pm} = \pm\lambda\left(\hat{H}_0 + \hat{H}_1 + \hat{H}_2\right), \tag{A.44}$$

where:

$$\hat{H}_0 = \frac{N|\zeta|}{1+|\zeta|^2}, \tag{A.45}$$

$$\hat{H}_1 = \frac{|\zeta|}{2}|\downarrow\rangle\langle\downarrow| + \frac{1}{2|\zeta|}|\uparrow\rangle\langle\uparrow| + \left(\frac{1}{2|\zeta|} - \frac{|\zeta|}{2}\right)\Delta\left(\hat{a}_\uparrow^\dagger\hat{a}_\uparrow\right), \tag{A.46}$$

$$\begin{aligned}\hat{H}_2 = {} & -\frac{1}{8}\frac{|\zeta|(1+|\zeta|^2)}{N}\left[|\downarrow\rangle\langle\downarrow| + \Delta\left(\hat{a}_\downarrow^\dagger\hat{a}_\downarrow\right)\right]^2 - \frac{1}{8}\frac{(1+|\zeta|^2)}{N|\zeta|^3}\left[|\uparrow\rangle\langle\uparrow| + \Delta\left(\hat{a}_\uparrow^\dagger\hat{a}_\uparrow\right)\right]^2 \\ & + \frac{1}{4}\frac{(1+|\zeta|^2)}{N|\zeta|}\left[|\downarrow\rangle\langle\downarrow| + \Delta\left(\hat{a}_\downarrow^\dagger\hat{a}_\downarrow\right)\right]\left[|\uparrow\rangle\langle\uparrow| + \Delta\left(\hat{a}_\uparrow^\dagger\hat{a}_\uparrow\right)\right],\end{aligned} \tag{A.47}$$

or, replacing $\Delta(\hat{a}_\uparrow^\dagger\hat{a}_\uparrow) = \Delta\hat{J}_z$ and $\Delta(\hat{a}_\downarrow^\dagger\hat{a}_\downarrow) = -\Delta\hat{J}_z$:

$$\hat{H}_0 = \frac{N|\zeta|}{1+|\zeta|^2}, \tag{A.48}$$

$$\hat{H}_1 = \frac{|\zeta|}{2}|\downarrow\rangle\langle\downarrow| + \frac{1}{2|\zeta|}|\uparrow\rangle\langle\uparrow| + \left(\frac{1}{2|\zeta|} - \frac{|\zeta|}{2}\right)\Delta\hat{J}_z, \tag{A.49}$$

$$\begin{aligned}\hat{H}_2 = &-\frac{1}{8}\frac{|\zeta|(1+|\zeta|^2)}{N}\left(|\downarrow\rangle\langle\downarrow| - \Delta\hat{J}_z\right)^2 - \frac{1}{8}\frac{(1+|\zeta|^2)}{N|\zeta|^3}\left(|\uparrow\rangle\langle\uparrow| + \Delta\hat{J}_z\right)^2 \\ &+\frac{1}{4}\frac{(1+|\zeta|^2)}{N|\zeta|}\left(|\downarrow\rangle\langle\downarrow| - \Delta\hat{J}_z\right)\left(|\uparrow\rangle\langle\uparrow| + \Delta\hat{J}_z\right).\end{aligned} \tag{A.50}$$

A.3.1 The Jaynes-Cummings approximation

So far the only restriction on the spin coherent state parameter has been $1/\sqrt{N} \ll |\zeta| \ll \sqrt{N}$. None of the analysis so far has assumed the bosonic approximation. Now we suppose that $|\zeta| \ll 1$. In this case the first term of $\hat{H}_1$ [equation (A.46)] is small and can be safely neglected for times $\lambda t \ll \frac{2\pi}{|\zeta|}$ because for those times we have $\exp\left[-i\lambda t\frac{|\zeta|}{2}|\downarrow\rangle\langle\downarrow|\right] \approx 1$. The second and third terms of $\hat{H}_1$ cannot be neglected, however, since $\frac{1}{|\zeta|} \gg 1$. The first term of $\hat{H}_2$ is

$$-\frac{1}{8}\frac{|\zeta|(1+|\zeta|^2)}{N}\left(|\downarrow\rangle\langle\downarrow| + \Delta\left(\hat{a}_\downarrow^\dagger\hat{a}_\downarrow\right)\right)^2 = -\frac{1}{8}\frac{|\zeta|(1+|\zeta|^2)}{N}|\downarrow\rangle\langle\downarrow| \tag{A.51}$$

$$-\frac{1}{4}\frac{|\zeta|(1+|\zeta|^2)}{N}\Delta\left(\hat{a}_\downarrow^\dagger\hat{a}_\downarrow\right)\otimes|\downarrow\rangle\langle\downarrow| \tag{A.52}$$

$$-\frac{1}{8}\frac{|\zeta|(1+|\zeta|^2)}{N}\left[\Delta\left(\hat{a}_\downarrow^\dagger\hat{a}_\downarrow\right)\right]^2 \tag{A.53}$$

Since the operator $\Delta\left(\hat{a}_\downarrow^\dagger\hat{a}_\downarrow\right)$ is of order $\sqrt{\mathrm{Var}\hat{J}_z} = \frac{\sqrt{N}|\zeta|}{1+|\zeta|^2}$ these terms (A.51), (A.52) and (A.53) are of order $\frac{|\zeta|}{N}$, $\frac{|\zeta|^2}{\sqrt{N}}$ and $|\zeta|^3$ respectively and can be neglected within the time $\lambda t \ll \frac{2\pi}{|\zeta|}$ already assumed. Similarly, the third term of $\hat{H}_2$ [equation (A.47)] is

$$\frac{1}{4}\frac{(1+|\zeta|^2)}{N|\zeta|}\left[|\downarrow\rangle\langle\downarrow| + \Delta\left(\hat{a}_\downarrow^\dagger \hat{a}_\downarrow\right)\right]\left[|\uparrow\rangle\langle\uparrow| + \Delta\left(\hat{a}_\uparrow^\dagger \hat{a}_\uparrow\right)\right] =$$

$$-\frac{1}{4}\frac{(1+|\zeta|^2)}{N|\zeta|}\Delta\hat{J}_z \otimes \hat{\sigma}_z \tag{A.54}$$

$$-\frac{1}{4}\frac{(1+|\zeta|^2)}{N|\zeta|}(\Delta\hat{J}_z)^2. \tag{A.55}$$

Again, using the fact that $\Delta(\hat{J}_z) \sim \sqrt{\mathrm{Var}\hat{J}_z} = \frac{\sqrt{N}|\zeta|}{1+|\zeta|^2}$ we find that term (A.54) is of order $\frac{1}{\sqrt{N}}$ and term (A.55) is of order $|\zeta|$. Both terms are also negligible for $\lambda t \ll \frac{2\pi}{|\zeta|}$. There is, however, a more significant contribution from the second term of $\hat{H}_2$:

$$-\frac{1}{8}\frac{(1+|\zeta|^2)}{N|\zeta|^3}\left[|\uparrow\rangle\langle\uparrow| + \Delta(\hat{a}_\uparrow^\dagger \hat{a}_\uparrow)\right]^2 = -\frac{1}{8}\frac{(1+|\zeta|^2)}{N|\zeta|^3}|\uparrow\rangle\langle\uparrow| \tag{A.56}$$

$$-\frac{1}{4}\frac{(1+|\zeta|^2)}{N|\zeta|^3}\Delta\hat{J}_z \otimes |\uparrow\rangle\langle\uparrow| \tag{A.57}$$

$$-\frac{1}{8}\frac{(1+|\zeta|^2)}{N|\zeta|^3}\left(\Delta\hat{J}_z\right)^2. \tag{A.58}$$

The term (A.57) is of order $\frac{1}{\sqrt{N}|\zeta|^2}$. For times $\lambda t \ll 2\pi\sqrt{N}|\zeta|^3$ this term can be safely neglected. Since (A.56) is of order $\frac{1}{N|\zeta|^3}$ it is smaller than (A.54) and can also be ignored for these times. The remaining term (A.53) is of order $\frac{1}{|\zeta|}$, however, and contributes significantly to the evolution on timescales of interest.

In summary, our final Hamiltonian for the the spin star model in the Jaynes-Cummings approximation is

$$\hat{H}_{SS}^{\pm} \approx \pm\lambda\left[\frac{N|\zeta|}{1+|\zeta|^2} + \frac{1}{2|\zeta|}|\uparrow\rangle\langle\uparrow| + \frac{1-|\zeta|^2}{2|\zeta|}\Delta(\hat{a}_\uparrow^\dagger \hat{a}_\uparrow) - \frac{1+|\zeta|^2}{8N|\zeta|^3}\left[\Delta(\hat{a}_\uparrow^\dagger \hat{a}_\uparrow)\right]^2\right]. \tag{A.59}$$

This approximation is valid for times $\lambda t \ll \frac{2\pi}{|\zeta|}$ and $\lambda t \ll 2\pi\sqrt{N}|\zeta|^3$.

A.3.2 The one-axis twisting approximation

Here we find an effective Hamiltonian beyond the Jaynes-Cummings approximation, when $|\zeta| \approx 1$. Setting $|\zeta| = 1$ in equations (A.48), (A.49) and (A.50) we

find that:

$$\hat{H}_0 = \frac{N}{2}, \tag{A.60}$$

$$\hat{H}_1 = \frac{1}{2}, \tag{A.61}$$

$$\hat{H}_2 = -\frac{1}{N}\left(\hat{J}_z + \frac{\hat{\sigma}_z}{2}\right)^2, \tag{A.62}$$

so that

$$\hat{H}^{\pm}_{SS} \approx \pm\lambda\left(\frac{N+1}{2} - \frac{1}{N}\left(\hat{J}_z + \frac{\hat{\sigma}_z}{2}\right)^2\right). \tag{A.63}$$

So that we can estimate the timescales where this approximation is valid, we derive this Hamiltonian in more detail below. Expanding the effective Hamiltonian (6.18):

$$\hat{H}^{\pm}_{SS} = \pm\sqrt{\hat{J}^2 - \hat{J}_z^2 - \hat{J}_z \otimes \hat{\sigma}_z}, \tag{A.64}$$

around the operator $\hat{J}^2$, we obtain:

$$\hat{H}^{\pm}_{SS} = \pm\lambda\sqrt{\hat{J}^2}\sum_{k=0}^{\infty} A_k \hat{M}^k, \tag{A.65}$$

where $\hat{M} = \frac{\hat{J}_z^2 + \hat{J}_z \otimes \hat{\sigma}_z}{\sqrt{\hat{J}^2}}$ and $A_0 = 1$, $A_1 = -1/2$ and $A_k = -(2k-3)!!/(2^k k!)$ (for $k \geq 2$) are coefficients whose absolute value is always less than unity. [Here $(2k-3)!!$ is a double factorial, i.e., the product of all odd positive integers less than or equal to $2k-3$.] Keeping only the first two terms in this expansion we have:

$$\hat{H}^{\pm}_{SS} \approx \pm\lambda\left(\sqrt{\hat{J}^2} - \frac{\hat{J}_z^2 + \hat{J}_z \otimes \hat{\sigma}_z}{2\sqrt{\hat{J}^2}}\right). \tag{A.66}$$

This can be rewritten as (6.19):

$$\hat{H}^{\pm}_{SS} \approx \pm\lambda\left(\sqrt{\hat{J}^2} + \frac{1}{8\sqrt{\hat{J}}} - \frac{\left(\hat{J}_z + \frac{\hat{\sigma}_z}{2}\right)^2}{2\sqrt{\hat{J}^2}}\right). \tag{A.67}$$

In the symmetric subspace of the N outer spins we have $\sqrt{\hat{J}^2} = \sqrt{\frac{N}{2}\left(\frac{N}{2}+1\right)} \approx \frac{N}{2}$ so that equations (A.67) and (A.63) are the same.

We write

$$\left|\tilde{\Psi}^{\pm}(t)\right\rangle = \exp\left[\pm\lambda\left(\sqrt{\hat{J}^2} + \frac{1}{8\sqrt{\hat{J}}} - \frac{\left(\hat{J}_z + \frac{\hat{\sigma}_z}{2}\right)^2}{2\sqrt{\hat{J}^2}}\right)\right]\left|\Psi^{\pm}(0)\right\rangle \tag{A.68}$$

for initial state $|\Psi^{\pm}(0)\rangle$ evolving by the truncated Hamiltonian (6.19). To see that this truncation is a good approximation, we show below that the fidelity of the state $\left|\tilde{\Psi}^{\pm}(t)\right\rangle$ to the state $e^{-it\hat{H}^{\pm}_{SS}}\left|\Psi^{\pm}(0)\right\rangle$ [evolving by Hamiltonian (A.64)] is close to unity. We write this fidelity as

$$\left|\left\langle\tilde{\Psi}^{\pm}(t)\right| e^{-it\hat{H}^{\pm}_{SS}}\left|\Psi^{\pm}(0)\right\rangle\right| \tag{A.69}$$

$$= \left|\left\langle\Psi^{\pm}(0)\right| \exp\left[\mp it\lambda\sqrt{\hat{J}^2}\sum_{k=2}^{\infty} A_k \hat{M}^k\right]\left|\Psi^{\pm}(0)\right\rangle\right| \tag{A.70}$$

$$= \left|\sum_{m=-N/2}^{N/2} |C_m|^2 \left\langle D^{\phi}_{\pm}(0)\right| \exp\left[\mp it\lambda\sqrt{\frac{N}{2}\left(\frac{N}{2}+1\right)}\sum_{k=2}^{\infty} A_k \left(\frac{m^2 + m\hat{\sigma}_z}{\frac{N}{2}\left(\frac{N}{2}+1\right)}\right)^k\right]\left|D^{\phi}_{\pm}(0)\right\rangle\right|, \tag{A.71}$$

where $|C_m|^2$ is the squared amplitude of the spin coherent state expansion coefficient, i.e. binomial coefficient [see equation (2.62)]. This binomial distribution $|C_m|^2$ has average value $\bar{m} = \left\langle \hat{J}_z \right\rangle = -\frac{N}{2}\left(\frac{1-|\zeta|^2}{1+|\zeta|^2}\right)$ and standard deviation $\delta m = \sqrt{\mathrm{Var}\hat{J}_z} = \frac{\sqrt{N}|\zeta|}{1+|\zeta|^2}$. In (A.71) we write $m = \bar{m} + (m - \bar{m})$ and replace all occurrences of $m - \bar{m}$ with the standard deviation δm. This is reasonable because the coefficient $|C_m|^2$ with

$$\frac{1}{\sqrt{N}} \ll |\zeta| \ll \sqrt{N} \qquad \text{and} \quad 1 \ll N, \tag{A.72}$$

is small unless m is in the range $\bar{m} \pm \delta m$. Only terms in this range will contribute significantly to the sum in (A.71). Expanding the exponential and only keeping the $k = 2$ term to lowest order in time gives

$$\left|\left\langle \tilde{\Psi}^{\pm}(t)\right| e^{-it\hat{H}^{\pm}_{SS}} \left|\Psi^{\pm}(0)\right\rangle\right| \tag{A.73}$$

$$\approx \left|1 \mp \sum_{m=-N/2}^{N/2} |C_m|^2 \frac{i\lambda t A_2}{\left[\frac{N}{2}\left(\frac{N}{2}+1\right)\right]^{3/2}} \left\langle D^{\phi}_{\pm}(0)\right| \left[(\bar{m}+\Delta m)^2 + (\bar{m}+\Delta m)\sigma_z\right]^2 \left|D^{\phi}_{\pm}(0)\right\rangle\right|$$

$$\approx \Big|1 \mp \frac{i\lambda t A_2}{\left[\frac{N}{2}\left(\frac{N}{2}+1\right)\right]^{3/2}} \left\langle D^{\phi}_{\pm}(0)\right| \Big[\frac{N^2(1-|\zeta|^2)^2}{4(1+|\zeta|^2)^2} + \frac{N|\zeta|^2}{(1+|\zeta|^2)^2} - \frac{N^{3/2}|\zeta|(1-|\zeta|^2)}{(1+|\zeta|^2)^2}$$

$$-\frac{N(1-|\zeta|^2)\sigma_z}{2(1+|\zeta|^2)} + \frac{\sqrt{N}|\zeta|\sigma_z}{1+|\zeta|^2}\Big]^2 \left|D^{\phi}_{\pm}(0)\right\rangle\Big|. \tag{A.74}$$

This is a complicated expression, but all terms (apart from unity) are negligible if

$$\lambda t \ll \frac{2}{N}\left(\frac{1+|\zeta|^2}{1-|\zeta|^2}\right)^4 \quad \text{and} \quad \lambda t \ll \frac{N(1+|\zeta|^2)^4}{8|\zeta|^4}. \tag{A.75}$$

For $|\zeta| = 1$ this simplifies to the condition that $\lambda t \ll N$.

References

Agarwal, G.S. (1981). Relation between atomic coherent-state representation, state multipoles, and generalized phase-space distributions. *Phys. Rev. A*, **24**, 2889–2896. 24

Agarwal, G.S., Puri, R.R. & Singh, R.P. (1997). Atomic Schrödinger cat states. *Phys. Rev. A*, **56**, 2249–2254. 114, 118, 121

Anza, F., Militello, B. & Messina, A. (2010). Tripartite thermal correlations in an inhomogeneous spin–star system. *Journal of Physics B: Atomic, Molecular and Optical Physics*, **43**, 205501. 69

Apostol, T.M. (1969). Calculus, volume 2: Multi-variable calculus and linear algebra with applications. *AMC*, **10**, 12. 52

Arecchi, F., Courtens, E., Gilmore, R. & Thomas, H. (1972). Atomic coherent states in quantum optics. *Physical Review A*, **6**, 2211. 18, 19, 23, 24, 33

Averbukh, I. & Perelman, N. (1989). Fractional revivals: Universality in the long-term evolution of quantum wave packets beyond the correspondence principle dynamics. *Physics Letters A*, **139**, 449 – 453. 110, 115, 118

Averbukh, I.S. (1992). Fractional revivals in the Jaynes-Cummings model. *Phys. Rev. A*, **46**, R2205–R2208. 112

Bennett, S.D., Yao, N.Y., Otterbach, J., Zoller, P., Rabl, P. & Lukin, M.D. (2013). Phonon-induced spin-spin interactions in diamond nanostructures: Application to spin squeezing. *Phys. Rev. Lett.*, **110**, 156402. 70, 118, 136, 141

Bernt, B.C. & Evans, R.J. (1981). The determination of Gauss sums. *Bull. Amer. Math. Soc.*, **5**, 107–129. 115

Berry, M., Marzoli, I. & Schleich, W. (2001). Quantum carpets, carpets of light. *Phys. World*, **14**, 39–44. 121

Braunstein, S.L. & Caves, C.M. (1994). Statistical distance and the geometry of quantum states. *Phys. Rev. Lett.*, **72**, 3439–3443. 57

Breuer, H.P. & Petruccione, F. (2007). Stochastic analysis and simulation of spin star systems. *Phys. Rev. E*, **76**. 69

Breuer, H.P., Burgarth, D. & Petruccione, F. (2004). Non-Markovian dynamics in a spin star system: Exact solution and approximation techniques. *Phys. Rev. B*, **70**, 045323. 69

Brune, M., Hagley, E., Dreyer, J., Maitre, X., Maali, A., Wunderlich, C., Raimond, J.M. & Haroche, S. (1996). Observing the progressive decoherence of the "meter" in a quantum measurement. *Phys. Rev. Lett.*, **77**, 4887–4890. 86

Bužek, V., Moya-Cessa, H., Knight, P. & Phoenix, S. (1992). Schrödinger-cat states in the resonant Jaynes-Cummings model: Collapse and revival of oscillations of the photon-number distribution. *Physical Review A*, **45**, 8190. 97, 112

Cahill, K.E. & Glauber, R.J. (1969). Density operators and quasiprobability distributions. *Phys. Rev.*, **177**, 1882–1902. 10

Chin, A.W., Huelga, S.F. & Plenio, M.B. (2012). Quantum metrology in non-Markovian environments. *Phys. Rev. Lett.*, **109**, 233601. 44

Chumakov, S.M., Frank, A. & Wolf, K.B. (1999). Finite Kerr medium: macroscopic quantum superposition states and Wigner functions on the sphere. *Physical Review A*, **60**, 1817–1823. 114, 121

Cramér, H. (1999). *Mathematical methods of statistics*, vol. 9. Princeton university press. 52

Dalvit, D.A.R., de Matos Filho, R.L. & Toscano, F. (2006). Quantum metrology at the Heisenberg limit with ion trap motional compass states. *New Journal of Physics*, **8**, 276. 14, 59

DiCarlo, L., Reed, M., Sun, L., Johnson, B., Chow, J., Gambetta, J., Frunzio, L., Girvin, S., Devoret, M. & Schoelkopf, R. (2010). Preparation and measurement of three-qubit entanglement in a superconducting circuit. *Nature*, **467**, 574–578. 71

Doherty, M.W., Dolde, F., Fedder, H., Jelezko, F., Wrachtrup, J., Manson, N.B. & Hollenberg, L.C.L. (2012). Theory of the ground-state spin of the nv^- center in diamond. *Phys. Rev. B*, **85**, 205203. 127

Dooley, S. & Spiller, T.P. (2014). Fractional revivals, multiple-Schrödinger-cat states, and quantum carpets in the interaction of a qubit with n qubits. *Phys. Rev. A*, **90**, 012320. 3, 70, 83, 111, 117, 122, 123, 124, 125

Dooley, S., McCrossan, F., Harland, D., Everitt, M.J. & Spiller, T.P. (2013). Collapse and revival and cat states with an n-spin system. *Phys. Rev. A*, **87**, 052323. 3, 86, 108

Dowling, J.P. & Milburn, G.J. (2003). Quantum technology: the second quantum revolution. *Philosophical Transactions of the Royal Society of London. Series A: Mathematical, Physical and Engineering Sciences*, **361**, 1655–1674. 1

Dowling, J.P., Agarwal, G.S. & Schleich, W.P. (1994). Wigner distribution of a general angular-momentum state: Applications to a collection of two-level atoms. *Phys. Rev. A*, **49**, 4101–4109. 24

Dutra, S., Knight, P. & Moya-Cessa, H. (1994). Large-scale fluctuations in the driven jaynes-cummings model. *Physical Review A*, **49**, 1993. 95

El-Orany, F.A.A. & Abdalla, M.S. (2011). Variance squeezing and entanglement of the XX central spin model. *Journal of Physics A: Mathematical and Theoretical*, **44**, 035302. 69

Ferrini, G., Minguzzi, A. & Hekking, F.W.J. (2008). Number squeezing, quantum fluctuations, and oscillations in mesoscopic number squeezing, quantum fluctuations, and oscillations in mesoscopic Bose Josephson junctions. *Phys. Rev. A*, **78**, 023606. 116

Gantsog, T. & Tanas, R. (1991). Discrete superpositions of coherent states and phase properties of elliptically polarized light propagating in a Kerr medium. *Quantum Optics: Journal of the European Optical Society Part B*, **3**, 33. 112

Gea-Banacloche, J. (1990). Collapse and revival of the state vector in the Jaynes-Cummings model: An example of state preparation by a quantum apparatus. *Phys. Rev. Lett.*, **65**, 3385–3388. 91

Gea-Banacloche, J. (1991). Atom- and field-state evolution in the Jaynes-Cummings model for large initial fields. *Phys. Rev. A*, **44**, 5913–5931. 82, 92, 95, 97, 112

Gerry, C. & Knight, P. (2005). *Introductory Quantum Optics*. Cambridge University Press, Cambridge, England. 4, 7, 8, 11, 14, 80, 86, 87, 89, 90, 91, 93

Gerry, C.C. (1998). Schrödinger cat states in a Josephson junction. *Phys. Rev. B*, **57**, 7474. 116

Gilchrist, A., Milburn, G.J., Munro, W.J. & Nemoto, K. (2003). Generating optical nonlinearity using trapped atoms. *arXiv preprint quant-ph/0305167*. 92

Giovannetti, V., Lloyd, S. & Maccone, L. (2004). Quantum-enhanced measurements: Beating the standard quantum limit. *Science*, **306**, 1330–1336. 37, 40

Giovannetti, V., Lloyd, S. & Maccone, L. (2011). Advances in quantum metrology. *Nature Photonics*, **5**, 222–229. 37, 40

Giraud, O., Braun, P. & Braun, D. (2008). Classicality of spin states. *Physical Review A*, **78**, 042112. 24

Glauber, R.J. (1963). Coherent and incoherent states of the radiation field. *Phys. Rev.*, **131**, 2766–2788. 8

Góra, P.F. & Jedrzejek, C. (1993). Superstructures, fractional revivals, and optical Schrödinger-cat states in the Jaynes-Cummings model. *Phys. Rev. A*, **48**, 3291–3300. 112, 114

Greiner, M., Mandel, O., Hansch, T.W. & Bloch, I. (2002). Collapse and revival of the matter wave field of a Bose-Einstein condensate. *Nature (London)*, **419**, 51–54. 110

Gross, C. (2010). *Spin squeezing and non-linear atom interferometry with Bose-Einstein condensates*. Ph.D. thesis, Universitat Heidelberg. 49

Gut, A. (2009). *An intermediate course in probability*. Springer. 56

Hamdouni, Y., Fannes, M. & Petruccione, F. (2006). Exact dynamics of a two-qubit system in a spin star environment. *Phys. Rev. B*, **73**, 245323. 147

Hillery, M. (1985). Classical pure states are coherent states. *Physics Letters A*, **111**, 409 – 411. 9

Holstein, T. & Primakoff, H. (1940). Field dependence of the intrinsic domain magnetization of a ferromagnet. *Phys. Rev.*, **58**, 1098–1113. 33

Hudson, R. (1974). When is the Wigner quasi-probability density non-negative? *Reports on Mathematical Physics*, **6**, 249–252. 10

Huelga, S.F., Macchiavello, C., Pellizzari, T., Ekert, A.K., Plenio, M.B. & Cirac, J.I. (1997). Improvement of frequency standards with quantum entanglement. *Phys. Rev. Lett.*, **79**, 3865–3868. 44, 48

Hunter, J., Hunter, J. & Box, G. (1978). Statistics for experimenters an introduction to design, data analysis, and model building. *Wiley series in probability and mathematical statistics.*. 39

Hutton, A. & Bose, S. (2004). Mediated entanglement and correlations in a star network of interacting spins. *Phys. Rev. A*, **69**, 042312. 68, 69, 72

Jaynes, E. & Cummings, F. (1963). Comparison of quantum and semiclassical radiation theories with application to the beam maser. *Proc. IEEE.*, **51**. 86

Jones, J.A., Karlen, S.D., Fitzsimons, J., Ardavan, A., Benjamin, S.C., Briggs, G.A.D. & Morton, J.J.L. (2009). Magnetic field sensing beyond the standard quantum limit using 10-spin noon states. *Science*, **324**, 1166–1168. 44, 70, 71

Kaplan, A.E., Marzoli, I., Lamb, W.E. & Schleich, W.P. (2000). Multimode interference: highly regular pattern formation in quantum wave-packet evolution. *Phys. Rev. A*, **61**, 032101. 121

Kenfack, A. & Życzkowski, K. (2004). Negativity of the Wigner function as an indicator of non-classicality. *Journal of Optics B: Quantum and Semiclassical Optics*, **6**, 396. 10

Kirchmair, G., Vlastakis, B., Leghtas, Z., Nigg, S., Paik, H., Ginossar, E., Mirrahimi, M., Frunzio, L., Girvin, S. & Schoelkopf, R. (2013). Observation of quantum state collapse and revival due to the single-photon Kerr effect. *Nature (London)*, **495**, 205–209. 112

Kitagawa, M. & Ueda, M. (1993). Squeezed spin states. *Phys. Rev. A*, **47**, 5138–5143. 27, 47, 114, 121, 126, 135

Klimov, A. & Saavedra, C. (1998). The Dicke model dynamics in a high detuning limit. *Physics Letters A*, **247**, 14 – 20. 118

Klimov, A. & Sanchez-Soto, L. (2000). Method of small rotations and effective hamiltonians in nonlinear quantum optics. *Physical Review A*, **61**, 063802. 80

Lee, H., Kok, P. & Dowling, J.P. (2002). A quantum rosetta stone for interferometry. *Journal of Modern Optics*, **49**, 2325–2338. 37, 40

Lee, S.Y., Lee, C.W., Nha, H. & Kaszlikowski, D. (2014). Quantum phase estimation with four-headed cat states. *arXiv preprint arXiv:1409.4220*. 14

Loudon, R. (1973). *The Quantum Theory of Light*. Clarendon, New York. 151

Lvovsky, A., Ghobadi, R., Chandra, A., Prasad, A. & Simon, C. (2013). Observation of micro-macro entanglement of light. *Nature Physics*, **9**, 541–544. 11

Ma, J., Wang, X., Sun, C. & Nori, F. (2011). Quantum spin squeezing. *Physics Reports*, **509**, 89 – 165. 29, 46, 47, 121, 126, 134, 135

Mandel, L. (1979). Sub-Poissonian photon statistics in resonance fluorescence. *Optics Letters*, **4**, 205–207. 12

Marcos, D., Wubs, M., Taylor, J.M., Aguado, R., Lukin, M.D. & Sørensen, A.S. (2010). Coupling nitrogen-vacancy centers in diamond to superconducting flux qubits. *Phys. Rev. Lett.*, **105**, 210501. 71

Matsuzaki, Y., Benjamin, S.C. & Fitzsimons, J. (2011). Magnetic field sensing beyond the standard quantum limit under the effect of decoherence. *Phys. Rev. A*, **84**, 012103. 44

Maurer, P.C., Kucsko, G., Latta, C., Jiang, L., Yao, N.Y., Bennett, S.D., Pastawski, F., Hunger, D., Chisholm, N., Markham, M., Twitchen, D.J., Cirac, J.I. & Lukin, M.D. (2012). Room-temperature quantum bit memory exceeding one second. *Science*, **336**, 1283–1286. 138

McDermott, R., Simmonds, R.W., Steffen, M., Cooper, K.B., Cicak, K., Osborn, K.D., Oh, S., Pappas, D.P. & Martinis, J.M. (2005). Simultaneous state measurement of coupled Josephson phase qubits. *Science*, **307**, 1299–1302. 71

Meekhof, D.M., Monroe, C., King, B.E., Itano, W.M. & Wineland, D.J. (1996). Generation of nonclassical motional states of a trapped atom. *Phys. Rev. Lett.*, **76**, 1796–1799. 86

Merzbacher, E. (1977). Quantum mechanics, 1970. *John Wiler & Sons, New York Zbl0102*, **42701**. 4

Milburn, G.J., Corney, J., Wright, E.M. & Walls, D.F. (1997). Quantum dynamics of an atomic Bose-Einstein condensate in a double-well potential. *Phys. Rev. A*, **55**, 4318–4324. 118

Militello, B. & Messina, A. (2011). Genuine tripartite entanglement in a spin-star network at thermal equilibrium. *Physical Review A*, **83**, 042305. 69

Munro, W.J., Nemoto, K., Milburn, G.J. & Braunstein, S.L. (2002). Weak-force detection with superposed coherent states. *Physical Review A*, **66**, 023819. 14

Neeley, M., Bialczak, R.C., Lenander, M., Lucero, E., Mariantoni, M., O'Connell, A.D., Sank, D., Wang, H., Weides, M., Wenner, J., Yin, Y., Yamamoto, T., Cleland, A.N. & Martinis, J.M. (2010). Generation of three-qubit entangled states using superconducting phase qubits. *Nature (London)*, **467**, 570–573. 71

Nielsen, M. & Chuang, I. (2000). *Quantum Computation and Quantum Information*. CUP. 16, 50

Niskanen, A.O., Harrabi, K., Yoshihara, F., Nakamura, Y., Lloyd, S. & Tsai, J.S. (2007). Quantum coherent tunable coupling of superconducting qubits. *Science*, **316**, 723–726. 71

Papoulis, A. & Pillai, S. (2002). *Probability, random variables, and stochastic processes*. McGraw-Hill electrical and electronic engineering series, McGraw-Hill. 34

Paris, M.G.A. (2009). Quantum estimation for quantum technology. *International Journal of Quantum Information*, **07**, 125–137. 50, 53, 60

Radcliffe, J.M. (1971). Some properties of coherent spin states. *Journal of Physics A: General Physics*, **4**, 313. 34

Raghavan, S., Pu, H., Meystre, P. & Bigelow, N. (2001). Generation of arbitrary Dicke states in spinor Bose–Einstein condensates. *Optics communications*, **188**, 149–154. 28

Reed, M., DiCarlo, L., Nigg, S., Sun, L., Frunzio, L., Girvin, S. & Schoelkopf, R. (2012). Realization of three-qubit quantum error correction with superconducting circuits. *Nature*, **482**, 382–385. 71

Robinett, R. (2004). Quantum wave packet revivals. *Physics Reports*, **392**, 1 – 119. 92, 110, 118

Saito, S., Zhu, X., Amsüss, R., Matsuzaki, Y., Kakuyanagi, K., Shimo-Oka, T., Mizuochi, N., Nemoto, K., Munro, W.J. & Semba, K. (2013). Towards realizing a quantum memory for a superconducting qubit: Storage and retrieval of quantum states. *Phys. Rev. Lett.*, **111**, 107008. 72

Scharfenberger, B. (2014). Unpublished (private communication). 145

Schlosshauer, M. (2007). *Decoherence and the Quantum to Classical Transition*. Springer. 1

Schrödinger, E. (1935). The present status of quantum mechanics. *Die Naturwissenschaften*, **23**, 1–26. 1

Shore, B.W. & Knight, P.L. (1993). The Jaynes-Cummings model. *Journal of Modern Optics*, **40**, 1195–1238. 97

Simmons, S., Jones, J.A., Karlen, S.D., Ardavan, A. & Morton, J.J.L. (2010). Magnetic field sensors using 13-spin cat states. *Phys. Rev. A*, **82**, 022330. 70, 71

Stanwix, P.L., Pham, L.M., Maze, J.R., Le Sage, D., Yeung, T.K., Cappellaro, P., Hemmer, P.R., Yacoby, A., Lukin, M.D. & Walsworth, R.L. (2010). Coherence of nitrogen-vacancy electronic spin ensembles in diamond. *Physical Review B*, **82**, 201201. 144

Sudarshan, E.C.G. (1963). Equivalence of semiclassical and quantum mechanical descriptions of statistical light beams. *Phys. Rev. Lett.*, **10**, 277–279. 8

Susskind, L. & Glogower, J. (1964). Quantum mechanical phase and time operator. *Physica*, **1**, 49–61. 151

Tara, K., Agarwal, G.S. & Chaturvedi, S. (1993). Production of Schrödinger macroscopic quantum-superposition states in a Kerr medium. *Phys. Rev. A*, **47**, 5024–5029. 112

Toscano, F., Dalvit, D.A.R., Davidovich, L. & Zurek, W.H. (2006). Sub-Planck phase-space structures and Heisenberg-limited measurements. *Phys. Rev. A*, **73**, 023803. 14, 48, 59

Tóth, G. & Petz, D. (2013). Extremal properties of the variance and the quantum fisher information. *Physical Review A*, **87**, 032324. 53

Tóth, G., Knapp, C., Gühne, O. & Briegel, H.J. (2007). Optimal spin squeezing inequalities detect bound entanglement in spin models. *Phys. Rev. Lett.*, **99**, 250405. 64

Tsomokos, D.I., Ashhab, S. & Nori, F. (2008). Fully connected network of superconducting qubits in a cavity. *New Journal of Physics*, **10**, 113020. 71

Twamley, J. & Barrett, S.D. (2010). Superconducting cavity bus for single nitrogen-vacancy defect centers in diamond. *Phys. Rev. B*, **81**, 241202. 71

Vlastakis, B., Kirchmair, G., Leghtas, Z., Nigg, S.E., Frunzio, L., Girvin, S.M., Mirrahimi, M., Devoret, M.H. & Schoelkopf, R.J. (2013). Deterministically encoding quantum information using 100-photon Schrödinger cat states. *Science*, **342**, 607–610. 1

Wernsdorfer, W. (2008). Quantum dynamics in molecular nanomagnets. *Comptes Rendus Chimie*, **11**, 1086 – 1109. 118

Wesenberg, J. & Mølmer, K. (2002). Mixed collective states of many spins. *Phys. Rev. A*, **65**, 062304. 18

Wineland, D.J., Bollinger, J.J., Itano, W.M. & Heinzen, D.J. (1994). Squeezed atomic states and projection noise in spectroscopy. *Phys. Rev. A*, **50**, 67–88. 46, 47

Wiseman, H. & Milburn, G. (2010). *Quantum Measurement and Control*. Cambridge. 50, 53

Wootters, W.K. (1981). Statistical distance and hilbert space. *Phys. Rev. D*, **23**, 357–362. 54, 55, 56

Yoshihara, F., Harrabi, K., Niskanen, A.O., Nakamura, Y. & Tsai, J.S. (2006). Decoherence of flux qubits due to $1/f$ flux noise. *Phys. Rev. Lett.*, **97**, 167001. 130

Yurke, B. & Stoler, D. (1986). Generating quantum mechanical superpositions of macroscopically distinguishable states via amplitude dispersion. *Phys. Rev. Lett.*, **57**, 13–16. 111

Zhang, Z. & Duan, L. (2014). Quantum metrology with dicke squeezed states. *arXiv preprint arXiv:1406.7626*. 147

Zhu, X., Saito, S., Kemp, A., Kakuyanagi, K., Karimoto, S.i., Nakano, H., Munro, W.J., Tokura, Y., Everitt, M.S., Nemoto, K., Kasu, M., Mizuochi, N. & Semba, K. (2011). Coherent coupling of a superconducting flux qubit to an electron spin ensemble in diamond. *Nature (London)*, **478**, 221–224. 72

Zhu, X., Matsuzaki, Y., AmsÃss, R., Kakuyanagi, K., Shimo-Oka, T., Mizuochi, N., Nemoto, K., Semba, K., Munro, W.J. & Saito, S. (2014). Observation of dark states in a superconductor diamond quantum hybrid system. *Nat Commun*, **5**. 72

Zurek, W.H. (2001). Sub-Planck structure in phase space and its relevance for quantum decoherence. *Nature*, **412**, 712–717. 15

Zurek, W.H. (2003). Decoherence and the transition from quantum to classical–revisited. *arXiv preprint quant-ph/0306072*. 1